

Alma Mater Studiorum – Università di Bologna

**DOTTORATO DI RICERCA IN**

**Scienze Biochimiche e Biotecnologiche**

**Ciclo XXIX**

**Settore Concorsuale di afferenza: 03/D1**

**Settore Scientifico disciplinare: CHIM/08**

**Design and Synthesis of New Chemical Entities to Exploring the Multifactorial  
Nature of Alzheimer's Disease**

**Presentata da: Roberta Caporaso**

**Coordinatore Dottorato**

**Prof. Santi Mario Spampinato**

**Relatore**

**Prof.ssa Anna Minarini**

**Correlatore**

**Prof.ssa Michela Rosini**

**Esame finale anno 2017**

# Contents

<b>Preface</b>	2
<b>Abstract</b>	3
<b>Chapter 1 - Introduction</b>	4
1.1 The multifactorial nature of Alzheimer's Disease (AD) pathogenesis	5
1.1.1 Etiology of AD and therapeutic approaches: what still lives on	7
1.2 The re-examination of A $\beta$ -centric approach	25
1.2.1 A $\beta$ and oxidative stress: a toxic vicious cycle	26
1.2.2 A $\beta$ role in p53-mediated neuronal death	32
1.2.3 A $\beta$ -mediated excitotoxicity	34
1.3 Multitarget strategies in AD	37
1.4 Natural multifunctional agents	47
<b>Chapter 2 - Aim of the thesis</b>	53
2.1 Nature-Inspired Modulators of AD: Focusing on Amyloid and Oxidative Stress	54
2.1.1 METHODS: Chemistry and Biology	59
2.1.2 Results and discussion	65
2.2 Design of MTDLs Combining Anti-aggregating and Antioxidant Profile with NMDAR Antagonism	79
2.2.1 METHODS: Chemistry and Biology	81
2.2.2 Conclusions	86
<b>Chapter 3 - Experimental section</b>	87
3.1 Chemistry	87
3.2 Biology	112
<b>Bibliography</b>	118
<b>Appendix</b>	134

# Preface

This PhD thesis has been carried out at the Department of Pharmacy and Biotechnology, Alma Mater Studiorum-University of Bologna (Italy), under the supervision of Prof. Anna Minarini.

The thesis project is devoted to the design and synthesis of small molecules targeting the multifactorial nature of neurodegenerative diseases, mainly in the fields of antioxidants and anti-aggregating agents.

Two main projects are herein described: the first one is focused on the development of nature-inspired multifunctional ligands as promising pharmacological tools to deepen insight into the complex nature of Alzheimer's disease, while the second one is devoted to the design and synthesis of new multi-target-directed ligands conveyed by memantine in the achievement of a site-specific mode of action.

The thesis is organized in 3 different chapters: the first chapter is an introduction about the physiopathological aspects and the intertwined mechanisms underpinning the etiology and progression of Alzheimer's disease.

Chapter 2 contains the drug design approaches used in each project, the synthetic methods and the biological evaluation assays of the new synthesized compounds. It also includes the results and discussions section.

Chapter 3 reports experimental procedures of synthesized compounds including chemical and biological methods.

I would like to sincerely thank and express my gratitude to Prof. Anna Minarini and to the research group involved in the present investigation, particularly Prof. Michela Rosini and Dr. Elena Simoni (University of Bologna), for the helpful discussions, guidance and encouragement in the project realization.

I would also like to thank Prof. Manuela Bartolini (University of Bologna) and Prof. Cristina Lanni and her group (University of Pavia) for biological investigations.

## Abstract

Alzheimer's disease (AD) is a multifactorial syndrome, with a complex interplay of genetic and biochemical factors contributing to the cognitive decline. Besides diffuse neuronal loss, AD brain shows protein folding defects, and there is growing evidence that amyloid- $\beta$  peptide ( $A\beta$ ) might trigger the disease process. In parallel, an increasing number of molecular targets, that may play an important role in the expression of its neurotoxicity, is emerging. In particular, the etiopathogenic loop generated by  $A\beta$  and oxidative stress indicates reactive oxygen species (ROS) overproduction as a crucial partner of  $A\beta$  toxicity. Moreover, a correlation between  $A\beta$ , oxidative stress and conformational changes of the transcription factor p53 has been suggested. In this context, (erythroid-derived 2)-like 2 (Nrf2) transcriptional pathway plays an important role as the major mechanism of defense in the cell against oxidative or electrophilic stress. Additionally, several evidences showed an attenuation of  $A\beta$ -induced oxidative cell death by means of activation of Nrf2 signaling, calling for a deeper investigation of Nrf2/ $A\beta$  cellular network.

Besides that, an excessive glutamatergic activity together with the hyperactivation of extrasynaptic *N*-methyl-D-aspartate receptors (NMDARs) has been widely documented in AD. In particular, a relationship between NMDARs hyperactivation, ROS production and  $A\beta$  toxicity has been well established in AD.

On the basis of these considerations, in order to obtain pharmacological tools to deepen insight into the cross-talk between  $A\beta$  functions and radical species in AD, in this project thesis new chemical entities have been synthesized combining natural privileged molecular fragments, which turned out to be versatile instruments to investigate  $A\beta$  causative role in AD.

Furthermore, based on the MTDL (multi-target-directed ligand) approach, aimed to obtain single molecules able to simultaneously hit multiple targets, in this work thesis, multifunctional ligands have been developed by combining the NMDAR antagonist memantine with natural pharmacophores exerting antioxidant and anti-aggregating activities.

# Chapter 1

## Introduction

AD is currently the most common neurodegenerative disorder, with both genetic and biochemical multiple factors contributing to the cognitive decline. In the United States, AD is ranked as the sixth leading cause of death among adults; worldwide, over 47 million people are afflicted by dementia, and this number is expected to increase, reaching more than 131 million by 2050, as populations age<sup>1</sup>. Furthermore, the huge majority of people with dementia don't receive a diagnosis, and so are unable to access care and treatment. Even when dementia is diagnosed, the limited available therapies and the fragmented care provided, which fall largely on families and caregivers, make AD one of the most serious diseases with social impact in the world, for which effective cures are urgently needed<sup>2</sup>.

As depicted by Alois Alzheimer in 1907, the neuropathological hallmarks observed in AD brain consist mainly of extracellular accumulation of aggregated A $\beta$ , that evolve in senile plaques and dystrophic neuritis, and intracellular neurofibrillary tangles (NFTs), formed by aggregates of hyperphosphorylated tau ( $\tau$ ) protein. Although the classical histopathological lesions are useful diagnostic markers, the cognitive impairment in patients with AD is closely associated with medial temporal lobe atrophy<sup>3</sup>, the progressive deterioration of the limbic system<sup>4, 5</sup>, neocortical regions<sup>6</sup>, and the basal forebrain<sup>7</sup>. Indeed, synapse loss in the neocortex and limbic system is the most specific pathological feature of the cognitive impairment in patients with AD<sup>8</sup>. Besides aggregation of A $\beta$  in amyloid plaques, several lines of investigation now support the view that increased levels of soluble A $\beta$ <sub>42</sub> oligomers might lead to synaptic damage and neurodegeneration<sup>9</sup>. These events result in the development of the typical symptoms of AD characterized by progressive impairments of cognitive functions, often accompanied by behavioral changes such as aggression and depression. In addition, memory loss with difficulty of performing familiar tasks, problems with language, disorientation in time space, and impaired judgment occur<sup>10</sup>. However, all these findings take place when the neurodegeneration is already evident, and there is no possibility for early detection. Consequently,

to date current medications only provide temporary benefits to patients by improving symptoms or retarding the progression of the pathology.

Despite the implication of senile plaques and neurofibrillary tangles in the pathogenesis and development of the disease is widely demonstrated, a complex network of events is involved in the etiology of AD. Therefore, the failure of properly facing this devastating illness might be explained partly by the lack of a unique exhaustive hypothesis able to explain the pathogenesis and the progression of the disease in its entirety.

### **1.1 The multifactorial nature of AD pathogenesis**

One of the biggest challenge for drug development programs is the research of an effective instrument able to explain adequately the molecular mechanisms responsible for the several histopathological changes observed in AD patients, as the current therapy offer only limited and temporary benefits to patients. The AD pathological hallmarks, such as A $\beta$  evolved in senile plaques and NFTs, have commonly been considered as causative features of the pathogenesis and progression of AD, leading over the years to the formulation of their respective hypotheses (amyloid cascade and tau hypothesis) as those mainly accredited to explain the etiology of the disease. However, after more than a century from its discovery, the scientific consensus is quite firm that, although its pathogenesis is not yet fully understood, AD is a multifactorial debilitating disorder caused by genetic, environmental and endogenous factors<sup>11</sup>. These factors include misfolding and dysfunctional trafficking proteins, often related to oxidative stress and free radical formation, mitochondrial dysfunction, metal dyshomeostasis and inflammation, and/or environmental factors strongly associated with age<sup>11</sup>.

None of these general events is *per se* sufficient to explain the wide spectrum of biochemical and pathological abnormalities found in AD (and generally in all neurodegenerative disorders), but there is a growing awareness that all these molecular events might coexist and influence each other (Fig.1.1).

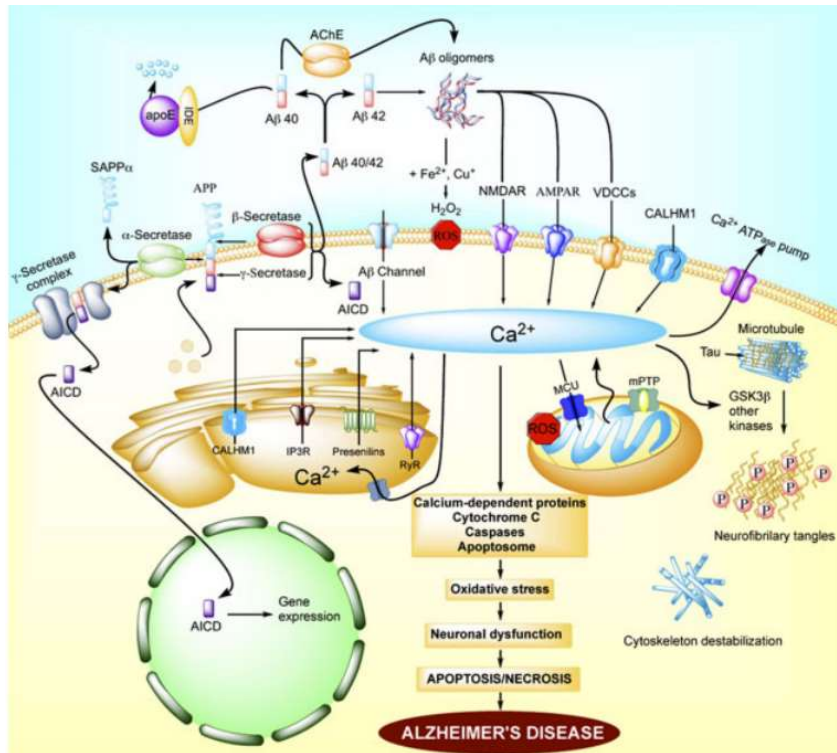


**Figure 1.1.** Interconnected pathways in AD<sup>12</sup>.

Genetic factors are particularly relevant in the early-onset familial AD, whose pathogenesis involves the apolipoprotein E (APOE) genotype. In the hereditary syndrome, that represents 3-4% of cases, APOE4 mutations constitute a high risk factor. Basically, APOE4 is closely connected to A $\beta$  for two reasons: (i) it increases A $\beta$  concentration by decreasing its clearance<sup>13, 14</sup>; (ii) it is able to enhance the activity of glycogen synthase kinase 3 $\beta$  (GSK-3 $\beta$ ), a kinase that hyperphosphorylates  $\tau$  protein, that in turn is essential for A $\beta$ -induced neurotoxicity<sup>15</sup>.

The environmental agents involved in AD are as important as genetic factors, and they include prions (atypical slow viruses), conventional viruses, metal neurotoxicants (e.g. aluminum) and diet, in particular dietary fat, while fish consumption was found to be a significant risk reduction factor<sup>16</sup>. Herpes simplex virus 1 (HSV1), present in the brain, stimulates nuclear factor kappa  $\beta$  (NF $\kappa$  $\beta$ ) which in turn up-regulates, among others, genes for stress-response proteins, leading to increase A $\beta$  formation<sup>17</sup>. HSV1 is also neurotropic and can produce Herpes simplex encephalitis (HSE) with AD-like impairment of short-term memory<sup>18</sup>. Another significant environmental factor that

contributes to A $\beta$ -neurotoxicity is chronic aluminum exposure. Aluminum salts, used as additives to enhance various characteristics of commercially-prepared foods and beverages, are routinely ingested with diet. As a consequence, accumulation of aluminum in aging neurons might contribute to neurofibrillary damage typical of AD progression<sup>19</sup>.

As for endogenous factors responsible for AD pathogenesis, besides the already mentioned hallmarks of the disease (i.e. A $\beta$  deposits and NFTs), decreased levels of some neurotransmitters involved in cognitive functions (e.g. acetylcholine, ACh) or overactivation of different receptors and channels (e.g. NMDARs) as well as metal dyshomeostasis and mitochondrial dysfunction are all strictly involved with the evolution of the disease. The interaction between toxic A $\beta$  species (likely oligomers) and metal ions such as Fe<sup>2+</sup> or Cu<sup>+</sup> activates the generation of ROS, representing a sort of initiator for the cascade of events leading to pathogenesis and progression of AD<sup>12</sup>.

On this basis, it is evident how the “one-molecule, one-target” paradigm in drug discovery lacks of any realistic foundation to face and overcome the complexity of the disease and the multiple crossroads between different pathways involved in the progression and cognitive decline of AD. Thus, the simultaneous action on different relevant targets crucial for the disease, by using a combination therapy or a single molecule able to interact with different targets in a parallel fashion, might be an effective strategy to better understand and prevent the progression of the disease.

### **1.1.1 Etiology of AD and therapeutic approaches: what still lives on**

The oldest hypothesis formulated to explain the etiology of AD was the cholinergic hypothesis, nearly 40 years ago, based on the evidence that several abnormalities in cholinergic neurotransmission were found in patients with AD. Later, amyloid cascade and  $\tau$  hypothesis came out as preeminent hypotheses because they were found to be responsible for key nodes in the pathological cascade leading to AD. Moreover, glutamatergic excitotoxicity, resulting from overactivation of NMDARs by glutamate, led to the formulation of glutamatergic hypothesis which links cognitive decline in AD patients to neuronal damage. In the last years, much attention has been devoted to oxidative stress as the redox impairment is one of the most prominent aspects of AD, despite it could be secondary to other pathological events.

Although each hypothesis has its own predominant features, altogether they have shown to be intertwined and to participate as active players in the intricate pathogenic scenario of AD.

### *Cholinergic hypothesis*

In the mid-1970s, several biochemical investigations of the brains of patients with AD showed substantial neocortical deficits in the enzyme responsible for the synthesis of ACh, choline acetyltransferase (ChAT)<sup>20-22</sup>. Besides that, consequent discoveries of reduced choline uptake, ACh release and degeneration of the basal forebrain nuclei confirmed an extensive deficit in presynaptic cholinergic transmission<sup>23</sup>. These studies, together with the emerging role of ACh in learning and memory<sup>24</sup>, led to the formulation of the “cholinergic hypothesis” of AD.

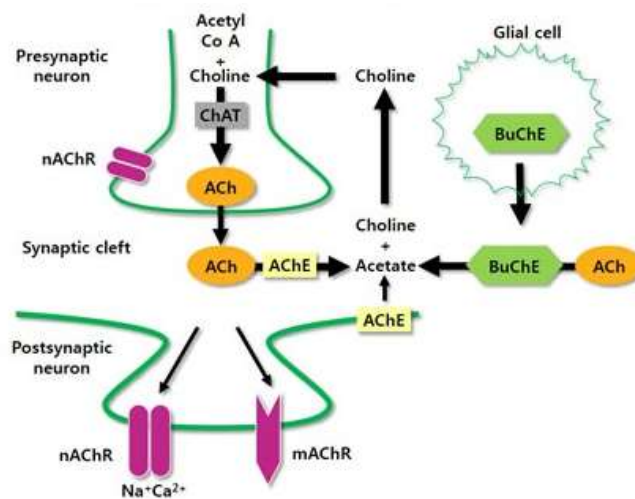


**Figure 1.2.** Functional features of the cholinergic system. ACh = acetylcholine; AChE = acetylcholinesterase<sup>25</sup>.

A large number of potential therapeutic strategies have been investigated with the attempt to correct ACh deficiency and loss of presynaptic cholinergic function, and to improve cholinergic neurotransmission: (i) increasing of ACh synthesis or ACh presynaptic release; (ii) stimulation of postsynaptic muscarinic (mAChRs) and nicotinic receptors (nAChRs); (iii) reduction of ACh synaptic degradation. Acetylcholinesterase (AChE) is the enzyme responsible for the hydrolysis of ACh in the synapse into choline and acetate, that can be in turn transported back into the presynaptic cell and used again for ACh synthesis. By inhibiting AChE an increased amount of ACh will be

available in the synapse to potentiate cholinergic transmission and keep nerve signal continue (Fig. 1.2). Currently, three AChE inhibitors (AChEIs) are marketed for the treatment of mild to moderate AD following approval by the U.S. Food and Drug Administration (FDA): donepezil, rivastigmine and galantamine (Fig. 1.3).

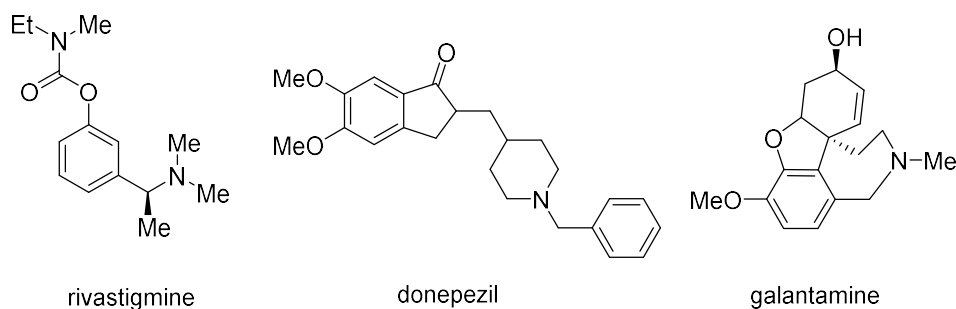


**Figure 1.3.** Chemical structures of the three AChEI drugs available for AD treatment.

Rivastigmine inhibits both AChE and butyrylcholinesterase (BChE), a cholinesterase mainly associated with glial cells that has shown to act probably as a compensatory mechanism for ACh metabolism<sup>26</sup>. Donepezil and galantamine selectively inhibit AChE. In addition, galantamine improves cholinergic transmission by acting as allosteric modulator of presynaptic nAChRs, thus increasing presynaptic ACh release and postsynaptic neurotransmission<sup>27</sup>. In fact, one of the most consistent cholinergic deficits is the reduced expression of nAChRs in the brain<sup>28</sup>. Expression of both  $\alpha 4\beta 2$  and  $\alpha 7$  nicotinic receptor subtypes, that predominate in the central nervous system (CNS) and are implicated in learning and memory processes, is reduced in AD. Thus, several subtype-selective agonists and partial agonists that target  $\alpha 4\beta 2$  as well as  $\alpha 7$  nAChR have been tested<sup>29</sup>. Currently, several compounds targeting nAChRs for mild to moderate AD are in clinical trial development: (i) EVP-6124 (FORUM Pharmaceuticals), an  $\alpha 7$  nAChR partial agonist; (ii) varenicline (Pfizer), an  $\alpha 4\beta 2$  nAChR partial agonist; (iii) AZD-3480 (AstraZeneca), a partial agonist for  $\alpha 4\beta 2$  and  $\alpha 2\beta 2$  nAChRs. Interestingly, since  $\alpha 4\beta 2$  nAChRs are lost early in AD,  $\alpha 4\beta 2$  nAChR single photon emission computed tomography (SPECT) and positron emission tomography (PET) radioligands are being developed and tested in clinical trials as potential diagnostic tools and biomarkers for AD staging<sup>29</sup>. Among mAChRs, M<sub>1</sub> subtype, widely expressed in CNS and

implicated in many physiological and pathological brain functions, is postulated to be an important therapeutic target for AD<sup>30</sup>, since several studies on M<sub>1</sub> mAChR-knockout mice showed a series of cognitive deficits and impairments in long-term potentiation. These evidence links M<sub>1</sub> subtype to multiple physiological functions such as synaptic plasticity and neuronal excitability differentiation. In support of this, cell line studies demonstrated that M<sub>1</sub>-allosteric modulators promoted a non-amyloidogenic pathway and decreased A $\beta$  production, indicating that M<sub>1</sub> modulation may have efficacy in the treatment of both symptomatic and pathologic features of AD<sup>31</sup>. Furthermore, administration of nonselective muscarinic antagonists can induce cognitive deficits and psychosis in humans<sup>32</sup>. Alternatively, antagonists of central presynaptic M<sub>2</sub> receptors may improve cognition by increasing the central release of ACh. Following this approach as well, high selectivity for one muscarinic receptor sub-type is required both for efficacy and to avoid cholinergic side effects<sup>33</sup>.

### ***Tau hypothesis***

The hypothesis of the hyperphosphorylation of  $\tau$  protein as one of the causal events of AD is justified by the presence of NFTs, primarily composed of paired helical filaments (PHFs) containing hyperphosphorylated  $\tau$  protein.  $\tau$  is a soluble microtubule-binding protein that stabilizes the microtubules in axons to ensure axonal transport and neuronal growth. As a consequence, the neurotoxicity mediated by NFTs is not only due to the direct toxic effects of aggregated  $\tau$ , but also to the loss of axonal transport, owing to sequestration of soluble  $\tau$  into hyperphosphorylated and aggregated forms that are no longer capable of supporting axonal transport. Destabilization of microtubules as well as direct toxic effects of soluble  $\tau$  aggregates and the formation of tangles may all contribute to  $\tau$ -mediated neurodegeneration. As a consequence, the best intervention is most likely to reduce the level of  $\tau$  in the brain. The strategies suggested over the years are mainly based on: (i) the inhibition of phosphorylation process (kinase inhibitors), (ii) the blockage of the formation of soluble  $\tau$  aggregates and NFTs (aggregation inhibitors), and (iii) the clearance enhancement of  $\tau$  and the degradation of its aggregates (clearance activators)<sup>34</sup> (Fig. 1.4).

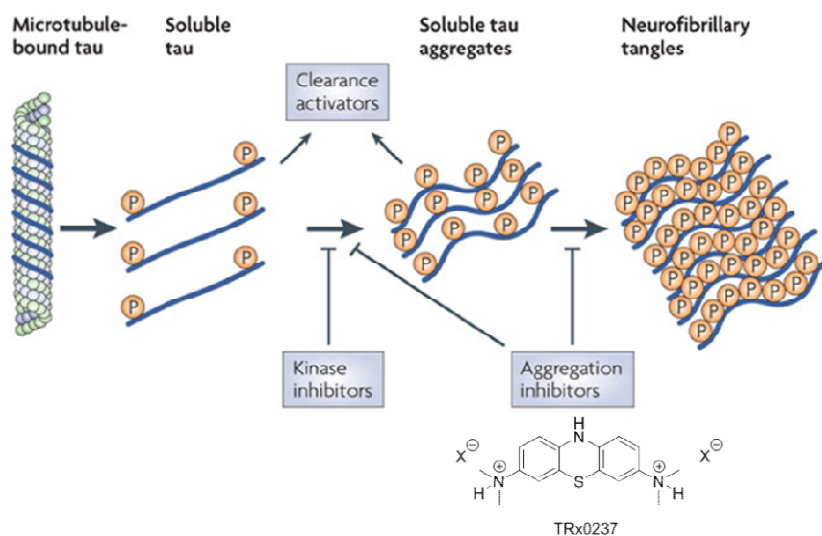


**Figure 1.4.** Tau  $\tau$ -pathology and major therapeutic approaches<sup>34</sup>.

From a drug development perspective, anti-aggregation approaches represent an appealing strategy, even if pose a number of issue regarding drug-like properties of candidates<sup>35</sup>. So far, the most successful therapeutic approach was prevention of aggregation regardless of phosphorylation or other modifications. In this sense, derivatives of methylene blue have been shown to inhibit the aggregation of  $\tau$ , thereby reducing oxidative stress, preventing mitochondrial damage, and preserving cognitive function in mice<sup>36</sup>. Among them, TRx0237 (TauRx Therapeutics Ltd.), a second-generation of  $\tau$  aggregation inhibitors, was the most successful, reaching phase III trial. Unfortunately, with the dismay of all researcher and media, it failed in people with mild to moderate AD for lack of efficacy<sup>37</sup>.

### ***NMDAR-mediated excitotoxicity***

Glutamate is the most abundant excitatory neurotransmitter in the CNS and is essential for the establishment of synaptic plasticity and the formation of memory and learning<sup>38</sup>. This fundamental activity of neuronal network building is significantly mediated by the ionotropic receptor family of *N*-methyl-D-aspartate (NMDA). NMDARs are characterized by high  $\text{Ca}^{2+}$  ions' permeability, voltage-dependent blockade by  $\text{Mg}^{2+}$  ions, and slower gating kinetics. Under physiological conditions, presynaptic depolarization promotes vesicles to release their contents of glutamate into

the synapses through exocytosis, where upon the released glutamate binds to post-synaptic ionotropic receptors, stimulating an influx of cations which depolarizes the post-synaptic cell<sup>39</sup>. To prevent over-stimulation, glutamate is removed by astrocytes and converted to L-glutamine through the action of glutamine synthetase, which is released to the extracellular fluid taken up by neurons (Fig. 1.5). The permanent presence of glutamate in the synaptic clefts leads to prolonged activation of NMDARs resulting into an excessive influx of  $\text{Ca}^{2+}$  that can lead to cell death through a process termed “excitotoxicity”. The massive influx of  $\text{Ca}^{2+}$  triggers a cascade of events leading to neuronal injury and death, which include: (i) the production of ROS and reactive nitrogen species (RNS); (ii) caspase and protease activation that damage cellular architecture and induce apoptosis; (iii) lipid peroxidation, which disrupts membrane integrity; (iv) toxic effects on mitochondrial functions; (v) stimulation of the p38 mitogen-activated kinase (MAPK) that induces transcription of proapoptotic factors<sup>40</sup>.

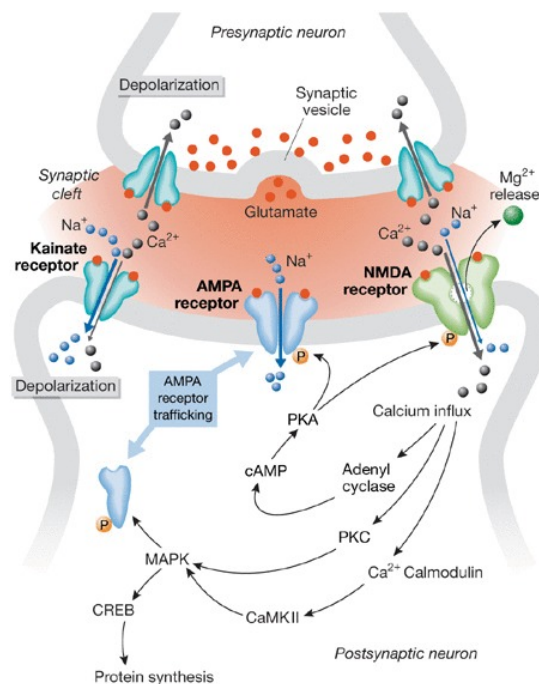


**Figure 1.5.** Glutamate receptors and synaptic plasticity<sup>41</sup>.

NMDARs are absolutely crucial for neuronal plasticity and normal neuronal functionality. Therefore, the generalized inhibition of normal excitatory synaptic activity has severe and unacceptable side effects<sup>40</sup>. One of the major reasons for therapeutic failure of promising drugs acting on this system is the lack of clinical tolerability, with the onset of stroke and traumatic brain

injury. To date, memantine, an old drug re-emerged for its ability of blocking excitotoxic cell death in a clinically tolerated manner<sup>42-44</sup>, is the only drug approved by U.S. FDA for the treatment of moderate to severe AD. Memantine is a low-to-moderate affinity, uncompetitive NMDARs antagonist, that preferentially blocks extrasynaptic NMDA channels when excessively activated. Because NMDARs during normal synaptic activity are opened for few milliseconds, memantine is unable to act, thus ensuring normal synaptic activity. Instead, during excitotoxic conditions, when NMDARs are activated for long periods of time, memantine becomes effective, blocking receptor activity. By manifesting a relatively fast off-rate from the channel at physiological resting potential, memantine does not accumulate in the channel, avoiding blockade of their normal function<sup>40</sup>. In addition, a large number of *in vivo* and *in vitro* studies confirm the neuroprotective properties of memantine, making this drug not only an enhancer of synaptic transmission but also a potential neuroprotective agent against glutamate-mediated neurotoxicity<sup>45</sup>. Besides the hyperactivation of NMDARs due to the permanent presence of glutamate in the synaptic cleft, decreased glutamate reuptake from microglia is another pathophysiological mechanism associates with excess of glutamate at excitatory synapses and consequent cytotoxicity.<sup>46</sup> Accordingly, riluzole, a US FDA-approved disease-modifying drug for amyotrophic lateral sclerosis, is in a phase II clinical trial in mild AD patients as inhibitor of presynaptic glutamate release and enhancer of glutamate transporter activity<sup>47</sup>.

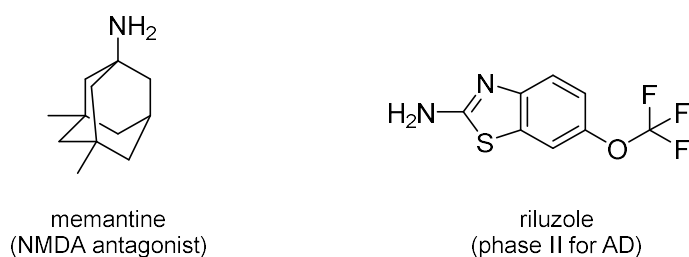


**Figure 1.6.** Drug (memantine) and drug candidate (riluzole) acting on glutamatergic system.

In the last decade, *Lipton et al.* reported a second generation of memantine derivatives, called NitroMemantines, designed to enhance neuroprotective efficacy of memantine without affecting safety<sup>40</sup>. The aimed goal was to block excitotoxicity by means of an additional modulatory site on NMDARs, in which *S*-nitrosylation, resulting from covalent bind of a nitro group to a crucial cysteine thiol residue(s) of the channel, occurs. This regulatory post-translational modification leads

to downregulation of excessive receptor activity, laying the foundations for novel therapeutics<sup>48</sup>. At basal levels, nitric oxide (NO), produced consequently to the mild-activation of synaptic NMDARs by a cascade of events that involve influx of  $\text{Ca}^{2+}$ , plays an important regulatory role in the CNS, promoting normal neuronal activity and neuronal differentiation or survival. By contrast, hyperactivation of extrasynaptic NMDARs leads to excessive production of NO (and ROS), contributing significantly to the etiology and pathophysiology of the disease. NO neuroprotective effects are partly mediated by NMDARs themselves *via* S-nitrosylation and consequent downregulation of receptors, as a sort of negative feedback to prevent their overactivation. S-Nitrosylation can occur on various cysteine residues on different NMDAR subunits, both on the GluN1 (NR1) and on the GluN2A (NR2A) subunit<sup>49-51</sup>. The presence of free thiol groups in these regions enhances S-nitrosylation of specific cysteines, leading to a series of polynitrosylation at the other NMDAR sites, thus inhibiting the activity of the receptor and so over-production of NO. In this context, NitroMemantines, bearing a nitro group ( $-\text{NO}_2$ ) tethered to the memantine moiety, offer the chance to antagonize hyperactivated NMDARs through two sites of action: (i) the ion channel where memantine itself binds, and (ii) an extra-cellular redox-sensitive thiol site of the receptor where  $-\text{NO}_2$  reacts to inhibit NMDAR activity (forming  $-\text{SNO}$  or  $-\text{SNO}_2$ ), causing desensitization.

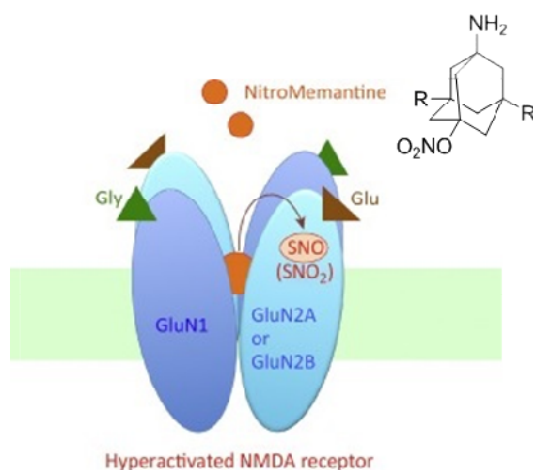


**Figure 1.7.** NitroMemantine-mediated inhibition of hyperactivated NMDARs. NMDARs is a heterodimer, composed of two GluN1 and two GluN2 sub-units. Excessive concentrations of glycine (Gly) and glutamate (Glu), co-agonists of the receptor, can trigger pathological activation of the NMDAR<sup>48</sup>.

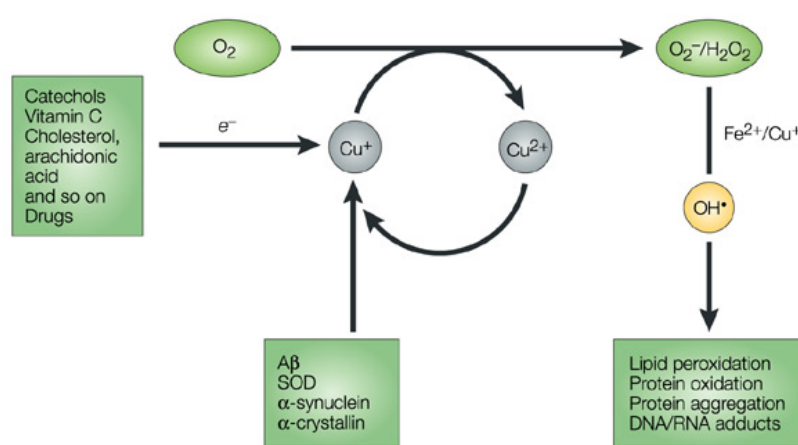
Taking advantage of an adamantane moiety that binds the excessively-open, extrasynaptic channels and using it to direct an NO-generating group to the redox-mediated regulatory sites on the receptor,

the new derivatives demonstrated to acting in a dual action, via channel blockade associated to allosteric redox modulation. In this manner, NitroMemantine drug can provide increased blockade of overactivated NMDARs through *S*-nitrosylation in addition to channel block, thus affording more neuroprotection than is offered by memantine. In addition, the lead NitroMemantine candidate, YQW-036/NMI-6979, has shown a favorable pharmacokinetic profile, excellent CNS penetration, and good safety index in early preclinical studies<sup>52</sup>. These compounds are currently being evaluated for clinical trials for AD and other neurological disorders<sup>48, 52</sup>.

### ***Oxidative stress in AD: primary cause or downstream event?***

Oxidative stress, defined as an imbalance in pro-oxidant and antioxidant homeostasis, is involved in various and numerous pathological states, including AD<sup>53</sup>. It is associated with increased production of ROS and RNS, including superoxide radical anion ( $O_2^{\cdot-}$ ), hydrogen peroxide ( $H_2O_2$ ), hydroxyl radical ( $HO^{\cdot}$ ), NO, and peroxynitrite ( $ONOO^-$ ). Mitochondria are the major source of ROS production as byproducts during oxidative phosphorylation<sup>54</sup>. Under normal conditions, the endogenous antioxidant enzymes acting as free radical scavengers control levels of ROS. These include superoxide dismutase (SOD), glutathione peroxidase (GSHPx), glutathione reductase, thioredoxins, and catalase<sup>55</sup>. In AD, the activity of antioxidant enzymes is reduced, thereby contributing to the unconstrained accumulation of oxidative damage<sup>56</sup>. When unbalanced, overproduction of ROS combines with the insufficient endogenous defense mechanisms, oxidative stress occurs. Several evidences have shown that mitochondrial dysfunction results in increased ROS production leading to the early stages of AD and contributing to the onset of A $\beta$  pathology<sup>53</sup>. Markers of oxidative stress including high levels of oxidized proteins, glycosylated products, lipid peroxidation, formation of aldehydes, free carbonyls, ketones, and oxidative modifications in RNA and nuclear and mitochondrial DNA were found in postmortem brain tissue and in peripheral systems (including cells and isolated mitochondria) from people with preclinical or early stages of AD<sup>57, 58</sup>. ROS can be generated by a large number of pathways, including the abnormal homeostasis of bioactive metals such as iron (Fe), copper (Cu) and zinc (Zn). In presence of the redox-active metal ions, like ferrous iron ( $Fe^{2+}$ ),  $H_2O_2$  can be converted to  $OH^{\cdot}$  through the “Fenton reaction”. The increased concentration of redox-active metals in the brain could lead to hypermetallation of proteins that normally bind metal ions at shielded sites (e.g. A $\beta$ ), releasing inappropriate radical

species. They can then interact with nearby cellular components, such as proteins, lipids and DNA, initiating neuronal cell death and neurodegeneration through a cascade of events<sup>59</sup> (Fig. 1.8). One of the downstream events that contributes to the apoptotic cascade is the dysregulation of intracellular calcium signaling, that can ultimately lead to the excitotoxic response through the activation of glutamate receptors<sup>60</sup>. However, if the disruption of calcium homeostasis is a cause or consequence of ROS generation, is still an open question, as increases in intracellular calcium have been reported to induce ROS production<sup>61</sup>.



Nature Reviews | Drug Discovery

**Figure 1.8.** ROS generation by abnormal reaction of O<sub>2</sub> with protein-bound Fe or Cu<sup>59</sup>.

The brain, compared with other organs, is particularly susceptible to the damaging effects of ROS because of its high content in polyunsaturated fatty acids (PUFAs), the poor levels of antioxidant defenses, the high oxidative metabolism and transition metal content, all acting as powerful pro-oxidants<sup>62</sup>. Peroxidation of the membrane lipid bilayer is one of the major sources of free radical-mediated injury that can propagate and amplify oxidative stress, directly damaging cell membranes, organelles and neurons. The oxidation of PUFAs by ROS at the membrane levels leads to the formation of reactive oxygenated  $\alpha,\beta$ -unsaturated aldehydes, which can act as “toxic second messengers”<sup>63</sup>. In fact, due to their amphiphilic nature, they can easily diffuse across membranes and form covalent adducts with cellular proteins altering their functions<sup>64</sup>. Covalent adduction of a lipid aldehyde to cysteine, lysine and histidine side chains leads to protein carbonylation, a type of protein oxidation that can be promoted by ROS. The resulting carbonylated proteins have been

implicated as causative in a variety of metabolic states, including AD<sup>65</sup>. One of the most abundant and cytotoxic lipid-derived alkenal is 4-hydroxy 2-nonenal (4-HNE). 4-HNE is able to readily react with various cellular components, such as DNA and proteins, to form 1,4-Michael type adducts with their nucleophilic thiol (-SH) or amino (-NH<sub>2</sub>) groups<sup>63</sup>. 4-HNE-protein adducts are one of key markers of lipid peroxidation found to be elevated in AD brain tissue. They lead to alteration of common pathways, such as antioxidant response, glucose metabolism and mitochondrial function that are known to contribute to cognitive decline<sup>62</sup>.

### *Amyloidogenic pathway*

The evidence of extracellular deposits of A $\beta$  in senile neuritic plaques together with genetic studies of AD led 25 years ago to the formulation of the amyloid hypothesis<sup>66</sup>.

A $\beta$  peptide comes from the proteolytic cleavage of amyloid- $\beta$  precursor protein (APP), a type I integral membrane glycoprotein, through the sequential action of two enzymes,  $\beta$ -secretase (also known as  $\beta$ -site APP cleaving enzyme 1, BACE1) and  $\gamma$ -secretase. The cleavage and processing of APP can be divided into an amyloidogenic pathway and a non-amyloidogenic pathway (Fig. 1.9).

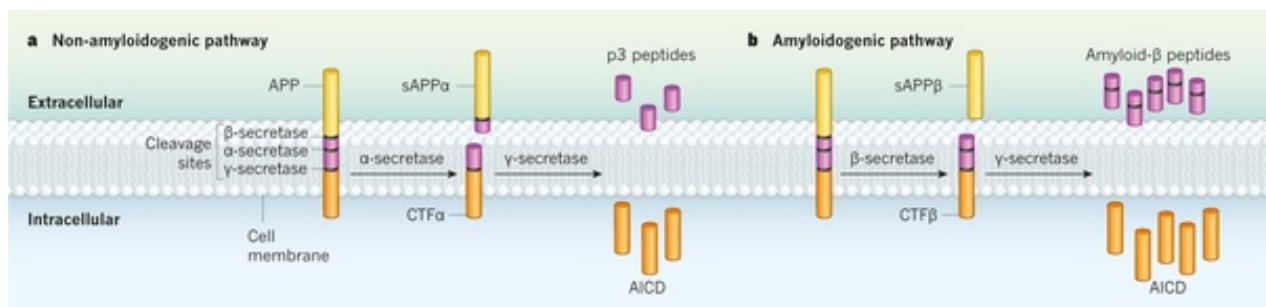


**Figure 1.9.** The production of A $\beta$  peptide<sup>66</sup>.

In the prevalent non-amyloidogenic pathway, APP is cleaved by the  $\alpha$ -secretase enzyme and leads to the formation of a soluble fragment, sAPP $\alpha$ , secreted into the extracellular medium and having neurotrophic and neuroprotective action<sup>67</sup>, and a C-terminal fragment of 83 amino acids (aa) (CTF $\alpha$ ), which remains anchored to the membrane. CTF $\alpha$  is in turn processed by a  $\gamma$ -secretase, producing a soluble extracellular non-amyloidogenic peptide, p3, and the APP intracellular domain (AICD)<sup>68</sup>.

The amyloidogenic pathway involves BACE1, which cleaves the extracellular domain of APP generating a soluble *N*-terminal fragment, sAPP $\beta$ , and a C-terminal fragment of 99aa (CTF $\beta$ ) which remains anchored to the membrane<sup>69</sup>. CTF $\beta$  is then processed by  $\gamma$ -secretase leading to release of A $\beta$  peptides of varying lengths and AICD fragment. The A $\beta_{40}$  variant is the most abundant and may actually be anti-amyloidogenic<sup>70</sup>, while A $\beta_{42}$  and A $\beta_{43}$  species are more hydrophobic and considered to be the more neurotoxic and prone to fibril formation than the shorter A $\beta_{40}$ <sup>66, 71</sup>.

The discovery that AD could be inherited in an autosomal dominant fashion has represented the strongest support for the articulation of the amyloid cascade hypothesis<sup>72</sup> (Fig. 1.10). Mutations in three genes are known to cause early-onset autosomal dominant familial AD (fAD): APP, PSEN1 and PSEN2, all involved in metabolism or stability of A $\beta$ . The gene APP encodes for APP, the holoprotein from which A $\beta$  is excised by BACE1 and  $\gamma$ -secretase, as mentioned before. Presenilin 1 (PSEN1)<sup>73</sup> and PSEN2<sup>74</sup> are both homologous proteins that form the catalytic active site of the  $\gamma$ -secretase complex<sup>75</sup>. Mutations or duplications in APP, or mutations in PSEN1 and PSEN2 can cause an increase in the production of longer, toxic A $\beta_{42/43}$  that are highly self-aggregating, leading to A $\beta$  deposition<sup>70</sup>.

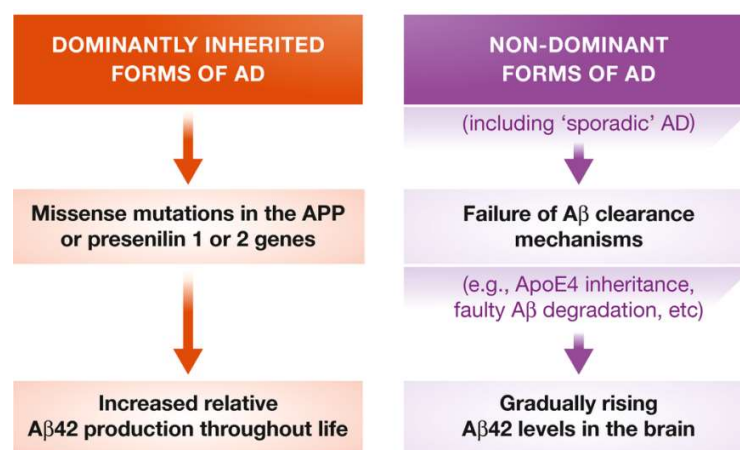


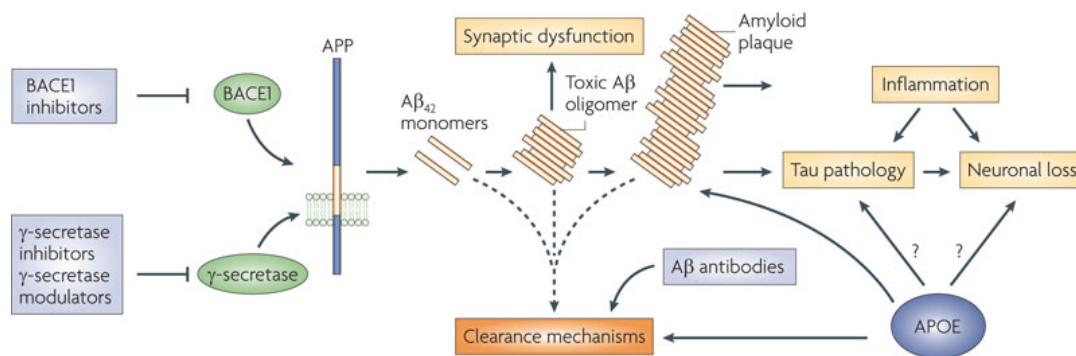
**Figure 1.10.** Sequence of events proposed by the amyloid cascade hypothesis leading to formation of toxic A $\beta_{42}$ <sup>76</sup>.

The major genetic risk factor of more common late-onset form of AD (sporadic AD, sAD) is caused by the  $\epsilon 4$  allele of the *APOE* gene (APOE4), as one of its functions appears to be correlated to the accumulation of intracellular A $\beta$ <sup>77</sup>. Humans possess three common *APOE* alleles: *APOE2*, *APOE3*

and *APOE4*<sup>78</sup>. While the expression of *APOE4* allele can promote amyloid build-up, development of plaques and vascular A $\beta$  deposits, *APOE3* can be considered to be neutral and *APOE2* is thought to be protective<sup>79</sup>. So far, it's not completely clear how the different APOE proteins mediate their effects in AD, but several experiments in PDAPP transgenic mice that harbored the human *APOE* genes have shown that A $\beta$  clearance (but not A $\beta$  production) is decreased by these proteins, with APOE2, APOE3 and APOE4 being increasingly less effective<sup>75</sup>. In particular, knock-in mice expressing human APOE2 have demonstrated to decrease A $\beta$  plaque pathology<sup>80</sup>. Furthermore, numerous studies indicate that APOE can also influence A $\beta$  metabolism, since in human APOE4 carriers displayed to accelerate amyloid plaque accumulation, with APOE4 promoting amyloid aggregation and deposition<sup>72</sup>.

Summing up, the most important genetic risk factor, APOE4, is associated with increased amyloid burden. Most importantly, all mutations that cause fAD increase A $\beta_{42}$  production or the ratio of A $\beta_{42}$  compared to the less aggregation-prone A $\beta_{40}$  isoform. All these alterations directly enhance amyloidogenic APP processing, in a way that promotes pathological aggregation of A $\beta$ . Thus, the predominant genetic risk factor in AD-related cognitive decline strongly supports the central etiologic role of A $\beta$  in the amyloid cascade hypothesis, that can in turn explain and incorporate several key data (pathological, phenotypical and genetic) relevant for the disease process. Moreover, other several arguments support the crucial role of A $\beta$  in the pathogenesis of AD: (i) amyloid deposits and neuritic plaques as key histopathological hallmark of AD, (ii) the acute synaptic toxicity effects shown by A $\beta$  oligomers, and (iii) the pro-inflammatory effects and neuronal toxicity caused by A $\beta$  fibrils.

Altogether these findings suggested multiple A $\beta$ -targeted therapeutic approaches with the aim to reduce the levels of A $\beta$ , including, among other strategies, modulation of A $\beta$  production, inhibition of A $\beta$  aggregation, enhancement of A $\beta$  clearance through immunotherapy, and APOE-related treatment approaches (Fig. 1.11).



Nature Reviews | Drug Discovery

**Figure 1.11.** The amyloid cascade and therapeutic points of intervention<sup>34</sup>.

### *Modulation of A $\beta$ production*

As depicted by the amyloid hypothesis, A $\beta$ , in particular the least soluble 42 amino-acid long A $\beta$ <sub>42</sub>, has a critical role in all forms of AD. Therefore, it's not surprising that one of the first direct approach in anti-amyloid therapy was to modulate A $\beta$ <sub>42</sub> production, by acting on the three key enzymes responsible to the cleavage of APP: BACE1,  $\gamma$ -secretase and  $\alpha$ -secretase. BACE1 and  $\gamma$ -secretase lead to the formation of toxic A $\beta$ <sub>42</sub> through the amyloidogenic pathway, thus the belonging strategies aim to reduce A $\beta$  production by the development of compound inhibitors.  $\alpha$ -secretase competes with BACE1 for the APP, leading to the non-amyloidogenic pathway, so the pursued approach in this case could be the stimulation of  $\alpha$ -secretase pathway, that can preclude the production of A $\beta$  by cleaving the peptide in two<sup>75</sup>.

$\gamma$ -secretase complex is composed of four different integral membrane proteins: presenilin (PSeN), nicastrin (NCSTN), alhaphrotein 1A (APH-1A) and presenilin enhancer 2 (PeN2), each of which could represent a possible target.  $\gamma$ -secretase is responsible for the processing of more than 70 transmembrane proteins involved in normal cellular processes besides APP, including regulation of cell adhesion, migration, neurite outgrowth, synaptogenesis, calcium homeostasis, transport of membrane proteins, and cell signaling<sup>81, 82</sup>. Thus, the identification of a selective inhibitor acting only on APP substrate represents a pressing concern in the drug development process<sup>83</sup>. In fact, one of the reasons that slowed the development of  $\gamma$ -secretase inhibitors (GSIs) has been the resulting toxicity attributed to the inhibition of one substrate in particular: the Notch receptor. The inhibition

of its proteolytic processing by GSIs lead to the suppression of intestinal goblet cell differentiation and to immunosuppression<sup>84</sup>. Several GSIs have failed advanced-phase clinical trials in AD, presumably for their mechanism-based toxicities. In particular, Semagacestat (Eli Lilly & Co.) that demonstrated safety and tolerability from Phase II studies, thus reaching pivotal Phase III studies, has failed not only for lacking efficacy but also for having worsened some patients' symptoms such as cognition and the ability to perform activities of daily living<sup>85</sup>. With the aim to block A $\beta$ <sub>42</sub> production without suppressing Notch cleavage, a the second generation of  $\gamma$ -secretase inhibitors and modulators was developed, including some non-steroidal anti-inflammatory drugs (NSAIDs). Several epidemiological studies had shown a lower incidence of AD in patient populations that used NSAIDs for other conditions, suggesting that this evidence was due to the reduction of neurotoxic inflammation by decreasing of cyclooxygenase (COX) activities<sup>86</sup>. However, a series of *in vitro* and *in vivo* studies demonstrated that NSAIDs were able to modulate  $\gamma$ -secretase cleavage by reducing toxic A $\beta$ <sub>42</sub> and, at the same time, by increasing the production of smaller A $\beta$  isoforms, such as A $\beta$ <sub>38</sub>, less toxic and less prone to aggregation<sup>87, 88</sup> (Fig. 1.12).

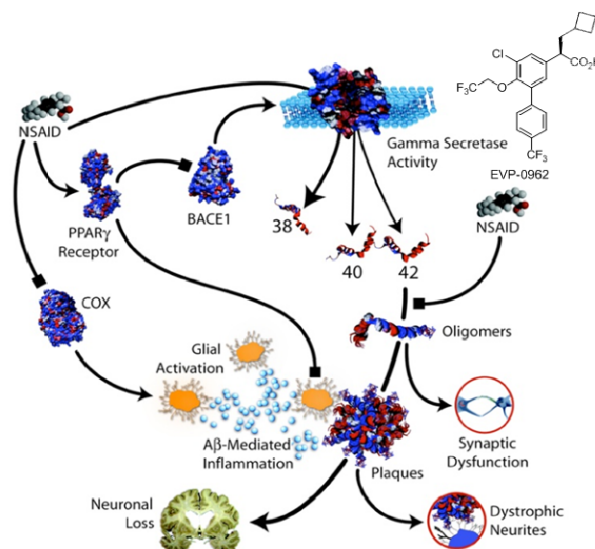


**Figure 1.12.** Potential protective mechanism of NSAIDs and EVP-0962 in AD<sup>89</sup>.

Besides targeting APP processing and A $\beta$  production and aggregation, a number of other mechanisms have been proposed to clarify the protective effects of NSAIDs in AD and the reduction of brain inflammation, all connected to their anti-inflammatory properties<sup>89</sup>: (i) the blockade of COX1-mediated inflammation in microglia that is associated with fibrillar A $\beta$  deposits and COX-

mediated synthesis of inflammatory prostaglandins<sup>90</sup>; (ii) stimulation of peroxisome proliferator-activated receptor- $\gamma$  (PPAR $\gamma$ ), a nuclear transcriptional regulator that inhibits the expression of pro-inflammatory genes<sup>91</sup>; (iii) reduction BACE1 gene transcription through overexpression of PPAR $\gamma$  and A $\beta$  secretion after stimulation of cell-lines with pro-inflammatory cytokines<sup>92</sup>. EVP-0962 is a potent, second generation  $\gamma$ -secretase modulator currently in a phase II trial (FORUM Pharmaceuticals, Inc.) for AD. It reduces the production of A $\beta_{42}$  specifically by modulating the APP cleavage toward the production of less toxic A $\beta_{38}$ , without affecting other  $\gamma$ -secretase substrates like Notch receptor<sup>83</sup> (Fig. 1.12).

The second main strategy to effectively block A $\beta$  production was targeting BACE1, because of its primary role in generation of A $\beta$ . BACE1 is a transmembrane aspartic protease of about 500 residues in length, with the active site located on the luminal side of the membrane, where APP cleavage occurs. The first generation of BACE1 peptidomimetic inhibitors was developed on the basis of the X-ray crystal structure of the enzyme<sup>93</sup>, resulting to be very effective and highly selective. Nevertheless, they failed because of low membrane permeability across the blood-brain barrier (BBB) and low oral bioavailability due to the required large molecular size to interact with the active site of the enzyme<sup>94</sup>. Thus, a new class of small molecules with the aim to easier penetrate BBB, albeit retaining a high affinity for BACE1, emerged. Among them, Eli Lilly's LY2886721, that initially showed reduction of A $\beta$  levels in plasma, was abandoned in 2013 because of liver toxicity<sup>95</sup>. However, some promising compounds showed satisfactory pharmacokinetics and provided encouraging clinical data in ongoing studies, and they are actually on Phase II/III trials (e.g. AZD3293, Eli Lilly & Co. and Astra Zeneca's)<sup>83</sup>.

Finally, the third strategy involving  $\alpha$ -secretase processing of APP can be considered a suitable treatment for AD, as it precludes A $\beta$  formation and reduce APP available for the amyloidogenic pathway<sup>96</sup>. Interestingly, several studies performed on current drugs in use for treatment of AD with different mechanism of action (e.g. Selegiline, a selective monamine oxidase inhibitor used to slow the progression of disease) showed an indirect  $\alpha$ -secretase activation by means of associated signaling cascades<sup>94, 97, 98</sup>. Thus, a wide number of indirect  $\alpha$ -secretase activators have reached clinical trials stage for AD. The most promising one is etazolate (EHT 0202), a selective GABA $_A$  receptor modulator, which has reached Phase II trials after demonstrating to stimulate sAPP $\alpha$  production, that is neurotrophic and precognitive, and protects against A $\beta$  induced toxicity in rat

cortical neurons<sup>99, 100</sup>. Another interesting compound currently in ongoing phase II/III trials is the polyphenol epigallocatechin-3-gallate (EGCG), that has been shown to stimulate  $\alpha$ -secretase via the protein kinase C pathway and reduce cerebral amyloid deposition in AD mice<sup>101, 102</sup>.

#### *Immunotherapy to enhance A $\beta$ clearance*

A $\beta$  content in the brain results from a balance between elevated production and decreased degradation, so it is comprehensible that, from a drug development perspective, enhancing A $\beta$  clearance could be a potential therapeutic strategy. Numerous enzymes called A $\beta$ -degrading proteases (A $\beta$ DPs), are involved in A $\beta$  degradation, including neprilysin, insulin-degrading enzyme and plasmin, and they can be functionally classified as endogenous (activated under physiological conditions) or pathogenic (activated under pathological conditions) regulators<sup>103</sup>. Thus, current treatments may aim at stimulating the expression of A $\beta$ DPs<sup>104</sup> or inhibiting the endogenous inhibitors that regulate A $\beta$ DPs<sup>105</sup>. However, in the last years the most extensively studied approach in A $\beta$ -targeted therapy, that led to the major contribution in terms of agents entered clinical trials, has become immunotherapy<sup>34</sup>. The systemic infusion of monoclonal antibodies (passive immunotherapy) directed at A $\beta$  has shown to directly prevent oligomerization and fibril formation<sup>106, 107</sup> and to dissolve A $\beta$  aggregates<sup>108</sup>, with high specificity and affinity toward the antigen. The model of antibody-mediated amyloid clearance mainly follows four possible mechanisms: (i) peripherally administered antibody reaches the CNS, binds to amyloid and triggers endogenous microglia to phagocytose the amyloid via Fc receptor-mediated clearance; (ii) antibody resolves amyloid deposits in the brain directly through interaction with aggregated A $\beta$  fibrils; (iii) amyloid-specific antibody acts as a peripheral sink for soluble A $\beta$  species, leading ultimately to the resolution of brain deposits by pulling soluble A $\beta$  into the periphery, where it is rapidly cleared; (iv) antibody rapidly binds to oligomeric A $\beta$  species, blocking their toxic effects without immediate impact on amyloid load. The choice of A $\beta$  antibody epitope (amino-terminal, mid-region, carboxy-terminal and conformational) is crucial, as affects the predominant mechanism of action and determines which A $\beta$  isoforms are cleared<sup>34</sup>. Notwithstanding the amino-terminus of A $\beta$  is the one accessible in both monomeric and aggregated species, antibodies that recognize this specific region have failed in clinical trials<sup>83</sup>. Bapineuzumab and gantenerumab, both directed against N-terminal epitope (the latter recognizes also mid-region) and targeted plaques, have failed in phase III trial for

AD, primary because clinical endpoints were not met. They were developed by building the antibody on an immunoglobulin G1 (IgG1) backbone, so they were considered “microglial clearance” antibody. A derivative of bapineuzumab, AAB-003, is currently in phase I trial and was engineered to reduce microglial activation. Roche and Genetec developed crenezumab by using an IgG4 backbone rather than an IgG1, thus reducing the overactivation of microglial cells and promoting microglial A $\beta$  phagocytosis in the brain<sup>109</sup>. Crenezumab, actually in phase III trial, has shown to recognize the mid-region epitope of A $\beta$ , which seems to be the main responsible for aggregation, and to identify preferentially oligomers, fibrils and plaques of A $\beta$  rather than monomeric forms<sup>83</sup>. Biogen’s aducanumab (phase III trial) is recently attracting attention for its ability to remove plaques and not just slowing further A $\beta$  accumulation<sup>110</sup>. Aducanumab is a human IgG1 monoclonal antibody obtained from healthy aged people who were supposed to develop antibodies against A $\beta$ . Aducanumab can selectively enter the brain by crossing BBB, reacts with soluble A $\beta$  oligomers and fibrils and reverse plaque deposition with slowing of cognitive decline, thereby emerging as an A $\beta$ -removing, disease-modifying therapy for AD<sup>111</sup>.

## 1.2 The re-examination of A $\beta$ -centric approach

In the pursuit of effective drugs for AD treatment it cannot be denied that A $\beta$ -modulating candidates are still holding a primary importance. According to the most recent analysis, 29 new drugs are in phase II/III clinical trial, and among them 15 are amyloid-related drugs<sup>112</sup>. Unfortunately, some of the most promising candidates have failed in late-phase studies.  $\gamma$ -Secretase inhibitors that decrease A $\beta$  production have failed in pivotal trials. Very recently, Merck announced that it will stop testing the BACE inhibitor verubecestat in people with mild to moderate AD, concluding that there was no chance to obtain a positive effect in the trial<sup>112</sup>. Despite the development of monoclonal antibodies against A $\beta$  is currently an encouraging issue in AD research, the top A $\beta$  drugs like bapineuzumab and solanezumab missed their primary end-point (Table 1.1)<sup>109</sup>.

Antibody name	Company	Status	Amyloid target
Bapineuzumab	Johnson & Johnson/ Pfizer	Failed phase III	Monomers, oligomers and plaques
Gantenerumab	Roche	Failed phase III, but trials ongoing*	Plaques
Solanezumab	Lilly	Failed phase III, but trials ongoing*	Soluble monomers
Aducanumab	Biogen	Phase III	Plaques and oligomers
Crenezumab	Genentech/ Roche	Phase III*	Oligomers
N3pG-A $\beta$	Lilly	Phase I	Plaques

**Table 1.1.** Selected A $\beta$ -targeted monoclonal antibodies. \*See text for details of ongoing prevention trials<sup>109</sup>.

Solanezumab, in phase III trial for patients with mild AD, was directed to soluble monomers of A $\beta$  but was not able to dismantle plaques already formed. It is for now in ongoing placebo-controlled trials of patient population with only the very earliest signs of cognitive decline or dominantly inherited AD with higher doses, as the antibody didn't show any safety flags in phase III trial. Bapineuzumab and gantenerumab both target plaques, but they have failed phase III probably due to the incidence of amyloid-related imaging abnormalities-edema (ARIA-E, defects characterized by evidence of brain-fluid accumulation in magnetic resonance imaging scans) that cut the antibody

doses. Gantenerumab is currently being assessed in a smaller trial of patients with autosomal dominant AD mutations<sup>109</sup>.

Growing amount of data, including a number of failed clinical trials, suggests that A $\beta$ -centered model is inadequate to target and treat AD in a satisfy manner, so that no new drug for the disease has been approved in the past 14 years. The extreme complexity of plaque production and assembly as well as the intertwined correlation of A $\beta$  with other crucial toxic partners of the pathogenic cascade suggests the linear structure of the amyloid hypothesis to be possibly too simplistic, calling for a deeper understanding of A $\beta$  role and its pathological mechanisms of action<sup>76, 113</sup>.

### **1.2.1 A $\beta$ and oxidative stress: a toxic vicious cycle**

Despite the extensive research made in recent years on the etiology and progression of AD, so far direct A $\beta$ -induced neurotoxicity has been difficult to be identified in animal models, suggesting the existence of key intermediates between amyloidosis and neurodegeneration<sup>114, 115</sup>.

Growing evidences highlight that A $\beta$  toxicity mechanism involves oxidative stress induction by increasing ROS production into the mitochondria<sup>116</sup>. Not surprisingly, as mitochondrial abnormalities, initially caused by gradual oxidative disturbances, are the major contributors of ROS to the cell. In this pathological conditions, the damaged mitochondria increase the release of ROS by decreasing efficiency, and contribute to other changes, including the oxidation of proteins and lipids and BACE1 up-regulation<sup>117, 118</sup>. The interaction between A $\beta$  oligomers, considered the highly toxic form<sup>119</sup>, and redox-active metals such as Fe<sup>2+</sup> and Cu<sup>+</sup> has been proposed as source of oxidative stress in AD, leading to generation of H<sub>2</sub>O<sub>2</sub><sup>120</sup>. The consequent peroxidative attack on membrane lipids yields to 4-HNE production with subsequent oxidative damage to membrane-bound and cytosolic and mitochondrial Ca<sup>2+</sup> overload. Cellular A $\beta$  directly attacks electron transport complex IV (cytochrome *c* oxidase) and key Krebs-cycle enzymes ( $\alpha$ -ketoglutarate and pyruvate dehydrogenase) and damages mitochondrial DNA (mtDNA). As a consequence, excessive amounts of ROS and RNS are generated at mitochondrial complex I and III, resulting in impairment of the electron transport chain, decreased production of ATP and caspase activation<sup>120, 121</sup> (Fig. 1.13).

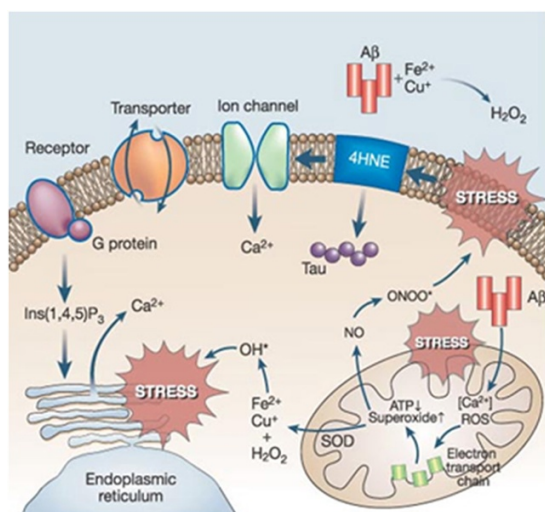


**Figure 1.13.** The neurotoxic action of A $\beta$  involving ROS and mitochondrial failure<sup>120</sup>.

Several studies reported that A $\beta$  induces lipid peroxidation of membranes and can directly react with 4-HNE. The increased toxicity associated with A $\beta$  oligomers may be attributable to its ability to reside in the lipid bilayer, where lipid peroxidation can occur. Indeed, the additions of A $\beta$  to neurons directly lead to formation of 4-HNE. This process exacerbates the formation of toxic A $\beta$  oligomers and insoluble aggregates, which, in turn, enhanced oxidative stress and formation of lipid peroxidation products, such as 4-HNE<sup>122</sup>. 4-HNE modifies the three histidyl residues of A $\beta$  leading to 4-HNE-modified A $\beta$  molecules with increased affinities for membrane lipids by adopting a similar conformation as mature amyloid fibrils<sup>123</sup>. It is known that A $\beta$  mediates impairment of glucose transport, with consequent decrease in cellular ATP levels. It has been suggested that this mechanism involves conjugation with 4-HNE to the neuronal glucose transport protein GLUT3, thus linking lipid peroxidation with adverse action of A $\beta$ <sup>124</sup>. One of the first research study conducted *in vitro* about the interaction between A $\beta$  and 4-HNE showed that 4-HNE modification of A $\beta$  results in a selective and efficient inhibition of degradation of oxidized proteins by 20S proteasome, leading to accumulation of oxidized substrates in neurons and consequently cell toxicity<sup>125</sup>. Indeed, 4-HNE enhances  $\gamma$ -secretase and BACE-1 activity and the overexpression of the latter, with significant increase of A $\beta$  production in neurons, establishing a direct relationship between oxidative stress and the amyloidogenic process of APP<sup>126</sup>.

All these findings clearly suggest that A $\beta$ -mediated cell toxicity may occur through oxidative stress, making A $\beta$  as a sort of prime initiator of damage induced by oxidative stress. One explanation for the easy oxidation of A $\beta$  could be the presence of methionine (Met) at residue 35 of A $\beta_{42}$ , which is particularly important for its oxidative role<sup>127</sup>. Met is an easily oxidizable amino acid that can undergo one or two-electron oxidation to form sulfuranyl radical cation or methionine sulfoxide, respectively. The proposed mechanism for A $\beta$ -induced oxidative stress and neurotoxicity by *Butterfield et al.* was based on the one-electron oxidation of Met-35 to form the sulfuranyl radical cation<sup>128</sup> (Fig. 1.14). Sulfur atom can be oxidized by superoxide radical anion, that in turn could reduce Cu<sup>2+</sup> to Cu<sup>+</sup> to produce damaging hydroxyl free radicals by Fenton reaction, or by Cu<sup>2+</sup> itself, that is shown to bind A $\beta$  with high affinity. The sulfuranyl radical cation, generated in the lipid bilayer because small oligomers of A $\beta$  come out from transmembrane APP protein, has the ability to abstract an allylic H-atom from the unsaturated acyl chains of lipid molecules, thereby leading to the initiation of lipid peroxidation processes. The resultant acid formed (pKa=5) can react with any base, for example, water, to lose proton and form reduced Met again<sup>128</sup>.

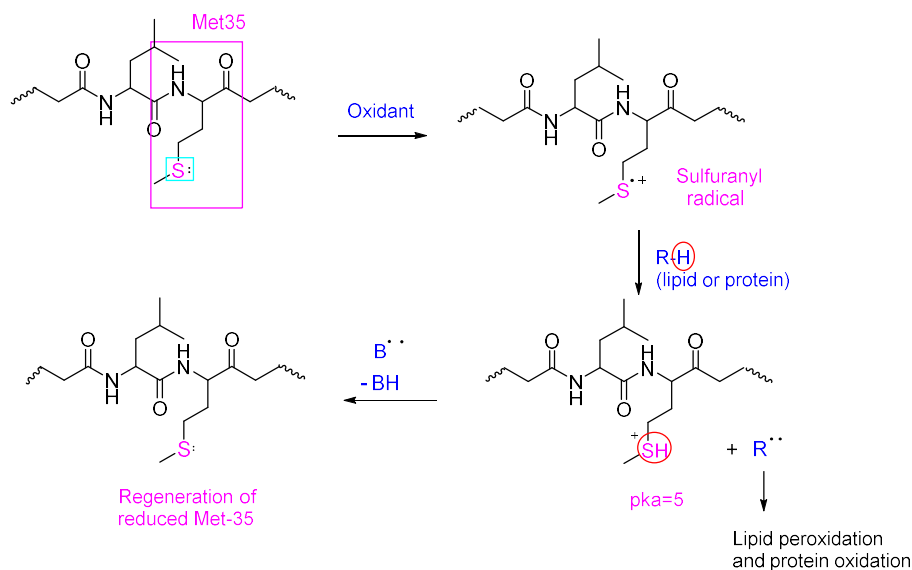


**Figure 1.14.** Methionine-35 residues in A $\beta$  can undergo one electron oxidation to form a sulfuranyl radical, which can then initiate the process of lipid peroxidation<sup>128</sup>.

This model of A $\beta_{42}$ -induced lipid peroxidation and subsequent oxidative damage to proteins is consistent with the results of *in vitro* and *in vivo* studies which showed that, by replacement of

Met35 with methylene moiety or leucine, no increase of oxidative stress and neurotoxicity was observed, suggesting that the sulfur atom of Met is key to the A $\beta$ <sub>42</sub>-mediated free radical formation<sup>128</sup>.

In addition to one-electron oxidation, the sulfur atom of Met35 of A $\beta$ <sub>42</sub> can undergo a two-electron oxidation leading to the formation of methionine sulfoxide (Met35SOx). Reversible oxidation of Met to protein-bound MetSOx is catalyzed by the enzyme methionine sulfoxide reductase A (MsrA), that serves as regulatory function and in cellular defense. The reversible oxidation-reduction cycle of Met involving MsrA may also act as general antioxidant mechanism, and a decrease in its activity has been implicated in AD<sup>129</sup>. It has been demonstrated that MsrA activity and mRNA levels increase in rat neuroblastoma cells when treated with A $\beta$ <sub>42</sub> modified with oxidized Met35, contrarily to that shown by the reduced peptide. The increased MsrA function and expression is associated with consequent reduced ROS generation, thus directly linking the redox state of Met35 to A $\beta$ <sub>42</sub> neurotoxic actions<sup>130</sup>. Moreover, the oxidation of Met35 to Met35SOx has been identified as potential modulator of A $\beta$  aggregation. Met35SOx is able to reduce  $\beta$ -strand content of the C-terminal hydrophobic region, that is believed to be necessary for aggregation, with a subsequent effect on the secondary structure of A $\beta$ , making the peptide potentially less prone to aggregation<sup>131</sup>. Additional NMR studies have shown that oxidation impedes A $\beta$  aggregation and fibrillation, thus suggesting a reduced propensity for  $\beta$ -strand structure in A $\beta$ <sup>132</sup>.

### ***Nrf2-ARE pathway in AD***

The Nrf2-antioxidant response element (ARE) transcriptional pathway is a primary sensor and the major mechanism of defense in the cell against oxidative or electrophilic stress via its ability to modulate the expression of cytoprotective genes, which include heme-oxygenase 1 (HO-1), glutathione *S*-transferase (GST) and NAD(P)H:quinone reductase (NQO1)<sup>133</sup>. Nrf2 activity is regulated by the cysteine-rich Kelch-like ECH-associated protein 1 (Keap1), a negative regulator protein that, under normal conditions, retains Nrf2 in the cytoplasm. When exposed to ROS or electrophiles<sup>134</sup>, the Nrf2 signaling pathway is activated: Keap1 is covalently modified at specific cysteine residues, resulting in a conformational change of the protein. This event dissociates Nrf2 from cytosolic Keap1 and promotes its nuclear translocation. Here, Nrf2 binds to ARE in the

promoter region of phase II genes to enhance the expression of a multitude of antioxidant and phase II enzymes that restore redox homeostasis (Fig. 1.15).

Keap1 plays a critical role in the maintenance of the cellular redox balance, as its conserved cysteine residues are responsible for the molecular switch triggered by intracellular redox changes that leads Nrf2 to translocate and activate gene transcription<sup>135</sup>. All the free radical scavenging enzymes represent a powerful antioxidant defense mechanism. For example, catalase, glutathione peroxidases and peroxiredoxins, are responsible, among other functions, for detoxification of H<sub>2</sub>O<sub>2</sub><sup>135</sup>. Inducible HO-1 and constitutive HO-2 protect brain cells from oxidative stress by degrading toxic heme into the antioxidants biliverdin, free iron and carbon monoxide. NQO1, mainly expressed in astrocytes and brain endothelial cells, catalyzes the obligatory 2-electron reduction of various broad array of exogenous and endogenous quinones to their corresponding hydroquinones by using either NADPH or NADH as the hydride donor, thus protecting against free radical toxicity<sup>136</sup>.

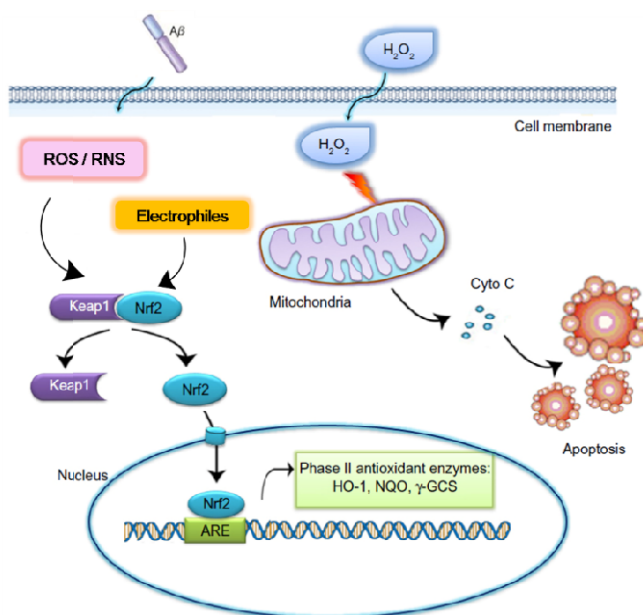


**Figure 1.15.** Nrf2 activation consequently to Aβ-mediated oxidative insult or electrophiles exposure. *Adapted from Ye, et al.*<sup>137</sup>

Given the involvement of oxidative stress in AD and its intertwined connection with Aβ, that in turn exacerbates oxidative damage, particular attention should be paid to the modulation of Nrf2 signaling, that represents a pivotal regulator of endogenous defense systems. In AD brain tissue, where chronic oxidative stress occurs, Nrf2 expression levels, as determined by immunoblotting, are

significantly decreased, becoming unresponsive to ROS insult. Moreover, Nrf2 is not a prevalent component of A $\beta$  or NFTs, suggesting that, despite the presence of oxidative stress, Nrf2-mediated transcription is not induced in AD neurons<sup>138</sup>.

Consequently, several experiments have shown that activation of Nrf2 pathway is beneficial in facing AD, on both pathological and symptomatic levels. Furthermore, recent studies have demonstrated a protection from A $\beta$ -induced neurotoxicity and attenuation of A $\beta$ -induced oxidative cell death through the activation of the Nrf2 signaling, thus establishing a relationship between A $\beta$ , oxidative stress and Nrf2. In NT2N neurons, a cell line model used for AD, oxidative stress can be inhibited in the presence of tert-butylhydroquinone (tBHQ), a known inducer of Nrf2. In addition, tBHQ showed to inhibit the formation of A $\beta$  plaques in response to H<sub>2</sub>O<sub>2</sub>/FeSO<sub>4</sub> and 4-HNE in the same cell line, increasing cell viability. This was the first report to suggest a neuroprotective effect of Nrf2 through suppression of A $\beta$  formation<sup>139</sup>.

Sulforaphane, another Nrf2 activator able to up-regulate expression of antioxidant enzymes such as NQO1 and HO-1, has demonstrated to protect the brain from A $\beta$ -induced toxicity in human neuroblastoma SH-SY5Y cells. Through the inhibition of ROS production due to the augmentation of antioxidant defenses, sulforaphane has shown to suppress A $\beta$ <sub>25-35</sub>-induced oxidative damage and cell death<sup>140</sup>. Very recently, sulforaphane also exhibited a reduction of A $\beta$ <sub>42</sub>-induced neuroinflammation in human THP-1 microglia-like cells<sup>141</sup>.

Pinocembrin, the natural flavonoid richly present in propolis, has been proven to exert neuroprotective effects against A $\beta$ -induced neurotoxicity through increase in Nrf2 protein levels and consequent induction of HO-1 expression<sup>142</sup>.

Several studies suggest that Nrf2 could mediate autophagy and alter processing/clearance of APP and/or A $\beta$ . Genetic deletion of Nrf2 in APP/PS1 transgenic mice (an AD model carrying overexpressing human APP and PSEN1) showed increased chronic inflammation and accumulation of insoluble APP fragments and A $\beta$ , as well as augmentation of multivesicular bodies, endosomes and lysosomes, leading to incomplete autophagic flux<sup>143</sup>. Hydrogen sulfide (H<sub>2</sub>S), recognized as endogenous cytoprotectant produced in the brain, improved learning and spatial memory deficits and reduce senile plaques and neuron loss in APP/PS1 transgenic mice through a protective mechanism that may be mediated by its activation of Nrf2-ARE signaling pathway<sup>144</sup>.

### 1.2.2 A $\beta$ role in p53-induced neuronal death

p53 is a tumor-suppressor protein and a transcription factor mainly involved in cancer, the primary function of which is to regulate several genes implicated in cell cycle control and apoptotic pathways<sup>145</sup>. Apoptosis exacerbation is a characteristic of aging and neurodegenerative disorders, therefore growing interest has been shown in the last decades towards the role and involvement of p53 in AD<sup>146</sup>.

In the CNS, p53 plays a pivotal role as activator of programmed cell-death signaling for newly born postmitotic neurons that are not appropriately differentiated. Besides that, p53 activation after chronic insult, oxidative stress or DNA damage also results in the induction of apoptosis or initiation of senescence<sup>147</sup>. Cell death by apoptosis occurs in a wide range of neurons in AD brain, and apoptotic neurons are often associated with increased levels of intracellular A $\beta$ <sup>148</sup>. In addition, several studies have shown that p53 expression is elevated in AD brain. It has been demonstrated that intracellular A $\beta$ <sub>42</sub> directly activates the transactivation of p53 promoter, resulting in p53-dependent neuronal apoptosis. Oxidative DNA damage owing to H<sub>2</sub>O<sub>2</sub> treatment triggers A $\beta$ <sub>42</sub> translocation into the nucleus and increasing p53 mRNA expression. Moreover, accumulation of A $\beta$ <sub>42</sub> and p53 was found in ill-shape neurons in both transgenic mice and human AD cases, thus linking intracellular A $\beta$ <sub>42</sub>/p53 pathway to neuronal loss<sup>149</sup>.

Another reasonable connection between p53 and neuronal aging may be its role on redox modulation. Following high stress levels, p53 is activated and accumulates to push further the cell oxidative balance toward a pro-oxidant state. In this condition, p53 induces pro-oxidant genes expression, thus increasing ROS production, and, at the same time, directly represses antioxidant genes (e.g. SOD2, GST, NQO1), facilitating apoptosis and influencing the aging process<sup>147</sup>. Furthermore, oxidative imbalance, resulting in a chronic exposure to ROS, can induce conformational changes in p53 tertiary structure, leading to the nonfunctional unfolded form of p53<sup>150</sup>. Unfolded p53 results in altered DNA binding properties and impairment of its transcriptional activity<sup>151</sup>. Several evidences confirm that conformational changes and functional alterations of p53 have been found in fibroblasts of patients with AD<sup>151-153</sup>.

Interestingly, besides oxidative stress, soluble nanomolar concentrations of A $\beta$  have been shown to alter protein conformational state of p53 by interfering with the homeodomain-interacting protein kinase 2 (HIPK2)<sup>154</sup> (Fig. 1.16).

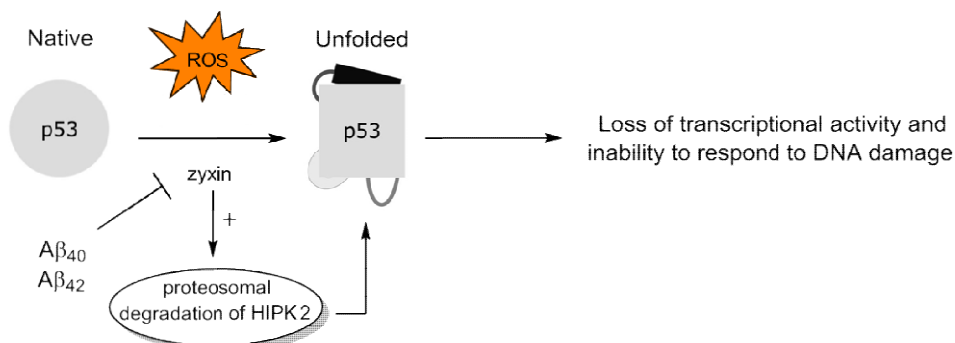


**Figure 1.16.** Loss of transcriptional activity of p53 mediated by its conformationally altered status. Chronic exposure to ROS and/or A $\beta_{40}$  or A $\beta_{42}$  can induce a switch toward the nonfunctional unfolded form of p53. Sublethal concentrations of A $\beta_{40}$  or A $\beta_{42}$  induce zyxin deregulation with further inhibition of HIPK2 expression and activity through degradation via the proteasome system. As a consequence, p53 changes the wild-type conformation with subsequent abolishment of transcriptional activity.

HIPK2, a co-repressor for several transcription factors, is responsible for p53 activation after exposure to genotoxic agents. In the absence of HIPK2, p53 loses its native conformation and DNA binding properties, by means of a process involving metallothionein 2A (MT2A) and Zn<sup>2+</sup>. It has been hypothesized that A $\beta$  is able to cause HIPK2 proteasomal degradation with consequent nuclear disappearance<sup>154</sup>. HIPK2 deregulation in turn results in the induction of MT2A that exerts its Zn<sup>2+</sup> chelator function leading to p53 misfolding. As a consequence, abolishment of wild type p53 DNA binding and transcriptional activity occurs<sup>154</sup>.

The ability of A $\beta$  to interfere with HIPK2 knockout is due to its interaction with zyxin<sup>155</sup>. Zyxin is an adaptor protein identified as a regulator of HIPK2-p53 signaling in response to DNA-damage, fundamental in maintaining HIPK2 stability and in turn p53 activity. Sublethal concentrations of intracellular A $\beta_{40}$  and A $\beta_{42}$  down-regulate zyxin protein levels, leading to HIPK2 degradation and p53 misfolding via MT2A up-regulation. As a result of this conformational change, p53 loses its transcriptional activity and becomes unable to respond to DNA damage<sup>155</sup>.

Thus, this A $\beta$ -mediated downregulation could be considered as a peripheral and early signature of AD that precedes the amyloidogenic pathway in the neurodegenerative cascade.

### 1.2.3 A $\beta$ -mediated excitotoxicity

As the neurotoxicity induced by A $\beta$  is, among other factors, related to the impairment of neuronal functions and synaptic plasticity, the interconnection between the toxic peptide and the glutamate system, in particular NMDARs, has to be investigated.

As mentioned before, excitotoxicity occurs when uncontrolled glutamate release overcomes the capacity of astrocyte to exert clearance mechanisms or the ability of one of five excitatory amino-acid transporters (EAATs) to uptake glutamate. The tripartite synapse is the main site where glutamatergic neurotransmission occurs, and it is composed by a presynaptic terminal, a postsynaptic spine and an astrocytic process<sup>156</sup>. During AD, these components that regulate extracellular glutamate levels become dysregulated, with consequences for extracellular NMDARs activation. In short, glutamate can be synthesized from glucose through the Krebs cycle or by glutamate-glutamine cycle in astrocytes. In the latter case, it is then transferred back to neurons where it is packaged presynaptically into synaptic vesicles by vesicular glutamate transporters (VGLUTs), and following presynaptic neuronal depolarization, released in the synaptic cleft. Here, it can activate ionotropic (including NMDARs) and metabotropic (mGluR1-8) receptors. Astrocytes may respond to neuronal activity through an elevation of internal Ca<sup>2+</sup> concentration, which further leads to the release of neurotransmitters able to cause feedback regulation of neuronal activity and synaptic efficacy. Glutamate is then cleared from the extracellular space via EAAT1/2 by astrocytes and *via* EAAT2/5 by the presynaptic terminal and then stored into vesicles.

NMDARs mediate the majority of excitatory neurotransmission and synaptic plasticity. While activation of synaptic NMDARs mediates neuronal survival through anti-apoptotic and antioxidant effect, activation of extrasynaptic NMDARs is associated with neurotoxicity and cell death<sup>157, 158</sup>.

In this context, A $\beta$ , in particular soluble oligomers, can severely affect the glutamatergic transmission and induce excitotoxicity through several mechanisms, including stimulation of glutamate release, inhibition of glutamate uptake, and alteration of receptors' activity<sup>156</sup> (Fig. 1.17). In pathological conditions, A $\beta$ <sub>42</sub> is able to stimulate astrocytic  $\alpha$ 7-nAChR resulting in increased Ca<sup>2+</sup> concentration and glutamate release, followed by activation of extracellular NMDARs and downstream toxicity<sup>159</sup>. Both oligomers and fibrils of A $\beta$  can directly bind with high affinity to  $\alpha$ 7-nAChR at presynaptic level, involved in the regulation of synaptic plasticity and responsible for the release of a variety of neurotransmitters (both excitatory and inhibitory) to the brain<sup>160</sup>. This

interaction leads to the formation of complexes that would alter glutamatergic transmission with consequent further degeneration<sup>45</sup>. Pathologically elevated levels of A $\beta$  are able to inhibit glutamate reuptake by interfering with astrocytes and reversing glutamate transporters at the synaptic cleft. These events result in increased extracellular glutamate concentration with subsequent desensitization of NMDARs and ultimately synaptic depression<sup>45, 156</sup>.

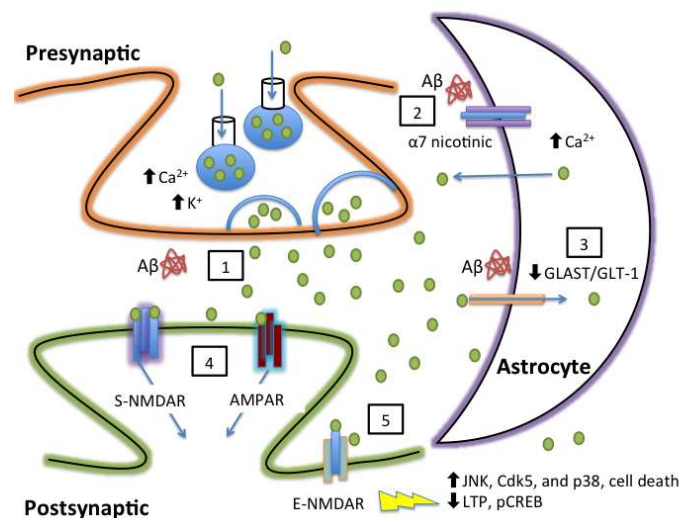


**Figure 1.17.** A $\beta$ -mediated increases in extracellular glutamate and the resulting excitotoxicity. (1) A $\beta$  increases presynaptic release of glutamate. (2) A $\beta$  elevates astrocytic calcium via stimulation of astrocytic  $\alpha 7$  nicotinic receptors, resulting in astrocytic glutamate release via an unknown mechanism. (3) A $\beta$  decreases glutamate clearance from the synapse, thereby prolonging the duration of glutamate in the synapse and potentially resulting in the spread of glutamate to neighboring synapses. (4) Prolonged activation of synaptic-NMDARs and AMPARs resulting from increased extracellular glutamate is predicted to cause desensitization and internalization of NMDA/AMPA, resulting in synaptic depression. (5) Glutamate spillover activates extracellular-NMDARs, resulting in multiple deleterious downstream events, including an increase in tau kinase activity, cell death, and blockade of long-term potentiation<sup>156</sup>.

A possible mechanism for the inhibition of glutamate transporters could be the A $\beta$ -induced increase of 4-HNE through lipid peroxidation, that in turn covalently modifies the glutamate transporters resulting in inhibition of glutamate uptake. It has been reported that A $\beta_{42}$  itself is able to increment 4-HNE conjugation to the glutamate transporters<sup>161</sup>. A $\beta_{42}$  oligomers have also been shown to induce overexpression of the activity-regulated cytoskeletal (Arc) gene (critical for memory consolidation), leading to loss of surface NMDARs and altered cell morphology with expected plasticity failure and memory dysfunction<sup>162</sup>. Several evidences support the specific effect of A $\beta$  on NMDARs. A $\beta$  may directly affect NMDARs function by partially relieving the voltage-dependent Mg<sup>2+</sup> block of

NMDARs, which allows the continuous entry of  $\text{Ca}^{2+}$  into neurons, thus altering the homeostasis and causing cell death<sup>163</sup>. The prolonged  $\text{Ca}^{2+}$  influx due to pathological activation of NMDARs could also lead in turn to intracellular generation of toxic  $\text{A}\beta$  oligomers, through a feedback mechanism that ultimately lead to exacerbate neurodegeneration<sup>163</sup>. In this regard, the strongest support for interactions between  $\text{A}\beta$ , glutamate and NMDARs in AD is provided by memantine. Numerous studies *in vitro* and *in vivo* demonstrated neuroprotective effects of memantine against  $\text{A}\beta_{42}$  toxicity and attenuation of its deleterious action. The vicious cycle of  $\text{A}\beta$  that activates NMDARs, which in turn increase its production, was blocked by memantine. Furthermore, memantine increases the levels of sAPP $\alpha$  likely by enhancing the  $\alpha$ -secretase (non-amyloidogenic) pathway<sup>163</sup> and has shown to decrease levels of secreted APP and lower  $\text{A}\beta_{42}$  secretion in neuroblastoma cells<sup>164</sup>. The effects of memantine on memory acquisition and spatial and non-spatial learning in APP/PS1 mutant mice have also been assessed, revealing the potential of this drug to provide symptomatic improvement in cognition and to reduce clinical worsening<sup>163</sup>.

### 1.3 Multitarget strategies in AD

Despite massive investments and research efforts, an effective drug for halting AD has yet to arrive, as current therapies offer only limited and temporary benefits to patients<sup>165</sup>. Therefore, drug research devotes to the discovery of small molecules able to modulate the biological function of a single protein target might be insufficient to counteract the multifaceted nature of AD. In light of this, the “one-molecule, one-target” paradigm has been challenged, and a more holistic approach has recently emerged<sup>166</sup>. This is the polypharmacological approach, that allows the modulation of several drug targets by overcoming the problems of drugs hitting only a single target<sup>167</sup>.

There are three possible approaches to polypharmacology<sup>11</sup>. First, when a single medicine is not sufficient to effectively treat a disease, it can be combined two or three different drugs with different therapeutic mechanism through a multiple-medication therapy (MMT, also termed as “cocktail” or “combination of drugs”). MMT has already proven successful in treatment of complex disease such as cancer, HIV infections and hypertension. In clinics, the coadministration of memantine (NMDARs antagonist) and AChEIs have provided evidence for enhanced therapeutic effects over AChEI monotherapy<sup>168</sup>. In this regard, the combination of memantine and galantamine has shown to enhance cognitive symptoms in animal models and improve neuroprotective effect of memantine<sup>169</sup>. However, this approach might be disadvantageous for patients with compliance problems. A second strategy might be the use of a combination of different therapeutic agents into the same formulation that act independently on different targets<sup>11</sup>. This is the so called multiple-compound medication (MCM, also referred to as “fixed-dose combination”), that is increasingly providing several marketing successes. To this end, Namzaric<sup>®</sup> (Actavis [USA] and Adamas Pharmaceuticals [USA]) (Fig. 1.18) is the controlled release formulation approved in December 2014 for the treatment of moderate to severe AD. It combines the AChEI donepezil with memantine in a once-daily fixed-dose combination product<sup>170</sup>. This strategy has the advantages to make dosing regimen simpler and thereby to improve patient compliance. However, combining several drugs in a single tablet exhibits the difficulty to deal with pharmacokinetic differences between the individual components. The drug-drug interactions, including competition for common metabolic pathways and chemical incompatibility, can lead to variability in drug exposure with consequent overdosing or undertreatment<sup>171</sup>.

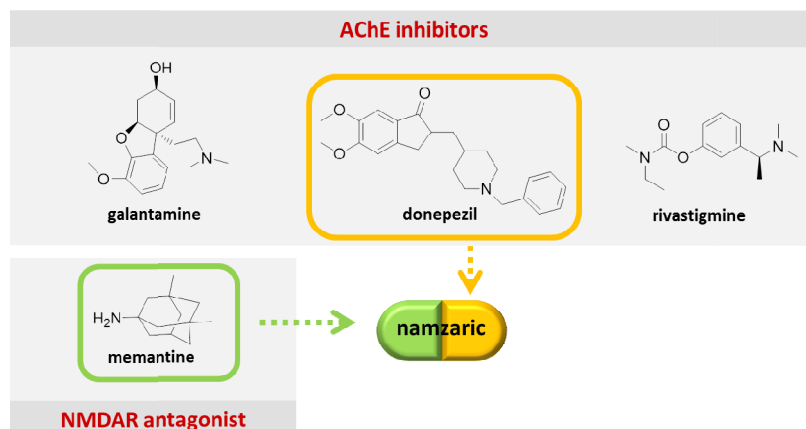


**Figure 1.18.** Current therapies for AD treatment. In the top frame, structures of the AChEIs galantamine, donepezil and rivastigmine. In the bottom frame, the structure of the NMDA antagonist memantine. Figure shows the combination of memantine and donepezil in the fixed-dose combination Namzanic<sup>®165</sup>.

In light of this, a third approach more recently emerged by shifting towards single compounds able to simultaneously hit multiple targets, termed “multi-target-directed ligands” (MTDLs). MTDLs would be effective in treating complex diseases because of their ability to interact with multiple points of a given pathogenic cascade thought to be responsible for the disease onset (Fig. 1.19). Clearly, therapy with a single drug that has different biological properties would have several advantages over MMT or MCM. Firstly, MTDLs might overcome the drawbacks owing to the different bioavailability, pharmacokinetics and metabolism of multiple single-drugs entities. Indeed, in terms of pharmacokinetic and absorption, distribution, metabolism, excretion and toxicity (ADMET) optimization, the clinical development of a single drug able to hit multiple targets should be simpler than an MMT/MCM approach. Furthermore, the risk of drug-drug interactions would be avoided and the therapeutic regimen greatly simplified<sup>11</sup>. However, despite the encouraging premises and the solid rationale, the design of MTDLs with predefined biological properties can be extremely challenging for medicinal chemists. The first critical point is the selection of biologically validated combinations of targets relevant to the disease, given the complexity of AD drug-target networks<sup>172</sup>. Further difficulties emerge in the hit identification and optimization processes to achieve multifunctional profiles. In this regard, several approaches have been suggested during the years to identify multitarget leads, for example *via* random screening against several targets.

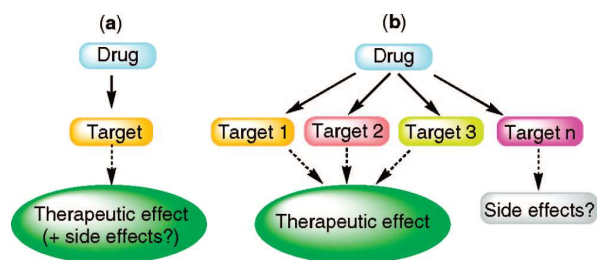


**Figure 1.19.** Pathways leading to the discovery of new medications: (a) Target-driven drug discovery approach, that is, the application of the current one-molecule-one-target paradigm. Although this approach has led to many effective drugs able to hit a single target, it is now well-documented that these drugs may represent the exception rather than the rule. (b) MTDLs approach to drug discovery. A drug, could recognize (in principle, with comparable affinities) different targets involved in the cascade of pathological events leading to a given disease. Thus, such a medication would be highly effective for treating multifactorial diseases. The design of such a drug may not be easy because it could also bind targets that are not involved with the disease and could be responsible (although not necessarily) for side effects. With MTDLs, the one-medication-one-disease paradigm finds a practical application<sup>11</sup>.

Virtual screening (pharmacophore-based) and computational docking (biostructure-based) have also been used to discover multitarget agents<sup>173</sup>. Besides these, the ligand-based approach is still the prevailing choice, which aim to combine two molecular fragments into a new single chemical entity. The incorporation of synergistic pharmacophores into a new dual-targeted molecule can be achieved with different strategies, leading to hybrid, fused or chimeric compounds. In lead optimization it has to deal with the main difficulty to balance multiple activities toward different target proteins, while keeping drug-like properties and controlling unintended off-target effects<sup>171</sup>.

Since 2005, literature has shown several promising results from applying MTDLs approach to drug design and development for neurodegenerative diseases. Indeed, several combinations of druggable targets have been proposed to achieve therapeutically acceptable pharmacological profiles. Among them, AChE arise as a crucial target for AD therapy. Three of the four drugs approved by the U.S. FDA for AD are AChEIs (Fig. 1.18). Indeed, one of the most widely adopted approaches to obtain novel MTDLs has been to modify the molecular structure of an AChEI in order to provide it with additional biological properties useful for treating AD<sup>11</sup>. New interest in this target emerges from the discovery of the AChE noncholinergic functions due to the presence of the peripheral anionic site (PAS), that is thought to be involved in the neurotoxic cascade of AD through AChE-induced A $\beta$  aggregation. Thus, dual-binding compounds able to simultaneously inhibit PAS may offer the possibility for turning AChEIs into potential disease-modifying agents<sup>174</sup>. Besides that, oxidative

stress, considered as a key event in AD onset and progression, recently emerged as capable of amplify the complexity of the disease, calling for antioxidant as beneficial therapeutic tools in AD treatment<sup>175</sup>. Furthermore, single molecules with antioxidant properties that can act at different levels in the neurodegenerative cascade, can exert additional neuroprotective effects against AD<sup>11, 166</sup>. The rational modification of AChEIs structures to provide them with antioxidant properties has led *Melchiorre et al.* to discover in 2005 the multifunctional bivalent ligand lipocrine (**1**)<sup>176</sup>. Compound **1** combines, in the same molecule, the structure of the natural antioxidant lipoic acid (LA) with the 6-chloro derivative of tacrine, the first AChEI approved for AD treatment (Fig. 1.20). Experimental evidence indicated that **1** could bind both catalytic and peripheral sites of AChE, thus acting as a mixed-type inhibitor. This bivalent interaction afforded one of the most potent AChEIs ever found ( $IC_{50} = 0.25$  nM), together with the ability to reduce AChE-induced A $\beta$  aggregation ( $IC_{50} = 45$   $\mu$ M). In addition, LA contributed to the multimodal profile of **1**, protecting human SH-SY5Y cells from ROS formation induced by oxidative stress (with **1** being more active than LA)<sup>175</sup>.

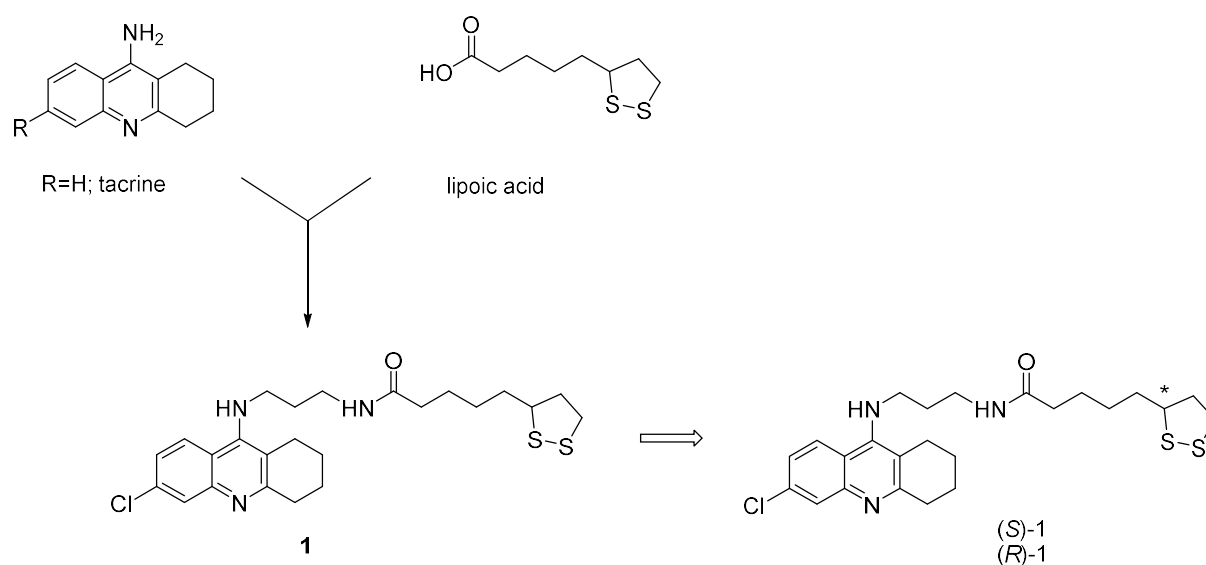


**Figure 1.20.** Design strategy of lipocrine (**1**) and its enantiomers merging the structures of tacrine and lipoic acid<sup>175</sup>.

In 2011, this study was expanded, exploiting the role of LA's stereochemistry<sup>177</sup>. In particular, it had been reported that stereochemistry is not significant for the protective effect of LA against oxidative cell damage<sup>178</sup>. However, to verify whether it could affect AChE inhibition, the two enantiomers of **1**, (*S*)-**1** and (*R*)-**1**, were synthesized and studied. Their inhibitory potencies were slightly different on AChE. Enantiomer (*R*)-**1** was only twice as potent as (*S*)-**1** ( $IC_{50} = 0.23$  nM and  $IC_{50} = 0.47$  nM,

respectively). The lack of a biologically significant difference between racemic **1** and the most active enantiomer (*R*)-**1** rationalized the design of new anticholinesterase LA adducts as racemic compounds. Compound **1** is currently marketed as a pharmacological tool for studying AD. Preliminary ADMET studies have investigated whether this lead compound could result in a suitable multifunctional drug for AD treatment<sup>175</sup>.

From 2005, other frameworks such as cystamine and ferulic acid (FA) with antioxidant properties have been exploited with the aim to enhance the pharmacological profile compared to the merely anticholinesterase activity<sup>179, 180</sup>. The resulting hybrid molecules **2** and **3** inhibited both catalytic activities of AChE and AChE-induced A $\beta$  aggregation and exerted antioxidant and/or neuroprotective activity by modulating A $\beta$  self-induced aggregation (Fig. 1.21).

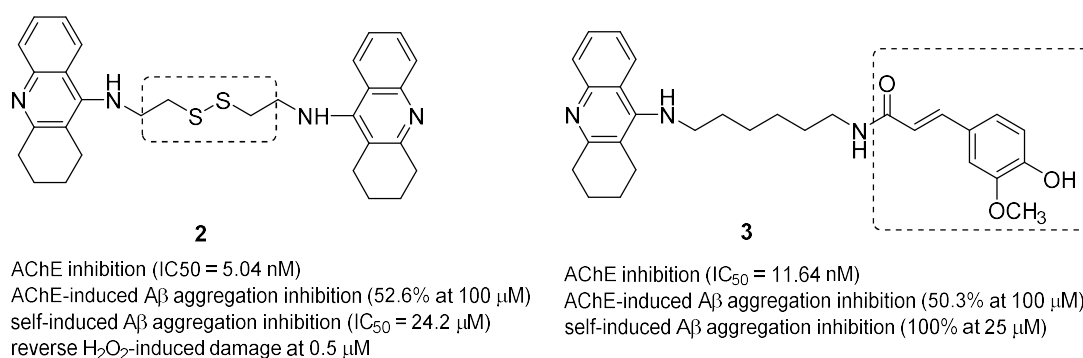


**Figure 1.21.** Structures of the multifunctional antioxidants **2** and **3**. Antioxidant features are highlighted with dashed boxes<sup>175</sup>.

Interestingly, the *in vitro* and *in vivo* studies of FA-tacrine adduct **3** clearly highlighted the well-established and existing correlation between oxidative stress and A $\beta$  processing and deposition. In fact, compound **3** has shown to prevent cell death and reduce intracellular ROS accumulation induced by A $\beta$ <sub>40</sub> in PC12 cells. It also improved the impairment of learning and memory on AD mice model. Moreover, it significantly increased choline acetyltransferase activity and reduced AChE efficacy after intracerebroventricular injection of A $\beta$ <sub>40</sub>, thus potentiating the cholinergic system<sup>180</sup>. In order to investigate molecular mechanisms underpinning its neuroprotective effects, **3** was also assayed in HT22 cells, proving to be able to protect against glutamate-induced cell injury and to activate Nrf2/ARE pathway by up-regulating the expression of HO-1<sup>181</sup>.

On the strength of these results, recently new hybrids combining hydroxycinnamic acids (including ferulic and caffeic acid) with cholinesterase inhibitory moieties emerged. In particular, caffeic acid (CA), with antioxidant and anti-aggregating profile, has been conjugated by means of a linker with rivastigmine, a marketed AChEI able to inhibit both AChE and BChE. The CA-rivastigmine adduct **4** emerged as the most interesting compound of the series, with an intriguing multifunctional profile (Fig. 1.22)<sup>182</sup>.

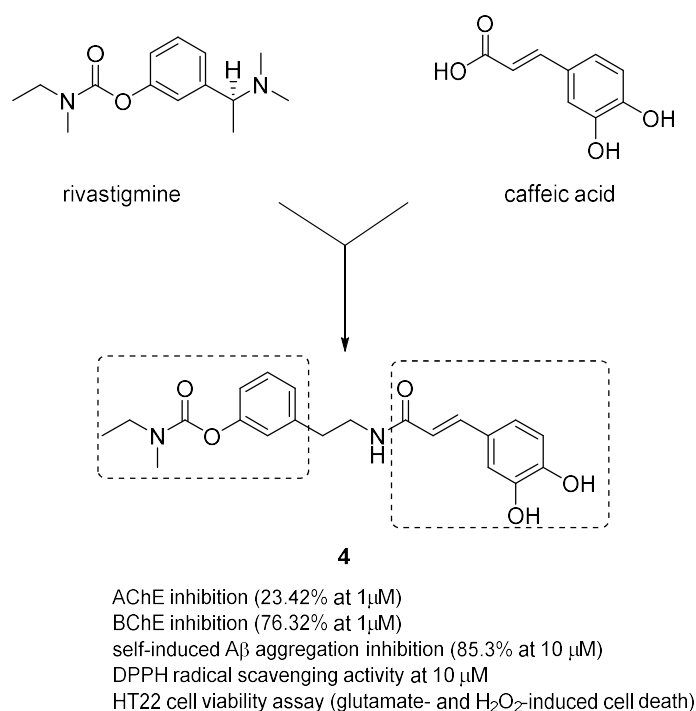


**Figure 1.22.** Design strategy for compound **4**.

It has been demonstrated that **4** is able to inhibit both AChE and BChE activities stronger than rivastigmine and to prevent A $\beta$  self-aggregation in a thioflavin-T (ThT)-based fluorometric assay. Moreover, it has shown to protect HT22 cells from glutamate- and H<sub>2</sub>O<sub>2</sub>-induced cell death and to scavenge free radicals in a more effective way compared to rivastigmine-FA hybrids. Finally, **4** also exerted copper-chelating properties probably due to its phenolic moiety, thus leading to inhibit Cu<sup>2+</sup>-induce A $\beta$  aggregation and oxidative stress<sup>182</sup>.

Altogether these findings clearly point out that endowing anticholinesterase agents with antioxidant ability could be a useful strategy for improving efficacy and expanding the therapeutic profile. Besides that, a combination of drugs affecting the cholinergic and glutamatergic system is becoming

more relevant in the last years. The rationale of designing MTDLs combining anticholinesterase activity with NMDAR antagonism is validated by the numerous evidence that in AD progression the impairment of cholinergic transmission goes hand-in-hand with glutamatergic synaptic loss and excitotoxic neuronal cell injury. As mentioned above, these two neurotransmitter systems influence each other, and has been demonstrated to be correlated with other primary insults typical of AD, i.e. A $\beta$ -induce toxicity<sup>45</sup>. Consequently, acting on these two pathological features of AD could lead to a synergistic or additive therapeutic goal<sup>183</sup>. In 2012, it was reported that subactive doses of memantine and galantamine afforded a significant cognitive enhancement in animal models, again supporting drug combinations as effective treatments of memory impairment<sup>184</sup>. This potential synergistic effect gave the rationale for developing a new class of MTDLs by chemically joining the structures of the two marketed drugs with the interposition of different spacers<sup>185</sup> (Fig. 1.23).

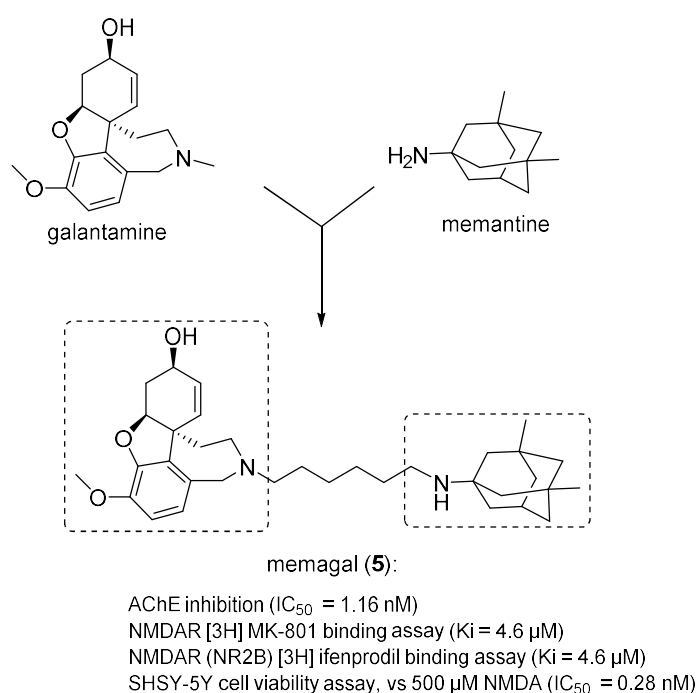


**Figure 1.23.** Design strategy of memagal (**5**) and its activity profile<sup>165</sup>.

Memagal (**5**) carrying an hexamethylene spacer, was the most promising hit of the series. With its optimal chain length, compound **5** showed a nanomolar AChE inhibitory activity along with an efficient binding affinity for both MK-801 and ifenprodil-binding sites of NMDAR. The *in vitro* profile was also strengthened by a prominent neuroprotective effect against NMDA-induced neurotoxicity in neuroblastoma cells<sup>185</sup>. Despite some open questions, compound **5** represents a

synergistic combination of two marketed drugs working together on the same excitotoxic cascade in a new single chemical entity, which offered the opportunity for studying the simultaneous modulation of cholinergic and glutamatergic systems in AD<sup>165</sup>.

In the pursuit of concomitant AChE and NMDAR inhibition, the withdrawn antihistamine drug dimebon attracted considerable interest because of the encouraging results obtained in clinical trials in terms of enhancing cognition in patients with mild to moderate AD<sup>186</sup>. Although its mechanism of action seemed to be centered on AChE inhibition and NMDAR antagonism, further ambiguous results in clinical studies gave much uncertainty about the real mechanism by which dimebon may benefit AD<sup>187</sup>. This contradictory story has been interpreted as the starting point to pursue a multitarget drug design approach and to gain balanced multitarget profile against the two targets. In particular, based on computational studies, the  $\gamma$ -carboline moiety of dimebon was selected as the key recognition fragment for AChE inhibition to be exploited in the search of an amplified drug activity profile. In 2013, a bivalent ligand approach led to a dimebon congener (**6**) with a markedly improved *in vitro* activities with respect to the parent compound<sup>188</sup> (Fig. 1.24). A significant increase of AChE inhibitory activity was reported for compound **6**, that was 454-fold more potent than the prototype. Additionally, the molecular duplication, while having no detrimental impact on molecular recognition at NMDAR, allowed to obtain an effective inhibitor activity against *in vitro* amyloid aggregation compared to the ineffective  $\gamma$ -carboline-containing monomer dimebon<sup>183</sup>.

More recently, hybrids combining the  $\gamma$ -carboline and the phenothiazine core of methylene blue were reported<sup>189</sup>. The new conjugates displayed micromolar to submicromolar inhibitory activity toward cholinesterase, with a marked selectivity against BChE over AChE. As for NMDA receptors, studies of the compounds binding to MK-801 and ifenprodil-binding sites revealed that conjugates **7** and **8**, carrying a 1-oxopropylene spacer, had improved affinity towards both NMDA-receptor binding sites compared to dimebon<sup>189</sup> (Fig. 1.24).

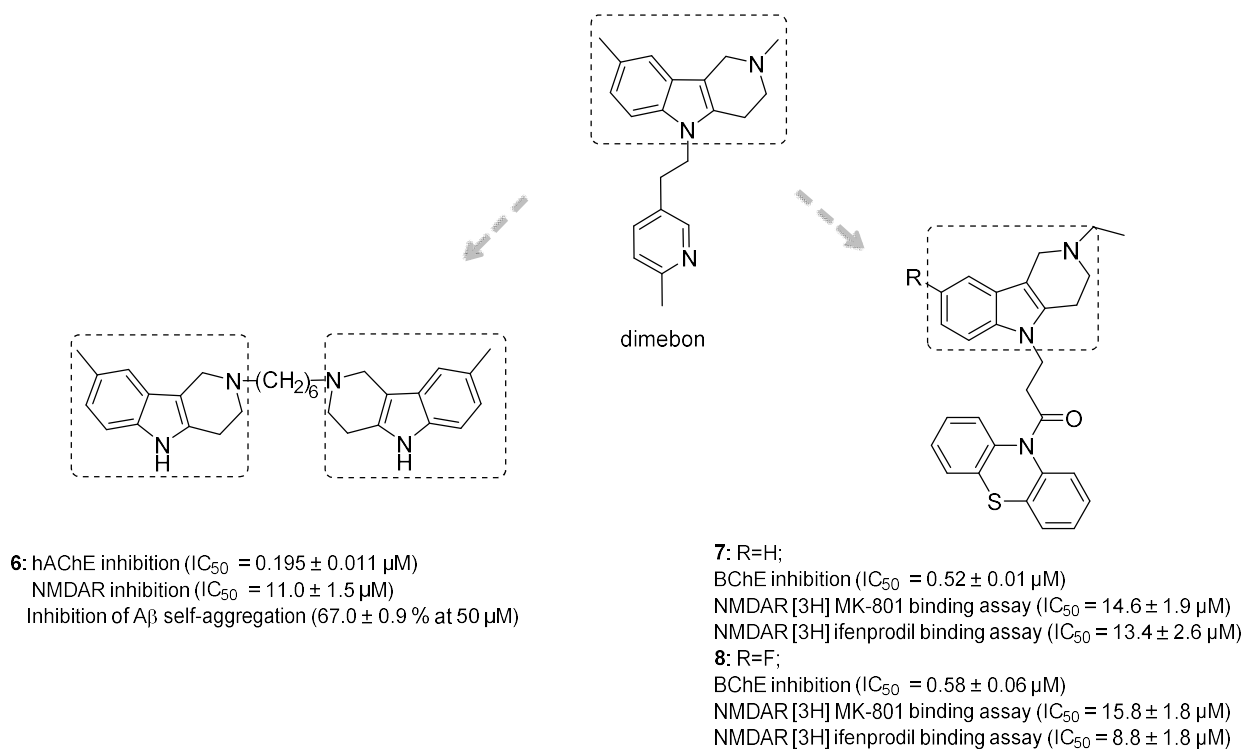


**Figure 1.24.** Design strategies and activity profiles of dimebon congeners **6-8** carrying a  $\gamma$ -carboline fragment<sup>165</sup>.

For several years, the amyloid cascade hypothesis for AD has represented the main issue underlying AD pathogenesis, according to which A $\beta$  misfolding and aggregation were the causative events leading to onset and progression of AD. However, the failure of purely anti-amyloid strategies has led to a critical rethink of A $\beta$ -centered model, especially concerning the relationship between the toxic peptide and other active players of the neurotoxic cascade<sup>165</sup>.

On this basis, the development of multifunctional anti-amyloid agents, that exert other biological properties in addition to the only anti-amyloidogenic one, could represent an added value for modulating the robust network of A $\beta$ -mediated events. In this context, the simultaneous modulation of hallmark proteins A $\beta$  and  $\tau$  has recently pursued in order to look into their complex interaction in AD pathogenesis<sup>165</sup>. In particular, a fragment-based approach was performed by merging the pharmacophoric features responsible for binding to BACE1 and GSK-3 $\beta$ , such as a guanidine function and a cyclic amide motif, respectively, into a single scaffold to obtain dual-inhibitors of A $\beta$  and  $\tau$  production. As a result, triazinone (**9**) was identified, which showed moderate and well-balanced *in vitro* potencies against the two targets<sup>190</sup> (Fig. 1.25).

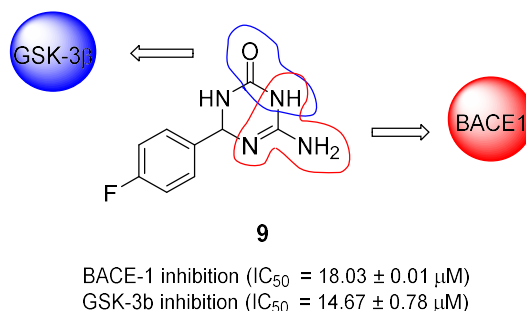


**Figure 1.25.** Design strategy and activity profile of triazinone **9**.

Moreover, compound **9** showed an interesting anti-inflammatory/neuroprotective profile, as GSK-3 $\beta$  is responsible, among other functions, to regulate microglia activation and inflammatory tolerance in astrocytes, playing a major role in neuroprotection and neurogenesis<sup>191</sup>. By inhibiting GSK-3 $\beta$  activity, compound **9** exerted effective neuroprotective and neurogenic activities and no sign of neuron neurotoxicity was detected in glial and neuronal cells. A preliminary pharmacokinetic assessment was also performed in mice, revealing good oral bioavailability and BBB penetration<sup>190</sup>. On these bases, **9** emerges as a promising AD modifier, pointing to triazinones as a new class of multitarget fragments able to tackle  $\tau$  and amyloid neurotoxic cascades<sup>165</sup>.

Thus, because of the multifactorial degenerative process which characterizes AD, a drug discovery program pointing to a single molecule able to hit several targets in this such complex disease might be a viable alternative strategy in the search of effective AD cures. Several challenges remain to be addressed to convert AD multitarget approaches into clinically acceptable tools. However, with its strengths and limitations, the rational design of compounds with multiple biological profile may represent a valuable strategy on the road to therapeutics for AD<sup>165</sup>.

## 1.4 Natural multifunctional agents

Considering the complex multifactorial scenario of AD, therapeutic agents acting on multiple levels of this chronic neurodegenerative disorder are needed, and might play a determining role in drug development and discovery. In this regard, natural products offer great chemical diversity and have already proven to be a rich source of therapeutics. In particular, plant-derived compounds have demonstrated potential health-promoting abilities in AD treatment<sup>192</sup>. Moreover, a number of epidemiological studies have reported a significant positive influence of consumption of polyphenolic phytochemical-rich foods on the prevention of neurological disorders, such as AD<sup>193</sup>. Indeed, several evidence suggest that these polyphenolic compounds might have pleiotropic protective effects by acting at different steps of the neurotoxic cascade. Because of their interesting anti-AD properties, including antiamyloidogenic, antioxidant and anti-inflammatory activities, their potential role as neuroprotective agents in AD is currently a source of inspiration and investigation for drug design.

Polyphenols are widely diffused in nature, in plants, fruits and vegetables, and are characterized by the presence of several hydroxyl groups on aromatic ring or more than one phenol structural unit (Fig. 1.26). Generally, polyphenols can react with one-electron oxidants as well as with metal ions capable of generating free radicals (e.g.  $\text{Fe}^{2+}$ ) to prevent ROS formation and quenching chain reactions in biological systems, thus protecting them against cellular damage. Indeed, it has been shown that several polyphenols exert antioxidant properties by acting as chain breakers or radicals scavengers depending on their chemical structure<sup>194</sup>.

Accumulating evidences suggest that, besides antioxidant features, polyphenols also exhibit additional activities in chronic and neurodegenerative diseases. In particular, in the past years various *in vitro* assays have demonstrated the ability of certain polyphenols to inhibit amyloid fibril formation and their associated cytotoxicity. The driving forces that lead to the formation of fibrillar assemblies seem to be primarily hydrogen bonds involving the polypeptide main chain and secondly stacking interactions of aromatic residues that may accelerate the assembly process. In view of their structural similarities, polyphenol common mechanism of inhibition of fibrils formation might be due to structural constrains and specific aromatic interactions which direct these inhibitors to the amyloidogenic core<sup>195, 196</sup>.

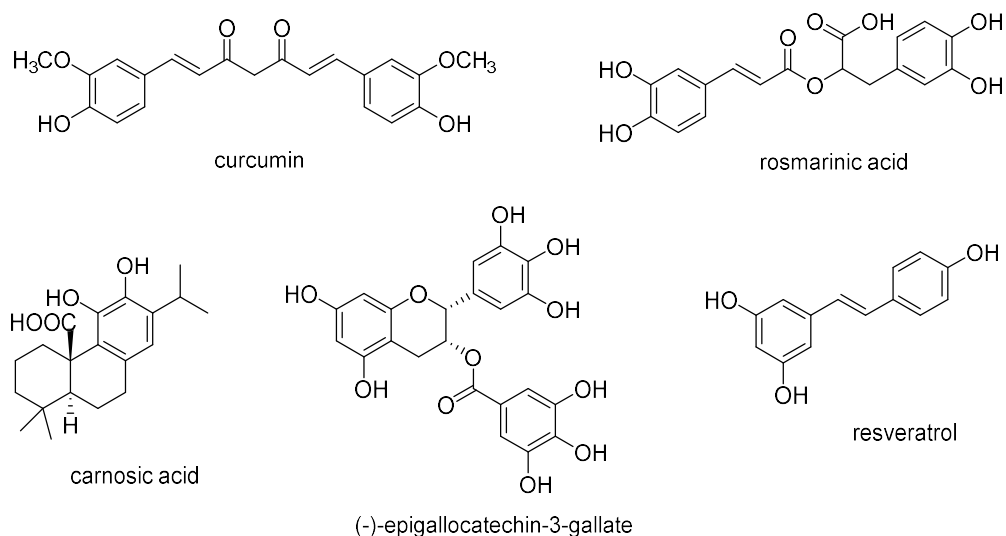


**Figure 1.26.** Chemical structures of some polyphenolic phytochemical compounds that have received attention for AD therapy.

Curcumin was the first polyphenol to be investigated with regard to its therapeutic potential in the pathophysiology of AD, owing to its pleiotropic activity. Curcumin has several functional groups wherein the planar aromatic ring systems are attached to  $\alpha,\beta$ -unsaturated carbonyl groups. The diketones generate stable enols that could be easily deprotonated to form enolates. The  $\alpha,\beta$ -unsaturated group can undergo nucleophilic addition and Michael reaction. Numerous evidence suggest that curcumin exert different neuroprotective activities, including antioxidant, anti-inflammatory and antiamyloidogenic properties<sup>197</sup>. In *in vitro* studies, curcumin has been reported to inhibit A $\beta$  aggregation, and A $\beta$ -induced inflammation, as well as BACE1 up-regulation and the activity of AChE. Moreover, it has demonstrated to attenuate the production of A $\beta$ -induced ROS<sup>198</sup>. In *in vivo* studies, oral administration of curcumin has resulted in the inhibition of A $\beta$  deposition, A $\beta$  oligomerization<sup>199</sup>,  $\tau$  phosphorylation<sup>200</sup>, and improvements in behavioral impairment in the brains of AD animal models. A recent study has characterized the interaction between A $\beta_{42}$  oligomers and some inhibitors including curcumin by means of NMR spectroscopy, revealing that the location of inhibitor binding influences the structure or formation of the different size oligomers. It has been demonstrated that curcumin binds to N-terminus of the peptide, thus capping the height of the oligomers that are formed<sup>201</sup>. Furthermore, previously it was reported that the enol form was the predominant species that interacted with the A $\beta$  aggregates, and that the requirements for anti-

aggregating activity were the coplanar structure and the double-bond conformation with certain optimal carbon chains<sup>202, 203</sup>. In addition, curcumin has been demonstrated to have a strong antioxidant neuroprotective effects, scavenging ROS and neutralizing NO-based free radicals. However, one of the causes of its failure in randomized control trials for AD was its low water solubility, which consequently led to poor bioavailability following oral administration or through parenteral route<sup>192</sup>.

Among polyphenols, EGCG is a very promising compound for AD therapy, currently in phase II/III trials as inducer of nonamyloidogenic APP metabolism through activation of  $\alpha$ -secretase. Additionally, an increasing number of publications reports the ability of EGCG to exert multiple heterogeneous pharmacological activities associated with beneficial health effects. It is a powerful free radical scavenger for the presence of the three hydroxyl groups on aromatic ring and the gallate moiety esterified in the tetrahydropyran ring<sup>204</sup>. It also regulates different survival genes and controls numerous antioxidant protective enzymes, i.e. SOD activity<sup>205</sup>. Furthermore, besides the attenuation of A $\beta$  neuropathology and the inhibition of A $\beta$  fibrils formation<sup>206</sup>, it was demonstrated that EGCG is able to restore mitochondrial respiratory rates, altered mitochondrial membrane potential, and ROS production<sup>207</sup>. Overall, this molecule has an intriguing profile if one considers that the targets involved (A $\beta$  and mitochondria) are intimately connected being amyloid responsible of mitochondrial dysfunction.

Resveratrol is a derivative of stilbene that exists in nature as two geometric isomers, *cis*- and *trans*-resveratrol. The more biologically active isomer is the *trans*-resveratrol, even if exposure to ultraviolet light leads to its conversion to the *cis* inactive form. Among other biological activities ascribable to its polyphenol features, the peculiar mechanism that makes resveratrol an auspicious neuroprotective agent in AD is its capability to interfere with the sirtuin pathway<sup>208</sup>. Sirtuins, particularly SIRT-1, may play an important role in protecting neurons from the devastating effects of ROS/RNS, A $\beta$  peptide, and other intracellular and extracellular insults that could be present in the brain with AD. Resveratrol-induced SIRT-1 overexpression has been found to deacetylate and suppress the activity of p53 in neurons, thus preventing their apoptotic death<sup>209</sup>. Moreover, it was observed that resveratrol-induced SIRT-1 also inhibited the signaling pathway of the nuclear factor kappa B (NF-Kb) in microglia and astrocytes, thus resulting in the protection against A $\beta$ -induced toxicity<sup>210</sup>.

The hydroxycinnamic acids belong to nonflavonoid polyphenols, and are widely distributed in plants and fruits (Fig. 1.27). They exhibit multiple biological profile with remarkable antioxidant, anti-inflammatory and cardioprotective activities, as well as anticancer and antiulcer properties<sup>211</sup>. Moreover, they demonstrated to exert neuroprotective ability by enhancing neuronal survival and promoting neurite outgrowth, a hallmark of neuronal differentiation<sup>212</sup>. Among these, caffeic acid has been reported to have neuroprotective effects against A $\beta$ -induced neurotoxicity and to improve cognitive impairments in AD mouse models<sup>213</sup>.

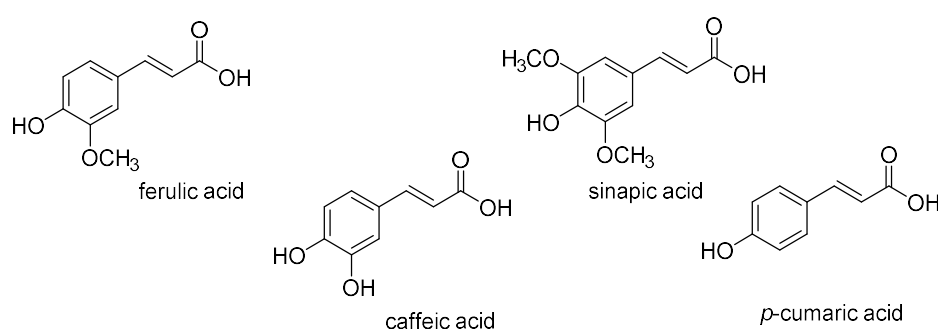


**Figure 1.27.** Chemical structures of some hydroxycinnamic acids.

The antioxidant activity of hydroxycinnamic acids is strongly dependent on their structural features, in particular the hydroxyl function(s) in the aromatic ring. The presence of catechol moiety is of significant importance, as well as the presence of three hydroxyl groups does not necessarily improve the activity. Conversely, the insertion of electron donating groups (e.g. methoxy) leads to decreased activity. This type of phenolic compounds often acts as radical-scavenger. However, other mechanisms of action have been suggested such as chelation of transition metals, like copper or iron, which are well-known catalysts of oxidative stress<sup>214</sup>.

In general, the antioxidant activity of polyphenols arises from the stimulation of antioxidant and detoxification defense systems expression through regulation of Nrf2/ARE signaling. Several data suggest that polyphenols are able to modify the capability of Keap1 in sequestering Nrf2, thus releasing it and promoting its translocation into the nucleus where can activate ARE-containing promoter of antioxidant genes<sup>215</sup>. This hypothesis is supported by the evidence that polyphenols, due to their electrophilic features, can react with cysteine sulfydryl groups of Keap1 and form with them direct covalent adducts that disrupts Keap1-Nrf2 interaction. S-Alkylation occurs since electrophilic

$\alpha,\beta$ -unsaturated carbonyl compounds have electron-deficient centers due to the electron density drawn to the carbonyl oxygen in the structure, that leaves the carbon  $\beta$  to the carbonyl relatively electron-deficient and more reactive for alkylation of cysteine thiol. However, an important issue with electrophilic compounds is that they can non-specifically react with other thiol groups in the cells, thereby inducing cell-toxicity<sup>216</sup>.

Interestingly, some polyphenols that themselves are not endowed with electrophilic properties, in response to oxidative insults can become electrophiles and activate Nrf2/ARE pathway. This concept of pro-electrophilic drugs (PEDs) has been used by Lipton et al. to investigate the potential therapeutic profile of carnosic acid (CA), a natural compound found in the herb rosemary. It has been demonstrated that, after exposure to oxidative stress that chemically converts it to the active electrophilic form, PED-CA induces the Keap1-Nrf2 transcriptional pathway and increases the levels of phase II antioxidant and anti-inflammatory enzymes in neural tissue, thus affording neuroprotection (Fig. 1.28). Redox-dependent generation of the active form of the drug might be therefore useful to prevent reactions with proteins containing thiol groups that would lead to neuronal injury<sup>217, 218</sup>.

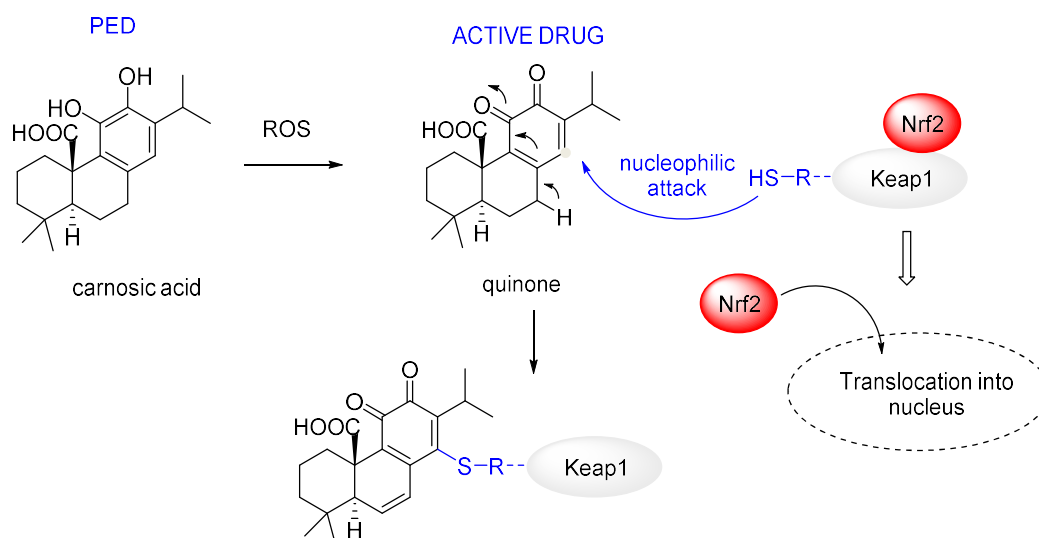


**Figure 1.28.** Schematic model showing action of a pro-electrophilic drugs (PEDs) in activating the Nrf2 transcriptional pathway. In this case, the PED carnosic acid (CA) is activated by reactive oxygen species (ROS) to the active quinone form, the reacts with a critical thiol (-SH) group on the cytoplasmic protein Keap1, which releases the transcription factor Nrf2. Nrf2 then is free to enter the nucleus where it transcriptionally activates phase 2 enzymes<sup>217</sup>. Adapted from Zhang, et al.<sup>217</sup>

In addition, in *in vivo* studies in two separate transgenic mouse models of AD, it has been demonstrated that CA improves learning and memory and decreases dendritic and synaptic loss and A $\beta$  deposition. This neuroprotective effect of CA might occur, at least in part, by activation of Keap1-Nrf2 pathway<sup>219</sup>.

Besides the wide class of polyphenols, natural herbal alternatives with pleiotropic useful properties might be sulfur-containing compounds present in garlic (*Allium sativum*), that has been recognized for its medicinal value centuries ago (Fig. 1.29).

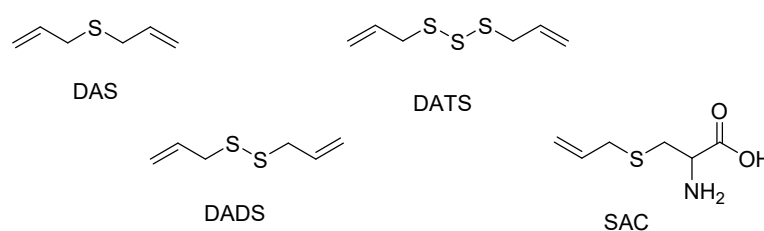


**Figure 1.29.** Chemical structures of sulfur-containing compounds present in garlic. DAS=diallyl sulphide; DATS=diallyl trisulphide; DADS=diallyl disulphide; SAC=S-allyl cysteine.

Major bioactive principles of garlic oil are organosulfur compounds with anti-inflammatory and antioxidant effects. It has been demonstrated that diallyl sulphide (DAS), diallyl disulphide (DADS) and diallyl trisulphide (DATS) are able to induce Nrf2-driven antioxidant gene expression, such as HO-1 and NQO1. In particular, it emerged that DATS, probably as mono-allyl mono-sulfide cleaved form, may directly interact with thiol groups of specific cysteine residues present in Keap1, thus disrupting Nrf2 binding and promoting its translocation into the nucleus<sup>220</sup>.

Several studies showed that garlic extract ameliorates symptoms associated with age and exhibits anti-aggregating efficacy and fibril degrading ability<sup>221</sup>. DADS and S-allyl cysteine (SAC) have been reported to prevent APP processing by amyloidogenic pathway, to reduce soluble and fibrillar A $\beta$  species and neuroinflammation. Moreover, they also decreased conformational change in  $\tau$  protein in a process involving GSK-3 $\beta$ <sup>222</sup> and they exerted anti-apoptotic properties<sup>223</sup>. In addition, SAC decreased the brain levels of A $\beta$ <sub>42</sub> by lowering BACE1 expression and activities<sup>224</sup>.

So far, the potential therapeutic application of garlic-derived organosulfur compounds has been limited by their volatile nature; however, to address this problem, numerous chemical derivatization approaches have been pursued, leading, among others, to interesting multifunctional compounds with multiple biological profile<sup>225, 226</sup>.

## Chapter 2

### **Aim of the thesis**

AD is a biologically multifaceted syndrome, with a complex interplay of genetic and biochemical factors contributing to the cognitive decline. Besides diffuse neuronal loss, AD brain shows protein folding defects, and there is growing evidence that A $\beta$  might trigger the disease process. However, A $\beta$ -centric drug programs have had limited success in AD clinical trials so far<sup>113</sup>. In parallel an increasing number of molecular targets, that may play an important role in the expression of A $\beta$ -induced neurotoxicity, is emerging. In particular, ROS overproduction emerged as a crucial partner of A $\beta$  toxicity, and A $\beta$  is in turn reported to exacerbate oxidative stress<sup>227</sup>, calling for a deeper investigation into this tangled cycle. Besides that, an excessive glutamatergic activity together with the hyperactivation of extrasynaptic NMDARs has been widely documented in AD. Overactivation of NMDARs drastically affects learning and memory processes, and promotes neurodegeneration. Moreover, a relationship between NMDARs hyperactivation, ROS production and A $\beta$  toxicity has been long well established in AD<sup>45</sup>.

Therefore, according to this puzzling scenario, in this work thesis different new nature-inspired molecules have been developed. In order to deepen insight the cross-talk between A $\beta$  functions and oxidative stress in AD, promising pharmacologic tools have been synthesized, which turned out to be versatile instruments to investigate A $\beta$  causative role in AD. Furthermore, based on the MTDL approach, multifunctional ligands were obtained by combining the NMDAR antagonist memantine with natural pharmacophores exerting antioxidant and anti-aggregating activities.

## 2.1 Nature-Inspired Modulators of AD: Focusing on Amyloid and Oxidative Stress

The amyloidogenic pathway is a prominent feature of AD. However, A $\beta$ -centric approaches have not yet resulted in clinically effective drugs. This has raised a degree of uncertainty in drug development programs, which has in turn led to a re-examination of the A $\beta$  controversial model. Besides the consolidated evidence that A $\beta$  might trigger the disease process, intertwined correlations between A $\beta$  and other main players of the disease have been identified. In particular, the vicious circle generated by A $\beta$  and oxidative stress offers a new key for reading A $\beta$  causative role. Oxidative stress is known to trigger the amyloidogenic pathway and promote A $\beta$  toxicity. On the other hand, several lines of evidence indicate that A $\beta$  exacerbates oxidative stress, with other cellular pathways emerging as determining mediators of this tangled cycle.

In this respect, regulation of p53 conformation and function may represent a crucial feature of this intricate scenario. Recent observations have showed that p53 may play a central role in aging and in neurodegenerative disorders since its conformational changes and functional alterations have been found in patients with AD<sup>147</sup>. In particular, subtoxic and chronic ROS exposure leads to impairment of wild-type p53 tertiary structure, inducing a switch toward the not functional unfolded form of p53<sup>228</sup>. Additionally, recent evidence showed that the alteration of the physiological functions of p53 can also result from the exposure to soluble non toxic A $\beta$ , suggesting an existing correlation among A $\beta$ , oxidative stress and p53 conformational changes in AD<sup>155</sup>.

In this context, Keap1-Nrf2 transcriptional pathway plays an important role as the major mechanism of defense in the cell against oxidative or electrophilic stress by controlling the expression of cytoprotective genes<sup>229</sup>. In particular, when exposed to oxidative insults, Keap1 undergoes conformational changes and disrupts Nrf2 binding, thus promoting its translocation into the nucleus and the activation of transcription-mediated protective responses. Interestingly, the Keap1-Nrf2 interaction can also be disrupted by small molecules with electrophilic properties able to covalently bind to Keap1 cysteine residues.<sup>187 189</sup> Recent studies have demonstrated a protection from A $\beta$ -induced neurotoxicity and attenuation of A $\beta$ -induced oxidative cell death by means of activation of the Keap1/Nrf2 signaling<sup>142</sup>.

In the search for valuable pharmacologic tools, aimed at deepening insight into AD cross-talk between A $\beta$  functions and oxidative stress, nature can be envisioned as a structural “muse”. Indeed, natural products offer a great chemical diversity, and have already proven to be a rich source of therapeutics<sup>230</sup>. Polyphenols are widely diffused in nature, and they have been shown to modulate several AD pathways, including oxidative injuries and A $\beta$  aggregation. Among them, proelectrophile compounds, which include hydroquinone cores of natural terpenoids and flavonoids, have attracted researchers’ interest due to their activation into electrophilic forms in response to pathological oxidation, offering prospects of minimal potential side effects.<sup>197</sup> Interestingly, many of them present a hydroxy-cinnamoyl function as a recurring motif. Among these, curcumin has emerged as a pleiotropic agent that, over the past decade, has been the object of intensive study, providing an outstanding platform for numerous biologically active ligands. On the other hand, garlic-derived organosulfur compound carrying allyl mercaptan moieties (i.e. DADS), are able to counteract oxidative stress through antioxidant enzyme expression<sup>220</sup>.

These structures have recently attracted the interest of the research group I joined during the three years of my PhD, leading to the identification of a small set of natural-product-inspired fragments by conjugating the cinnamoyl function of curcumin to the allyl mercaptan moiety of DADS (Fig. 2.1, Table 2.1).

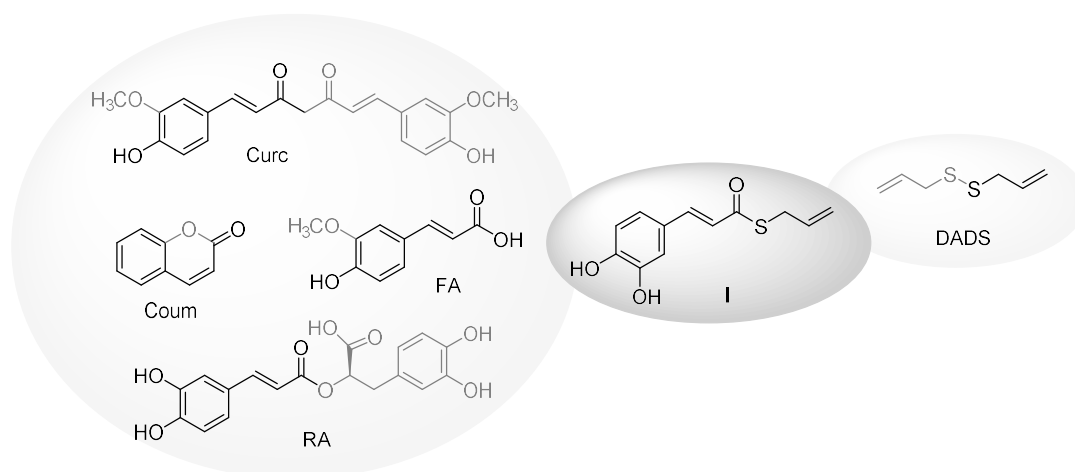


**Figure 2.1.** Design strategy of compound I. Leftside: Curc (curcumin), Coum (coumarin), FA (ferulic acid), RA (rosmarinic acid). Rightside: DADS (diallyl disulfide).

Among others, compound **I** emerged as the most promising derivative of that series, combining an efficient anti-aggregating activity to a good antioxidant profile. Moreover, based on previous structure-activity relationship (SAR) studies (Table 2.1), the thioester function was identified as a structural requirement for anti-aggregating activity. Indeed, when thioester was replaced with an ester or an amide (**V** or **VI** respectively), the anti-aggregating efficacy gradually decreased. Therefore, **I** was endowed with the optimal structural requirements being the lead compound of the present PhD project. Particularly, this work was centered on performing systematic and/or bioisosteric modifications of **I**'s building fragments, leading to the synthesis of nature-inspired hybrids that lack key features of symmetric prototypes, such as the  $\beta$ -diketone function of curcumin and the disulfide bridge of DADS, and merge into new chemical entities.

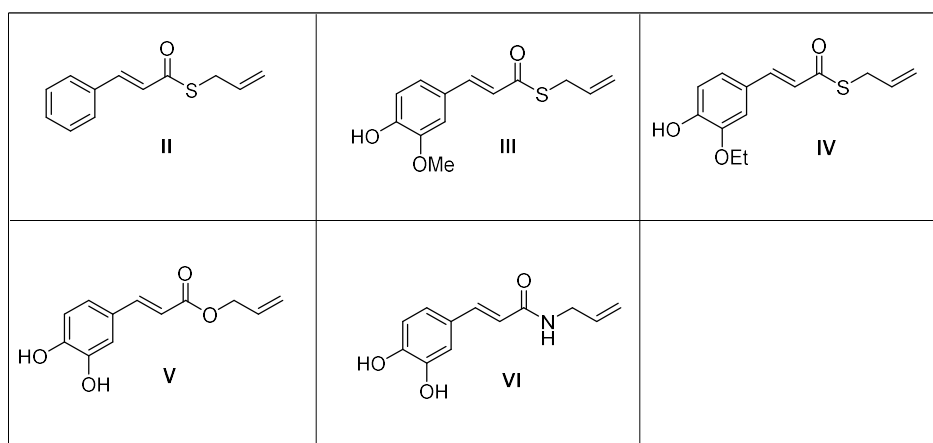


**Table 2.1.** Previously synthesized compounds.

Initially, to expand and complete SAR studies on catechol group, compounds **1-4** differing in the aromatic substitution pattern were synthesized (Fig. 2.2). In particular, to assess the radical scavenging activity related to the stabilization of phenolic groups, and the importance of the catechol moiety for anti-aggregating properties, *para*- and *meta*-coumaric acid were esterified with allyl mercaptan (**1** and **2**, respectively), and the catechol group was masked with methoxy- or ethoxy-functions (**3** and **4**, respectively).

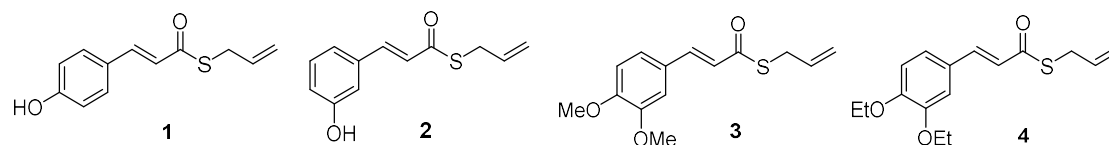


**Figure 2.2.** Structure of compounds 1-4.

Then, the focus has been shifted on the chemical tether between the catechol and thioester functions in order to investigate the role of aliphatic skeleton of **1** in amyloid recognition and for antioxidant efficacy (Fig. 2.3). In **5** the cinnamoyl double bond was saturated with the aim to assess the importance of electronic conjugation of the catechol moiety and thioester function for target identification. Conversely, in **6** the conjugation was kept and only the distance was shortened, by removing the ethylene group and directly binding the thioester side chain to the catechol group.

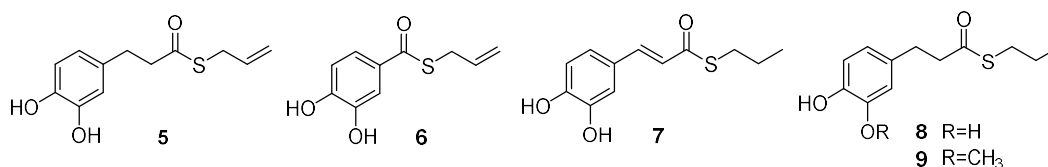


**Figure 2.3.** Structure of compounds 5-9.

In **7** and **8** the terminal allyl moiety was replaced by propyl group to verify its role in anti-aggregating and antioxidant activities and the possibility of further functionalization in that position. Finally, **9** was purposely synthesized by lacking both electrophilic functionalities (catechol moiety and cinnamoyl double bond) with the aim to remove the thought fundamental requirements for anti-aggregating activity and using it as negative control.

Since catechols are substrates for catechol *O*-methyl transferase (COMT), in order to improve the metabolic stability and the pharmacokinetic, a small set of (bio)isosteres was designed to overcome the conceivable toxicological limitations associated with these peculiar structures. In particular, for **10** and **11** the catechol ring was substituted by resorcinol and 2-hydroxymethyl phenol respectively, both not anymore suitable substrates of COMT (Fig. 2.4).

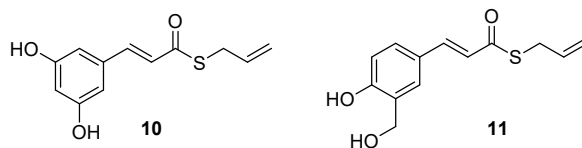


**Figure 2.4.** Structure of compounds **10** and **11**.

Compounds **12-15** were designed following the bioisosteric replacement of catechol ring by an indazole fragment<sup>231</sup> functionalized in 5' (**12** and **13**) or 6' (**14** and **15**) (Fig. 2.5). In this way, the indazole ring should presumably allow to preserve anti-aggregating activity, avoiding enzymatic degradation due to COMT activity.

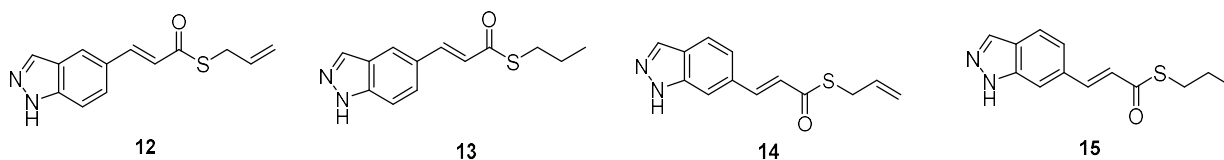


**Figure 2.5.** Structure of compounds **12-15**.

Because of the high susceptibility of its carbonyl center to undergo hydrolysis reactions, also the thioester function was replaced by bioisosteric fragments. In **16** and **17** the thioester group was substituted by an *N*-methyl propylamide and an *N*-propyl sulfonamide, respectively (Fig. 2.6). In particular, *N*-methyl amides have been recently used as isosteres for thioester bond in natural compounds, with the result to display an increased stability as compared to parent compound<sup>232</sup>.

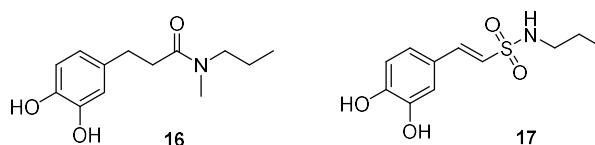


**Figure 2.6.** Structure of compounds **16** and **17**.

## 2.1.1 METHODS: Chemistry and Biology

### Chemistry

Syntheses of compounds **1-17** were carried out following different standard procedures outlined in Schemes 1-4.

Syntheses of the thioesters **1-10** and *N*-methyl amide derivative **16** were accomplished in two different ways (method A and B) according to Scheme 1. The synthesis of **3** and **4** was carried out by one pot reaction with minor modifications of literature procedure referred to caffeate esters<sup>233</sup>. As reported in Scheme 1 (method A), this procedure allowed Meldrum's acid mono-thioesterification with allyl sulphide to give the non-isolable intermediate, which was then readily condensed with the appropriate aldehyde affording cinnamic derivatives **3** and **4** with moderate to good yields. Unfortunately, this convenient method was not effective to access the other derivatives due to the presence of hydroxyl groups that led to undesired by-products. It has been therefore used an alternative procedure, which minimized side-reactions and purification efforts (Scheme 1, method B). *tert*-Butyldimethylsilyl (TBDMS)-protection of the alcohols **24-30** followed by coupling reaction with *N,N*-dicyclohexylcarbodiimide (DCC) in presence of 4-dimethylaminopyridine (DMAP) gave the intermediates **38-46**. Finally, treatment of **38-46** with tetrabutylammonium fluoride (TBAF) effected desilylation to give the final compounds **1, 2, 5-10** and **16**.

Compound **11** was efficiently synthesized according to the synthetic strategy outlined in Scheme 2. The key steps for the formation of the hydroxycinnamic intermediate **52** were achieved by Bouveault aldehyde synthesis followed by Knoevenagel condensation with some modifications of literature procedure<sup>234</sup>. 4-bromosalicyl alcohol (**48**) was prepared by reduction of the commercially available 5-bromosalicyl aldehyde (**47**) following a standard literature procedure<sup>235</sup>. Protection of the alcohol as isopropylidene acetal (**49**) was carried out and optimized by microwave assisted synthesis, shortening time reaction with quantitative yield. The resulting isopropylidene acetal **49** was treated first with *n*-butyllithium in tetrahydrofuran (THF) and afterwards with *N,N*-dimethyl formamide (DMF). This led via bromo/lithium-exchange to 4-formylsalicyl alcohol isopropylidene acetal (**50**) that was then condensed with malonic acid to afford acrylic acid derivative **51**, whose isopropylidene acetal group was readily cleaved with catalytic amounts of HCl to obtain the key

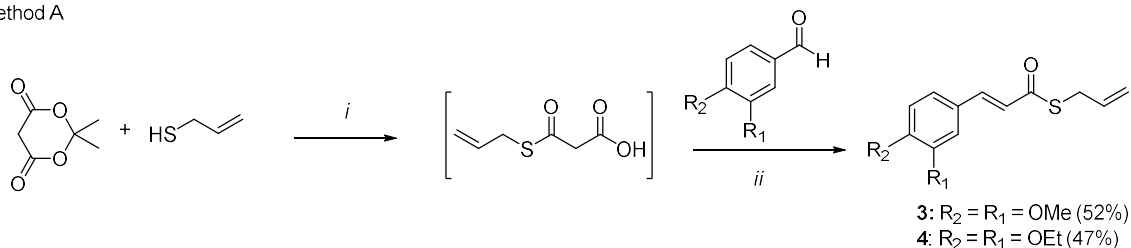
intermediate **52**<sup>234</sup>. The subsequent re-protection of the alcoholic functions with *tert*-butyldimethylsilyl chloride (TBDMS-Cl), whose cleavage is compatible with thioester group in the last step, followed by coupling reaction with *N*-(3-dimethylaminopropyl)-*N'*-ethylcarbodiimide hydrochloride (EDC) in presence of 1-hydroxybenzotriazole hydrate (HOBT) gave intermediate **54**. Likewise to previous hydroxycinnamic compounds, treatment of **54** with TBAF effected desilylation to give the final compounds **11**.

Syntheses of indazole derivatives **12-15** were carried out following the standard procedures outlined in Scheme 3. Commercially available indazole-5-carboxyaldehyde (**55**) and indazole-6-carboxyaldehyde (**56**) underwent to Knoevenagel condensation to afford  $\alpha,\beta$ -unsaturated acids **57** and **58**. *N*-protected indazole with *tert*-butyloxycarbonyl (Boc) group, needed to limit undesired side by products, followed by coupling reaction with EDC in presence of HOBT and the appropriate nucleophile gave the intermediates **61-64**. Finally, deprotection of the Boc group was accomplished by treatment with hydrochloridric acid in dichloromethane (CH<sub>2</sub>Cl<sub>2</sub>) followed by purification under basic conditions to afford the final compounds **12-15**.

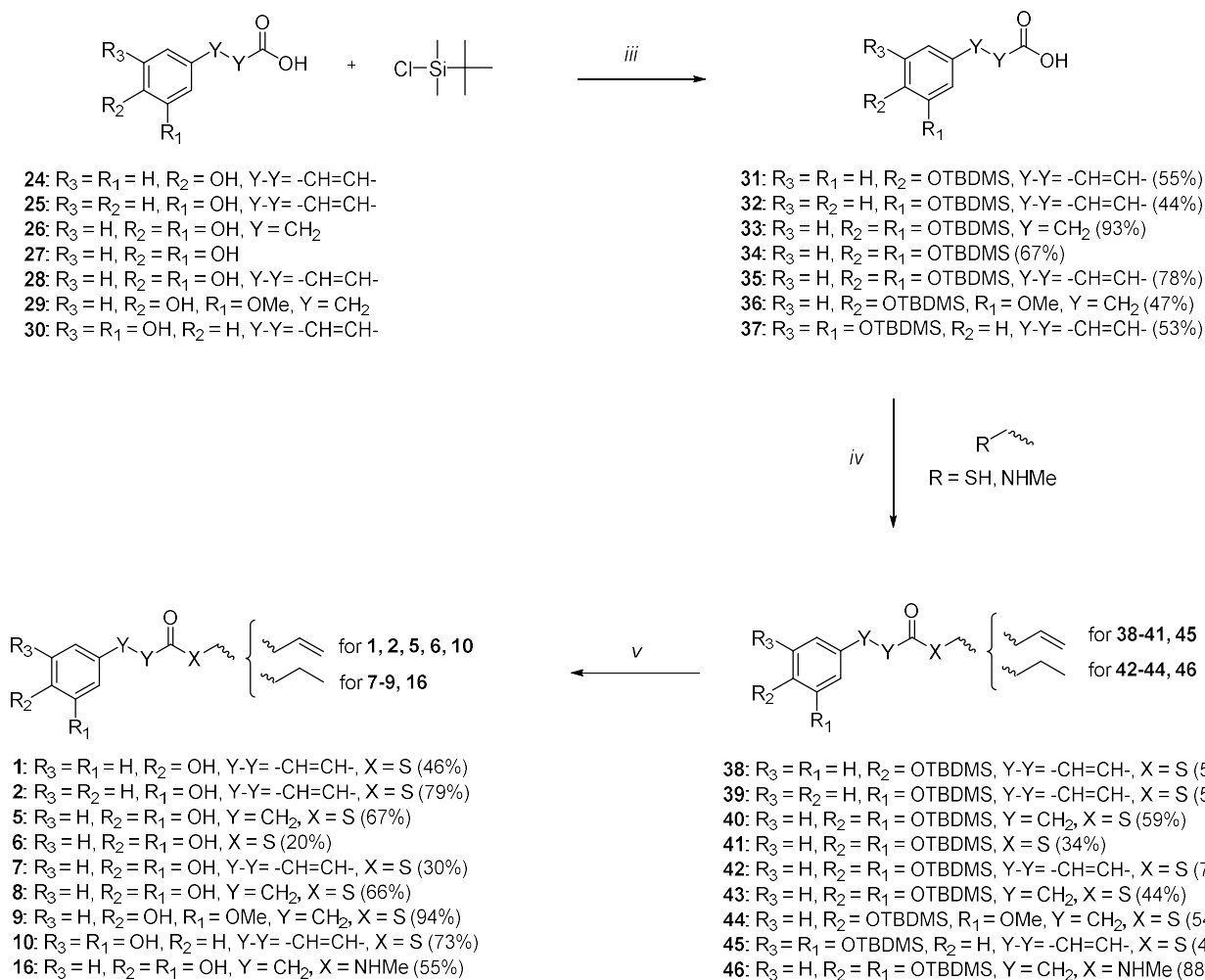
The synthesis of sulfonamide derivative **17** was outlined in Scheme 4. Reaction of ethyl bromoacetate (**65**) with Na<sub>2</sub>SO<sub>3</sub> following a literature procedure<sup>236</sup> afforded intermediate **66**, which was converted to the sulfonyl chloride **67** via chlorination using phosphorus pentachloride (PCl<sub>5</sub>). Then amidation of compound **67** with propylamine gave the intermediate **69** following ethyl ester hydrolysis. Further condensation of compounds **69** with 3,4-dihydroxybenzaldehyde in presence of catalytic amounts of pyrrolidine and acetic acid afforded the desired side chain **17** in moderate yield. The unreacted benzaldehyde was neutralized as hydrazone derivative by means of Girard's reagent T in presence of acetic acid.

<sup>1</sup>H NMR spectra show that all hydroxycinnamic compounds have an *E* configuration as indicated by the large spin coupling constants (around 16 Hz) of  $\alpha$ -H and  $\beta$ -H on double bonds.

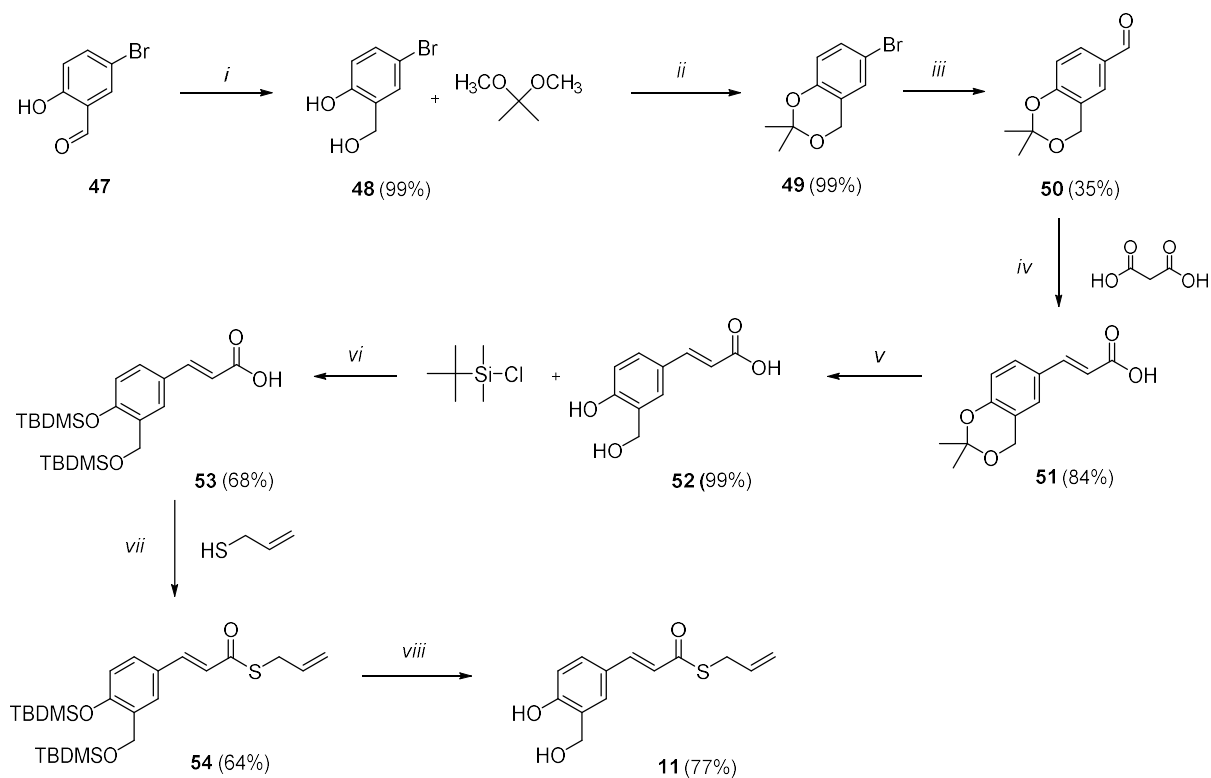
Method A



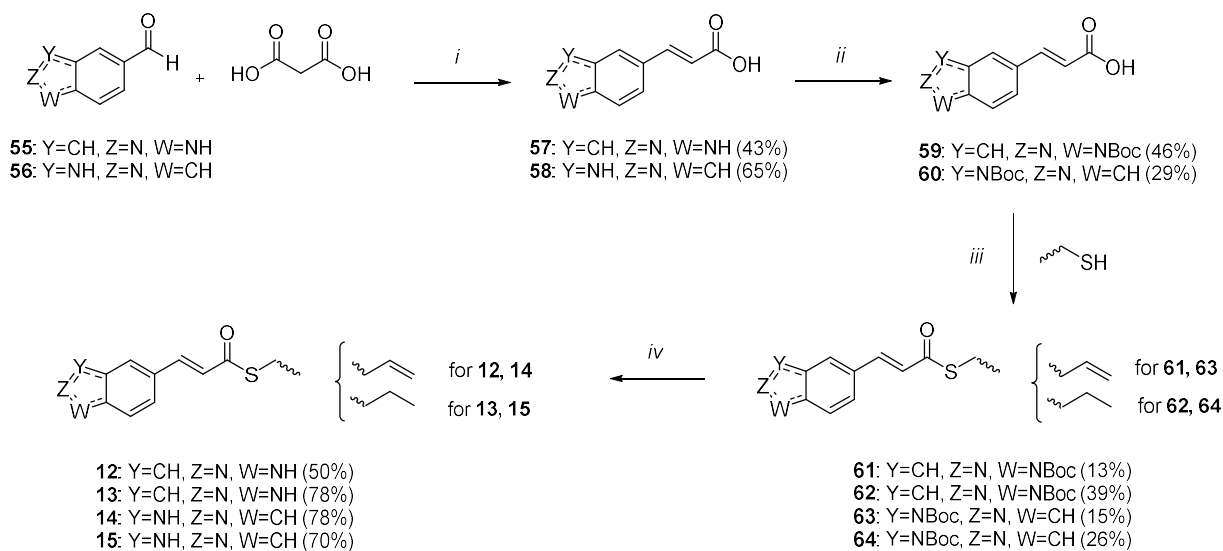
Method B



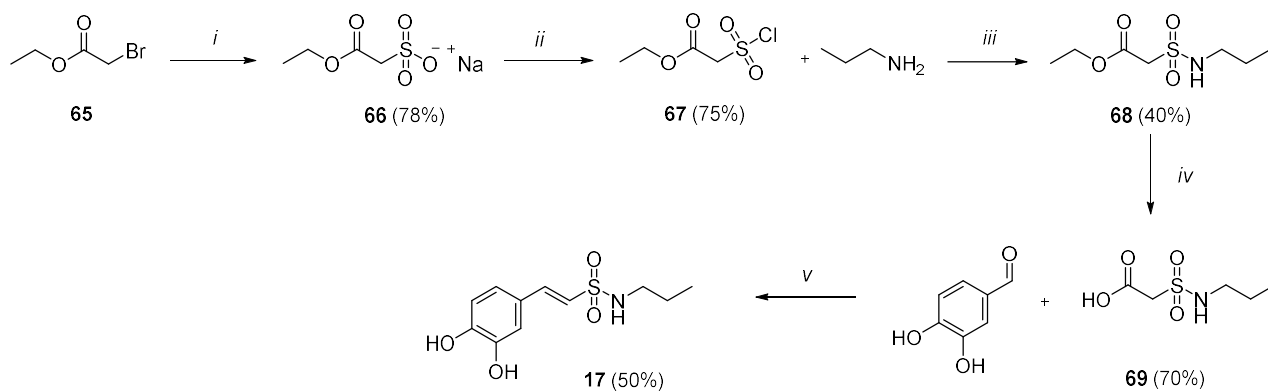
**Scheme 1.** Reagents and conditions: (i) toluene, reflux, 7 h; (ii) pyridine, piperidine, rt, 4 d; (iii) DMF, imidazole,  $\text{N}_2$ , rt, o/n; (iv) DCC, DMAP,  $\text{CH}_2\text{Cl}_2$ ,  $\text{N}_2$ , o/n,  $0^\circ\text{C}$ -rt; (v) TBAF, THF,  $\text{N}_2$ , 30', rt.



**Scheme 2.** Reagents and conditions: (i)  $\text{NaBH}_4$ , EtOH, 2 h,  $0^\circ\text{C}$ -rt; (ii) *p*TsOH,  $\text{Na}_2\text{SO}_4$ , MW, 20',  $60^\circ\text{C}$ ; (iii) *n*-BuLi, THF, DMF, 3 h,  $-78^\circ\text{C}$ ; (iv) pyridine, aniline, toluene, 5 h, reflux; (v) HCl 12N,  $\text{CH}_3\text{CN}/\text{H}_2\text{O}$  (cat.), 5', reflux; (vi) DMF, imidazole,  $\text{N}_2$ , 30', rt; (vii) EDC, HOBT,  $\text{CH}_2\text{Cl}_2$ ,  $\text{N}_2$ , o/n,  $0^\circ\text{C}$ -rt; (viii) TBAF, THF,  $\text{N}_2$ , 30', rt.



**Scheme 3.** Reagents and conditions: (i) pyridine, aniline, toluene, 2 h, reflux; (ii)  $\text{Boc}_2\text{O}$ ,  $\text{Et}_3\text{N}$ , DMAP, THF/ $\text{H}_2\text{O}$ , 2 d, rt; (iii) EDC, HOBT, DMF/ $\text{CH}_2\text{Cl}_2$ ,  $\text{N}_2$ , 24 h,  $0^\circ\text{C}$ -rt; (iv) HCl 4M in dioxane, MeOH, 4 h, rt.



**Scheme 4.** Reagents and conditions: (i)  $\text{Na}_2\text{SO}_3$ ,  $\text{H}_2\text{O}/\text{EtOH}$ , 1 h,  $50^\circ\text{C}$ ; (ii)  $\text{PCl}_5$ , 1 h, reflux; (iii) DBU,  $\text{K}_2\text{CO}_3$ ,  $\text{CH}_2\text{Cl}_2$ , 3 h, reflux; (iv) NaOH 10%  $\text{H}_2\text{O}$ , 3 h,  $0^\circ\text{C}$ -rt; (v) pyrrolidine, acetic acid, THF, 8 h, reflux, then Girard's reagent T, acetic acid,  $\text{CH}_2\text{Cl}_2$ ,  $10^\circ$ .

## Biology

Initially, the biological evaluation of synthesized compounds has been focused on lead compound **I** and its analogues lacking *m*- or *p*-hydroxyl function (**1** and **2**). They were first tested *in vitro* to assess their anti-aggregating properties towards A $\beta$ <sub>42</sub>, and then assayed in neuroblastoma cells to explore their ability to counteract oxidative stress and to exert neuroprotective effect against A $\beta$ <sub>42</sub>-induced toxicity. The efficacy of **I**, **1** and **2** in modulating A $\beta$ -induced conformational state alteration of p53 protein was also investigated.

Afterwards, previously synthesized compounds **II-VI** and the new ones **3-9** were investigated to assess their antioxidant and anti-aggregating properties. The efficacy in inhibiting fibrilization of amyloidogenic isoform A $\beta$ <sub>42</sub> was first studied *in vitro* by a fluorescence-based assay. In this case as well, they were then assayed in human SH-SY5Y neuroblastoma cells to explore their ability to contrast oxidative stress and to exert neuroprotective effect against A $\beta$ <sub>42</sub>-induced toxicity. To draw connections between the structural requirements involved in inhibition of amyloid aggregation and transcription-based antioxidant responses, selected compounds were studied as Nrf2 inducers in human SH-SY5Y neuroblastoma cells, and the ability of promoting the endogenous up-regulation of the Nrf2-dependent defensive gene NQO1 was also assessed.

Isosteres **10-17** are currently in ongoing studies to assess their ability to inhibit amyloid aggregation by a fluorescence-based assay and to counteract H<sub>2</sub>O<sub>2</sub>-induced oxidative stress in SH-SY5Y neuroblastoma cells by using the fluorescent probe dichlorofluorescein diacetate (DCF-DA) as a specific marker for quantitative intracellular ROS formation.

NMR investigation on selected synthesized compounds are currently ongoing using <sup>15</sup>N-labeled A $\beta$ <sub>42</sub> peptide. This study should allow us to evaluate the capacity of the new small molecules to interact with A $\beta$ <sub>42</sub> monomers and to identify the specific residues of A $\beta$ <sub>42</sub> that bind the inhibitors or that are indirectly influenced by the binding.

## 2.1.2 Results and discussion

### Focusing on amyloid-based molecular mechanism of AD (compounds **I**, **1** and **2**)<sup>237</sup>

Synthesized compounds **I**, **1** and **2** were first tested to evaluate their possible anti-aggregating properties by means of a thioflavin T (ThT)-based fluorometric assay, commonly used to monitor A $\beta$  fibrillization and its inhibition. Curcumin, that is a consolidated prototype for AD studies, was herein used as reference compound. The evaluation of **I**, **1** and **2** clearly highlights a strong influence of the aryl pattern on the ability to prevent the A $\beta$ <sub>42</sub> self-assembly process. Interestingly, the catechol moiety (compound **I**) emerged as essential for activity. **I**, at 1/1 ratio with A $\beta$ <sub>42</sub> almost completely inhibited A $\beta$ <sub>42</sub> self-aggregation (% inhibition > 90%, IC<sub>50</sub> = 12.5 ± 0.9  $\mu$ M), resulting even more effective than curcumin (% inhibition = 73.7%) and showing an inhibitory potency similar to the well known multipotent compound bis(7)tacrine (IC<sub>50</sub> = 8.4 ± 1.4  $\mu$ M). Noteworthy, in the same experimental conditions, a complete loss of the anti-aggregating efficacy was observed for **1** and **2**, lacking the *m*- or *p*-hydroxyl function, respectively (Fig. 2.7). This striking result points to the catechol moiety as a key recognition fragment for inhibition of amyloid aggregation.

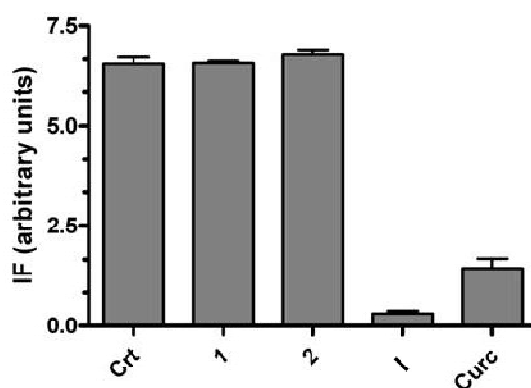


**Figure 2.7.** Inhibition of A $\beta$ <sub>42</sub> aggregation by **I**, **1** and **2** or curcumin (Curc), as determined by a ThT-based assay. ThT-related fluorescence intensity of A $\beta$ <sub>42</sub> (50  $\mu$ M) samples after a 24 h incubation period in the absence (Ctrl) or in the presence of the indicated test compounds (all at 50  $\mu$ M). Values are the mean.SEM of two independent measurements each performed in duplicate. *The assays were performed by Prof. . Bartolini's research group, University of Bologna, Italy.*

Motivated by the promising results, **I**'s mode of action was investigated at a molecular level using an orthogonal method, electrospray ionization-ion trap-mass spectrometry (ESI-IT-MS) in flow injection mode, which allows to detect and quantitate the monomeric form of A $\beta$ <sub>42</sub>.<sup>238</sup> In the used

experimental conditions, in the absence of any inhibitor, a progressive decrease in the monomer content, expressed as the sum of the native ( $A\beta_{42}$  Native) and oxidized form ( $A\beta_{42}$  Ox) of  $A\beta_{42}$ , is observed within 24 h, due to inclusion of  $A\beta$  monomers into growing stable oligomers. In agreement with this trend, when  $A\beta_{42}$  was incubated alone, a dramatic decrease (83%) in monomer content was observed after 24h incubation (Fig. 2.8). Conversely, when treating  $A\beta_{42}$  with **I** in a peptide/inhibitor ratio of 1:1, a high monomer content was detected after 24h incubation, meaning that **I** strongly inhibited monomer inclusion into growing amyloid oligomers (Fig. 2.8). Curcumin, tested in the same conditions, resulted to be a much weaker inhibitor of the early phase  $A\beta_{42}$  aggregation. These results clearly support the anti-aggregating activity resulting from the ThT-based assay. Moreover, they showed that **I** was able to strongly retard the  $A\beta$  overall assembly process by acting at monomer level in the early stage of amyloid aggregation and strongly preventing the formation of stable soluble oligomers. This is of utmost importance due to the cytotoxic effects exerted by soluble aggregation intermediates<sup>119, 239, 240</sup>.

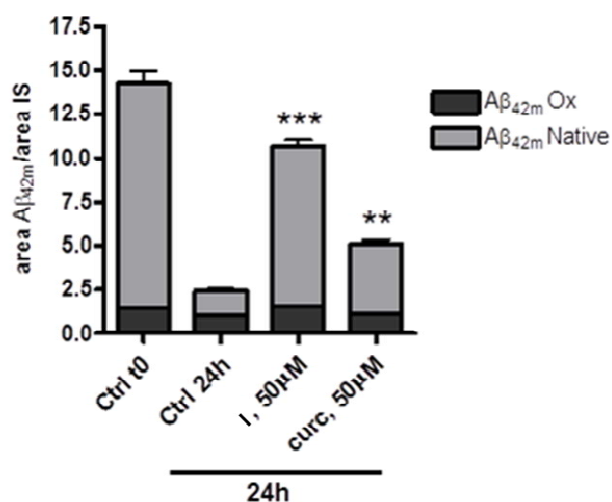


**Figure 2.8.** Inhibition of  $A\beta_{42}$  aggregation by **I** and curcumin (Curc), both at 50  $\mu$ M, as determined by ESI-IT-MS. The total  $A\beta_{42}$  monomer ( $A\beta_{42m}$ ) content in the absence (Ctrl) and in the presence of inhibitor is displayed as the sum of the native ( $A\beta_{42}$  Native) and oxidized ( $A\beta_{42}$  Ox) forms of  $A\beta_{42}$ . IS: internal standard (reserpine); \*\* $p < 0.01$ , \*\*\* $p < 0.001$  versus Ctrl 24 h; Dunnett's multiple comparison test<sup>237</sup>.

Since natural polyphenols can act as either antioxidant or pro-oxidant agents<sup>241</sup>, based on previous studies on myricetin that revealed pro-oxidant properties toward  $A\beta_{42}$  peptide<sup>242</sup> we sought to verify whether **I**, bearing a catechol moiety, could partially exert its inhibitory activity through an

oxidation-based mechanism. The oxidized form of A $\beta$ <sub>42</sub> (A $\beta$ <sub>42</sub>Ox) was shown to be less prone to aggregate than the native one (A $\beta$ <sub>42</sub> Native), thus accounting for a slower aggregation rate<sup>243</sup>. Based on the different molecular weight, both the native and oxidized forms of A $\beta$ <sub>42</sub> can be detected by MS analysis. When treating A $\beta$ <sub>42</sub> samples with **I** in a peptide/inhibitor ratio of 1:1, only a slightly increase of the oxidized species at 24h respect to the initial content was observed, thus excluding a significant oxidation-mediated mode of inhibition (Fig. 2.8). Hence, based on these results, a stabilization of the A $\beta$ <sub>42</sub> monomeric form and inhibition of its inclusion onto the growing oligomers, which greatly retards the overall A $\beta$  assembly process, can be rather postulated.

To determine whether **I** may exert any neuroprotective effect against A $\beta$ <sub>42</sub>-induced toxicity, a cell viability study in SH-SY5Y human neuroblastoma cells was performed using the MTT assay (Fig. 2.9).

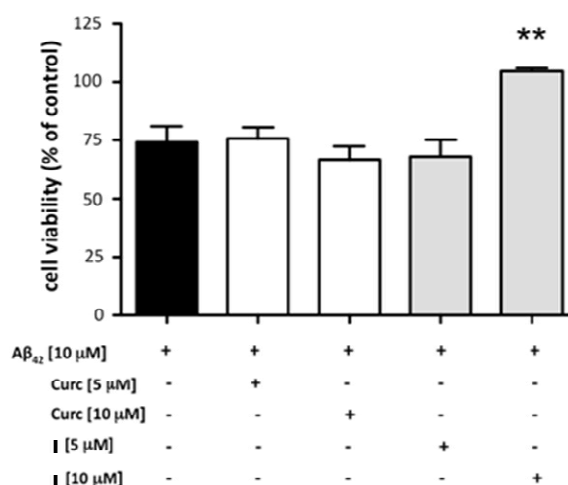


**Figure 2.9.** Effect of curcumin (Curc) and compound **I** on A $\beta$ <sub>42</sub>-mediated cytotoxicity in neuroblastoma cells. SH-SY5Y cells were pretreated for 24 h with curcumin or compound **I** at 5 or 10  $\mu$ M and then incubated for an additional 24 h with A $\beta$ <sub>42</sub> at 10  $\mu$ M. Cell viability was determined by MTT assay. Data are expressed as percentage cell viability versus control; \*\*p<0.01 versus Ab42; Dunnett's multiple comparison test<sup>237</sup>.

The results clearly showed that **I** was able to exert a dose-dependent protective effect. Indeed, while at 5  $\mu$ M **I** could not prevent A $\beta$ <sub>42</sub> cytotoxicity, a strong protective effect was observed when **I** was assayed at 10  $\mu$ M. At this concentration **I** almost completely prevented the A $\beta$ -induced cell death. In the same assay, curcumin was not able to counteract A $\beta$  toxicity even at 10  $\mu$ M concentration.

Afterwards, to determine the potential interest of thioesters **I**, **1** and **2** as antioxidants, we evaluated their protective effects against H<sub>2</sub>O<sub>2</sub>-induced oxidative damage. In comparison to untreated neuroblastoma cells (dashed line, Fig. 2.10), the intracellular DCF fluorescence intensity in H<sub>2</sub>O<sub>2</sub>-treated cells significantly increased (grey line, Fig. 2.10), revealing that curcumin and all compounds significantly suppressed H<sub>2</sub>O<sub>2</sub>-induced intracellular ROS production (Fig. 2.10), with **1** being strongly more effective in counteracting ROS formation.

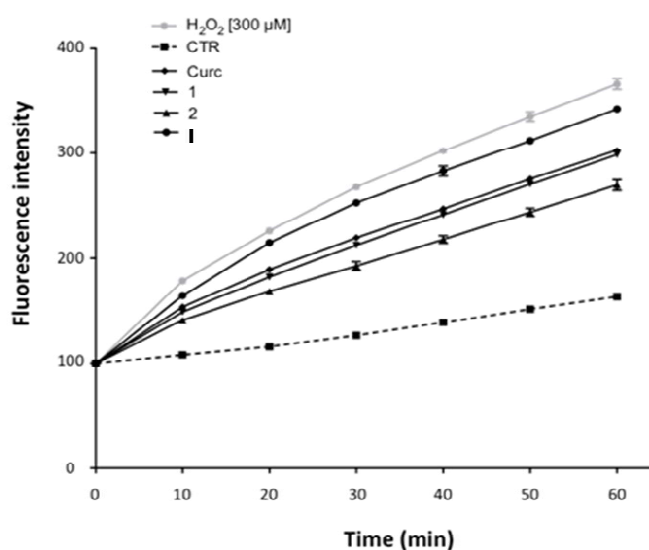


**Figure 2.10.** Compounds **I**, **1** and **2** reverse ROS-formation-induced oxidative stress. Cells were pretreated with curcumin (Curc) and compounds **I**, **1** and **2** (5 μM) for 24 h and then loaded with 25 μM DCF-DA for 45 min. DCF-DA was removed, and cells were then exposed to 300 μM H<sub>2</sub>O<sub>2</sub>. Intracellular ROS levels were determined on the basis of DCF fluorescence by using a fluorescent microplate. The graph shows the intracellular fluorescence intensity of DCF. SD at various time treatments. Fluorescence intensity for curcumin and compounds **I**, **1** and **2** at any time is significant, with  $p < 0.001$  versus H<sub>2</sub>O<sub>2</sub>; Dunnett's multiple comparison test<sup>237</sup>.

To corroborate the correlation between Aβ peptide, oxidative stress and p53 conformational changes compounds **I**, **1** and **2** were further investigated in a neuroblastoma cell line to verify whether they may affect the alterations in zyxin-HIPK2-p53 pathway mediated by soluble sublethal Aβ concentrations. The hypothesis that Aβ induces zyxin and HIPK2 deregulation and consequently the p53 conformational change may be related to the capability of the peptide to alter oxidative homeostasis. In this respect, compounds with antioxidant activity should reduce Aβ-mediated p53 conformational change.

To this aim, we first characterized SH-SY5Y neuroblastoma cells in term of HIPK2 and zyxin expression and p53 conformational status. A sublethal concentration of A $\beta$ <sub>42</sub> (10 nM) significantly reduced HIPK2 and zyxin protein levels (Fig. 2.11a). The conformational status of p53 was analyzed by immunoprecipitation using two conformation-specific antibodies, i.e., PAb1620 and PAb240, which discriminate folded versus unfolded p53 tertiary structure, respectively<sup>244</sup>. In neuroblastoma cells, A $\beta$ <sub>42</sub> induced the expression of unfolded p53, as recognized by PAb240 antibody (Fig. 2.11b).

On this basis, neuroblastoma cells were then treated with 10 nM A $\beta$ <sub>42</sub> in the presence of compounds **I**, **1** and **2** at the concentration of 5  $\mu$ M, resulting in a significantly lowered level of unfolded p53 as shown by a lower intensity of the PAb240 positive band in comparison with that obtained when cells were treated with A $\beta$ <sub>42</sub> alone, with **2** being significantly more effective (Fig. 2.11c). These data show that pre-treatment of neuroblastoma cells, in particular with compound **2**, for which marked antioxidant properties are not accompanied by any anti-aggregating activity, prevented A $\beta$ -induced p53 conformational changes. This finding supports an involvement of the oxidative stress in A $\beta$  function.

Since A $\beta$ -induced p53 conformational changes have been shown to contribute to the accumulation of cell damage and to hinder apoptotic programs of cells when exposed to noxae<sup>154, 155, 245</sup>, we sought to study cell sensitivity to doxorubicin, a genotoxic agent able to induce apoptosis in a p53-dependent manner<sup>246-248</sup>. Notably, cells treated with 5  $\mu$ M of **I**, **1** and **2** and 10 nM of A $\beta$ <sub>42</sub> showed to be more vulnerable to doxorubicin in comparison with cells treated with A $\beta$ <sub>42</sub> alone. Doxorubicin induced a reduction of about 30% of cell viability in A $\beta$ -treated cells, while the reduction of cell viability was about 50% in the presence of A $\beta$ <sub>42</sub> and of each tested compound (Fig. 2.11d). The obtained results indicate that compounds **I**, **1** and **2** may prevent the production of the unfolded isoform of p53 induced by A $\beta$ , making the cells more sensitive and able to respond to an insult.

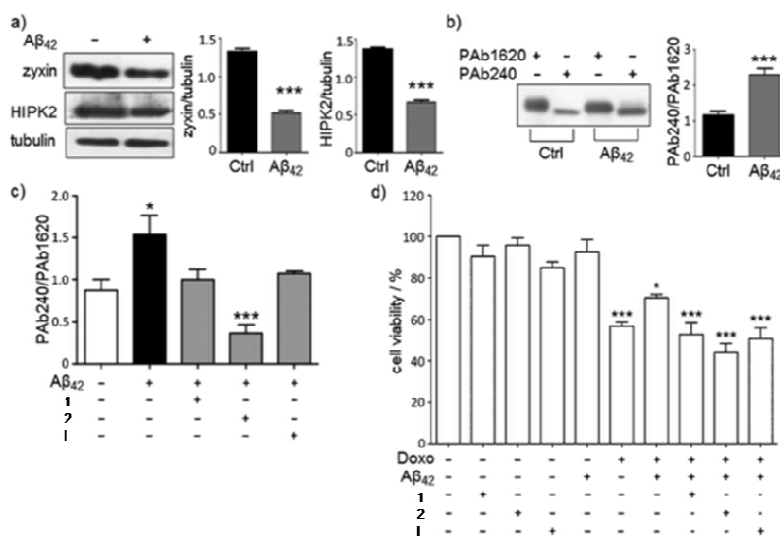


**Figure 2.11.** Compounds **I**, **1** and **2** positively modulate alterations in the zyxin–HIPK2–p53 pathway mediated by soluble sub-lethal levels of A $\beta$ <sub>42</sub>. **a)** Total cell extracts of SH-SY5Y cells treated with 10 nM A $\beta$ <sub>42</sub> for 48 h were analyzed for zyxin and HIPK2 expression. Anti-tubulin was used as the protein loading control. **b)** SHSY5Y cell lysates were immunoprecipitated with PAb240 or PAb1620 antibody. Immunoprecipitates were analyzed by western blot with the CM1 polyclonal anti-p53 antibody. **c)** Total cell extracts of SH-SY5Y cells incubated for 48 h with 10 nM A $\beta$ <sub>42</sub> and then treated with 5  $\mu$ M compounds **I**, **1** and **2** for 24 h were analyzed for the conformational state of p53. Cell lysates were immunoprecipitated with PAb240 or PAb1620 antibody. Immunoprecipitates were analyzed by western blot with the CM1 polyclonal anti-p53 antibody. After densitometric analysis, data were expressed as integrated density of the ratio of PAb240/PAb1620 antibodies signal and represent the mean. SEM of at least three independent experiments; \* $p < 0.05$ , \*\*\* $p < 0.001$  versus A $\beta$  treatment; Tukey’s multiple comparison test. **d)** SH-SY5Y cells were incubated with 10 nM A $\beta$ <sub>42</sub> for 24 h and then treated for an additional 24 h with compounds **I**, **1** and **2** at 5  $\mu$ M. Cells were then resuspended in fresh medium and finally exposed to 0.5  $\mu$ M doxorubicin for 24 h. Cell viability was determined by MTT assay. Data are expressed as percentage cell viability versus control; \* $p < 0.05$ , \*\*\* $p < 0.001$  versus control; Bonferroni multiple comparison test<sup>237</sup>.

In conclusion, in the present study a preliminary small set of nature-inspired multifunctional ligands **I**, **1** and **2** was synthesized and investigated aiming to a deeper comprehension of A $\beta$  functions and causative role in AD. These structures represent a noteworthy chance to gain insight the cross-talk between oxidative damage and A $\beta$  pathways, with p53 emerging as a possible mediator of this functional interplay.

Interestingly, compound’s pharmacological profile was strategically tuned by the hydroxyl substituents on the aromatic moiety. Notably, out of the three synthesized derivatives, only catechol **I** inhibited A $\beta$  fibrils formation, underling the importance of the catechol group. By acting at the early stage of amyloid aggregation, **I** strongly prevented the formation of cytotoxic stable oligomeric intermediates. Conversely, although to a different extent, all hybrids were able to decrease ROS formation and inhibit A $\beta$ -induced p53 conformational changes, with the stronger

antioxidant **2**, which lacks anti-aggregating properties, being significantly more effective. These findings suggest the involvement of radical species in the loss of p53 conformation and function induced by subtoxic A $\beta$ . Most importantly, they also point to the newly synthesized multifunctional molecules as promising pharmacologic instruments to shed light on the interconnection between the overproduction of radical species and A $\beta$  as well as molecular mechanisms potentially involved in chronic A $\beta$  injuries.

### A rational approach for targeting Nrf2/A $\beta$ connection in AD (compounds II-VI and 3-9)

Given the particular interest into the cross-talk between amyloid and oxidative stress, we went further in the search for versatile tools to investigate the molecular mechanisms potentially involved in chronic A $\beta$  damage. In particular, the focus moved towards the possibility to analyze and/or modulate the A $\beta$ /Nrf2 *liaison* in order to get a better understanding of this intricate scenario. Based on the previous identification of a small set of nature-inspired ligands (**I**, **1** and **2**) exerting a peculiar “on-off” pattern of control of the anti-aggregating efficacy<sup>237</sup>, SAR of compounds **II-VI** and **3-9** have been delineated by investigating antioxidant and anti-aggregating properties. Herein, derivative **I** has represented the driving motif for systematic modifications.

Initially, a cell viability assay was performed exposing SH-SY5Y human neuroblastoma cells to compounds **II-VI** and **3-9** (Fig. 2.12).

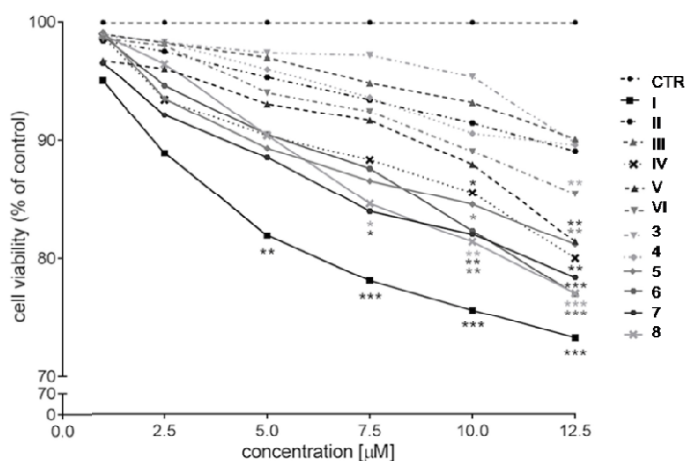


**Figure 2.12.** Cellular toxicity of compounds **II-VI**, **3-9** on human neuroblastoma SH-SY5Y cells. Concentration-dependent cell toxicity profile for reference compound **I** is also showed. Cells were treated with 1  $\mu$ M, 2.5  $\mu$ M, 5  $\mu$ M, 7.5  $\mu$ M, 10  $\mu$ M and 12.5  $\mu$ M of each compound for 24 h. Cell viability was assessed by MTT assay. Data are expressed

as percentage of cell viability versus CTR; \*  $p < 0.05$ , \*\* $p < 0.01$ , \*\*\* $p < 0.001$  versus CTR; Dunnett's multiple comparison test. *The assays were performed by Prof. C. Lanni's research group, University of Pavia, Italy.*

As shown in figure 2.12, all the compounds were well tolerated (reduction of cell viability of about 10%) at a concentration up to 5  $\mu\text{M}$ , resulting significantly less toxic than prototype **I**, that at this concentration determined a slight decrease (about 20%) of cell viability.

As previously seen, derivative **I** was identified as a good inhibitor of  $\text{A}\beta_{42}$  self-aggregation. Its anti-aggregating profile seemed to be strictly related to the catechol moiety, as a complete loss of efficacy was observed following single removal of the *m*- or *p*-hydroxyl function. Starting from this result, the inhibition of  $\text{A}\beta_{42}$  self-aggregation of newly synthesized compounds was assessed to corroborate the importance of the catechol group in anti-amyloid efficacy (Table 2.2).

<i>Compd</i>	% inhibition ( $\pm$ SEM) [I] = 50 $\mu\text{M}$	$\text{IC}_{50}$ $\mu\text{M}$ ( $\pm$ SEM)
<b>I</b>	> 90%	12.5 $\pm$ 0.9
<b>II</b>	< 10 %	nd
<b>III</b>	< 10 %	nd
<b>IV</b>	< 10 %	nd
<b>V</b>	68.8 $\pm$ 7.9	34.6 $\pm$ 6.8
<b>VI</b>	36.3 $\pm$ 7.6	nd
<b>3</b>	< 10%	nd
<b>4</b>	< 10%	nd
<b>5</b>	> 90%	8.72 $\pm$ 0.61
<b>6</b>	49.1 $\pm$ 6.3	nd
<b>7</b>	> 90%	3.99 $\pm$ 0.39
<b>8</b>	> 90%	3.80 $\pm$ 0.44

**Table 2.2.** Inhibition of  $\text{A}\beta_{42}$  50  $\mu\text{M}$  self-aggregation by compounds I-VI and 3-8 at [Inhibitor] = 50  $\mu\text{M}$ . The  $\text{A}\beta_{42}$ /inhibitor ratio was equal to 1/1. For compounds showing a % inhibition higher than 50% when screened at 50  $\mu\text{M}$  the  $\text{IC}_{50}$  value was determined. Values are the mean of two independent experiments each performed in duplicate. nd stands for not determined. SEM = standard error of the mean. *The assays were performed by Prof. M. Bartolini's research group, University of Bologna, Italy.*

As depicted in Table 2.2, the removal or masking into a methoxy- or ethoxy-function of one or both the hydroxyl substituents of **I** resulted in a complete loss of anti-aggregating efficacy (compounds **II-IV**, **3**, **4**), highlighting the importance of catechol moiety. Focusing then on thioester function, it emerged that replacement of this moiety with an ester or an amide, affording compounds **V** and **VI**, respectively, resulted in a gradual decrease in the ability of limiting fibril formation (Table 2.2). This finding suggest that the thioester moiety is a second requisite of relevance to guarantee anti-aggregating efficacy. For compound **5**, where saturation of the cinnamoyl double bond avoids conjugation of the catechol moiety and the thioester function, a slight increase in activity is observed with respect to prototype **I**, suggesting that no electronic influence between the two groups is required. Conversely, when the conjugation persists but the distance is shortened, as in **6**, a significant drop in activity is detected (Table 2.2), revealing the importance of the relative position of the catechol group and the thioester side chain in amyloid recognition. Interestingly, the anti-aggregating effect was even higher when the terminal allyl moiety of most active compounds **I** and **6** was replaced with an alkyl function, affording **7** and **8**, respectively (Table 2.2). This modification, in addition to potentiating prototype's efficacy, opens perspectives for further functionalization in this position as a promising multitarget drug discovery strategy.

Following the data on ThT assay, the more active compound **8** was studied to assess the ability of exert neuroprotective effect against A $\beta$ <sub>42</sub>-induced toxicity in SH-SY5Y human neuroblastoma cells, using **I** as the reference compound. According to previous data, **I** was able to prevent A $\beta$ <sub>42</sub> cytotoxicity only when used at 10  $\mu$ M. Compound **8** showed a strong protective effect as at 5  $\mu$ M almost completely prevented the A $\beta$ <sub>42</sub>-induced cell death, resulting to be more effective than **I** (Fig. 2.13). These data are in agreement with the inhibitory potency (as IC<sub>50</sub> values) determined by ThT-based assay, which showed a 3.3-fold higher anti-aggregating activity for **8** compared to **I** (Table 2.2).

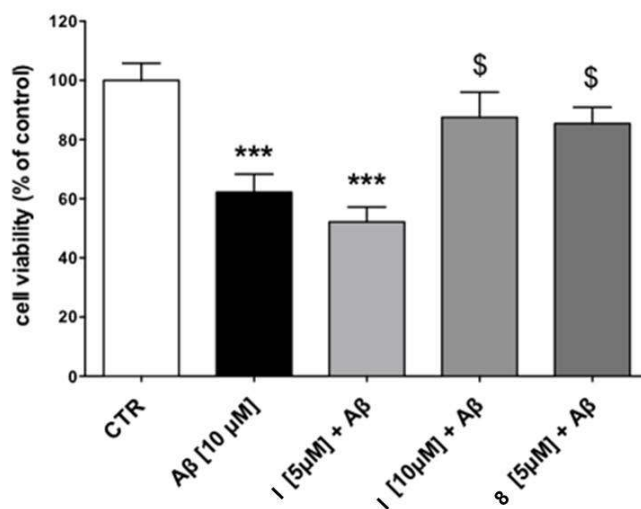


**Figure 2.13.** Effect of **I** and **8** on Aβ<sub>42</sub>-mediated toxicity in neuroblastoma cells. SH-SY5Y cells were co-incubated for 24 h with 5 μM and 10 μM compound **I** or with 5 μM compound **8** in presence of 10 μM Aβ<sub>42</sub>. Cell viability was determined by MTT assay. Data are expressed as percentage of cell viability versus CTR; \*\*\*p<0.001 versus CTR, § p<0.05 versus Aβ<sub>42</sub>; Dunnett's multiple comparison test. The assays were performed by Prof. C. Lanni's research group, University of Pavia, Italy.

To determine the potential interest of compounds **II-VI** and **3-8** as antioxidants their scavenger ability was evaluated when co-incubated with 300 μM H<sub>2</sub>O<sub>2</sub>, using prototype **I** as comparison.

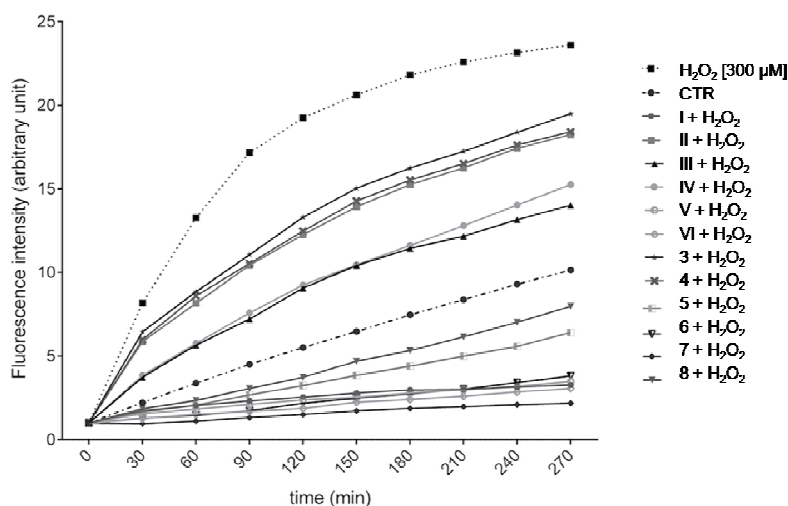


**Figure 2.14.** Compounds **I-VI** and **3-8** reverse ROS formation induced by H<sub>2</sub>O<sub>2</sub>-induced oxidative stress in SH-SY5Y neuroblastoma cells. Cells were loaded with 25 μM DCFH-DA for 45 min. DCFH-DA was removed by centrifugation, cells were resuspended in PBS into a black 96-wells plate and exposed to 5 μM concentration of compounds **I-VI** and **3-8** and 300 μM H<sub>2</sub>O<sub>2</sub>. ROS levels were determined from 0 to 270 min using a fluorescence microplate reader. Fluorescence intensity for all compounds is significant at any time from 30 to 270 min with p<0.001 versus H<sub>2</sub>O<sub>2</sub>.

Dunnett's multiple comparison test. *The assays were performed by Prof. C. Lanni's research group, University of Pavia, Italy*

Treatment with all compounds significantly suppressed H<sub>2</sub>O<sub>2</sub>-induced intracellular ROS production, albeit to a different extent. In particular, catechol-based derivatives **I**, **V**, **VI**, and **5-8** emerged as the most potent antioxidants as, at any time tested, they were able to keep ROS levels below those observed for control (Fig. 2.14). This strong antioxidant activity was particularly evident for compounds where conjugation between the catechol moiety and the carbonyl function (**I**, **V**, **VI**, **6** and **7**) occurs, while compounds **5** and **8**, lacking the cinnamoyl double bond, were slightly less effective.

Based on the (pro)electrophilic features of synthesized compounds, a number of catechol-based derivatives were selected to be studied as Nrf2 inducers. The catechol group represented a prerequisite for exploring the amyloid/Nrf2 cellular network due to its "on-off" control of anti-aggregating activity. Moreover, catechols, which become active *ortho*-quinones on oxidation, prospect benefits of proelectrophiles, which should provide neuroprotection in oxidative conditions<sup>219</sup>. In addition, catechol-bearing compounds **I**, **V**, **VI**, and **5-8** can count on more favorable scavenger abilities (as underpinned by their ability to reverse H<sub>2</sub>O<sub>2</sub>-induced ROS formation), which can significantly contribute to the overall antioxidant profile of the new molecules. Some of the selected compounds also presented an electrophilic  $\alpha,\beta$ -unsaturated carbonyl group (Michael acceptor functionality), which may represent an additional source for Nrf2 activation. To discriminate the individual contribution of the two (pro)electrophilic features, compound **III**, where the Michael acceptor is not associated to the catechol moiety, and a new compound (**9**) lacking both electrophilic functionalities (purposely synthesized) were tested for comparison. Nrf2 protein levels were evaluated by western immunoblotting in SH-SY5Y cells after treatment for 24 h with compounds **I**, **III**, **V**, **VI**, and **5-9** at 5  $\mu$ M concentration. Interestingly, all compounds with the exception of **9** increased Nrf2 levels when compared to control (Fig. 2.15), suggesting that Nrf2 modulation can be driven by both the catechol function and the  $\alpha,\beta$ -unsaturated carbonyl group, while the other structural features seemed to have modest relevance in this respect. In particular, differently from what observed for the anti-aggregating activity, the thioester group is not a key feature for inducing Nrf2 activation, as demonstrated by the strong efficacy elicited by ester derivative **V**. The lack of efficacy observed for compound **9** suggests that nucleophilic addition

of Keap1 cysteine residues to (pro)electrophilic portions of the molecule may represent the initiating event of the transcriptional process.

Total Nrf2 protein expression levels										
	CTR	I	III	V	VI	5	6	7	8	9
<b>Nrf2/ tubulin</b>	100,0	411,3	339,9	383,1	188,0	372,3	198,7	231,5	367,3	138,7
<b>SEM</b>	7,835	42,60	43,64	28,51	21,18	58,03	28,04	15,89	63,32	14,44
<b>P-value</b>	/	< 0,0001	< 0,0001	< 0,0001	0,5640	0,0002	0,4378	0,1617	< 0,0001	0,9813

**Figure 2.15.** Activation of Nrf2-mediated phase II detoxification pathway. Total cellular extracts of SH-SY5Y cells treated for 24 h with 5 $\mu$ M concentration of compounds **I**, **III**, **V**, **VI**, and **5-9** were analyzed for Nrf2 expression by western blot. Anti tubulin was used as protein loading control. Results are shown as ratio Nrf2/tubulin (% of CTR)  $\pm$  SEM. Dunnett's multiple comparison test. *The assays were performed by Prof. C. Lanni's research group, University of Pavia, Italy.*

Thus, the attention was paid on the activation of Nrf-2 signalling by analyzing its translocation into nucleus and its ability to induce NQO1, a prototypical cytoprotective Nrf2-target gene related to cellular stress response. In particular, compounds **I**, **III**, **V**, **5** and **8**, have been assayed, which increased significantly the protein levels of Nrf2, carrying alternatively or simultaneously the two (pro)electrophilic features responsible for Nrf2 induction. Compound **9** was also tested as negative control. All compounds, with the only exception of **9**, induced remarkable Nrf2 nuclear translocation, with catechol derivatives **I**, **V**, **5** and **8** being slightly more effective than **III**, lacking the catechol moiety (Fig. 2.16a). Moreover, when analyzing the induction of NQO1, all the compounds but **9** increased NQO1 levels, with the same trend of activity detected for Nrf2 activation and translocation to the nucleus (Fig. 2.16b). Noteworthy, the combined presence of the two (pro)electrophilic features, as in **I**, did not result in a synergistic efficacy (compare activity of **I** with that of **5** and **8**, which only carry the catechol group). This can be possibly ascribed to the conjugation, occurring in **I**, between the two features, that consequently may not behave as separate entities.

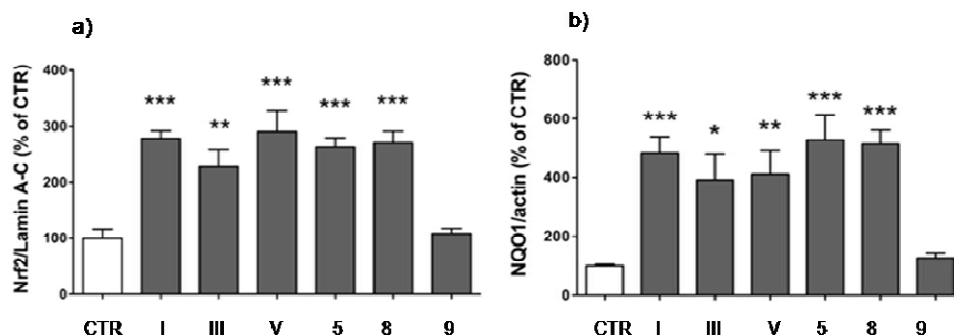


**Figure 2.16.** Activation of Nrf2-mediated phase II detoxification pathway. **a)** Nuclear cellular extracts of SH-SY5Y cells were treated for 3 h with compounds **I**, **III**, **V**, **5**, **8**, and **9** at 5  $\mu$ M concentration and homogenized to obtain nuclear fraction. Nrf2 expression was determined by western blot. Anti lamin A-C was used as protein loading control. Results are shown as ratio Nrf2/lamin A-C (% of CTR)  $\pm$  SEM. \*\* $p$ <0.01 and \*\*\* $p$ <0.001 versus CTR; Dunnett's multiple comparison test. **b)** Total cellular extracts of SH-SY5Y cells treated for 24 h with 5  $\mu$ M concentration of compounds **I**, **III**, **V**, **5**, **8**, and **9** were analyzed for NQO1 expression by western blot. Anti-actin was used as protein loading control. Results are shown as ratio NQO1/actin (% of CTR)  $\pm$  SEM. \* $p$ <0.05, \*\* $p$ <0.01 and \*\*\* $p$ <0.001 versus CTR; Dunnett's multiple comparison test. *The assays were performed by Prof. C. Lanni's research group, University of Pavia, Italy.*

In conclusion, in the present work SAR studies on the catechol derivative **I** have been expanded through systematic modifications of its structure, with the aim to obtain more effective anti-aggregating and antioxidant properties. Based on the growing evidence that an alteration of the Nrf2-mediated antioxidant response is reported to involve the toxic amyloid peptide, we investigated the antioxidant profile of the compounds by analyzing their ability to trigger the Nrf2 pathway in terms of up-regulation of Nrf2 expression, translocation into the nucleus and induction of the Nrf2-dependent defensive gene NQO1.

Interestingly, in SH-SY5Y neuroblastoma cells, all compounds tested exerted remarkable free radical scavenging properties and protected against oxidative stress through electrophilic activation of Nrf2-mediated response. This multimodal profile was accompanied by a significant reduction of the cytotoxicity with respect to **I**.

Regarding the needed requisites for A $\beta$  recognition, the catechol function and the thioester group were identified as driving forces of anti-aggregating efficacy. In particular, compound **8** emerged above others, that joined the above-mentioned antioxidant effects to a marked ability of preventing the formation of cytotoxic stable oligomeric intermediates, being significantly more effective than prototype **I**. Most importantly, different chemical features were necessary to regulate Nrf2 and A $\beta$  activities, allowing us to distinctly tune the two pathways. These findings point to compound **8** and

its derivatives as powerful tools for investigating the therapeutic potential of the Nrf2/A $\beta$  cellular network in AD.

Moreover, ongoing studies on isosteres **10-17** should allow us to shed light on the molecular mechanism whereby these promising tools would interact with A $\beta$  and to identify the needed residues of the inhibitors that are involved in amyloid recognition.

## 2.2 Design of MTDLs Combining Anti-aggregating and Antioxidant Profile with NMDAR Antagonism

The growing comprehension of the molecular mechanisms responsible for etiology and progression of AD underpinned how the “one-molecule, one-target” paradigm is *per se* not sufficient to face and overcome the complexity of the disease, due to the multiple crossroads between different pathways involved in the progression and cognitive decline of AD. Besides the consolidated evidence that A $\beta$  triggers the disease process by stimulating ROS overproduction and promoting neurotoxicity, a correlation among the toxic amyloid peptide, oxidative stress and excitotoxic neuronal injury, that can ultimately lead to cell death, is well established.

The prolonged activation of NMDARs due to the persisting of glutamate in the synaptic clefts results into a massive influx of Ca<sup>2+</sup> into the cells through the receptor’s associated ion channels. This leads to the production of damaging ROS and RNS, and activation of proteolytic processes responsible to contribute to the cascade of events leading to neuronal loss. In particular, oxidative stress and increased intracellular Ca<sup>2+</sup> levels generated in response to A $\beta$  insults have been shown to enhance glutamate-related neurotoxicity. Indeed, several evidence suggest a direct effect of A $\beta$  on NMDARs responses, thus enhancing excitotoxicity<sup>40</sup>. A $\beta$  is responsible for increasing extracellular glutamate and its presynaptic release, and, among other factors, is related to the impairment of neuronal functions and synaptic plasticity, suggesting an involvement of glutamate system on its-induced toxicity.

Whit these concepts in mind, the proposal of effectively counteract AD by acting on different targets relevant for the disease, exploiting a combination therapy or a single molecule able to interact with multiple targets in a parallel fashion, might be an helpful strategy to better understand and prevent the progression of the disease. Therefore, MTDLs approach in drug discovery and development programs is being more and more pursued, aiming to identify single molecules able to hit altogether several targets.

In this respect, the analysis of these information prompted us to design and synthesized multifunctional ligands that would join NMDAR antagonism to antioxidant and anti-aggregating properties (Fig. 2.17).

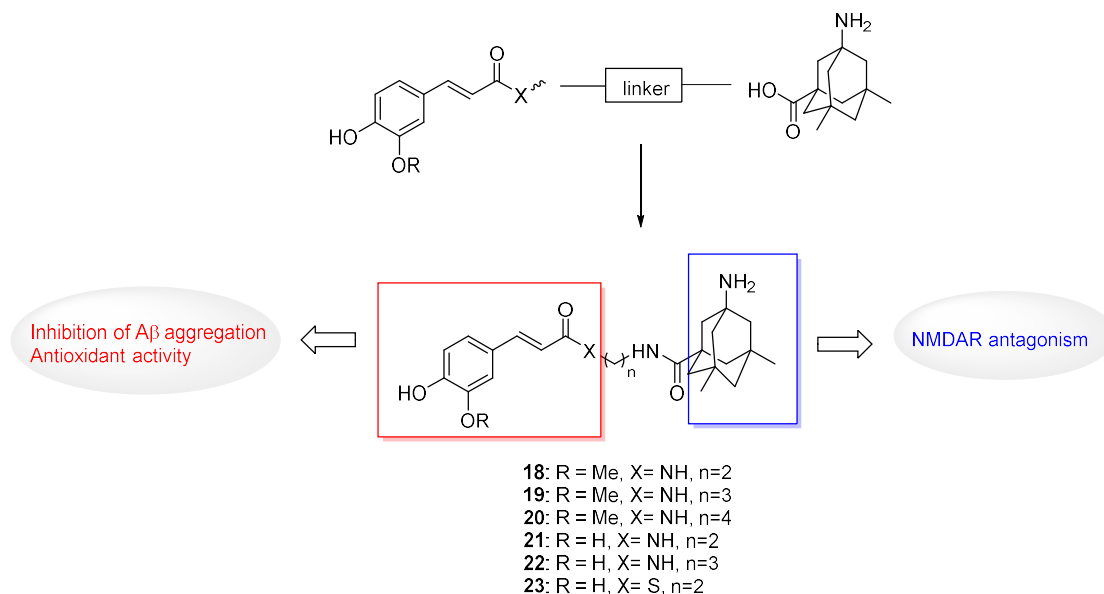


**Figure 2.17.** Drug design of MTDLs **18-23**.

Based on our previous SAR studies of a set of nature-inspired multifunctional ligands, we selected two compounds, **I** and **VI** (Fig. 2.1, Table 2.1), with an intriguing multimodal profile. Albeit to a different extent, they were able to inhibit A $\beta$ <sub>42</sub> self-aggregation and to counteract oxidative stress by reducing ROS formation in neuroblastoma cells. In particular, compound **I** showed a good anti-aggregating profile with an IC<sub>50</sub> value of 12.5 ± 0.9 μM, which is similar to that of the well known multipotent compound bis(7)tacrine (IC<sub>50</sub> = 8.4 ± 1.4 μM). Taking inspiration from nature, we also chose ferulic acid that can exert its antioxidant properties both as direct scavenger of free radicals and through activation of Nrf2-ARE pathway.

In order to join the multiple hydroxycinnamic derivatives' activities to an effective NMDAR antagonism, we focused our attention on memantine, currently one of the four drugs approved from U.S. FDA for AD treatment. To preserve its bridgehead amine free, that is protonated under physiological conditions and is responsible for the biological activity by binding at or near Mg<sup>2+</sup> site in the NMDAR-associated channel, the adamantane structure was functionalized with carboxylic function, thus allowing the conjugation with pharmacophores by means of different length spacers. Memantine is a low affinity, open-channel blockers that enters the channel preferentially when it is pathologically activated for long periods of time<sup>40</sup>. This peculiar pharmacologic profile allows memantine to interact with extrasynaptic NMDARs, that are hyperactivated under pathological

conditions and promoted cell death through, among others, a mechanism involving ROS production<sup>249</sup>. Driven by memantine in the achievement of NMDARs at extrasynaptic sites, MTDLs **18-23** should exert a strengthened pharmacological profile together with a site-specific mode of action.

## 2.2.1 METHODS: Chemistry and Biology

### Chemistry

Syntheses of compounds **18-23** were outlined according to Schemes 5-7.

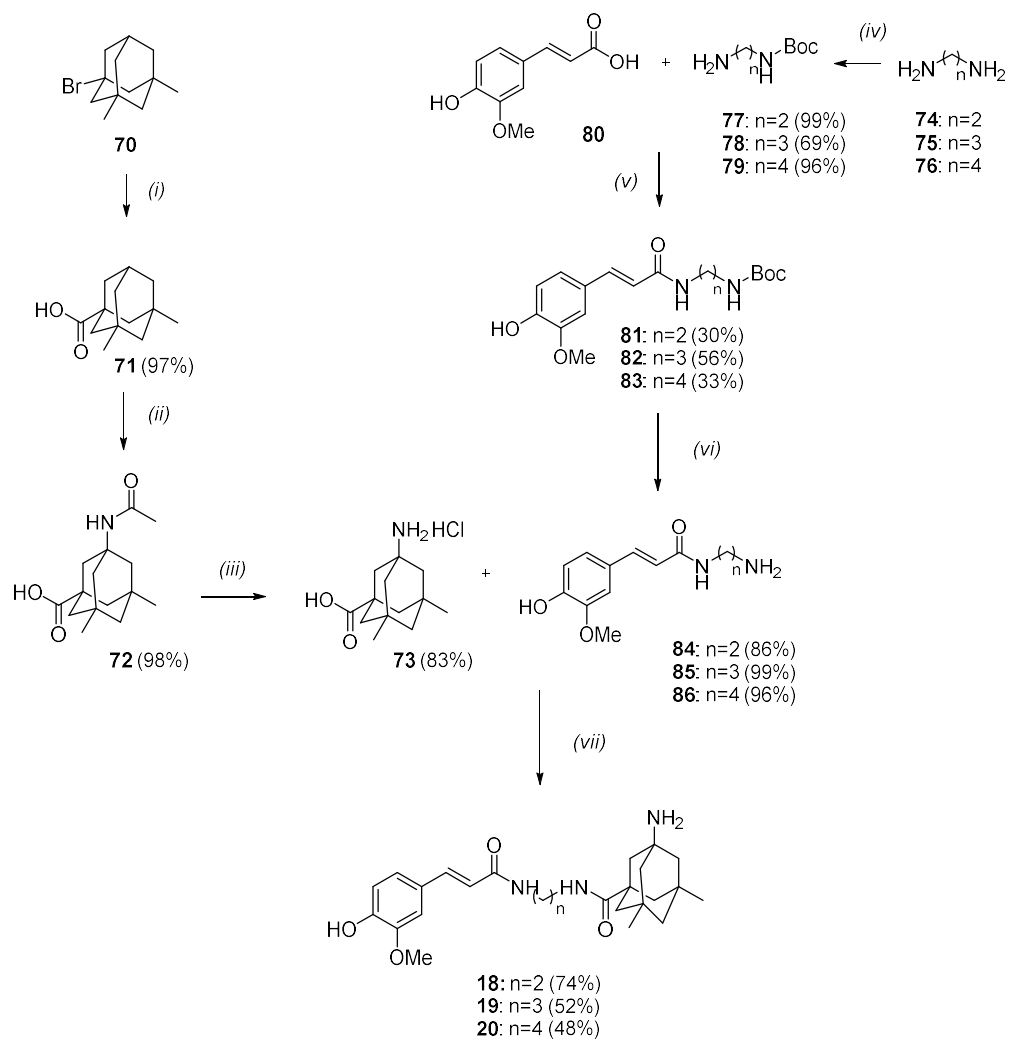
The synthesis of the key intermediate **73** as hydrochloride salt, in which the primary amine has to be unmasked, was the common point of all synthetic routes (Scheme 5). A Ritter-type protocol was set out that allows for *direct* C–H bond amidation of the adamantane fragment<sup>250</sup>. In order to activate the adamantane tertiary C–H bonds, a mixture of nitrating acid (HNO<sub>3</sub>/H<sub>2</sub>SO<sub>4</sub>) has been used, so that under these conditions the key single electron oxidizer NO<sub>2</sub><sup>+</sup> is generated in situ. This procedure yields a “(radical)cation solution” that can be quenched with the nucleophile acetonitrile, affording adamantane acetamide (**72**) in good yield. Finally, hydrolysis of **72** afforded 1-amino-3,5-dimethyladamantane (**73**).

Compounds **18-20** in which ferulic acid was conjugated with memantine were prepared following the synthetic route described in Scheme 5. The appropriate partially Boc-protected diamine (**77-79**), having only one primary amine free, was condensed with commercially available ferulic acid **80** in presence of EDC and HOBt to give intermediates **81-83**. Cleavage of protecting group in presence of acidic conditions afforded compounds **84-86**, that following conjugation with **73** afforded final compounds **18-20**.

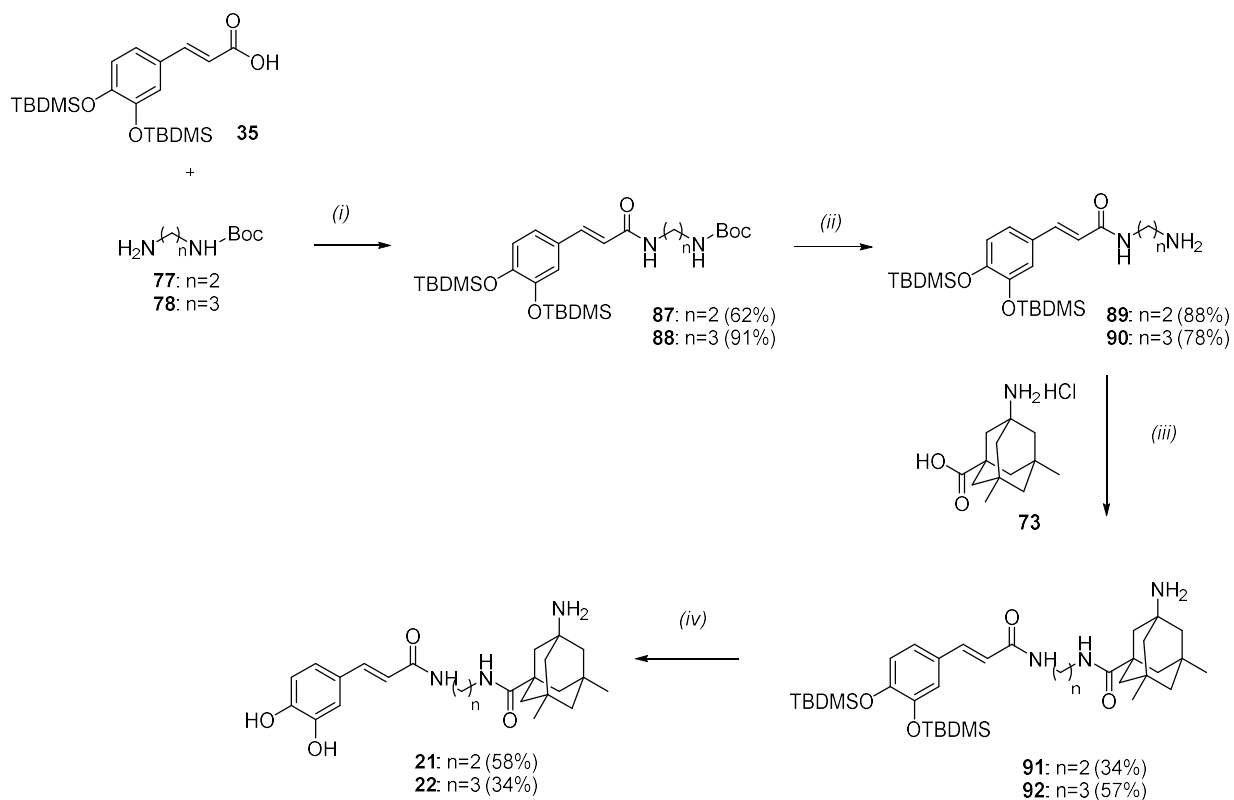
Syntheses of caffeic acid derivatives **21** and **22** was outlined in Scheme 6. TBDMS-protected acid **35** was condensed with the appropriate mono-protected amine (**77-78**) to afford intermediates **89-90** following removal of Boc-protecting group. Conjugation of **73** with **89-90** and subsequent desilylation of alcoholic functions in presence of acetyl chloride (AcCl) afforded final compounds **21-22**.

Synthesis of thioester derivative **23** was performed according to Scheme 7. Selective *S*-trityl protection of cysteamine hydrochloride, performed and optimized with microwave assisted

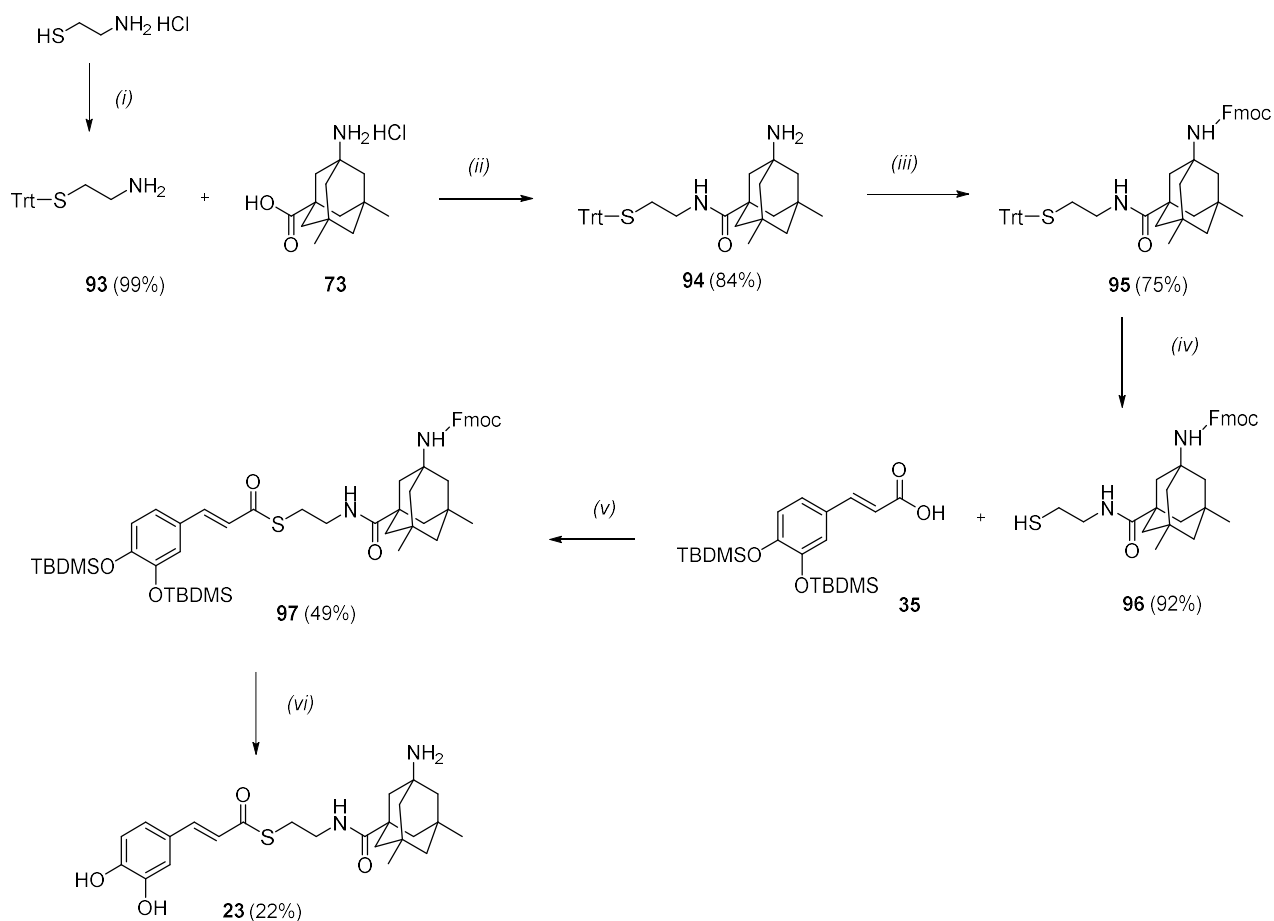
synthesis, followed by amidation reaction in presence of **73** gave the intermediate **94** that was *N*-protected with 9-fluorenylmethoxycarbonyl (Fmoc)-protecting group in order to limit undesired side products and avoid the intramolecular *S*- to *N*-acyl migration in further reaction conditions. Detritylation of thioether **95** in presence of trifluoroacetic acid (TFA) and triethylsilane (Et<sub>3</sub>SiH) afforded the intermediate **96** with the free thiol function that was readily condensed with TBDMS-protected caffeic acid (**35**) to gave intermediate **97**. Finally, the simultaneous cleavage of both TBDMS- and Fmoc-protecting groups in presence of TBAF afforded in one step reaction the final compound **23** after treatment with (benzotriazol-1-yloxy)tris(dimethylamino)phosphonium hexafluorophosphate (BOP) reagent in order to remove quaternary ammonium salts impurities.



**Scheme 5.** Reagents and conditions: (i) formic acid,  $\text{H}_2\text{SO}_4$ , 5 h, then o/n at  $4^\circ\text{C}$ ; (ii)  $\text{HNO}_3$ ,  $\text{H}_2\text{SO}_4$ , oleum, then  $\text{CH}_3\text{CN}$ , 12 h,  $0^\circ\text{C}$ -rt; (iii)  $\text{HCl}$  12 N, reflux, 80 h; (iv)  $\text{Boc}_2\text{O}$ ,  $\text{CH}_2\text{Cl}_2$ , 12 h,  $0^\circ\text{C}$ -rt; (v) EDC, HOBT, DMF,  $\text{Et}_3\text{N}$ ,  $\text{N}_2$ , 12 h,  $0^\circ\text{C}$ -rt; (vi)  $\text{HCl}$  4 M in dioxane,  $\text{CH}_2\text{Cl}_2$ , 90',  $0^\circ\text{C}$ -rt; (vii) EDC, HOBT, DMF,  $\text{N}_2$ , 36 h,  $0^\circ\text{C}$ -rt.



**Scheme 6.** Reagents and conditions: (i) EDC, HOBT, DMF,  $\text{Et}_3\text{N}$ ,  $\text{N}_2$ , 24 h,  $0^\circ\text{C}$ -rt; (ii) HCl 4 M in dioxane,  $\text{CH}_2\text{Cl}_2$ ,  $90^\circ$ ,  $0^\circ\text{C}$ ; (iii) EDC, HOBT, DMF,  $\text{N}_2$ , 36 h,  $0^\circ\text{C}$ -rt; (iv) MeOH, AcCl,  $0^\circ\text{C}$ , 1h.



**Scheme 7.** Reagents and conditions: (i) TrCl, DMF, 60°C, 20', MW; (ii) EDC, HOBT, DMF, N<sub>2</sub>, 36 h, 0°C-rt; (iii) Fmoc-Cl, CH<sub>2</sub>Cl<sub>2</sub>, aq. Na<sub>2</sub>CO<sub>3</sub> 10%, 1.5 h, 0°C-rt; (iv) TFA, Et<sub>3</sub>SiH, CH<sub>2</sub>Cl<sub>2</sub>, 10'; (v) EDC, HOBT, DIPEA, DMF, N<sub>2</sub>, 3 h, 0°C-rt; (vi) TBAF, THF, N<sub>2</sub>, 1 h, then BOP reagent in CH<sub>2</sub>Cl<sub>2</sub>, 30'.

## Biology

Compounds **18-23** are currently in ongoing studies to assess their ability to inhibit amyloid aggregation by a fluorescence-based assay.

The ability of counteracting H<sub>2</sub>O<sub>2</sub>-induced oxidative stress in neuroblastoma cells will also be assessed by using the fluorescent probe DCF-DA as a specific marker for quantitative intracellular ROS formation.

In parallel, to verify the capability of **18-23** to join the anti-aggregating/antioxidant activity to the neuroprotective effect of NMDA antagonists, they have been studied at recombinant NMDARs, heteromeric assemblies composed of three different subunits, NR1, NR2, and occasionally NR3, most of them probably comprising two NR1 and two NR2 (NR2A-D) subunits. In particular, the activity profile of **18-23** was evaluated at NR1/NR2A NMDARs expressed by *Xenopus laevis* oocytes, using memantine as the reference compound.

### 2.2.2 Conclusions

Over the years, research interest in MTDL design laid the foundations for discovery of several MTDLs to combat neurodegenerative diseases, including AD. In the present study, the MTDL approach allowed us to rationally design compounds **18-23** by integrating synergistic fragments into a new single chemical entities, with the aim to endow them with anti-aggregating and/or antioxidant efficacy with NMDAR blocking activity.

Currently, we are waiting for anti-aggregating efficacy of synthesized compounds, with special attention on the most promising derivative **23**, being confident that the biological profile of the parent compound **I** may be preserved. Moreover, conveyed by memantine in reaching extrasynaptic NMDARs, synthesized compounds should hopefully exert an antioxidant site-specific activity, in addition to NMDAR antagonism.

## Chapter 3

### Experimental section

#### 3.1 Chemistry

**General Chemical methods.** Chemical reagents were purchased from Sigma Aldrich, Fluka and Lancaster (Italy). Melting points were taken in glass capillary tubes on Buchi SMP-20 apparatus and are uncorrected. Nuclear magnetic resonance spectra (NMR) were recorded at 400 MHz for  $^1\text{H}$  and 100 MHz for  $^{13}\text{C}$  on Varian VXR 400 spectrometer. Chemical shifts are reported in parts per millions (ppm) relative to tetramethylsilane (TMS), and spin multiplicities are given as s (singlet), br s (broad singlet), d (doublet), dd (double doublet), t (triplet), q (quartet), or m (multiplet). Direct infusion ESI-MS mass spectra were recorded on a Waters ZQ 4000 apparatus. Microwave assisted synthesis was performed by using CEM Discover® SP apparatus (2.45 GHz, maximum power of 300W). Chromatographic separations were performed on silica gel columns by flash (Kieselgel 40, 0.040-0.063 mm, Merck) chromatography. Reactions were followed by thin-layer chromatography (TLC) on Merck (0.25 mm) glass-packed precoated silica gel plates (60 F254), then visualized in an iodine chamber or with an UV lamp or  $\text{KMnO}_4$ . Compounds were named following IUPAC rules as applied by ChemBioDraw Ultra (version 15.1). Final compounds **1-17** were >95% pure as determined by HPLC analyses. The analyses were performed under reversed-phase conditions on a Phenomenex Jupiter C18 (150x4.6 mm I.D.) column, using as the mobile phase a binary mixture of  $\text{H}_2\text{O}$ /acetonitrile (60/40, v/v for **1, 2**; 30/70, v/v for **3, 4**; 50/50, v/v for **5, 8, 9, 12-17**; 65/35, v/v for **6, 7, 10, 11**) with UV detection at  $\lambda = 302$  nm (for **1-4, 6, 7, 10-15**) or 254 nm (for **5, 8, 9, 16, 17**) and a flow rate of 0.7 mL/min. Analyses were performed on a liquid chromatograph model PU-1585 UV equipped with a 20  $\mu\text{L}$  loop valve (Jasco Europe, Italy).

**General procedure for compounds 3 and 4.** To a solution of Meldrum's acid (1 equiv, 4.05 mmol) in toluene (8 mL) was slowly added 2-propen thiol (1 equiv, 4.05 mmol). The mixture was refluxed for 7 h. After the formation of the intermediate, the reaction was cooled to room temperature followed by sequential addition of the appropriate aldehyde (0.4 equiv, 1.6 mmol), pyridine (400  $\mu$ L) and piperidine (40  $\mu$ L). The stirring continued at room temperature 4 days. Following evaporation of the solvent, the residue was purified by column chromatography on silica gel to yield the desired cinnamic derivatives **3** and **4**.

**S-allyl (E)-3-(3,4-dimethoxyphenyl)prop-2-enethioate (3).** **3** was synthesized from 3,4-dimethoxybenzaldehyde (266 mg, 1.6 mmol). Elution with petroleum ether/ethyl acetate (7:3) afforded **3** as a white solid: 220 mg (52%), m.p.= 123 °C.  $^1\text{H}$  NMR (400 MHz,  $\text{CDCl}_3$ )  $\delta$  7.57 (d,  $J$  = 16 Hz, 1H), 7.13 (dd,  $^1J$  = 8 Hz,  $^2J$  = 2 Hz, 1H), 7.05 (d,  $J$  = 2 Hz, 1H), 6.86 (d,  $J$  = 8 Hz, 1H), 6.59 (d,  $J$  = 16 Hz, 1H), 5.91-5.84 (m, 1H), 5.29 (d,  $J$  = 19.6, 1H), 5.13 (d,  $J$  = 11.6, 1H), 3.92 (s, 6H), 3.67 (d,  $J$  = 8 Hz, 2H).  $^{13}\text{C}$ -NMR (100 MHz,  $\text{CDCl}_3$ )  $\delta$  188.88, 151.44, 149.25, 140.77, 133.21, 126.95, 123.26, 122.58, 117.86, 111.04, 109.74, 55.98 (2 C), 31.71. MS [ $\text{ESI}^+$ ]  $m/z$  265 [ $\text{M}+1$ ] $^+$ .

**S-allyl (E)-3-(3,4-diethoxyphenyl)prop-2-enethioate (4).** **4** was synthesized from 3,4-diethoxybenzaldehyde (314 mg, 1.6 mmol). Crystallization from ethanol gave **4** as a white solid: 220 mg (47%), m.p. =145 °C;  $^1\text{H}$  NMR (400 MHz,  $\text{CDCl}_3$ )  $\delta$  7.53 (d,  $J$ =15.6 Hz, 1H), 7.09-7.05 (m, 2H), 6.83 (d,  $J$ =8 Hz, 1H), 6.57 (d,  $J$ =15.6 Hz, 1H), 5.89-5.83 (m, 1H), 5.27 (d,  $J$ =17.2 Hz, 1H), 5.11 (d,  $J$ =10.4 Hz, 1H), 4.13-4.08 (m, 4H), 3.66 (d,  $J$ =6.8 Hz, 2H), 1.47-1.44 (m, 6H).  $^{13}\text{C}$ -NMR (100 MHz,  $\text{CDCl}_3$ )  $\delta$  188.76, 151.28, 148.79, 140.90, 133.27, 126.75, 123.21, 122.36, 117.78, 112.63, 112.0, 64.58 (2 C), 31.67, 14.74 (2 C). MS [ $\text{ESI}^+$ ]  $m/z$  315 [ $\text{M}+\text{Na}$ ] $^+$ .

**General procedure for the intermediates 31-37, 53.** To a solution of the appropriate acid **24-30** and **52** (1 equiv) in dry DMF (5 mL) were added TBDMS-Cl (2-3 equiv) and imidazole (5 equiv) under nitrogen atmosphere. After leaving the reaction to room temperature overnight, the mixture was concentrated to dryness, and the residue purified by column chromatography on silica gel to yield the desired intermediates **31-37, 53**. Compounds **24-29** are commercially available; **30** was

synthesized as described in the literature for the synthesis of *trans*-cinnamic acid through the Knoevenagel-Doebner reaction<sup>233</sup>.

**(E)-3-(4-((*tert*-butyldimethylsilyl)oxy)phenyl)acrylic acid (31).** **31** was synthesized from **24** (500 mg, 3.04 mmol). Elution with petroleum ether/ethyl acetate (6:4) afforded **31** as a waxy solid; yield: 466 mg (55%); <sup>1</sup>H NMR (400 MHz, CDCl<sub>3</sub>) δ 7.71 (d, *J* = 16.0 Hz, 1H), 7.45 (d, *J* = 8.0 Hz, 2H), 6.85 (d, *J* = 8.0 Hz, 2H), 6.31 (d, *J* = 16.0 Hz, 1H), 0.99 (s, 9H), 0.23 (s, 6H).

**(E)-3-(3-((*tert*-butyldimethylsilyl)oxy)phenyl)acrylic acid (32).** **32** was synthesized from **25** (500 mg, 3.04 mmol). Elution with petroleum ether/ethyl acetate (7:3) afforded **32** as a waxy solid; yield: 370 mg (44%); <sup>1</sup>H NMR (400 MHz, CDCl<sub>3</sub>) δ 7.72 (d, *J* = 16.0 Hz, 1H), 7.24 (t, *J* = 8.0 Hz, 1H), 7.13 (d, *J* = 8.0 Hz, 1H), 7.00 (s, 1H), 6.87 (d, *J* = 8.0 Hz, 1H), 6.40 (d, *J* = 16.0 Hz, 1H), 0.98 (s, 9H), 0.20 (s, 6H).

**3-(3,4-bis((*tert*-butyldimethylsilyl)oxy)phenyl)propanoic acid (33).** **33** was synthesized from **26** (500 mg, 2.75 mmol). Elution with petroleum ether/ethyl acetate (8:2) afforded **33** as a waxy solid: 1050 mg (93 %); <sup>1</sup>H NMR (400 MHz, CDCl<sub>3</sub>) δ 6.76 (d, *J* = 8 Hz, 1H), 6.69 (s, 1H), 6.65 (d, *J* = 8 Hz, 1H), 2.85-2.84 (m, 2H), 2.66-2.64 (m, 2H), 1.00 (s, 18H), 0.20 (s, 12H). <sup>13</sup>C NMR (100 MHz, CDCl<sub>3</sub>) 179.36, 146.80, 145.42, 133.40, 121.28, 121.16, 121.14, 35.98, 30.05, 26.08 (6 C), 18.56 (2 C), -3.96 (4 C).

**3,4-bis((*tert*-butyldimethylsilyl)oxy)benzoic acid (34).** **34** was synthesized from **27** (500 mg, 3.24mmol). Elution with petroleum ether/ethyl acetate (9:1) afforded **24** as a waxy solid: 830 mg (67%); <sup>1</sup>H NMR (400 MHz, CDCl<sub>3</sub>) δ 7.62-7.57 (m, 2H), 6.85 (d, *J* = 8.4 Hz, 1H), 0.98 (s, 18H), 0.21 (s, 12H). <sup>13</sup>C NMR (100 MHz, CDCl<sub>3</sub>) δ 169.30, 152.45, 147.39, 130.24, 129.56, 121.53, 120.92, 25.08 (6 C), 18.35 (2 C), -3.86 (4 C).

**(E)-3-(3,4-bis((*tert*-butyldimethylsilyl)oxy)phenyl)acrylic acid (35).** **35** was synthesized from **28** (500 mg, 2.78mmol). Elution with petroleum ether/ethyl acetate (8:2) afforded **35** as a waxy solid: 885 mg (78%); <sup>1</sup>H NMR (400 MHz, CDCl<sub>3</sub>) δ 7.67 (d, *J* = 16 Hz, 1H), 7.04 (d, *J* = 8 Hz, 1H), 7.03

(s, 1H), 6.82 (d,  $J = 8$  Hz, 1H), 6.22 (d,  $J = 16$  Hz, 1H), 0.96 (s, 18H), 0.19 (s, 12H).  $^{13}\text{C}$  NMR (100 MHz,  $\text{CDCl}_3$ ) 172.58, 149.84, 147.21, 146.87, 127.66, 122.65, 121.14, 120.58, 114.88, 25.82 (6 C), 18.43 (2 C), -4.09 (4 C).

**3-(4-((*tert*-butyldimethylsilyl)oxy)-3-methoxyphenyl)propanoic acid (36).** **36** was synthesized from **29** (300mg, 1.52mmol). Elution with petroleum ether/ethyl acetate (7:3) afforded **36** as a waxy solid: 220 mg (47 %);  $^1\text{H}$  NMR (400MHz,  $\text{CDCl}_3$ )  $\delta$  6.78 (d,  $J = 8$ Hz, 1H), 6.71 (d,  $J = 1.6$  Hz, 1H), 6.66 (dd,  $^1J = 8$  Hz,  $^2J = 1.6$ , 1H), 3.79 (s, 3H), 2.9 (t,  $J = 8$  Hz, 2H), 2.66 (t,  $J = 8$  Hz, 2H), 1.01 (s, 9H), 0.16 (s, 6H).  $^{13}\text{C}$  NMR (100 MHz,  $\text{CDCl}_3$ )  $\delta$  179.50, 150.93, 143.60, 133.78, 121.00, 120.46, 112.52, 55.60, 36.10, 30.48, 25.87 (3 C), 18.56, -4.51 (2 C).

**3,5-bis((*tert*-butyldimethylsilyl)oxy)benzoic acid (37).** **37** was synthesized from **30** (300 mg, 1.95 mmol). Elution with petroleum ether/ethyl acetate (8.5:1.5) afforded **37** as a waxy solid: 360 mg (53 %);  $^1\text{H}$  NMR (400 MHz,  $\text{CDCl}_3$ )  $\delta$  7.65 (d,  $J = 16$  Hz, 1H), 6.65 (s, 2H), 6.38 (d,  $J = 7.2$  Hz, 1H) 6.33 (s, 1H), 0.98 (s, 18H), 0.20 (s, 12H).

**(*E*)-3-(4-((*tert*-butyldimethylsilyl)oxy)-3-(((*tert*-butyldimethylsilyl)oxy)methyl)phenyl)acrylic acid (53).** **53** was synthesized from **52** (250 mg, 1.29 mmol). Elution with petroleum ether/ethyl acetate (8:2) afforded **37** as a waxy yellow solid: 370 mg (68 %);  $^1\text{H}$ NMR (400MHz,  $\text{CDCl}_3$ )  $\delta$  7.76 (d,  $J = 16$ Hz, 1H), 7.69 (s, 1H), 7.33 (d,  $J = 8.4$  Hz, 1H), 6.75 (d,  $J = 8.4$  Hz, 1H), 6.32 (d,  $J = 16$ Hz, 1H), 4.74 (s, 2H), 1.01 (s, 9H), 0.97 (s, 9H), 0.24 (s, 6H), 0.12 (s, 6H).  $^{13}\text{C}$  NMR (100MHz,  $\text{CDCl}_3$ )  $\delta$  172.50, 154.54, 147.29, 132.97, 128.05, 127.32, 127.16, 118.11, 114.55, 60.28, 25.96 (3 C), 25.61 (3 C), 18.45, 18.21, -4.22 (2 C), -5.37 (2 C).

**General procedure for the intermediates 38-46.** To an ice-cooled solution of the appropriate protected acid (**31-37**) (1 equiv) in dry  $\text{CH}_2\text{Cl}_2$  (4 mL) was added DCC (1.1 equiv) and DMAP (cat.). The reaction mixture was stirred for 10 min, followed by addition of the appropriate nucleophile (3 equiv). Stirring was then continued at room temperature overnight, and the reaction worked up by filtration and evaporation. The crude was purified by chromatography on silica gel.

**(S)-allyl (E)-3-(4-((tert-butyldimethylsilyl)oxy)phenyl)prop-2-ene-thioate (38).** **38** was synthesized from **31** (160 mg, 0.575 mmol). Elution with petroleum ether/ethyl acetate (9.8:0.2) afforded **38** as a waxy solid: 100 mg (52%);  $^1\text{H}$  NMR (400 MHz,  $\text{CDCl}_3$ )  $\delta$  7.57 (d,  $J = 15.6$  Hz, 1H), 7.43 (d,  $J = 8.0$  Hz, 2H), 6.84 (d,  $J = 8.0$  Hz, 2H), 6.59 (d,  $J = 15.6$  Hz, 1H), 5.88–5.83 (m, 1H), 5.28 (d,  $J = 17.0$  Hz, 1H), 5.13 (d,  $J = 10.0$  Hz, 1H), 3.66 (d,  $J = 6.8$ , 2H), 0.98 (s, 9H), 0.22 (s, 6H).

**(S)-allyl (E)-3-(3-((tert-butyldimethylsilyl)oxy)phenyl)prop-2-ene-thioate (39).** **39** was synthesized from **32** (370 mg, 1.33 mmol). Elution with petroleum ether/ethyl acetate (9.8:0.2) afforded **39** as a waxy solid: 260 mg (58%);  $^1\text{H}$  NMR (400 MHz,  $\text{CDCl}_3$ )  $\delta$  7.57 (d,  $J = 15.6$  Hz, 1H), 7.15 (t,  $J = 8$  Hz, 1H), 7.13 (s, 1H), 6.88 (d,  $J = 8.0$  Hz, 1H), 6.70 (d,  $J = 8.0$  Hz, 1H), 6.66 (d,  $J = 16.0$  Hz, 1H), 5.88–5.83 (m, 1H), 5.28 (d,  $J = 16.0$  Hz, 1H), 5.13 (d,  $J = 10.0$  Hz, 1H), 3.66 (d,  $J = 6.4$  Hz, 2H), 0.97 (s, 9H), 0.20 (s, 6H).

**S-allyl 3-(3,4-bis((tert-butyldimethylsilyl)oxy)phenyl)propanethioate (40).** **40** was synthesized from **33** (300 mg, 0.73 mmol) and 2-propene-1-thiol. Elution with petroleum ether/ethyl acetate (9.7:0.3) afforded **40** as a waxy solid: 200 mg (59%);  $^1\text{H}$  NMR (400 MHz,  $\text{CDCl}_3$ )  $\delta$  6.71 (d,  $J = 8$  Hz, 1H), 6.62–6.57 (m, 2H), 5.78–5.73 (m, 1H), 5.20 (dd,  $^1J = 16.8$  Hz,  $^2J = 1.2$  Hz, 1H), 5.07 (d,  $J = 8$  Hz, 1H), 3.51 (d,  $J = 8$  Hz, 2H), 2.84–2.77 (m, 4H), 0.97 (s, 18H), 0.17 (s, 12H).  $^{13}\text{C}$ -NMR (100 MHz,  $\text{CDCl}_3$ )  $\delta$  198.09, 146.78 (2 C), 145.42, 133.22, 121.34, 121.24, 121.10, 117.99, 45.79, 31.09, 30.86, 26.09 (6 C), 18.57 (2 C), -3.96 (4 C).

**S-allyl 3,4-bis((tert-butyldimethylsilyl)oxy)benzothioate (41).** **41** was synthesized from **34** (330 mg, 0.862 mmol) and 2-propene-1-thiol. Elution with petroleum ether/ethyl acetate (8:2) afforded **41** as a waxy solid: 130 mg (34%);  $^1\text{H}$  NMR (400 MHz,  $\text{CDCl}_3$ )  $\delta$  7.51–7.47 (m, 2H), 6.84 (d,  $J = 8$  Hz, 1H), 5.88 (m, 1H), 5.30 (d,  $J = 17.2$  Hz, 1H), 5.13 (d,  $J = 10$  Hz, 1H), 3.69 (d,  $J = 6.8$  Hz, 2H), 0.99 (s, 18H), 0.22 (s, 12H).  $^{13}\text{C}$  NMR (100 MHz,  $\text{CDCl}_3$ )  $\delta$  190.30, 151.34, 146.49, 134.01, 130.94, 120.42, 117.82, 115.96, 114.76, 32.28, 25.72 (6 C), 18.57 (2 C), -4.06 (4 C).

**S-propyl (E)-3-(3,4-bis((tert-butyldimethylsilyloxy)phenyl)prop-2-enethioate (42).** **42** was synthesized from **35** (480 mg, 1.174 mmol) and 1-propanethiol. Elution with petroleum ether/ethyl acetate (9.8:0.2) afforded **42** as a waxy solid: 430 mg (78%); <sup>1</sup>H NMR (400 MHz, CDCl<sub>3</sub>) δ 7.49 (d, *J* = 16 Hz, 1H), 7.05-7.01 (m, 2H), 6.82 (d, *J* = 8.4 Hz, 1H), 6.52 (d, *J* = 16 Hz, 1H), 2.99 (t, *J* = 7.2 Hz, 2H), 1.70-1.64 (m, 2H), 1.03-0.97 (m, 18H+3H), 0.21 (s, 12H). <sup>13</sup>C NMR (100 MHz, CDCl<sub>3</sub>) δ 190.70, 145.84, 144.52, 141.95, 126.95, 122.98, 121.65, 115.54, 114.83, 32.14, 24.08, 25.52 (6 C), 18.53 (2 C), 13.32, -4.16 (4 C).

**S-propyl 3-(3,4-bis((tert-butyldimethylsilyloxy)phenyl)propanethioate (43).** **43** was synthesized from **33** (300 mg, 0.73mmol) and 1-propanethiol. Elution with petroleum ether/ethyl acetate (9.7:0.3) afforded **43** as a waxy solid: 342 mg (44%); <sup>1</sup>H NMR (400 MHz, CDCl<sub>3</sub>) δ 6.72 (d, *J* = 8 Hz, 1H), 6.64 (s, 1H), 6.61 (d, *J* = 8 Hz, 1H), 2.86-2.79 (m, 6H), 1.60-1.55 (m, 2H), 0.99-0.93 (m, 18H+3H), 0.18 (s, 12H). <sup>13</sup>C NMR (100 MHz, CDCl<sub>3</sub>) δ 198.86, 146.74, 145.35, 133.35, 121.33, 121.25, 121.06, 45.91, 30.94, 30.87, 26.07 (6 C), 23.07, 18.54 (2 C), 13.45, -3.98 (4 C).

**S-propyl 3-(4-((tert-butyldimethylsilyloxy)-3-methoxyphenyl)propanethioate (44).** **44** was synthesized from **36** (110 mg, 0.35mmol) and 1-propanethiol. Elution with petroleum ether/ethyl acetate (9.5:0.5) afforded **44** as a pale oil: 70 mg (54%); <sup>1</sup>H NMR (400MHz, CDCl<sub>3</sub>) δ 6.75 (d, *J* = 8Hz, 1H), 6.67 (d, *J* = 2Hz, 1H), 6.63 (dd, <sup>1</sup>*J* = 8Hz, <sup>2</sup>*J* = 2 Hz, 1H), 3.78 (s, 3H), 2.91-2.86 (m, 2H), 2.85-2.82 (m, 4H), 1.62-1.56 (m, 2H), 0.99 (s, 9H), 0.97-0.94 (m, 3H), 0.14 (s, 6H). <sup>13</sup>C NMR (100MHz, CDCl<sub>3</sub>) δ 198.96, 150.90, 143.55, 143.55, 133.69, 120.90, 112.54, 55.57, 45.95, 31.38, 30.88, 25.83 (3 C), 23.06, 18.53, 13.39, -4.56 (2 C).

**S-allyl (E)-3-(3,5-bis((tert-butyldimethylsilyloxy)phenyl)prop-2-enethioate (45).** **45** was synthesized from **37** (360 mg, 0.88 mmol) and 2-propene-1-thiol. Elution with petroleum ether/ethyl acetate (9.7:0.3) afforded **45** as a pale oil: 170 mg (41%); <sup>1</sup>H NMR (400 MHz, CDCl<sub>3</sub>) δ 7.46 (d, *J* = 15.6 Hz, 1H), 6.62-6.57 (m, 3H), 6.36 (s, 1H), 5.82-5.88 (m, 1H), 5.28 (d, *J* = 17.2 Hz, 1H), 5.12 (d, *J* = 10.4 Hz, 1H), 3.66 (d, *J* = 6.8 Hz, 2H), 0.96 (s, 18H), 0.19 (s, 12H).

**3-(3,4-bis((*tert*-butyldimethylsilyl)oxy)phenyl)-*N*-methyl-*N*-propylpropanamide (46).** **46** was synthesized from **33** (80 mg, 0.19 mmol) and *N*-methylpropan-1-amine. Elution with petroleum ether/ethyl acetate (7:3) afforded **46** as a pale oil: 80 mg (88%); <sup>1</sup>H NMR (400 MHz, CDCl<sub>3</sub>) δ 6.72 (d, *J* = 8Hz, 1H), 6.68 (s, 1H), 6.63 (d, *J* = 8Hz, 1H), 3.32-3.13 (m, 2H), 2.91-2.88 (m, 3H), 2.86-2.81 (m, 2H), 2.56-2.52 (m, 2H), 1.54-1.52 (m, 2H), 0.89 (s, 18H), 0.87 (t, *J* = 8Hz, 3H), 0.18 (s, 12 H). <sup>13</sup>C NMR (100 MHz, CDCl<sub>3</sub>) δ 172.01, 146.72, 145.24, 134.24, 121.52, 121.31, 121.06, 51.74, 49.61, 35.93, 35.36, 33.65, 31.20, 30.97, 26.15 (6 C), 21.84, 20.71, 18.62 (2 C), 11.48, 11.29, -3.91 (4 C).

**General procedure for compounds 1, 2, 5-10, 11, 16.** To a solution of the appropriate organosilane intermediate **38-46**, **54** (1 equiv) in THF (5 mL) was added TBAF (4 equiv) and stirring was continued at room temperature. After 20-30 min, the reaction was quenched by addition of saturated aqueous NH<sub>4</sub>Cl solution; the aqueous phase was extracted with EtOAc (3 x 10 mL), and the combined organic layer was dried over Na<sub>2</sub>SO<sub>4</sub>. Following evaporation of the solvent, the residue was purified by column chromatography on silica gel.

**(*S*)-allyl (*E*)-3-(4-hydroxyphenyl)prop-2-enethioate (1).** **1** was synthesized from **38** (100 mg, 0.299 mmol). Elution with petroleum ether/ethyl acetate (7:3) afforded **1** as a waxy solid: 30 mg (46%); <sup>1</sup>H NMR (400 MHz, CDCl<sub>3</sub>) δ 7.56 (d, *J* = 16.0 Hz, 1H), 7.42 (d, *J* = 8.0 Hz, 2H), 6.84 (d, *J* = 8.0 Hz, 2H), 6.58 (d, *J* = 16.0 Hz, 1H), 5.88–5.81 (m, 1H), 5.29-5.25 (d, *J* = 17.0 Hz, 1H), 5.13–5.10 (d, *J* = 10.0 Hz, 1H), 3.65 (d, *J* = 8.0 Hz, 2H); <sup>13</sup>C NMR (100 MHz, CDCl<sub>3</sub>) δ 189.97, 158.23, 140.83, 133.05, 130.44, 126.66, 122.29, 118.02, 116.03, 31.80. MS [ESI<sup>+</sup>] *m/z* 243 [M+Na]<sup>+</sup>.

**(*S*)-allyl (*E*)-3-(3-hydroxyphenyl)prop-2-enethioate (2).** **2** was synthesized from **39** (210 mg, 0.63 mmol). Elution with dichloromethane/methanol (9.7:0.3) afforded **2** as a waxy solid: 110 mg (79%); <sup>1</sup>H NMR (400 MHz, CDCl<sub>3</sub>) δ 7.54 (d, *J* = 16.0 Hz, 1H), 7.24 (t, *J* = 8.0 Hz, 1H), 7.08 (d, *J* = 8.0 Hz, 1H), 7.02 (s, 1H), 6.90 (d, *J* = 8.0 Hz, 1H), 6.58 (d, *J* = 16.0 Hz, 1H), 6.09 (br s, 1H), 5.88–5.81 (m, 1H), 5.28 (d, *J* = 16.0 Hz, 1H), 5.13 (d, *J* = 10 Hz, 1H), 3.65 (d, *J* = 6.4 Hz, 2H); <sup>13</sup>C NMR (100 MHz, CDCl<sub>3</sub>) δ 190.33, 156.20, 140.85, 135.43, 132.75, 130.22, 124.89, 121.12, 118.31, 118.05, 114.91, 31.94. MS [ESI<sup>-</sup>] *m/z* 219 [M-H]<sup>-</sup>.

**S-allyl 3-(3,4-dihydroxyphenyl)propanethioate (5).** **5** was synthesized from **40** (130 mg, 0.28 mmol). Elution with petroleum ether/ethyl acetate (5.5:4.5) afforded **5** as a waxy oil: 45 mg (67%);  $^1\text{H}$  NMR (400 MHz,  $\text{CDCl}_3$ )  $\delta$  6.77 (d,  $J = 8$  Hz, 1H), 6.69 (s, 1H), 6.61 (d,  $J = 8$  Hz, 1H), 5.84-5.73 (m, 1H), 5.22 (d,  $J = 17.2$  Hz, 1H), 5.10 (d,  $J = 10.8$  Hz, 1H), 3.53 (d,  $J = 7.2$  Hz, 2H), 2.89-2.80 (m, 4H).  $^{13}\text{C}$  NMR (100 MHz,  $\text{CDCl}_3$ )  $\delta$  199.25, 143.71, 142.18, 132.95 (2 C), 120.77, 118.18, 115.56, 115.50, 45.68, 31.96, 30.91. MS [ $\text{ESI}^+$ ]  $m/z$  261 [ $\text{M}+\text{Na}$ ] $^+$ .

**S-allyl 3,4-dihydroxybenzothioate (6).** **6** was synthesized from **41** (130 mg, 0.296 mmol). Elution with dichloromethane/methanol (9.8:0.2) afforded **6** as a dark oil: 15 mg (20%);  $^1\text{H}$  NMR (400 MHz,  $\text{CD}_3\text{OD}$ )  $\delta$  7.41-7.38 (m, 2H), 6.81 (d,  $J = 8.4$  Hz, 1H), 5.91-5.82 (m, 1H), 5.27 (d,  $J = 16.8$  Hz, 1H), 5.09 (d,  $J = 9.6$  Hz, 1H), 3.66 (d,  $J = 6.8$  Hz, 2H).  $^{13}\text{C}$  NMR (100 MHz,  $\text{CD}_3\text{OD}$ )  $\delta$  191.30, 152.35, 146.49, 135.01, 130.24, 121.53, 117.92, 115.92, 114.96, 32.38. MS [ $\text{ESI}^+$ ]  $m/z$  209 [ $\text{M}+1$ ] $^+$ .

**S-propyl (E)-3-(3,4-dihydroxyphenyl)prop-2-enethioate (7).** **7** was synthesized from **42** (430 mg, 0.921 mmol). Elution with dichloromethane/methanol (9.6:0.4) afforded **7** as a pale oil: 63 mg (30%);  $^1\text{H}$  NMR (400 MHz,  $\text{CDCl}_3$ )  $\delta$  7.50 (d,  $J = 15.6$  Hz, 1H), 7.10 (s, 1H), 7.02 (d,  $J = 8$  Hz, 1H), 6.88 (d,  $J = 8$  Hz, 1H), 6.56 (d,  $J = 15.6$  Hz, 1H), 2.98 (t,  $J = 7.2$  Hz, 2H), 1.69-1.64 (m, 2H), 1.00 (t,  $J = 7.2$  Hz, 3H).  $^{13}\text{C}$  NMR (100 MHz,  $\text{CDCl}_3$ )  $\delta$  191.80, 146.88, 144.02, 140.92, 127.25, 122.98 (2 C), 115.74, 114.93, 31.13, 23.08, 13.52. MS [ $\text{ESI}$ ]  $m/z$  237 [ $\text{M}-1$ ].

**S-propyl 3-(3,4-dihydroxyphenyl)propanethioate (8).** **8** was synthesized from **43** (119 mg, 0.25 mmol). Elution with petroleum ether/ethyl acetate (5.5:4.5) afforded **8** as a waxy oil: 41 mg (66%);  $^1\text{H}$  NMR (400 MHz,  $\text{CDCl}_3$ )  $\delta$  6.76 (d,  $J = 8.4$  Hz, 1H), 6.68 (d,  $J = 2$  Hz, 1H), 6.59 (dd,  $^1J = 8.4$ ,  $^2J = 2$  Hz, 1H), 2.86-2.81 (m, 6H), 1.58-1.57 (m, 2H), 0.94 (t,  $J = 7.2$  Hz, 3H).  $^{13}\text{C}$  NMR (100 MHz,  $\text{CDCl}_3$ )  $\delta$  200.23, 143.60, 142.07, 132.89, 120.61, 115.44, 115.39, 45.71, 30.92, 30.88, 22.82, 13.27. MS [ $\text{ESI}^+$ ]  $m/z$  263 [ $\text{M}+\text{Na}$ ] $^+$ .

**S-propyl 3-(4-hydroxy-3-methoxyphenyl)propanethioate (9).** **9** was synthesized from **44** (70 mg, 0.189 mmol). Elution with petroleum ether/ethyl acetate (5.5:4.5) afforded **9** as a pale oil: 45 mg (94%);  $^1\text{H}$  NMR (400 MHz,  $\text{CDCl}_3$ )  $\delta$  6.83-6.81 (m, 1H), 6.68 (s, 1H), 6.66 (d,  $J = 2$  Hz, 1H), 3.86

(s, 3H), 2.92-2.80 (m, 6H), 1.61-1.56 (m, 2 H), 0.95 (t,  $J = 8$  Hz, 3H).  $^{13}\text{C}$  NMR (100 MHz,  $\text{CDCl}_3$ )  $\delta$  199.14, 146.62, 144.23, 132.25, 121.10, 114.56, 111.14, 56.07, 46.15, 31.47, 30.10, 23.16, 13.51. MS [ESI<sup>+</sup>] ( $m/z$ ) 277 [M+Na]<sup>+</sup>.

**S-allyl (*E*)-3-(3,5-dihydroxyphenyl)prop-2-enethioate (10).** **10** was synthesized from **45** (170 mg, 0.366 mmol). Elution with dichloromethane/methanol (9.5:0.5) afforded **10** as a pale oil: 63 mg (73%);  $^1\text{H}$  NMR (400 MHz,  $\text{CD}_3\text{OD}$ )  $\delta$  7.43 (d,  $J = 15.6$  Hz, 1H), 6.67 (d,  $J = 16$  Hz, 1H), 6.52 (s, 2H), 6.34 (s, 1H), 5.87-5.79 (m, 1H), 5.25 (d,  $J = 16.8$  Hz, 1H), 5.08 (d,  $J = 10$  Hz, 1H), 3.63 (d,  $J = 6.4$  Hz, 2H).  $^{13}\text{C}$  NMR (100 MHz,  $\text{CD}_3\text{OD}$ )  $\delta$  190.72, 160.04, 142.38, 137.10, 134.55, 125.38, 118.14, 107.80, 106.22, 32.40. MS [ESI<sup>+</sup>]  $m/z$  237 [M+1]<sup>+</sup>.

**S-allyl (*E*)-3-(4-hydroxy-3-(hydroxymethyl)phenyl)prop-2-enethioate (11).** **11** was synthesized from **54** (270 mg, 0.56 mmol). Elution with petroleum ether/ethyl acetate (5:5) afforded **11** as a pale green solid: 108 mg (77%);  $^1\text{H}$  NMR (400 MHz,  $\text{CD}_3\text{OD}$ )  $\delta$  7.55-7.51 (m, 2H), 7.35 (dd,  $^1J = 8.4$  Hz,  $^2J = 2.4$  Hz, 1H), 6.78 (d,  $J = 8.4$  Hz, 1H), 6.62 (d,  $J = 16$  Hz, 1H), 5.86-5.79 (m, 1H), 5.21 (dd,  $^1J = 16.8$  Hz,  $^2J = 1.6$  Hz, 1H) 5.06 (dd,  $^1J = 10$  Hz,  $^2J = 1.6$ , 1H) 4.63 (s, 2H), 3.60 (d,  $J = 8$  Hz, 2H).  $^{13}\text{C}$  NMR (100 MHz,  $\text{CD}_3\text{OD}$ )  $\delta$  189.41, 157.73, 141.17, 133.42, 129.13, 128.31, 128.26, 125, 27, 121.01, 116.64, 114.10, 59.16, 31.00. MS [ESI<sup>-</sup>] ( $m/z$ ) 249[M-1]<sup>-</sup>.

**3-(3,4-dihydroxyphenyl)-*N*-methyl-*N*-propylpropanamide (16).** **16** was synthesized from **46** (80 mg, 0.171 mmol). Elution with petroleum ether/ethyl acetate (1:9) afforded **16** as a pale oil: 23 mg (55%);  $^1\text{H}$  NMR (400 MHz,  $\text{CDCl}_3$ )  $\delta$  6.76 (d,  $J = 8$  Hz, 1H), 6.75 (d,  $J = 2$  Hz, 1H), 6.54 (dd,  $^1J = 8$  Hz,  $^2J = 2$  Hz, 1H), 3.32-3.13 (m, 2H), 2.90-2.87 (m, 3H) 2.84-2.79 (m, 2H), 2.61-2.55 (m, 2 H), 1.52-1.49 (m, 2H), 0.87-81 (m, 3H).  $^{13}\text{C}$  NMR (100 MHz,  $\text{CDCl}_3$ )  $\delta$  173.31, 144.14, 142.818, 132.76, 119.79, 115.43, 115.07, 51.80, 49.83, 35.83, 35.47, 34.95, 33.79, 31.03, 30.78, 29.58, 21.42, 20.27, 11.08, 10.93. MS [ESI<sup>+</sup>]( $m/z$ )238[M+1]<sup>+</sup>.

**4-bromosalicyl alcohol (48).**  $\text{NaBH}_4$  (376 mg, 10 mmol) was added to a stirring solution of 5-bromo-2-hydroxybenzaldehyde (**47**) (2 g, 10 mmol) in EtOH (30 mL) in an ice bath. The reaction mixture was stirred at room temperature for 2 h. After that, the solvent was removed, 1 N aqueous

HCl (40 mL) was added to the residue and extracted with Et<sub>2</sub>O. The solvent was evaporated under vacuum to give the desired compound **48** as pale oil: 2 g (99%); <sup>1</sup>H NMR (400 MHz, CDCl<sub>3</sub>) δ 7.29 (dd, <sup>1</sup>J = 8.8 Hz, <sup>2</sup>J = 2.4 Hz, 1H), 7.15 (d, *J* = 2.4 Hz, 1H), 6.67 (d, *J* = 8.8 Hz, 1H), 5.08 (br s, 1H), 4.82 (s, 2H). <sup>13</sup>C NMR (100 MHz, CDCl<sub>3</sub>) δ 155.29, 132.18, 130.41, 126.57, 118.51, 111.98, 64.13.

**4-bromosalicyl alcohol isopropylidene acetal (49).** A mixture of **48** (2 g, 10 mmol), 2,2-dimethoxypropane (6 mL, 50 mmol), *p*-toluenesulfonic acid monohydrate (190 mg, 10 mmol) and anhydrous sodium sulfate (2.88 g) in dry DMF (1.5 mL) was placed in a microwave (60 °C, 250 Psi, 80 W) for 20 min. The solvent was removed under reduced pressure and the residue was dissolved in ethyl acetate and water. The aqueous phase was extracted twice with ethyl acetate (5 mL). The combined organic phases were washed twice with NaOH 1 M and water (20 mL), dried with sodium sulfate and concentrated under reduced pressure to give **49** as yellow oil: 2.4 g (99%); <sup>1</sup>H NMR (400 MHz, CDCl<sub>3</sub>) δ 7.23 (dd, <sup>1</sup>J = 8.8 Hz, <sup>2</sup>J = 2.4 Hz, 1H), 7.08 (d, *J* = 2.4 Hz, 1H), 6.68 (d, *J* = 8.8 Hz, 1H), 4.78 (s, 2H), 1.51 (s, 6H). <sup>13</sup>C NMR (100 MHz, CDCl<sub>3</sub>) δ 150.33, 130.99, 127.35, 121.35, 118.92, 112.39, 99.79, 60.36, 24.61 (2 C).

**4-formylsalicyl alcohol isopropylidene acetal (50).** Under nitrogen atmosphere, **49** (2.40 g, 9.90 mmol) was dissolved in dry THF (65 mL), cooled down to -78 °C and *n*-butyllithium (9 mL, 2.5 M in hexane) was added dropwise. The reaction mixture was stirred for 2 h at -78 °C and then treated with dry DMF (13 mL, 97.3 mmol) as solution in dry THF (13 mL), stirring at the same temperature for 45 min. The reaction mixture was warmed slowly up to room temperature, then diluted with ethyl ether, washed (3 x H<sub>2</sub>O, 1 x brine) and dried with sodium sulfate. The solvent was removed in vacuo and the residue was purified by flash chromatography (petroleum ether/ethyl acetate 8:2) to afford compound **50** as pale oil: 720 mg (35%); <sup>1</sup>H NMR (400 MHz, CDCl<sub>3</sub>) δ 9.82 (s, 1H), 7.67 (dd, <sup>1</sup>J = 8.8 Hz, <sup>2</sup>J = 2 Hz, 1H), 7.51 (d, *J* = 2 Hz, 1H), 6.90 (d, *J* = 8.8 Hz, 1H), 4.87 (s, 2H), 1.54 (s, 6H). <sup>13</sup>C NMR (100 MHz, CDCl<sub>3</sub>) δ 190.70, 156.77, 130.40, 129.44, 126.89, 119.74, 117.718, 100.75, 60.56, 24.78(2 C).

**(E)-3-(2,2-dimethyl-4H-benzo[d][1,3]dioxin-6-yl)acrylic acid (51).** To a solution of **50** (200 mg, 1.04 mmol) and malonic acid (117 mg, 1.12 mmol) in toluene were added pyridine (0.13 mL, 1.60

mmol) and aniline (0.014 mL) and the reaction mixture was stirred at 100 °C for 5 h. The precipitate was filtered off and washed with water to give **51** as a yellow solid: 540 mg (84%); <sup>1</sup>H NMR (400 MHz, DMSO-*d*<sub>6</sub>) δ 12.22 (br s, 1H), 7.50 (d, *J* = 8.4 Hz, 1H), 7.48-7.43 (m, 2H), 6.81 (d, *J* = 8.4 Hz, 1H), 6.34 (d, *J* = 16 Hz, 1H), 4.83 (s, 2H), 1.47 (s, 6H). <sup>13</sup>C NMR (100 MHz, DMSO-*d*<sub>6</sub>) δ 167.73, 152.64, 143.71, 128.31, 126.51, 125.42, 119.94, 116.99, 116.80, 99.92, 59.94, 24.57 (2 C).

**(*E*)-3-(4-hydroxy-3-(hydroxymethyl)phenyl)acrylic acid (52).** Two drops of HCl 12 N were added to a solution of **51** (100 mg, 0.43 mmol) in 3 mL of CH<sub>3</sub>CN/H<sub>2</sub>O (7:3) and the reaction mixture was brought to boil with a heat gun for 30 s. This procedure was repeated until the deprotection has been completed (5 min, monitoring by TLC, dichloromethane/methanol/acetic acid, 9:1:0.1). The solvent was removed in vacuo to give **52** as dark solid: 83 mg (99%); <sup>1</sup>H NMR (400 MHz, DMSO-*d*<sub>6</sub>) δ 9.95 (br s, 1H), 7.57 (d, *J* = 2 Hz, 1H), 7.49 (d, *J* = 16 Hz, 1H), 3.78 (dd, <sup>1</sup>*J* = 8.4 Hz, <sup>2</sup>*J* = 2 Hz, 1H), 6.80 (d, *J* = 8.4 Hz, 1H), 6.24 (d, *J* = 16 Hz, 1H), 4.47 (s, 2H). <sup>13</sup>C NMR (100 MHz, DMSO-*d*<sub>6</sub>) δ 167.94, 156.61, 144.59, 129.30, 128.33, 127.45, 125.03, 115.12, 115.03, 58.01.

***S*-allyl (*E*)-3-(4-((tert-butyldimethylsilyl)oxy)-3-(((tert-butyldimethylsilyl)oxy)methyl) phenyl) prop-2-ene-thioate (54).** To an ice-cooled solution of the protected acid (**53**) (370 mg, 0.88 mmol) in dry CH<sub>2</sub>Cl<sub>2</sub> (2.5 mL) was added HOBt (155 mg, 1.14 mmol) and EDC (178 mg, 1.14 mmol). The reaction mixture was stirred for 10 min, followed by addition of 2-propene-1-thiol (0.3 mL, 3.52 mmol). Stirring was then continued at room temperature overnight, and the solvent evaporated under vacuum. The crude was purified by chromatography on silica gel using petroleum ether/ethyl acetate (9.7:0.3) as mobile phase, affording compound **54** as pale oil: 270 mg (64%); <sup>1</sup>H NMR (400 MHz, CDCl<sub>3</sub>) δ 7.68 (s, 1H), 7.61 (d, *J* = 16 Hz, 1H), 7.32 (d, *J* = 8 Hz, 1H), 6.74 (d, *J* = 8 Hz, 1H), 6.61 (d, *J* = 16 Hz, 1H), 5.87-5.84 (m, 1H), 5.16-5.08 (m, 2H), 4.74 (s, 2H), 3.67 (d, *J* = 4 Hz, 2H), 1.01 (s, 9H), 0.97 (s, 9H), 0.24 (s, 6H), 0.12 (s, 6H). <sup>13</sup>C NMR (100 MHz, CDCl<sub>3</sub>) δ 189.06, 154.48, 141.13, 133.21, 132.10, 128.04, 127.41, 127.07, 122.41, 118.15, 117.78, 60.25, 42.26, 25.95 (3 C), 25.61 (3 C), 18.44, 18.21, -4.21 (2 C), -5.36 (2 C).

**General procedure for the intermediates 57 and 58.** To a solution of commercially available aldehydes **55** and **56** (1 equiv) and malonic acid (1.08 equiv) in toluene (2.2 mL) were added

pyridine (1.54 equiv) and aniline (0.045 mL) and the reaction mixture was stirred at 100 °C for 90 min. The precipitate was filtered off and purified by flash chromatography on silica gel using dichloromethane/methanol (9:1) as mobile phase.

**(E)-3-(1H-indazol-5-yl)acrylic acid (57).** Synthesized from **55** (500 mg, 3.42 mmol) affording **57** as white solid: 280 mg (43%); <sup>1</sup>H NMR (400 MHz, CD<sub>3</sub>OD) δ 8.06 (s, 1H), 7.89 (s, 1H), 7.67 (dd, <sup>1</sup>J = 9.2 Hz, <sup>2</sup>J = 8 Hz, 1H), 7.58 (d, J = 16 Hz, 1H), 7.53 (d, J = 8.8 Hz, 1H), 6.50 (d, J = 16 Hz, 1H).

**(E)-3-(1H-indazol-6-yl)acrylic acid (58).** Synthesized from **56** (500 mg, 3.42 mmol) affording **58** as white solid: 420 mg (65%); <sup>1</sup>H NMR (400 MHz, DMSO-*d*<sub>6</sub>) δ 8.04 (s, 1H), 7.72 (d, J = 8.8 Hz, 1H), 7.66 (s, 1H), 7.46 (d, J = 16 Hz, 1H), 7.38 (d, J = 8.8 Hz, 1H), 6.54 (d, J = 16 Hz, 1H).

**General procedure for the intermediates 59 and 60.** To a solution of the appropriate acid **57** and **58** (1 equiv) in 4.5 mL of THF/H<sub>2</sub>O (2:1) were added Boc<sub>2</sub>O (3 equiv), Et<sub>3</sub>N (1.5 equiv) and DMAP (cat.). The reaction mixture was stirred at room temperature for 2 d, then the solvent was removed and the crude purified by flash chromatography on silica gel using dichloromethane/methanol (9:1) as mobile phase.

**(E)-3-(1-(tert-butoxycarbonyl)-1H-indazol-5-yl)acrylic acid (59).** Synthesized from **57** (280 mg, 1.48 mmol) affording **59** as white solid: 200 mg (46%); <sup>1</sup>H NMR (400 MHz, CD<sub>3</sub>OD) δ 8.27 (s, 1H), 8.08 (s, 1H), 7.98-7.92 (m, 1H), 7.85-7.79 (m, 1H), 7.70 (d, J = 14.8 Hz, 1H), 6.57 (d, J = 15.6 Hz, 1H), 1.70 (s, 9H).

**(E)-3-(1-(tert-butoxycarbonyl)-1H-indazol-6-yl)acrylic acid (60).** Synthesized from **58** (420 mg, 2.23 mmol) to give **60** as white solid: 186 mg (29%); <sup>1</sup>H NMR (400 MHz, CD<sub>3</sub>OD) δ 8.31 (s, 1H), 8.30 (s, 1H), 7.86 (d, J = 8 Hz, 1H), 7.79 (d, J = 16 Hz, 1H), 7.65 (d, J = 8 Hz, 1H), 6.62 (d, J = 16 Hz, 1H), 1.75 (s, 9H).

**General procedure for the intermediates 61-64.** To an ice-cooled solution of the appropriate protected acid (**59** and **60**) (1 equiv) in 1.5 mL of dry CH<sub>2</sub>Cl<sub>2</sub>/DMF (1:2) was added EDC (1.3 equiv) and HOBt (1.3 equiv). The reaction mixture was stirred for 30 min at 0 °C, followed by addition of the appropriate nucleophile (3 equiv). Stirring was then continued at room temperature for 24 h, then the solvent was removed under vacuum and the crude purified by flash chromatography on silica gel using petroleum ether/ethyl acetate (8:2) as the mobile phase.

**tert-butyl (E)-5-(3-(allylthio)-3-oxoprop-1-en-1-yl)-1H-indazole-1-carboxylate (61).** Synthesized from **59** (100 mg, 0.442 mmol) and 2-propene-1-thiol (0.109 mL, 1.32 mmol) to give **61** as white solid: 20 mg (13%); <sup>1</sup>H NMR (400 MHz, CDCl<sub>3</sub>) δ 8.20 (s, 1H), 8.19 (d, *J* = 8.8 Hz, 1H), 7.88 (s, 1H), 7.74 (d, *J* = 8.8 Hz, 1H), 7.72 (d, *J* = 16 Hz, 1H), 6.76 (d, *J* = 16 Hz, 1H), 5.90-5.83 (m, 1H) 5.30 (d, *J* = 16.8 Hz, 1H), 5.14 (d, *J* = 10.4 Hz, 1H), 3.68 (d, *J* = 6.8 Hz, 2H), 1.73 (s, 9H).

**tert-butyl (E)-5-(3-oxo-3-(propylthio)prop-1-en-1-yl)-1H-indazole-1-carboxylate (62).** Synthesized from **59** (100 mg, 0.442 mmol) and 1-propanethiol (0.120 mL, 1.32 mmol) to give **61** as white solid: 60 mg (39%); <sup>1</sup>H NMR (400 MHz, CDCl<sub>3</sub>) δ 8.19 (s, 1H), 8.18 (d, *J* = 8.4 Hz, 1H), 7.87 (s, 1H), 7.74 (s, 1H), 7.69 (d, *J* = 16.4 Hz, 1H), 6.75 (d, *J* = 16 Hz, 1H), 3.01-2.98 (m, 2H), 1.72 (s, 9H), 1.70-1.65 (m, 2H), 1.01 (t, *J* = 7.6 Hz, 2H).

**tert-butyl (E)-6-(3-(allylthio)-3-oxoprop-1-en-1-yl)-1H-indazole-1-carboxylate (63).** Synthesized from **60** (86 mg, 0.380 mmol) and 2-propene-1-thiol (0.09 mL, 1.14 mmol) to give **63** as white solid: 20 mg (15%); <sup>1</sup>H NMR (400 MHz, CDCl<sub>3</sub>) δ 8.38 (s, 1H), 8.15 (s, 1H), 7.71 (d, *J* = 15.6 Hz, 1H), 7.71 (d, *J* = 8.8 Hz, 1H), 7.49 (d, *J* = 8.4 Hz, 1H), 6.82 (d, *J* = 15.6 Hz, 1H), 5.90-5.83 (m, 1H) 5.30 (d, *J* = 16.8 Hz, 1H), 5.14 (d, *J* = 10.4 Hz, 1H), 3.68 (d, *J* = 6.8 Hz, 2H), 1.73 (s, 9H).

**tert-butyl (E)-6-(3-oxo-3-(propylthio)prop-1-en-1-yl)-1H-indazole-1-carboxylate (64).** Synthesized from **60** (100 mg, 0.442 mmol) and 1-propanethiol (0.120 mL, 1.32 mmol) to give **64** as white solid: 40 mg (26%); <sup>1</sup>H NMR (400 MHz, CDCl<sub>3</sub>) δ 8.38(s, 1H), 8.15 (s, 1H), 7.71 (d, *J* = 15.6 Hz, 1H), 7.70 (d, *J* = 8.8 Hz, 1H), 7.49 (d, *J* = 8.4 Hz, 1H), 6.82 (d, *J* = 15.6 Hz, 1H), 3.00 (t, *J* = 7.2 Hz, 2H), 1.73 (s, 9H), 1.70 -1.62 (m, 2H), 1.01 (t, *J* = 7.2 Hz, 3H).

**General procedure for compounds 12-15.** To an ice-cooled solution of the appropriate *N*-protected intermediate **61-64** in methanol (0.5 mL) HCl 4M in dioxane was added and the reaction mixture was stirred for 4 h at 0 °C. The solvent was then removed under vacuum and the crude purified by column chromatography on silica gel using dichloromethane/methanol/ammonia solution 30% (9.5:0.5:0.05) as the mobile phase.

***S*-allyl (*E*)-3-(1*H*-indazol-5-yl)prop-2-enethioate (12).** Synthesized from **61** (20 mg) to give **12** as white solid: 7 mg (50%); <sup>1</sup>H NMR (400 MHz, CD<sub>3</sub>OD) δ 8.11 (s, 1H), 8.04 (s, 1H), 7.76 (d, *J* = 15.6 Hz, 1H), 7.73 (d, *J* = 8.8 Hz, 1H), 7.56 (d, *J* = 8.8 Hz, 1H), 6.86 (d, *J* = 15.6 Hz, 1H), 5.91-5.80 (m, 1H), 5.28 (d, *J* = 15.6 Hz, 1H), 5.10 (d, *J* = 10.4 Hz, 1H), 3.67 (d, *J* = 6.4 Hz, 2H). <sup>13</sup>C NMR (100 MHz, CD<sub>3</sub>OD) δ 190.76, 142.85, 135.99, 134.86, 128.70, 126.89, 124.88, 124.16, 118.14, 112.10, 32.49. MS [ESI-] *m/z* 243 [M-1]-.

***S*-propyl (*E*)-3-(1*H*-indazol-5-yl)prop-2-enethioate (13).** Synthesized from **62** (60 mg) to give **13** as white solid: 33 mg (78%); <sup>1</sup>H NMR (400 MHz, CD<sub>3</sub>OD) δ 8.10 (s, 1H), 8.01 (s, 1H), 7.72 (d, *J* = 15.6 Hz, 1H), 7.71 (d, *J* = 9.2 Hz, 1H), 7.55 (d, *J* = 8.8 Hz, 1H), 6.83 (d, *J* = 15.6 Hz, 1H), 2.98 (t, *J* = 7.2 Hz, 2H), 1.68-1.63 (m, 2H), 1.01 (t, *J* = 7.4 Hz, 3H). <sup>13</sup>C NMR (100 MHz, CD<sub>3</sub>OD) δ 191.45, 141.45, 134.73, 130.32, 129.09, 125.64, 125.19, 112.71, 31.70, 24.31, 13.61. MS [ESI+] *m/z* 247 [M+1]+.

***S*-allyl (*E*)-3-(1*H*-indazol-6-yl)prop-2-enethioate (14).** Synthesized from **63** (20 mg) to give **14** as white solid: 11 mg (78%); <sup>1</sup>H NMR (400 MHz, CD<sub>3</sub>OD) δ 8.06 (s, 1H), 8.00 (s, 1H), 7.79 (d, *J* = 8.4 Hz, 1H), 7.76 (d, *J* = 15.6 Hz, 1H), 7.47 (d, *J* = 8.4 Hz, 1H), 6.93 (d, *J* = 15.6 Hz, 1H), 5.91-5.83 (m, 1H), 5.29 (d, *J* = 15.2 Hz, 1H), 5.11 (d, *J* = 8.8 Hz, 1H), 3.68 (d, *J* = 7.2 Hz, 2H). <sup>13</sup>C NMR (100 MHz, CD<sub>3</sub>OD) δ 191.12, 142.16, 134.44, 133.91, 125.93, 122.25, 120.63, 117.97, 32.27, 26.24. MS [ESI-] *m/z* 243 [M-1]-.

***S*-propyl (*E*)-3-(1*H*-indazol-6-yl)prop-2-enethioate (15).** Synthesized from **64** (40 mg) to give **15** as white solid: 20 mg (70%); <sup>1</sup>H NMR (400 MHz, CD<sub>3</sub>OD) δ 8.55 (s, 1H), 7.94 (d, *J* = 8.8 Hz, 1H),

7.88 (s, 1H), 7.72 (d,  $J = 15.6$  Hz, 1H), 7.62 (d,  $J = 8.8$  Hz, 1H), 6.98 (d,  $J = 16$  Hz, 1H), 2.99 (t,  $J = 7.4$  Hz, 2H), 1.69-1.63 (m, 2H), 1.01 (t,  $J = 7.4$  Hz, 3H).  $^{13}\text{C}$  NMR (100 MHz,  $\text{CD}_3\text{OD}$ )  $\delta$  191.13, 140.41, 137.63, 128.18, 123.58, 122.87, 113.38, 31.63, 24.04, 13.51. MS [ESI-]  $m/z$  245 [M-1]-.

**Sodium 2-ethoxy-2-oxoethanesulfonate (66).**  $\text{Na}_2\text{SO}_3$  (1.5 g, 0.011 mol) was dissolved in water (5 mL) and a solution of ethyl bromoacetate (**65**, 2 g, 0.012 mol) in ethanol (2.5 mL) was added dropwise at 5-10 °C. The reaction mixture was heated to 50 °C for 1 h. After then, the solution was evaporated until dryness. Acetic acid (20 mL) and ethyl acetate (10 mL) were added to the residue, and the mixture was heated to 100 °C for 1 h. The hot mixture was filtered, and other 100 mL ethyl acetate was poured into the filtrate. The white crystals were filtered, washed with ethyl acetate, and dried to yield **66** as white solid: 2.0 g (78%);  $^1\text{H}$  NMR (400 MHz,  $\text{DMSO}-d_6$ )  $\delta$  4.02 (q,  $J = 7.1$  Hz, 2H), 3.44 (s, 2H), 1.16 (t,  $J = 7.1$  Hz, 3H).  $^{13}\text{C}$  NMR (100 MHz,  $\text{DMSO}-d_6$ )  $\delta$  166.51, 60.07, 56.71, 14.03. MS [ESI-]  $m/z$  167 [M-Na]-.

**Ethyl 2-(chlorosulfonyl)acetate (67).**  $\text{PCl}_5$  (300 mg, 1.44 mmol) was mixed thoroughly with compound **66** (250 mg, 1.31 mmol) and heated to 100 °C for 1 h in a pressure tube under reflux. Then, the reaction mixture was cooled to room temperature and 3 mL of toluene was added, stirring for 10 min. The reaction solution was filtered, and the solvent was evaporated under reduced pressure to obtain **66** as a yellow oil: 180 mg (75%);  $^1\text{H}$  NMR (400 MHz,  $\text{CDCl}_3$ )  $\delta$  4.60 (s, 2H), 4.32 (q,  $J = 7.1$  Hz, 2H), 1.33 (t,  $J = 7.2$  Hz, 3H).  $^{13}\text{C}$  NMR (100 MHz,  $\text{CDCl}_3$ )  $\delta$  160.23, 67.24, 63.64, 13.96.

**Ethyl 2-(*N*-propylsulfamoyl)acetate (68).** Compound **67** (1.11 g, 5.89 mmol) was added to a solution of 1,8-Diazabicyclo[5.4.0]undec-7-ene (DBU, 878  $\mu\text{L}$ , 5.89 mmol), 1-propanamine hydrochloride (1.13 g, 11.78 mmol), and  $\text{K}_2\text{CO}_3$  (1.63 g, 11.78 mmol) in dry  $\text{CH}_2\text{Cl}_2$  (20 mL) at 0 °C. The mixture was refluxed for 3 h, cooled, and evaporated. The crude residue was dissolved in EtOAc (60 mL), washed with 1 M aqueous HCl (3 x 60 mL) and brine (30 mL), dried over  $\text{Na}_2\text{SO}_4$  and evaporated to give **68** as a dark yellow oily residue that was used in the next step without purification: 450 mg (40%);  $^1\text{H}$  NMR (400 MHz,  $\text{CDCl}_3$ )  $\delta$  4.92 (br s, 1H), 4.24 (q,  $J = 7.1$  Hz, 2H),

3.97 (s, 2H), 3.12-3.08 (m, 2H), 1.65 – 1.53 (m, 2H), 1.34-1.28 (m, 3H), 0.95 (t,  $J = 7.4$  Hz, 3H).  $^{13}\text{C}$  NMR (100 MHz,  $\text{CDCl}_3$ )  $\delta$  164.12, 62.46, 55.04, 45.48, 23.26, 13.98, 11.08.

**2-(*N*-propylsulfamoyl)acetic acid (69).** A cold solution of NaOH (580 mg, 14.5 mmol) in  $\text{H}_2\text{O}$  (15 mL) was added dropwise to **68** (450 mg, 2.15 mmol). Stirring was continued for 3 h, and the solution was washed with EtOAc (2 x 10 mL). The aqueous layer was acidified with 2 M aqueous HCl to pH 2 and extracted with EtOAc (3 x 15 mL). The combined extracts were dried over  $\text{Na}_2\text{SO}_4$ , filtered, and evaporated to afford **69** as yellow waxy solid: 270 mg (70%);  $^1\text{H}$  NMR (400 MHz,  $\text{DMSO}-d_6$ )  $\delta$  13.00 (br s, 1H), 7.29 (t,  $J = 5.8$  Hz, 1H), 4.02 (s, 2H), 2.94-2.89 (m, 2H), 1.62 – 1.36 (m, 2H), 0.85 (t,  $J = 7.4$  Hz, 3H).  $^{13}\text{C}$  NMR (100 MHz,  $\text{DMSO}-d_6$ )  $\delta$  164.92, 56.32, 44.41, 22.75, 11.09.

**(*E*)-2-(3,4-dihydroxyphenyl)-*N*-propylethene-1-sulfonamide (17).** To a solution of **69** (260 mg, 1.43 mmol) in THF (6 mL) was added 3,4-dihydroxybenzaldehyde (188 mg, 1.36 mmol), pyrrolidine (cat.) and acetic acid (cat.) and the solution was refluxed for 8 h. Afterwards, the solvent was removed under *vacuum*, the crude was dissolved in  $\text{CH}_2\text{Cl}_2$  (3 mL) and Girard's reagent T (911 mg, 5.44 mmol) and acetic acid (3.4 mL, 61.2 mmol) were added. After stirring for 10 min, the solvent was evaporated and the crude purified by flash chromatography using petroleum ether/ethyl acetate (5:5) to afford **17** as green solid: 180 mg (50%);  $^1\text{H}$  NMR (400 MHz,  $\text{CD}_3\text{OD}$ )  $\delta$  7.64 (d,  $J = 15.4$  Hz, 1H), 7.40 (d,  $J = 2.0$  Hz, 1H), 7.33 (dd,  $J = 8.2, 2.0$  Hz, 1H), 7.19 (d,  $J = 8.2$  Hz, 1H), 7.05 (d,  $J = 15.4$  Hz, 1H), 5.26 (br s, 2H), 3.31 (t,  $J = 7.1$  Hz, 2H), 1.98 – 1.87 (m, 2H), 1.33 (t,  $J = 7.5$  Hz, 3H).  $^{13}\text{C}$  NMR (100 MHz,  $\text{CD}_3\text{OD}$ )  $\delta$  149.41, 146.74, 142.24, 126.02, 123.05, 122.60, 116.43, 115.14, 45.60, 24.12, 11.47. MS [ESI-]  $m/z$  256 [M-1]-.

**(1*r*,3*R*,5*S*,7*r*)-3,5-dimethyladamantane-1-carboxylic acid (71).** To a solution of 1-bromo-3,5-dimethyladamantane (**70**, 1.23 mL, 6.17 mmol) in  $\text{H}_2\text{SO}_4$  (45 mL) was added dropwise formic acid (4.5 mL) and the reaction mixture was stirred for 5 h at room temperature. The reaction was quenched with ice and left standing in a refrigerator overnight. The precipitated was filtered off and dried to afford **71** as white solid: 1.24 g (97%);  $^1\text{H}$  NMR (400 MHz,  $\text{DMSO}-d_6$ )  $\delta$  12.02 (br s, 1H), 2.04 (br s, 1H), 1.61 (s, 2H), 1.45-1.36 (m, 4H), 1.34-1.26 (m, 4H), 1.14-1.07 (m, 2H), 0.80 (s, 6H).

**(1*r*,3*s*,5*R*,7*S*)-3-acetamido-5,7-dimethyladamantane-1-carboxylic acid (72).** 1.24 g (5.95 mmol) of **71** was suspended in HNO<sub>3</sub> (3.60 mL) and cooled to 0 °C with an ice bath. After the addition of H<sub>2</sub>SO<sub>4</sub> (6 mL), the mixture was stirred at 0 °C for 10 min. 2.10 mL of oleum (25% SO<sub>3</sub>) was then added and the mixture stirred for 30 min at 0 °C and 1 h at room temp. After cooling to 0 °C, 3.6 mL of technical grade acetonitrile was added, the mixture was stirred for 10 min at 0 °C and 12 h at room temp. Finally, the mixture was poured onto ca. 2 kg of ice with shaking and left standing in a refrigerator overnight. The colorless precipitate was collected via suction filtration to give **72** as white solid: 1.57 g, (98%); <sup>1</sup>H NMR (400 MHz, DMSO-*d*<sub>6</sub>) δ 7.39 (br s, 1H), 1.84 (s, 2H), 1.73 (s, 3H), 1.57-1.47 (m, 4H), 1.41-1.32 (m, 4H), 1.09-1.05 (m, 2H), 0.84 (s, 6H).

**(1*r*,3*s*,5*R*,7*S*)-3-amino-5,7-dimethyladamantane-1-carboxylic acid hydrochloride (73).** **72** was refluxed in HCl 12 N (36-38%) for 80 h. After evaporation of the acid under reduced pressure to dryness, the crude product were treated with ethyl acetate and collected via suction filtration to afford **73** as white solid: 1.25 g, (83%); <sup>1</sup>H NMR (400 MHz, DMSO-*d*<sub>6</sub>) δ 12.33 (br s, 1H), 8.35 (br s, 3H), 7.33 [t, *J*(<sup>15</sup>N-H) = 50.8 Hz, 1H], 1.76 (s, 2H), 1.47-1.34 (m, 8H), 1.12-1.09 (m, 2H), 0.88 (s, 6H).

**General procedure for the intermediates 77-79.** To an ice-cooled solution of the appropriate diamine (**74-76**, 5-10 equiv) in CH<sub>2</sub>Cl<sub>2</sub> (30-40 mL) was added dropwise a solution of Boc<sub>2</sub>O (1 equiv) in CH<sub>2</sub>Cl<sub>2</sub> (30-40 mL). The solution was stirred at room temperature for 12 h, then evaporated under vacuo and purified by flash chromatography on silica gel using dichloromethane/methanol/ammonia solution 30% (8:2:0.2) as mobile phase.

**tert-butyl (2-aminoethyl)carbamate (77).** Synthesized from 1,2-ethanediamine (**74**, 6 g, 0.10 mol) to give **77** as a pale oil: 1.7 g (99%); <sup>1</sup>H NMR (400 MHz, CDCl<sub>3</sub>) δ 5.03 (br s, 1H exch with D<sub>2</sub>O), 3.19-3.15 (m, 2H), 2.80 (t, *J* = 5.8 Hz, 2H), 2.13 (br s, 2H exch with D<sub>2</sub>O), 1.42 (s, 9H).

**tert-butyl (3-aminopropyl)carbamate (78).** Synthesized from 1,3-propanediamine (**75**, 3.41 g, 0.046 mol) to give **78** as a pale oil: 1.1 g (69%); <sup>1</sup>H NMR (400 MHz, CDCl<sub>3</sub>) δ 4.80 (br s, 1H exch

with D<sub>2</sub>O), 3.21-3.19 (m, 2H), 2.79-2.75 (m, 2H), 1.82 (br s, 2H, exch with D<sub>2</sub>O), 1.64-1.60 (m, 2H), 1.43 (s, 9H).

***tert*-butyl (4-aminobutyl)carbamate (79).** Synthesized from 1,4-butanediamine (**76**, 2 g, 0.023 mol) to give **79** as a pale oil: 0.83 g (96%); <sup>1</sup>H NMR (400 MHz, CDCl<sub>3</sub>) δ 5.95 (br s, 1H exch with D<sub>2</sub>O), 3.24-3.19 (m, 2H), 2.79-2.72 (m, 2H), 2.34 (br s, 2H exch with D<sub>2</sub>O), 1.59-1.52 (m, 4H), 1.38 (s, 9H).

**General procedure for the intermediates 81-83, 87, 88.** To an ice-cooled solution of the appropriate acid (**35** and **80**) (1 equiv) in dry DMF (3-4 mL) was added HOBt (1.3 equiv) and EDC (1.3 equiv). The reaction mixture was stirred for 10 min, followed by addition of Et<sub>3</sub>N (1.3 equiv) and the appropriate mono-protected diamine (**77-79**) (1 equiv). Stirring was then continued at room temperature overnight, and the solvent evaporated under *vacuum*. The crude was purified by flash chromatography on silica gel using dichloromethane/methanol (9.5:0.5) as mobile phase. The intermediate **80** was synthesized as described in the literature for the synthesis of *trans*-cinnamic acid through the Knoevenagel-Doebner reaction.

***tert*-butyl (E)-(2-(3-(4-hydroxy-3-methoxyphenyl)acrylamido)ethyl)carbamate (81).** **81** was synthesized from **80** (400 mg, 2.06 mmol) and **77** (330 mg, 2.06 mmol) to afford **81** as waxy solid: 200 mg (30%); <sup>1</sup>H NMR (400 MHz, CDCl<sub>3</sub>) δ 7.50 (d, *J* = 15.6 Hz, 1H), 6.99 (d, *J* = 8 Hz, 1H), 6.94 (s, 1H), 6.88 (d, *J* = 8.4 Hz, 1H), 6.60 (br s, 1H), 6.26 (d, *J* = 15.6 Hz, 1H), 5.33 (br s, 1H), 3.85 (s, 3H), 3.50-3.46 (m, 2H), 3.33-3.30 (m, 2H), 1.42 (s, 9H).

***tert*-butyl (E)-(3-(3-(4-hydroxy-3-methoxyphenyl)acrylamido)propyl)carbamate (82).** **82** was synthesized from **80** (100 mg, 0.51 mmol) and **78** (174 mg, 0.51 mmol) to afford **82** as waxy solid: 100 mg (56%); <sup>1</sup>H NMR (400 MHz, CDCl<sub>3</sub>) δ 7.55 (d, *J* = 15.2 Hz, 1H), 7.05 (d, *J* = 8 Hz, 1H), 7.01 (s, 1H), 6.90 (d, *J* = 8 Hz, 1H), 6.50 (br s, 1H), 6.30 (d, *J* = 15.2 Hz, 1H), 4.96 (br s, 1H), 3.92 (s, 3H), 3.44-3.40 (m, 2H), 3.23-3.19 (m, 2H), 1.67-1.61 (m, 2H), 1.45 (s, 9H).

***tert*-butyl (*E*)-(4-(3-(4-hydroxy-3-methoxyphenyl)acrylamido)butyl)carbamate (83).** **83** was synthesized from **80** (400 mg, 2.06 mmol) and **79** (188 mg, 2.06 mmol) to afford **83** as waxy green solid: 230 mg (33%); <sup>1</sup>H NMR (400 MHz, CDCl<sub>3</sub>) δ 7.52 (d, *J* = 15.2 Hz, 1H), 7.03 (d, *J* = 8.4 Hz, 1H), 6.98 (s, 1H), 6.88 (d, *J* = 8 Hz, 1H), 6.25 (d, *J* = 15.2 Hz, 1H), 6.01 (br s, 1H), 4.64 (br s, 1H), 3.89 (s, 3H), 3.39-3.38 (m, 2H), 3.17-3.13 (m, 2H), 1.60-1.55 (m, 4H), 1.43 (s, 9H).

***tert*-butyl (*E*)-(2-(3-(3,4-bis((*tert*-butyldimethylsilyloxy)phenyl)acrylamido)ethyl)carbamate (87).** **87** was synthesized from **35** (600 mg, 1.47 mmol) and **77** (236 mg, 1.47 mmol). Elution with petroleum ether/ethyl acetate (6:4) afforded **87** as brown oil: 500 mg (62%); <sup>1</sup>H NMR (400 MHz, CDCl<sub>3</sub>) δ 7.47 (d, *J* = 15.6 Hz, 1H), 6.97 (d, *J* = 9.2 Hz, 1H), 6.97 (s, 1H), 6.19 (d, *J* = 15.6 Hz, 1H), 3.48-3.47 (m, 2H), 3.33 (br, 2H), 1.43 (s, 9H), 0.98 (s, 18H), 0.20 (s, 12H).

***tert*-butyl (*E*)-(3-(3-(3,4-bis((*tert*-butyldimethylsilyloxy)phenyl)acrylamido)propyl)carbamate (88).** **88** was synthesized from **35** (520 mg, 1.28 mmol) and **78** (174 mg, 1.28 mmol). Elution with petroleum ether/ethyl acetate (5.5:4.5) afforded **88** as brown oil: 660 mg (91%); <sup>1</sup>H NMR (400 MHz, CDCl<sub>3</sub>) δ 7.46 (d, *J* = 15.6 Hz, 1H), 6.97-6.94 (m, 2H), 6.76-6.74 (m, 1H), 6.25 (d, *J* = 15.6 Hz, 1H), 3.40-3.36 (m, 2H), 3.16-3.14 (m, 2H), 1.64-1.61 (m, 2H), 1.40 (s, 9H), 0.94 (s, 18H), 0.17 (s, 12H).

**General procedure for the intermediates 84-86, 89, 90.** To an ice-cooled solution of the appropriate Boc-protected intermediate (**81-83**, **87**, **88**, 1 equiv) in CH<sub>2</sub>Cl<sub>2</sub> (2-3 mL) was added HCl 4 M in dioxane (2-3 mL) and the reaction mixture was stirred at 0 °C for 90 min. The solvent was evaporated and the crude purified by flash chromatography on silica gel using dichloromethane/methanol/ammonia solution 30% (8:2:0.2) affording desired intermediates as free bases.

**(*E*)-*N*-(2-aminoethyl)-3-(4-hydroxy-3-methoxyphenyl)acrylamide (84).** Synthesized from **81** (200 mg, 0.60 mmol) to give **84** as pale yellow solid: 120 mg (86%); <sup>1</sup>H NMR (400 MHz, DMSO-*d*<sub>6</sub>) δ 8.34 (t, *J* = 5.4 Hz, 1H), 7.72 (d, *J* = 15.6 Hz, 1H), 7.53 (s, 1H), 7.41-7.38 (m, 1H), 7.20 (d, *J* =

7.6 Hz, 1H), 6.86 (d,  $J = 15.6$  Hz, 1H), 4.21 (s, 3H), 3.59-3.55 (m, 2H), 3.04-3.00 (m, 2H), 2.92 (br s, 2H).

**(*E*)-*N*-(3-aminopropyl)-3-(4-hydroxy-3-methoxyphenyl)acrylamide (85).** Synthesized from **82** (100 mg, 0.30 mmol) to give **85** as pale green solid: 71 mg (99%);  $^1\text{H}$  NMR (400 MHz,  $\text{CD}_3\text{OD}$ )  $\delta$  7.40 (d,  $J = 15.6$  Hz, 1H), 7.10 (s, 1H), 7.00-6.98 (m, 1H), 6.77 (d,  $J = 8.4$  Hz, 1H), 6.48 (d,  $J = 15.6$  Hz, 1H), 3.84 (s, 3H), 3.38 (t,  $J = 6.4$  Hz, 2H), 2.96 (t,  $J = 7.2$  Hz, 2H), 1.95-1.88 (m, 2H).

**(*E*)-*N*-(4-aminobutyl)-3-(4-hydroxy-3-methoxyphenyl)acrylamide (86).** Synthesized from **83** (230 mg, 0.63 mmol) to give **86** as pale green solid: 160 mg (96%);  $^1\text{H}$  NMR (400 MHz,  $\text{CD}_3\text{OD}$ )  $\delta$  7.39 (d,  $J = 15.6$  Hz, 1H), 7.05 (s, 1H), 6.96 (d,  $J = 7.6$  Hz, 1H), 6.73 (d,  $J = 8.4$  Hz, 1H), 6.40 (d,  $J = 15.6$  Hz, 1H), 3.82 (s, 3H), 3.31-3.23 (m, 2H), 2.80-2.78 (m, 2H), 1.59-1.58 (m, 4H).

**(*E*)-*N*-(2-aminoethyl)-3-(3,4-bis((*tert*-butyldimethylsilyl)oxy)phenyl)acrylamide (89).** Synthesized from **87** (500 mg, 0.91 mmol) to give **89** as pale green solid: 360 mg (88%);  $^1\text{H}$  NMR (400 MHz,  $\text{DMSO-}d_6$ )  $\delta$  7.29 (d,  $J = 15.6$  Hz, 1H), 7.04 (d,  $J = 6.8$  Hz, 1H), 7.04 (s, 1H), 6.87 (d,  $J = 9.2$  Hz, 1H), 6.44 (d,  $J = 15.6$  Hz, 1H), 3.17-3.14 (m, 2H), 2.62 (t,  $J = 6.4$  Hz, 2H), 0.95 (s, 18H), 0.20 (s, 12H).

**(*E*)-*N*-(3-aminopropyl)-3-(3,4-bis((*tert*-butyldimethylsilyl)oxy)phenyl)acrylamide (90).** Synthesized from **88** (610 mg, 1.08 mmol) to give **90** as pale green solid: 390 mg (78%);  $^1\text{H}$  NMR (400 MHz,  $\text{CDCl}_3$ )  $\delta$  7.46 (d,  $J = 15.6$  Hz, 1H), 6.99-6.96 (m, 2H), 6.78 (d,  $J = 8.4$  Hz, 1H), 6.62 (br s, 1H), 6.21 (d,  $J = 15.6$  Hz, 1H), 3.50-3.46 (m, 2H), 2.87 (t,  $J = 6.2$  Hz, 2H), 2.57 (br s, 2H), 1.77-1.74 (m, 2H), 0.97 (s, 18H), 0.19 (s, 12H).

**General procedure for compounds 18-20 and intermediates 91, 92.** To an ice-cooled solution of the hydrochloride salt **73** (1 equiv) in dry DMF (3 mL) was added HOBt (1.3 equiv) and EDC (1.3 equiv) under nitrogen atmosphere. The reaction mixture was stirred for 10 min, followed by addition of the appropriate intermediates (**84-86**, **89**, **90**) (2 equiv). Stirring was continued at room temperature for 36-48 h, and then the solvent evaporated under *vacuum*. The crude was purified by

column chromatography on silica gel using dichloromethane/methanol/ammonia solution 30% (8.5:1.5:0.15) as mobile phase.

**(1*r*,3*s*,5*R*,7*S*)-3-amino-*N*-(2-((*E*)-3-(4-hydroxy-3-methoxyphenyl)acrylamido)ethyl)-5,7-dimethyladamantane-1-carboxamide (18).** Synthesized from **73** (64 mg, 0.24 mmol) and **84** (115 mg, 0.48 mmol) to give **18** as green solid: 80 mg (74%); <sup>1</sup>H NMR (400 MHz, DMSO-*d*<sub>6</sub>) δ 7.99 (t, *J* = 5.6 Hz, 1H), 7.46 (t, *J* = 5.2 Hz, 1H), 7.32 (d, *J* = 15.6 Hz, 1H), 7.11 (s, 1H), 6.99-6.97 (m, 1H), 6.80 (d, *J* = 8.4 Hz, 1H), 6.40 (d, *J* = 15.6 Hz, 1H), 3.80 (s, 3H), 3.20-3.17 (m, 2H), 3.15-3.12 (m, 2H), 1.40 (s, 2H), 1.29-1.23 (m, 4H), 1.16-1.12 (m, 4H), 1.01 (s, 2H), 0.82 (s, 6H). <sup>13</sup>C NMR (100 MHz, DMSO-*d*<sub>6</sub>) δ 176.77, 166.17, 148.84, 148.27, 139.55, 126.70, 121.97, 119.25, 116.10, 111.23, 55.96, 51.30, 49.90, 49.79, 49.03, 46.18, 44.55, 44.10, 38.90, 32.95, 30.19. MS [ESI+] *m/z* 442 [M+1]<sup>+</sup>.

**(1*r*,3*s*,5*R*,7*S*)-3-amino-*N*-(3-((*E*)-3-(4-hydroxy-3-methoxyphenyl)acrylamido)propyl)-5,7-dimethyladamantane-1-carboxamide (19).** Synthesized from **73** (37 mg, 0.14 mmol) and **85** (71 mg, 0.28 mmol) to give **19** as green solid: 31 mg (52%); <sup>1</sup>H NMR (400 MHz, CD<sub>3</sub>OD) δ 7.42 (d, *J* = 15.6 Hz, 1H), 7.10 (s, 1H), 7.01-6.98 (m, 1H), 6.76 (d, *J* = 8 Hz, 1H), 6.39 (d, *J* = 15.6 Hz, 1H), 3.85 (s, 3H), 3.27 (t, *J* = 6.8 Hz, 2H), 3.21 (t, *J* = 6.4 Hz, 2H), 1.69-1.66 (m, 2H), 1.61 (s, 2H), 1.43 (s, 4H), 1.30-1.25 (m, 4H), 1.12 (s, 2H), 0.90 (s, 6H). <sup>13</sup>C NMR (100MHz, CD<sub>3</sub>OD) δ 177.79, 168.00, 148.87, 148.00, 140.82, 126.55, 121.91, 117.08, 115.16, 110.09, 54.95, 50.48, 48.96, 48.41, 48.28, 44.09, 43.78, 43.43, 36.40, 36.37, 32.47, 28.98, 28.60. MS [ESI+] *m/z* 455 [M+1]<sup>+</sup>.

**(1*r*,3*s*,5*R*,7*S*)-3-amino-*N*-(4-((*E*)-3-(4-hydroxy-3-methoxyphenyl)acrylamido)butyl)-5,7-dimethyladamantane-1-carboxamide (20).** Synthesized from **73** (89 mg, 0.30 mmol) and **86** (160 mg, 0.61 mmol) to give **20** as green solid: 68 mg (48%); <sup>1</sup>H NMR (400 MHz, CD<sub>3</sub>OD) δ 7.40 (d, *J* = 15.6 Hz, 1H), 7.05 (s, 1H), 6.98-6.95 (m, 1H), 6.73 (d, *J* = 8 Hz, 1H), 6.37 (d, *J* = 15.6 Hz, 1H), 3.82 (s, 3H), 3.27-3.25 (m, 2H), 3.16-3.13 (m, 2H), 1.54-1.50 (m, 6H), 1.40-1.34 (m, 4H), 1.27-1.21 (m, 4H), 1.07 (s, 2H), 0.86 (s, 6H). <sup>13</sup>C NMR (100 MHz, CD<sub>3</sub>OD) δ 177.94, 167.90, 149.828, 148.28, 140.76, 126.04, 122.02, 116.86, 115.50, 110.03, 54.92, 49.76, 49.12, 49.09, 48.47, 44.22, 44.09, 43.91, 38.77, 38.63, 32.46, 28.76, 26.53, 26.44. MS [ESI+] *m/z* 470 [M+1]<sup>+</sup>.

**(1*r*,3*s*,5*R*,7*S*)-3-amino-*N*-(2-((*E*)-3-(3,4-bis((*tert*-butyldimethylsilyloxy)phenyl)acrylamido)ethyl)-5,7-dimethyladamantane-1-carboxamide (91).** Synthesized from **73** (46 mg, 0.18 mmol) and **89** (160 mg, 0.35 mmol) to give **91** as green solid: 40 mg (34%); <sup>1</sup>H NMR (400 MHz, CDCl<sub>3</sub>) δ 7.45 (d, *J* = 15.6 Hz, 1H), 6.989 (d, *J* = 8.0 Hz, 1H), 6.946 (s, 1H), 6.77 (d, *J* = 8.0 Hz, 1H), 6.26 (d, *J* = 15.6, 1H), 3.48-3.41 (m, 4H), 1.68 (s, 2H), 1.41 (s, 4H), 1.39-1.34 (m, 6H), 0.96 (s, 18H), 0.87 (s, 6H), 0.18 (s, 12H).

**(1*r*,3*s*,5*R*,7*S*)-3-amino-*N*-(3-((*E*)-3-(3,4-bis((*tert*-butyldimethylsilyloxy)phenyl)acrylamido)propyl)-5,7-dimethyladamantane-1-carboxamide (92).** Synthesized from **73** (110 mg, 0.42 mmol) and **90** (390 mg, 0.84 mmol) to give **92** as green solid: 160 mg (57%); <sup>1</sup>H NMR (400 MHz, CDCl<sub>3</sub>) δ 7.46 (d, *J* = 15.6 Hz, 1H), 6.99-6.94 (m, 2H), 6.81 (br s, 1H), 6.77 (d, *J* = 8 Hz, 1H), 6.61 (br s, 1H), 6.27 (d, *J* = 15.6 Hz, 1H), 3.33-3.27 (m, 4H), 1.64-1.62 (m, 2H), 1.60 (s, 2H), 1.42 (s, 4H), 1.25-1.21 (m, 4H), 1.08 (s, 2H), 0.96 (s, 18H), 0.87 (s, 6H), 0.17 (s, 12H).

**General procedure for compounds 21 and 22.** To an ice-cooled solution of the appropriate protected-alcohol **91** and **92** (1 equiv) in methanol (1-2 mL) was added acetyl chloride (0.45 equiv). The reaction mixture was stirred for 1 h at 0 °C, then the solvent was removed under *vacuum*. The crude was purified by column chromatography on silica gel using dichloromethane/methanol/ammonia solution 30% (7:3:0.3) as mobile phase.

**(1*r*,3*s*,5*R*,7*S*)-3-amino-*N*-(2-((*E*)-3-(3,4-dihydroxyphenyl)acrylamido)ethyl)-5,7-dimethyladamantane-1-carboxamide (21).** Synthesized from **91** (30 mg, 0.04 mmol) to give **21** as pale green solid: 12 mg (58%); <sup>1</sup>H NMR (400 MHz, CD<sub>3</sub>OD) δ 7.34 (d, *J* = 15.6 Hz, 1H), 6.95 (s, 1H), 6.84 (d, *J* = 7.6 Hz, 1H), 6.70 (d, *J* = 8.4 Hz, 1H), 6.29 (d, *J* = 15.6 Hz, 1H), 3.37-3.36 (m, 2H), 3.27 (t, *J* = 1.6 Hz, 2H), 1.85 (s, 2H), 1.57 (s, 2H), 1.39 (s, 2H), 1.27 (s, 2H), 1.25 (s, 2H), 1.09 (s, 2H), 0.87 (s, 6H). <sup>13</sup>C NMR (100 MHz, CD<sub>3</sub>OD) δ 178.17, 168.50, 148.24, 145.71, 141.23, 126.33,

120.81, 116.48, 115.04, 113.35, 50.37, 48.97, 44.05, 43.73, 43.38, 39.33, 38.51, 32.44, 29.32, 28.60.  
MS [ESI+]  $m/z$  428 [M+1]<sup>+</sup>.

**(1*r*,3*s*,5*R*,7*S*)-3-amino-*N*-(3-((*E*)-3-(3,4-dihydroxyphenyl)acrylamido)propyl)-5,7-dimethyladamantane-1-carboxamide (22).** Synthesized from **92** (160 mg, 0.24 mmol) to give **22** as pale green solid: 35 mg (34%); <sup>1</sup>H NMR (400 MHz, DMSO-*d*<sub>6</sub>) δ 8.00 (br s, 1H), 7.50 (br s, 1H), 7.22 (d, *J* = 16 Hz, 1H), 6.94 (s, 1H), 6.82 (d, *J* = 8 Hz, 1H), 6.73 (d, *J* = 8 Hz, 1H), 6.30 (d, *J* = 15.6 Hz, 1H), 3.12-3.05 (m, 4H), 1.57-1.51 (m, 4H), 1.33-1.23 (m, 8H), 1.05 (s, 2H), 0.85 (s, 6H). <sup>13</sup>C NMR (100 MHz, DMSO-*d*<sub>6</sub>) δ 175.91, 165.89, 147.81, 146.02, 139.46, 126.73, 120.76, 118.87, 116.19, 114.26, 51.43, 50.52, 49.48, 49.02, 48.60, 44.27, 43.88, 36.90, 36.83, 32.90, 29.91, 29.76. MS [ESI+]  $m/z$  442 [M+1]<sup>+</sup>.

**2-(tritylthio)ethan-1-amine (93).** A mixture of 2-aminoethane-1-thiol hydrochloride (300 mg, 2.64 mmol) and trityl chloride (490 mg, 1.76 mmol) in 1.5 mL of dry DMF was placed in a microwave (60 °C, 250 Psi, 80 W) for 20 min. The solvent was removed under reduced pressure and the crude purified by flash chromatography on silica gel using dichloromethane/methanol/ammonia solution 30% (9:1:0.1) as mobile phase to give **93** as waxy pale yellow solid: 540 mg (99%); <sup>1</sup>H NMR (400 MHz, CDCl<sub>3</sub>) δ 7.40 (d, *J* = 7.6 Hz, 6H), 7.26 (t, *J* = 7.6 Hz, 6H), 7.19 (d, *J* = 7.2 Hz, 3H), 2.56 (t, *J* = 6.4 Hz, 2H), 2.32 (t, *J* = 6.4 Hz, 2H), 1.75 (br s, 2H exch with D<sub>2</sub>O). <sup>13</sup>C NMR (100 MHz, CDCl<sub>3</sub>) δ 144.85, 129.57, 129.54, 127.92, 127.87, 126.66, 66.58, 40.89, 35.91.

**(1*r*,3*s*,5*R*,7*S*)-3-amino-5,7-dimethyl-*N*-(2-(tritylthio)ethyl)adamantane-1-carboxamide (94).** To an ice-cooled solution of **73** (228 mg, 0.88 mmol) in dry DMF (2.5 mL) under nitrogen atmosphere was added HOBt (154 mg, 1.14 mmol) and EDC (191 mg, 1.14 eq). The reaction mixture was stirred for 15 min, followed by addition dropwise of **93** (540 mg, 1.76 mmol) in dry DMF (2.5 mL). Stirring was then continued at room temperature for 36 h, and then the solvent evaporated under *vacuum*. The crude was purified by column chromatography on silica gel using dichloromethane/methanol/ammonia solution 30% (9:1:0.1) as mobile phase to give **94** as white solid: 378 mg (84%); <sup>1</sup>H NMR (400 MHz, CDCl<sub>3</sub>) δ 7.39 (d, *J* = 7.6 Hz, 6H), 7.27 (t, *J* = 7.6 Hz, 6H), 7.20 (d, *J* = 7.6 Hz, 3H), 5.78 (t, *J* = 4.0 Hz, 1H), 3.07 (dd, <sup>1</sup>*J* = 12.2, <sup>2</sup>*J* = 6.0 Hz, 2H), 2.36 (t,

$J = 6.0$  Hz, 2H), 2.25 (br s, 2H), 1.53 (s, 2H), 1.35 (q,  $J = 12.3$  Hz, 4H), 1.26 (s, 4H), 1.10 (s, 2H), 0.89 (s, 6H).  $^{13}\text{C}$  NMR (100 MHz,  $\text{CDCl}_3$ )  $\delta$  176.36, 144.59, 129.50, 127.95, 126.79, 66.69, 50.61, 50.56, 50.11, 49.52, 45.68, 44.38, 44.35, 37.98, 33.02, 32.15, 29.60.

**(9H-fluoren-9-yl)methyl** **((1s,3R,5S,7r)-3,5-dimethyl-7-((2-(tritylthio)ethyl)carbamoyl)adamantan-1-yl)carbamate (95)**. To a solution of **94** (390 mg, 0.74 mmol) in  $\text{CH}_2\text{Cl}_2$  (3.5 mL) was added aqueous solution of  $\text{Na}_2\text{CO}_3$  10% (2 mL) and the reaction mixture was cooled down to 0 °C. A solution of Fmoc-Cl (212 mg, 0.82 mmol) in  $\text{CH}_2\text{Cl}_2$  (2 mL) was added dropwise and then stirred at room temperature for 90 min. The solvent was removed under *vacuum* and the crude purified by flash chromatography on silica gel using petroleum ether/ethyl acetate (7:3) as mobile phase to afford **95** as waxy solid: 410 mg (75%);  $^1\text{H}$  NMR (400 MHz,  $\text{CDCl}_3$ )  $\delta$  7.74 (d,  $J = 7.6$  Hz, 2H), 7.56 (d,  $J = 7.6$  Hz, 2H), 7.42-7.36 (m, 8H), 7.31-7.24 (m, 8H), 7.20 (t,  $J = 7.2$  Hz, 3H), 5.79 (br s, 1H), 4.70 (br s, 1H), 4.33 (s, 2H), 4.18 (t,  $J = 4.6$  Hz, 1H), 3.09 (dd,  $^1J = 6.4$  Hz,  $^2J = 5.6$  Hz, 2H), 2.37 (t,  $J = 6.4$  Hz, 2H), 1.86 (s, 2H), 1.69-1.56 (m, 4H), 1.49-1.38 (m, 4H), 1.14 (s, 2H), 0.91 (s, 6H).  $^{13}\text{C}$  NMR (100 MHz,  $\text{CDCl}_3$ )  $\delta$  175.82, 144.45, 143.86, 141.15, 129.36, 127.82, 127.48, 126.89, 126.65, 124.78, 119.83, 66.56, 53.27, 52.59, 49.44, 47.15, 46.71, 44.28, 43.77, 41.58, 37.90, 32.54, 31.97, 29.39.

**(9H-fluoren-9-yl)methyl** **((1s,3r,5R,7S)-3-((2-mercaptoethyl)carbamoyl)-5,7-dimethyladamantan-1-yl)carbamate (96)**. To an ice-cooled solution of **95** (250 mg, 0.33 mmol) in  $\text{CH}_2\text{Cl}_2$  (8 mL) was added trifluoroacetic acid (3 mL) and triethylsilane (0.1 mL) and the reaction mixture was stirred at room temp for 10 min. The solvent was evaporated and the crude purified by flash chromatography on silica gel using petroleum ether/ethyl acetate (5:5) as mobile phase to afford **96** as waxy solid: 155 mg (92%);  $^1\text{H}$  NMR (400 MHz,  $\text{CDCl}_3$ )  $\delta$  7.76 (d,  $J = 8.0$  Hz, 2H), 7.58 (d,  $J = 8.0$  Hz, 2H), 7.40 (t,  $J = 8.0$  Hz, 2H), 7.33-7.30 (m, 2H), 6.06 (br s, 1H), 4.72 (br s, 1H), 4.34 (s, 2H), 4.20 (t,  $J = 6.4$  Hz, 1H), 3.40 (dd,  $^1J = 12.4$  Hz,  $^2J = 6.2$  Hz, 2H), 2.65 (dd,  $^1J = 14.7$  Hz,  $^2J = 6.4$  Hz, 2H), 1.94 (s, 2H), 1.65-1.47 (m, 8H), 1.16 (s, 2H), 0.92 (s, 6H).  $^{13}\text{C}$  NMR (100 MHz,  $\text{CDCl}_3$ )  $\delta$  176.32, 143.96, 141.28, 127.61, 126.99, 124.93, 119.96, 65.86, 52.74, 49.52, 47.26, 46.89, 44.46, 44.02, 42.13, 41.69, 32.67, 29.49, 24.57.

***S*-2-(((1*r*,3*s*,5*R*,7*S*)-3-(((9*H*-fluoren-9-yl)methoxy)carbonyl)amino)-5,7-dimethyladamantane-1-carboxamido)ethyl) (E)-3-(3,4-bis((*tert*-butyldimethylsilyl)oxy)phenyl)prop-2-enethioate (97).** To an ice-cooled solution of **73** (65 mg, 0.26 mmol) in CH<sub>2</sub>Cl<sub>2</sub> (2 mL) under nitrogen atmosphere was added HOBt (28 mg, 0.33 mmol) and EDC (40 mg, 0.33 mmol). The reaction mixture was stirred at 0 °C for 30 min, followed by addition of DIPEA (32 μL) and **35** (80 mg, 0.26 mmol). After stirring at room temp for 3 h, the solvent was removed under *vacuum* and the crude purified by flash chromatography on silica gel using petroleum ether/ethyl acetate (6:4) as mobile phase to afford **97** as waxy solid: 70 mg (49%); <sup>1</sup>H NMR (400 MHz, CDCl<sub>3</sub>) δ 7.75 (d, *J* = 7.2 Hz, 2H), 7.57 (d, *J* = 7.6 Hz, 2H), 7.52 (d, *J* = 16.0 Hz, 1H), 7.39 (t, *J* = 8.0 Hz, 2H), 7.31 (t, *J* = 8.0 Hz, 2H), 7.04 (d, *J* = 8.0 Hz, 1H), 7.01 (s, 1H), 6.81 (d, *J* = 8.0 Hz, 1H), 6.54 (d, *J* = 16.0 Hz, 1H), 4.68 (br s, 1H), 4.32 (s, 2H), 4.19 (t, *J* = 6.2 Hz, 1H), 3.49 (dd, <sup>1</sup>*J* = 12.0 Hz, <sup>2</sup>*J* = 6.2 Hz, 2H), 3.16 (t, *J* = 6.2 Hz, 2H), 1.89 (s, 2H), 1.66-1.13 (m, 10H), 0.98 (s, 18H), 0.88 (s, 6H), 0.21 (s, 12H). <sup>13</sup>C NMR (100 MHz, CDCl<sub>3</sub>) δ 190.31, 147.30, 144.01, 141.45, 141.29, 127.61, 127.35, 127.01, 122.75, 122.33, 121.25, 120.94, 119.96, 47.29, 46.83, 41.76, 39.81, 28.26, 25.86, 25.83, 18.49, 18.40, - 4.07, - 4.12.

***S*-2-(((1*r*,3*s*,5*R*,7*S*)-3-amino-5,7-dimethyladamantane-1-carboxamido)ethyl) (E)-3-(3,4-dihydroxyphenyl)prop-2-enethioate (23).** To a solution of **97** (140 mg, 0.16 mmol) in THF (2 mL) was added TBAF (0.18 mL, 0.8 mmol) and stirring was continued under nitrogen atmosphere at room temperature. After 1 h, the solvent evaporated under *vacuum*, the crude was washed with diethyl ether and dried under *vacuo*. The residue was then dissolved in CH<sub>2</sub>Cl<sub>2</sub> (4 mL) and BOP reagent (495 mg, 1.12 mmol) was added. The reaction mixture was stirred for 30 min, followed by decantation. The resulting solution was filtered and evaporated, and the residue was purified by column chromatography on silica gel using dichloromethane/methanol/ammonia solution 30% (7:3:0.3) as mobile phase to give **23** as green solid: 14 mg (22%). <sup>1</sup>H NMR (400 MHz, CD<sub>3</sub>OD) δ 7.49 (d, *J* = 15.6 Hz, 1H), 7.04 (s, 1H), 6.96 (d, *J* = 8.4 Hz, 1H), 6.75 (d, *J* = 8.4 Hz, 1H), 6.59 (d, *J* = 15.6 Hz, 1H), 3.40 (t, *J* = 6.4 Hz, 2H), 3.16-3.13 (m, 2H), 1.63 (s, 2H), 1.42 (s, 4H), 1.33 (s, 4H), 1.14 (s, 2H), 0.91 (s, 6H). <sup>13</sup>C NMR (100 MHz, CD<sub>3</sub>OD) δ 191.44, 179.42, 151.87, 147.69, 143.53, 126.66, 124.13, 121.95, 116.93, 115.12, 52.24, 50.55, 50.04, 45.68, 45.36, 44.73, 40.64, 34.08, 30.99, 30.96, 30.21, 29.09. MS [ESI+] *m/z* 443 [M+1]<sup>+</sup>.

## 3.2 Biology

### *Sample preparation for A $\beta$ <sub>42</sub> self-aggregation.*

1,1,1,3,3,3-Hexafluoro-2-propanol (HFIP)-pretreated A $\beta$ <sub>42</sub> samples (Bachem AG, Switzerland) were resolubilized with a CH<sub>3</sub>CN/0.3 mM Na<sub>2</sub>CO<sub>3</sub>/250 mMNaOH (48.4:48.4:3.2) mixture to have a stable stock solution ([A $\beta$ <sub>42</sub>]=500  $\mu$ M)<sup>251</sup>. Tested inhibitors were dissolved in MeOH and diluted in the assay buffer. Experiments were performed by incubating the peptide diluted in 10 mMphosphate buffer (pH 8.0) containing 10 mM NaCl at 30°C (Thermomixer Comfort, Eppendorf, Italy) for 24 h (final A $\beta$  concentration=50  $\mu$ M) with and without inhibitor.

***Inhibition of A $\beta$ <sub>42</sub> self-aggregation: ThT assay.*** Inhibition studies were performed by incubating A $\beta$ <sub>42</sub> samples in the assay conditions reported above, with and without tested inhibitors. Inhibitors were first screened at 50  $\mu$ M in a 1:1 ratio with A $\beta$ <sub>42</sub>. To quantify amyloid fibril formation, the ThT fluorescence method was used.<sup>252, 253</sup> After incubation, samples were diluted to a final volume of 2.0 mL with 50 mM glycine-NaOH buffer (pH = 8.5) containing 1.5  $\mu$ M ThT. A 300-seconds-time scan of fluorescence intensity was carried out ( $\lambda_{exc}$  = 446 nm;  $\lambda_{em}$  = 490 nm), and values at plateau were averaged after subtracting the background fluorescence of 1.5  $\mu$ M ThT solution. Blanks containing inhibitor and ThT were also prepared and evaluated to account for quenching and fluorescence properties. The fluorescence intensities were compared and the % inhibition was calculated. For compounds **I**, **V**, **5**, **7** and **8**, the IC<sub>50</sub> value was also determined. To this aim four increasing concentrations were tested. IC<sub>50</sub> value was obtained from the % inhibition vs log[inhibitor] plot.

***Inhibition of A $\beta$ <sub>42</sub> self-aggregation by I, as determined by flow injection ESI-MS.*** Inhibition studies were performed by incubating A $\beta$ <sub>42</sub> samples in the assay conditions reported above, with and without the tested inhibitor **I** or curcumin. At t = 0 and t = 24 h, aliquots with and without inhibitor were analyzed by flow injection-ESI-IT-MS. LC-MS analyses were performed as described in Fiori *et al.*<sup>242</sup> Briefly, the A $\beta$ <sub>42</sub> samples were analyzed by 10- $\mu$ L loop injection after previous addition of reserpine as internal standard. ESI-IT-MS analyses were performed on a Jasco PU-1585 Liquid Chromatograph (Jasco, Tokyo, Japan) interfaced with LCQ Duo Mass Spectrometer (ThermoFinnigan, San Jose, CA, USA) equipped with an electrospray ionization (ESI) source

operating with an ion trap analyzer. The mobile phase consisted of 0.1% (v/v) formic acid in acetonitrile/water 30/70. ESI system employed a 4.5 kV spray voltage and a capillary temperature of 200°C. Mass spectra were operated in positive polarity, in the scan range of 200-2000  $m/z$  and at the scan rate of 3 microscans/sec. Single ion monitoring (SIM) chromatograms for the quantitative analysis were reconstructed at the base peaks corresponding to the differently charged amyloid monomer ions (Native, N) and oxidized ions (Ox). The ratio between the total monomer area and the IS area was used for A $\beta$ <sub>42</sub> monomer determination. The  $\text{Area}_{\text{total monomer}}/\text{Area}_{\text{IS}}$  ratio at  $t_0$  is considered as 100% of the monomer content. The results were expressed as means  $\pm$  SD of three independent experiments and a p value < 0.05 was considered statistically significant (Dunnett's Multiple Comparison Test).

**Reagents for cellular experiments.** All culture media, supplements and Foetal Bovine Serum (FBS) were obtained from Euroclone (Life Science Division, Milan, Italy). Electrophoresis reagents were obtained from Bio-Rad (Hercules, CA, USA). All other reagents were of the highest grade available and were purchased from Merck KGaA (Darmstadt, Germany) unless otherwise indicated. A $\beta$ <sub>42</sub> was solubilized in dimethyl sulfoxide (DMSO) at the concentration of 100  $\mu\text{M}$  and frozen in stock aliquots that were diluted at the final concentration of 10 nM prior to use. For each experimental setting, one aliquot of the stock was thawed out and diluted at the final concentration of 10 nM to minimize peptide damage as a result of repeated freeze and thaw. The A $\beta$ <sub>42</sub> concentration was chosen following dose-response experiments (data not shown), for which maximal modulation of the p53 structure and its transcriptional activity were obtained at 10 nM. All the experiments performed with A $\beta$  were made in 1% of serum. H<sub>2</sub>O<sub>2</sub> was diluted to working concentration (300  $\mu\text{M}$ ) in phosphate buffer saline (PBS) at the moment of use. Mouse monoclonal anti  $\alpha$ -tubulin was purchased from Sigma-Aldrich (St. Louis, MO, USA). Host-specific peroxidase conjugated IgG secondary antibodies were obtained from Pierce (Rockford, IL, USA).

**Cell cultures.** Human neuroblastoma SH-SY5Y cell line from European Collection of Cell Cultures (ECACC No. 94030304) were cultured in medium with equal amount of Eagle's minimum essential medium and Nutrient Mixture Ham's F-12, supplemented with 10% foetal bovine serum, glutamine (2mM), penicillin/streptomycin, non-essential aminoacids at 37 °C in 5% CO<sub>2</sub>/95% air.

**Cell viability.** The mitochondrial dehydrogenase activity that reduces 3-(4,5-dimethylthiazol-2-yl)-2,5-diphenyl-tetrazolium bromide (MTT, Sigma, St Louis, MO, USA) was used to determine cellular viability, in a quantitative colorimetric assay. At day 0 SH-SY5Y cells were plated at a density of  $2.5 \times 10^4$  viable cells per well in 96-well plates. After treatment, according to the experimental setting, cells were exposed to an MTT solution in PBS (1 mg/mL). Following 4 h incubation with MTT and treatment with SDS for 24 h, cell viability reduction was quantified by using a BIO-RAD microplate reader (Model 550; Hercules, CA, USA) or synergy HT multi-detection microplate reader (Bio-Tek).

**Measurement of intracellular ROS.** 2',7'-Dichlorofluorescein diacetate (DCF-DA; Sigma–Aldrich) was used to estimate intracellular ROS. Briefly, cells ( $2 \times 10^4$  cells per well) were pretreated with reference curcumin and compounds **I-VI**, **1-9** (5  $\mu$ M) for 24 h and then loaded with 25  $\mu$ M DCF-DA at 37 °C for 45 min. DCF-DA was removed after centrifuge and cells were resuspended in PBS and then exposed to 300  $\mu$ M H<sub>2</sub>O<sub>2</sub>. The results were visualized by using a Synergy HT microplate reader (BioTek) with excitation and emission wavelengths of 485 and 530 nm, respectively.

**Immunodetection of zyxin and HIPK2.** Cell monolayers were washed twice with ice cold PBS, lysed on the tissue culture dish by addition of ice-cold lysis buffer (50 mM Tris/HCl pH 7.4, 150 mM NaCl, 50 mM EDTA, 0.2 mM 4-(2-aminoethyl)benzenesulfonylfluoride hydrochloride (AEBSF), 20  $\mu$ g/mL leupeptin, 25  $\mu$ g/mL aprotinin, 0,5  $\mu$ g/mL pepstatin A and 1% Triton X-100) and an aliquot was used for protein analysis with the Pierce Bicinchoninic Acid kit, for protein quantification. Cell lysates were diluted in sample buffer (62.5 Mm Tris/HCl pH 6.8, 2% SDS, 10% glycerol, 50 mM dithiothreitol, 0.1% bromophenol blue) and subjected to Western blot analysis. Proteins were subjected to SDS-PAGE (8%) and then transferred onto PVDF membrane 0.45 $\mu$ m (Immobilion, Millipore Corp, Bedford, MA,USA). The membrane was blocked for 1 h with 5% non-fat dry milk in Tris-buffered saline containing 0.1% Tween 20 (TBST). Membranes were immunoblotted with the rabbit anti human zyxin or HIPK2 polyclonal antibody (at 1:1000 dilution in 5% non fat dry milk, from Cell Signaling Technology, EuroClone, Milan, Italy). The detection was carried out by incubation with horseradish peroxidase conjugated goat anti-rabbit IgG (1:5000

dilution in 5% non fat dry milk, from Pierce, Rockford, IL, USA) for 1 h. The blots were then washed extensively and the proteins of interest were visualized using an enhanced chemiluminescent method (Pierce, Rockford, IL, USA). Tubulin was also performed as a normal control of proteins.

***p53 conformational immunoprecipitation.*** p53 conformational state was analyzed by immunoprecipitation as detailed previously<sup>151</sup>. Briefly, cells were lysed in immunoprecipitation buffer (10 mM Tris, pH 7.6, 140 mM NaCl, and 0.5% NP40 including protease inhibitors); 100 µg of total cell extracts were used for immunoprecipitation experiments performed in a volume of 500 µL with 1 µg of the conformation-specific antibodies PAb1620 (wild-type specific) or PAb240 (mutant specific) (Neomarkers, CA, USA). Immunocomplexes were separated by 10% SDS-PAGE and immunoblotting was performed with rabbit anti-p53 antibody (FL393) (Santa Cruz, CA, USA). Immunoreactivity was detected with the ECL-chemiluminescence reaction kit (Amersham, Little Chalfont, UK).

***Immunodetection of Nrf2 and NQO-1.*** Cell monolayers were washed twice with ice cold PBS, lysed on the tissue culture dish by addition of ice-cold lysis buffer (50 mM Tris/HCl pH 7.4, 150 mM NaCl, 50 mM EDTA, 0.2 mM 4-(2-aminoethyl) benzenesulfonylfluoride hydrochloride (AEBSF), 20 µg/mL leupeptin, 25 µg/mL aprotinin, 0.5 µg/mL pepstatin A and 1% Triton X-100) and an aliquot was used for protein analysis with the Bradford assay, for protein quantification. Cell lysates were diluted in sample buffer (62.5 mM Tris/HCl pH 6.8, 2% SDS, 10% glycerol, 50 mM dithiothreitol, 0.1% bromophenol blue) and subjected to Western blot analysis. Proteins were subjected to SDS-PAGE (10%) and then transferred onto PVDF membrane 0.45 µm (Merck KGaA Darmstadt, Germany). The membrane was blocked for 1 h with 5% BSA in Tris-buffered saline containing 0.1% Tween 20 (TBST). Membranes were immunoblotted with the rabbit anti human Nrf2 polyclonal antibody (at 1:2000 in 5% BSA) and the mouse anti-NQO-1 monoclonal antibody (1:1000 in 5% BSA) (Novus, Bio-technie Minneapolis, USA). The detection was carried out by incubation with horseradish peroxidase conjugated goat anti-rabbit IgG for Nrf-2 or rabbit anti-mouse for NQO-1 (1:5000 dilution in 5% BSA, from Merck KGaA Darmstadt, Germany) for 1 h. The blots were then washed extensively and the proteins of interest were visualized using an

enhanced chemiluminescent method (Pierce, Rockford, IL, USA). Tubulin was also performed as a normal control of proteins (Merck KGaA Darmstadt, Germany).

***Subcellular fractionation for Nrf2 nuclear translocation.***  $5 \times 10^6$  SH-SY5Y cells were seeded in 100 mm<sup>2</sup> dishes and treated for 3 h with 5  $\mu$ M compounds **I**, **III**, **V**, **5**, **7**, **9**; afterwards the medium was removed, and cells were washed twice with ice-cold PBS. Cells were subsequently homogenized 15 times using a glass-glass dounce homogenizer in 0.32 M sucrose buffered with 20 mM Tris-HCl (pH 7.4) containing 2 mM EDTA, 0.5 mM EGTA, 50 mM  $\beta$ -mercaptoethanol, and 20  $\mu$ g/ml leupeptin, apotrinin and pepstatin. The homogenate was centrifuged at 300 $\times$ g for 5 min to obtain the nuclear fraction. An aliquot of the nuclear fraction was used for protein assay by the Bradford method, whereas the remaining was boiled for 5 min after dilution with sample buffer and subjected to polyacrylamide gel electrophoresis and immunoblotting as described.

***Densitometry and statistics.*** All the experiments, unless specified, were performed at least three times. Following acquisition of the Western blot image through an AGFA scanner and analysis by means of the Image 1.47 program (Wayne Rasband, NIH, Research Services Branch, NIMH, Bethesda, MD, USA), the relative densities of the bands were expressed as arbitrary units and normalized to data obtained from control sample run under the same conditions. Data were analyzed by analysis of variance (ANOVA) followed when significant by an appropriate post hoc comparison test as indicated in figure legend. The reported data are expressed as means  $\pm$  SEM of at least three independent experiments. A p value < 0.05 was considered statistically significant.

## **ABBREVIATIONS**

ANOVA, analysis of variance; Boc<sub>2</sub>O: di-*tert*-butyl dicarbonate; Bop: (benzotriazol-1-yloxy)tris(dimethylamino)phosphonium hexafluorophosphate; DBU: 1,8-Diazabicyclo[5.4.0]undec-7-ene; DCFH-DA, dichloro-dihydro-fluorescein diacetate; DCC, *N,N*-dicyclohexylcarbodiimide; DIPEA: *N,N*-diisopropylethylamine; DMAP, 4-dimethylaminopyridine; DMF, *N,N*-dimethylformamide; DMSO, dimethyl sulfoxide; EDC: *N*-(3-dimethylaminopropyl)-*N'*-ethylcarbodiimide hydrochloride; ESI-MS, electrospray ionisation mass spectrometry; FBS, Foetal

Bovine Serum; Fmoc-Cl: 9-fluorenylmethoxycarbonyl chloride; Girard's reagent T: (carboxymethyl)trimethylammonium chloride hydrazide; GST, glutathione S-transferase; HOBt: 1-hydroxybenzotriazole hydrate; HPLC, high performance liquid chromatography; HO-1, heme oxygenase-1; MTT, 3-(4,5-dimethylthiazol-2-yl)-2,5-diphenyl-tetrazolium bromide; Et<sub>3</sub>N: triethylamine; NMR, nuclear magnetic resonance; NQO1, NAD(P)H:quinone reductase; Nrf2, nuclear factor (erythroid-derived 2)-like 2; PBS, phosphate buffer saline; PCl<sub>5</sub>: phosphorus pentachloride; TBAF, tetrabutylammonium fluoride; TBDMS-Cl, *tert*-butyldimethylsilyl chloride; TBST, Tris-buffered saline containing 0.1% Tween 20; THF, tetrahydrofuran; TLC, thin layer chromatography; TMS, tetramethylsilane; ThT, thioflavin T; UV, ultraviolet.

## **Bibliography**

1. Alzheimer's Disease International WaR. <https://alz.co.uk/research/WorldAlzheimerReport2016.pdf>.
2. Centers for Disease Control and Prevention. <https://www.cdc.gov/aging/aginginfo/alzheimers.htm>.
3. Ballard, C.; Gauthier, S.; Corbett, A.; Brayne, C.; Aarsland, D.; Jones, E., Alzheimer's disease. *Lancet* **2011**, *377* (9770), 1019-31.
4. Arnold, S. E.; Hyman, B. T.; Flory, J.; Damasio, A. R.; Van Hoesen, G. W., The topographical and neuroanatomical distribution of neurofibrillary tangles and neuritic plaques in the cerebral cortex of patients with Alzheimer's disease. *Cereb Cortex* **1991**, *1* (1), 103-16.
5. Klucken, J.; McLean, P. J.; Gomez-Tortosa, E.; Ingelsson, M.; Hyman, B. T., Neuritic alterations and neural system dysfunction in Alzheimer's disease and dementia with Lewy bodies. *Neurochem Res* **2003**, *28* (11), 1683-91.
6. Terry, R. D.; Peck, A.; DeTeresa, R.; Schechter, R.; Horoupian, D. S., Some morphometric aspects of the brain in senile dementia of the Alzheimer type. *Ann Neurol* **1981**, *10* (2), 184-92.
7. Teipel, S. J.; Flatz, W. H.; Heinsen, H.; Bokde, A. L.; Schoenberg, S. O.; Stöckel, S.; Dietrich, O.; Reiser, M. F.; Möller, H. J.; Hampel, H., Measurement of basal forebrain atrophy in Alzheimer's disease using MRI. *Brain* **2005**, *128* (Pt 11), 2626-44.
8. DeKosky, S. T.; Scheff, S. W.; Styren, S. D., Structural correlates of cognition in dementia: quantification and assessment of synapse change. *Neurodegeneration* **1996**, *5* (4), 417-21.
9. Benilova, I.; Karran, E.; De Strooper, B., The toxic A $\beta$  oligomer and Alzheimer's disease: an emperor in need of clothes. *Nat Neurosci* **2012**, *15* (3), 349-57.
10. Sun, H. Q.; Zhang, X.; Huang, W. J.; Chen, W. W., The news advances on Alzheimer's disease's therapeutics. *Eur Rev Med Pharmacol Sci* **2016**, *20* (9), 1903-10.
11. Cavalli, A.; Bolognesi, M. L.; Minarini, A.; Rosini, M.; Tumiatti, V.; Recanatini, M.; Melchiorre, C., Multi-target-directed ligands to combat neurodegenerative diseases. *J Med Chem* **2008**, *51* (3), 347-72.
12. León, R.; Garcia, A. G.; Marco-Contelles, J., Recent advances in the multitarget-directed ligands approach for the treatment of Alzheimer's disease. *Med Res Rev* **2013**, *33* (1), 139-89.
13. Bales, K. R.; Dodart, J. C.; DeMattos, R. B.; Holtzman, D. M.; Paul, S. M., Apolipoprotein E, amyloid, and Alzheimer disease. *Mol Interv* **2002**, *2* (6), 363-75, 339.
14. DeMattos, R. B.; Cirrito, J. R.; Parsadanian, M.; May, P. C.; O'Dell, M. A.; Taylor, J. W.; Harmony, J. A.; Aronow, B. J.; Bales, K. R.; Paul, S. M.; Holtzman, D. M., ApoE and clusterin cooperatively suppress Abeta levels and deposition: evidence that ApoE regulates extracellular Abeta metabolism in vivo. *Neuron* **2004**, *41* (2), 193-202.
15. Takashima, A.; Noguchi, K.; Sato, K.; Hoshino, T.; Imahori, K., Tau protein kinase I is essential for amyloid beta-protein-induced neurotoxicity. *Proc Natl Acad Sci U S A* **1993**, *90* (16), 7789-93.
16. Grant, W. B.; Campbell, A.; Itzhaki, R. F.; Savory, J., The significance of environmental factors in the etiology of Alzheimer's disease. *J Alzheimers Dis* **2002**, *4* (3), 179-89.

17. Itzhaki, R. F.; Wozniak, M. A., Alzheimer's disease and infection: Do infectious agents contribute to progression of Alzheimer's disease? *Alzheimers Dement* **2010**, *6* (1), 83-4; author reply 85.
18. Banatvala, J. E., Herpes simplex encephalitis. *Lancet Infect Dis* **2011**, *11* (2), 80-1.
19. Walton, J. R., Aluminum involvement in the progression of Alzheimer's disease. *J Alzheimers Dis* **2013**, *35* (1), 7-43.
20. Bowen, D. M.; Smith, C. B.; White, P.; Davison, A. N., Neurotransmitter-related enzymes and indices of hypoxia in senile dementia and other abiotrophies. *Brain* **1976**, *99* (3), 459-96.
21. Davies, P.; Maloney, A. J., Selective loss of central cholinergic neurons in Alzheimer's disease. *Lancet* **1976**, *2* (8000), 1403.
22. Perry, E. K.; Gibson, P. H.; Blessed, G.; Perry, R. H.; Tomlinson, B. E., Neurotransmitter enzyme abnormalities in senile dementia. Choline acetyltransferase and glutamic acid decarboxylase activities in necropsy brain tissue. *J Neurol Sci* **1977**, *34* (2), 247-65.
23. Rylett, R. J.; Ball, M. J.; Colhoun, E. H., Evidence for high affinity choline transport in synaptosomes prepared from hippocampus and neocortex of patients with Alzheimer's disease. *Brain Res* **1983**, *289* (1-2), 169-75.
24. Drachman, D. A.; Leavitt, J., Human memory and the cholinergic system. A relationship to aging? *Arch Neurol* **1974**, *30* (2), 113-21.
25. TWO-GATHER Symposium (access on 15/02/2017). [http://www.whosaeng.com/imgdata/whosaeng\\_com/201305/2013053039373546.jpg](http://www.whosaeng.com/imgdata/whosaeng_com/201305/2013053039373546.jpg).
26. Xie, W.; Stribley, J. A.; Chatonnet, A.; Wilder, P. J.; Rizzino, A.; McComb, R. D.; Taylor, P.; Hinrichs, S. H.; Lockridge, O., Postnatal developmental delay and supersensitivity to organophosphate in gene-targeted mice lacking acetylcholinesterase. *J Pharmacol Exp Ther* **2000**, *293* (3), 896-902.
27. Scott, L. J.; Goa, K. L., Galantamine: a review of its use in Alzheimer's disease. *Drugs* **2000**, *60* (5), 1095-122.
28. Francis, P. T.; Palmer, A. M.; Snape, M.; Wilcock, G. K., The cholinergic hypothesis of Alzheimer's disease: a review of progress. *J Neurol Neurosurg Psychiatry* **1999**, *66* (2), 137-47.
29. Dineley, K. T.; Pandya, A. A.; Yakel, J. L., Nicotinic ACh receptors as therapeutic targets in CNS disorders. *Trends Pharmacol Sci* **2015**, *36* (2), 96-108.
30. Jiang, S.; Li, Y.; Zhang, C.; Zhao, Y.; Bu, G.; Xu, H.; Zhang, Y. W., M1 muscarinic acetylcholine receptor in Alzheimer's disease. *Neurosci Bull* **2014**, *30* (2), 295-307.
31. Jones, C. K.; Brady, A. E.; Davis, A. A.; Xiang, Z.; Bubser, M.; Tantawy, M. N.; Kane, A. S.; Bridges, T. M.; Kennedy, J. P.; Bradley, S. R.; Peterson, T. E.; Ansari, M. S.; Baldwin, R. M.; Kessler, R. M.; Deutch, A. Y.; Lah, J. J.; Levey, A. I.; Lindsley, C. W.; Conn, P. J., Novel selective allosteric activator of the M1 muscarinic acetylcholine receptor regulates amyloid processing and produces antipsychotic-like activity in rats. *J Neurosci* **2008**, *28* (41), 10422-33.
32. Foster, D. J.; Choi, D. L.; Conn, P. J.; Rook, J. M., Activation of M1 and M4 muscarinic receptors as potential treatments for Alzheimer's disease and schizophrenia. *Neuropsychiatr Dis Treat* **2014**, *10*, 183-91.
33. Clader, J. W.; Wang, Y., Muscarinic receptor agonists and antagonists in the treatment of Alzheimer's disease. *Curr Pharm Des* **2005**, *11* (26), 3353-61.
34. Citron, M., Alzheimer's disease: strategies for disease modification. *Nat Rev Drug Discov* **2010**, *9* (5), 387-98.

35. Bulic, B.; Pickhardt, M.; Schmidt, B.; Mandelkow, E. M.; Waldmann, H.; Mandelkow, E., Development of tau aggregation inhibitors for Alzheimer's disease. *Angew Chem Int Ed Engl* **2009**, *48* (10), 1740-52.
36. Baddeley, T. C.; McCaffrey, J.; Storey, J. M.; Cheung, J. K.; Melis, V.; Horsley, D.; Harrington, C. R.; Wischik, C. M., Complex disposition of methylthioninium redox forms determines efficacy in tau aggregation inhibitor therapy for Alzheimer's disease. *J Pharmacol Exp Ther* **2015**, *352* (1), 110-8.
37. Alzheimer's Association International Conference 2016. Alzforum (n.d.). Retrieved March 5, 2017, from. <http://www.alzforum.org/news/conference-coverage/first-phase-3-trial-tau-drug-lmtm-did-not-work-period>.
38. Butterfield, D. A.; Pocernich, C. B., The glutamatergic system and Alzheimer's disease: therapeutic implications. *CNS Drugs* **2003**, *17* (9), 641-52.
39. Walton, H. S.; Dodd, P. R., Glutamate-glutamine cycling in Alzheimer's disease. *Neurochem Int* **2007**, *50* (7-8), 1052-66.
40. Lipton, S. A., Paradigm shift in neuroprotection by NMDA receptor blockade: memantine and beyond. *Nat Rev Drug Discov* **2006**, *5* (2), 160-70.
41. Voglis, G.; Tavernarakis, N., The role of synaptic ion channels in synaptic plasticity. *EMBO Rep* **2006**, *7* (11), 1104-10.
42. Seif el Nasr, M.; Peruche, B.; Rossberg, C.; Mennel, H. D.; Krieglstein, J., Neuroprotective effect of memantine demonstrated in vivo and in vitro. *Eur J Pharmacol* **1990**, *185* (1), 19-24.
43. Chen, H. S.; Pellegrini, J. W.; Aggarwal, S. K.; Lei, S. Z.; Warach, S.; Jensen, F. E.; Lipton, S. A., Open-channel block of N-methyl-D-aspartate (NMDA) responses by memantine: therapeutic advantage against NMDA receptor-mediated neurotoxicity. *J Neurosci* **1992**, *12* (11), 4427-36.
44. Lipton, S. A., Prospects for clinically tolerated NMDA antagonists: open-channel blockers and alternative redox states of nitric oxide. *Trends Neurosci* **1993**, *16* (12), 527-32.
45. Esposito, Z.; Belli, L.; Toniolo, S.; Sancesario, G.; Bianconi, C.; Martorana, A., Amyloid  $\beta$ , glutamate, excitotoxicity in Alzheimer's disease: are we on the right track? *CNS Neurosci Ther* **2013**, *19* (8), 549-55.
46. Pereira, A. C.; Lambert, H. K.; Grossman, Y. S.; Dumitriu, D.; Waldman, R.; Jannetty, S. K.; Calakos, K.; Janssen, W. G.; McEwen, B. S.; Morrison, J. H., Glutamatergic regulation prevents hippocampal-dependent age-related cognitive decline through dendritic spine clustering. *Proc Natl Acad Sci U S A* **2014**, *111* (52), 18733-8.
47. Fumagalli, E.; Funicello, M.; Rauen, T.; Gobbi, M.; Mennini, T., Riluzole enhances the activity of glutamate transporters GLAST, GLT1 and EAAC1. *Eur J Pharmacol* **2008**, *578* (2-3), 171-6.
48. Nakamura, T.; Lipton, S. A., Protein S-Nitrosylation as a Therapeutic Target for Neurodegenerative Diseases. *Trends Pharmacol Sci* **2016**, *37* (1), 73-84.
49. Lipton, S. A.; Choi, Y. B.; Pan, Z. H.; Lei, S. Z.; Chen, H. S.; Sucher, N. J.; Loscalzo, J.; Singel, D. J.; Stamler, J. S., A redox-based mechanism for the neuroprotective and neurodestructive effects of nitric oxide and related nitroso-compounds. *Nature* **1993**, *364* (6438), 626-32.
50. Choi, Y. B.; Tenneti, L.; Le, D. A.; Ortiz, J.; Bai, G.; Chen, H. S.; Lipton, S. A., Molecular basis of NMDA receptor-coupled ion channel modulation by S-nitrosylation. *Nat Neurosci* **2000**, *3* (1), 15-21.

51. Lei, S. Z.; Pan, Z. H.; Aggarwal, S. K.; Chen, H. S.; Hartman, J.; Sucher, N. J.; Lipton, S. A., Effect of nitric oxide production on the redox modulatory site of the NMDA receptor-channel complex. *Neuron* **1992**, *8* (6), 1087-99.
52. Takahashi, H.; Xia, P.; Cui, J.; Talantova, M.; Bodhinathan, K.; Li, W.; Saleem, S.; Holland, E. A.; Tong, G.; Piña-Crespo, J.; Zhang, D.; Nakanishi, N.; Larrick, J. W.; McKercher, S. R.; Nakamura, T.; Wang, Y.; Lipton, S. A., Pharmacologically targeted NMDA receptor antagonism by NitroMemantine for cerebrovascular disease. *Sci Rep* **2015**, *5*, 14781.
53. Uttara, B.; Singh, A. V.; Zamboni, P.; Mahajan, R. T., Oxidative stress and neurodegenerative diseases: a review of upstream and downstream antioxidant therapeutic options. *Curr Neuropharmacol* **2009**, *7* (1), 65-74.
54. Quinlan, C. L.; Perevoshchikova, I. V.; Hey-Mogensen, M.; Orr, A. L.; Brand, M. D., Sites of reactive oxygen species generation by mitochondria oxidizing different substrates. *Redox Biol* **2013**, *1*, 304-12.
55. Tönnies, E.; Trushina, E., Oxidative Stress, Synaptic Dysfunction, and Alzheimer's Disease. *J Alzheimers Dis* **2017**.
56. Kim, T. S.; Pae, C. U.; Yoon, S. J.; Jang, W. Y.; Lee, N. J.; Kim, J. J.; Lee, S. J.; Lee, C.; Paik, I. H.; Lee, C. U., Decreased plasma antioxidants in patients with Alzheimer's disease. *Int J Geriatr Psychiatry* **2006**, *21* (4), 344-8.
57. Smith, M. A.; Rudnicka-Nawrot, M.; Richey, P. L.; Praprotnik, D.; Mulvihill, P.; Miller, C. A.; Sayre, L. M.; Perry, G., Carbonyl-related posttranslational modification of neurofilament protein in the neurofibrillary pathology of Alzheimer's disease. *J Neurochem* **1995**, *64* (6), 2660-6.
58. Butterfield, D. A.; Di Domenico, F.; Barone, E., Elevated risk of type 2 diabetes for development of Alzheimer disease: a key role for oxidative stress in brain. *Biochim Biophys Acta* **2014**, *1842* (9), 1693-706.
59. Barnham, K. J.; Masters, C. L.; Bush, A. I., Neurodegenerative diseases and oxidative stress. *Nat Rev Drug Discov* **2004**, *3* (3), 205-14.
60. Mattson, M. P.; Chan, S. L., Neuronal and glial calcium signaling in Alzheimer's disease. *Cell Calcium* **2003**, *34* (4-5), 385-97.
61. Lewén, A.; Matz, P.; Chan, P. H., Free radical pathways in CNS injury. *J Neurotrauma* **2000**, *17* (10), 871-90.
62. Di Domenico, F.; Tramutola, A.; Butterfield, D. A., Role of 4-hydroxy-2-nonenal (HNE) in the pathogenesis of Alzheimer disease and other selected age-related neurodegenerative disorders. *Free Radic Biol Med* **2016**.
63. Esterbauer, H.; Schaur, R. J.; Zollner, H., Chemistry and biochemistry of 4-hydroxynonenal, malonaldehyde and related aldehydes. *Free Radic Biol Med* **1991**, *11* (1), 81-128.
64. Perluigi, M.; Coccia, R.; Butterfield, D. A., 4-Hydroxy-2-nonenal, a reactive product of lipid peroxidation, and neurodegenerative diseases: a toxic combination illuminated by redox proteomics studies. *Antioxid Redox Signal* **2012**, *17* (11), 1590-609.
65. Curtis, J. M.; Hahn, W. S.; Long, E. K.; Burrill, J. S.; Arriaga, E. A.; Bernlohr, D. A., Protein carbonylation and metabolic control systems. *Trends Endocrinol Metab* **2012**, *23* (8), 399-406.
66. Canter, R. G.; Penney, J.; Tsai, L. H., The road to restoring neural circuits for the treatment of Alzheimer's disease. *Nature* **2016**, *539* (7628), 187-196.
67. Lichtenthaler, S. F.; Haass, C., Amyloid at the cutting edge: activation of alpha-secretase prevents amyloidogenesis in an Alzheimer disease mouse model. *J Clin Invest* **2004**, *113* (10), 1384-7.

68. Lammich, S.; Kojro, E.; Postina, R.; Gilbert, S.; Pfeiffer, R.; Jasionowski, M.; Haass, C.; Fahrenholz, F., Constitutive and regulated alpha-secretase cleavage of Alzheimer's amyloid precursor protein by a disintegrin metalloprotease. *Proc Natl Acad Sci U S A* **1999**, *96* (7), 3922-7.
69. Tang, B. L.; Liou, Y. C., Novel modulators of amyloid-beta precursor protein processing. *J Neurochem* **2007**, *100* (2), 314-23.
70. Kim, J.; Onstead, L.; Randle, S.; Price, R.; Smithson, L.; Zwizinski, C.; Dickson, D. W.; Golde, T.; McGowan, E., Abeta40 inhibits amyloid deposition in vivo. *J Neurosci* **2007**, *27* (3), 627-33.
71. Jarrett, J. T.; Berger, E. P.; Lansbury, P. T., The carboxy terminus of the beta amyloid protein is critical for the seeding of amyloid formation: implications for the pathogenesis of Alzheimer's disease. *Biochemistry* **1993**, *32* (18), 4693-7.
72. Musiek, E. S.; Holtzman, D. M., Three dimensions of the amyloid hypothesis: time, space and 'wingmen'. *Nat Neurosci* **2015**, *18* (6), 800-6.
73. Sherrington, R.; Rogaev, E. I.; Liang, Y.; Rogaeva, E. A.; Levesque, G.; Ikeda, M.; Chi, H.; Lin, C.; Li, G.; Holman, K.; Tsuda, T.; Mar, L.; Foncin, J. F.; Bruni, A. C.; Montesi, M. P.; Sorbi, S.; Rainero, I.; Pinessi, L.; Nee, L.; Chumakov, I.; Pollen, D.; Brookes, A.; Sanseau, P.; Polinsky, R. J.; Wasco, W.; Da Silva, H. A.; Haines, J. L.; Pericak-Vance, M. A.; Tanzi, R. E.; Roses, A. D.; Fraser, P. E.; Rommens, J. M.; St George-Hyslop, P. H., Cloning of a gene bearing missense mutations in early-onset familial Alzheimer's disease. *Nature* **1995**, *375* (6534), 754-60.
74. Rogaev, E. I.; Sherrington, R.; Rogaeva, E. A.; Levesque, G.; Ikeda, M.; Liang, Y.; Chi, H.; Lin, C.; Holman, K.; Tsuda, T., Familial Alzheimer's disease in kindreds with missense mutations in a gene on chromosome 1 related to the Alzheimer's disease type 3 gene. *Nature* **1995**, *376* (6543), 775-8.
75. Karran, E.; Mercken, M.; De Strooper, B., The amyloid cascade hypothesis for Alzheimer's disease: an appraisal for the development of therapeutics. *Nat Rev Drug Discov* **2011**, *10* (9), 698-712.
76. Selkoe, D. J.; Hardy, J., The amyloid hypothesis of Alzheimer's disease at 25 years. *EMBO Mol Med* **2016**, *8* (6), 595-608.
77. LaFerla, F. M.; Green, K. N.; Oddo, S., Intracellular amyloid-beta in Alzheimer's disease. *Nat Rev Neurosci* **2007**, *8* (7), 499-509.
78. Nickerson, D. A.; Taylor, S. L.; Fullerton, S. M.; Weiss, K. M.; Clark, A. G.; Stengård, J. H.; Salomaa, V.; Boerwinkle, E.; Sing, C. F., Sequence diversity and large-scale typing of SNPs in the human apolipoprotein E gene. *Genome Res* **2000**, *10* (10), 1532-45.
79. Farrer, L. A.; Cupples, L. A.; Haines, J. L.; Hyman, B.; Kukull, W. A.; Mayeux, R.; Myers, R. H.; Pericak-Vance, M. A.; Risch, N.; van Duijn, C. M., Effects of age, sex, and ethnicity on the association between apolipoprotein E genotype and Alzheimer disease. A meta-analysis. APOE and Alzheimer Disease Meta Analysis Consortium. *JAMA* **1997**, *278* (16), 1349-56.
80. Fagan, A. M.; Watson, M.; Parsadanian, M.; Bales, K. R.; Paul, S. M.; Holtzman, D. M., Human and murine ApoE markedly alters A beta metabolism before and after plaque formation in a mouse model of Alzheimer's disease. *Neurobiol Dis* **2002**, *9* (3), 305-18.
81. Lleó, A.; Saura, C. A.,  $\gamma$ -secretase substrates and their implications for drug development in Alzheimer's disease. *Curr Top Med Chem* **2011**, *11* (12), 1513-27.
82. Pardossi-Piquard, R.; Checler, F., The physiology of the  $\beta$ -amyloid precursor protein intracellular domain AICD. *J Neurochem* **2012**, *120 Suppl 1*, 109-24.

83. Graham, W. V.; Bonito-Oliva, A.; Sakmar, T. P., Update on Alzheimer's Disease Therapy and Prevention Strategies. *Annu Rev Med* **2017**, *68*, 413-430.
84. Wong, G. T.; Manfra, D.; Poulet, F. M.; Zhang, Q.; Josien, H.; Bara, T.; Engstrom, L.; Pinzon-Ortiz, M.; Fine, J. S.; Lee, H. J.; Zhang, L.; Higgins, G. A.; Parker, E. M., Chronic treatment with the gamma-secretase inhibitor LY-411,575 inhibits beta-amyloid peptide production and alters lymphopoiesis and intestinal cell differentiation. *J Biol Chem* **2004**, *279* (13), 12876-82.
85. Imbimbo, B. P.; Panza, F.; Frisardi, V.; Solfrizzi, V.; D'Onofrio, G.; Logroscino, G.; Seripa, D.; Pilotto, A., Therapeutic intervention for Alzheimer's disease with  $\gamma$ -secretase inhibitors: still a viable option? *Expert Opin Investig Drugs* **2011**, *20* (3), 325-41.
86. Akiyama, H.; Barger, S.; Barnum, S.; Bradt, B.; Bauer, J.; Cole, G. M.; Cooper, N. R.; Eikelenboom, P.; Emmerling, M.; Fiebich, B. L.; Finch, C. E.; Frautschy, S.; Griffin, W. S.; Hampel, H.; Hull, M.; Landreth, G.; Lue, L.; Mrak, R.; Mackenzie, I. R.; McGeer, P. L.; O'Banion, M. K.; Pachter, J.; Pasinetti, G.; Plata-Salaman, C.; Rogers, J.; Rydel, R.; Shen, Y.; Streit, W.; Strohmeyer, R.; Tooyoma, I.; Van Muiswinkel, F. L.; Veerhuis, R.; Walker, D.; Webster, S.; Wegrzyniak, B.; Wenk, G.; Wyss-Coray, T., Inflammation and Alzheimer's disease. *Neurobiol Aging* **2000**, *21* (3), 383-421.
87. Weggen, S.; Eriksen, J. L.; Das, P.; Sagi, S. A.; Wang, R.; Pietrzik, C. U.; Findlay, K. A.; Smith, T. E.; Murphy, M. P.; Bulter, T.; Kang, D. E.; Marquez-Sterling, N.; Golde, T. E.; Koo, E. H., A subset of NSAIDs lower amyloidogenic Abeta42 independently of cyclooxygenase activity. *Nature* **2001**, *414* (6860), 212-6.
88. Weggen, S.; Eriksen, J. L.; Sagi, S. A.; Pietrzik, C. U.; Ozols, V.; Fauq, A.; Golde, T. E.; Koo, E. H., Evidence that nonsteroidal anti-inflammatory drugs decrease amyloid beta 42 production by direct modulation of gamma-secretase activity. *J Biol Chem* **2003**, *278* (34), 31831-7.
89. Imbimbo, B. P.; Solfrizzi, V.; Panza, F., Are NSAIDs useful to treat Alzheimer's disease or mild cognitive impairment? *Front Aging Neurosci* **2010**, *2*.
90. Hoozemans, J. J.; Rozemuller, J. M.; van Haastert, E. S.; Veerhuis, R.; Eikelenboom, P., Cyclooxygenase-1 and -2 in the different stages of Alzheimer's disease pathology. *Curr Pharm Des* **2008**, *14* (14), 1419-27.
91. Sastre, M.; Dewachter, I.; Landreth, G. E.; Willson, T. M.; Klockgether, T.; van Leuven, F.; Heneka, M. T., Nonsteroidal anti-inflammatory drugs and peroxisome proliferator-activated receptor-gamma agonists modulate immunostimulated processing of amyloid precursor protein through regulation of beta-secretase. *J Neurosci* **2003**, *23* (30), 9796-804.
92. Sastre, M.; Dewachter, I.; Rossner, S.; Bogdanovic, N.; Rosen, E.; Borghgraef, P.; Evert, B. O.; Dumitrescu-Ozimek, L.; Thal, D. R.; Landreth, G.; Walter, J.; Klockgether, T.; van Leuven, F.; Heneka, M. T., Nonsteroidal anti-inflammatory drugs repress beta-secretase gene promoter activity by the activation of PPARgamma. *Proc Natl Acad Sci U S A* **2006**, *103* (2), 443-8.
93. Ghosh, A. K.; Bilcer, G.; Harwood, C.; Kawahama, R.; Shin, D.; Hussain, K. A.; Hong, L.; Loy, J. A.; Nguyen, C.; Koelsch, G.; Ermolieff, J.; Tang, J., Structure-based design: potent inhibitors of human brain memapsin 2 (beta-secretase). *J Med Chem* **2001**, *44* (18), 2865-8.
94. De Strooper, B.; Vassar, R.; Golde, T., The secretases: enzymes with therapeutic potential in Alzheimer disease. *Nat Rev Neurol* **2010**, *6* (2), 99-107.
95. Study of LY2886721 in mild cognitive impairment due to Alzheimer's disease or mild Alzheimer's disease. <https://clinicaltrials.gov/ct2/show/NCT01561430>.

96. Kuhn, P. H.; Wang, H.; Dislich, B.; Colombo, A.; Zeitschel, U.; Ellwart, J. W.; Kremmer, E.; Rossner, S.; Lichtenthaler, S. F., ADAM10 is the physiologically relevant, constitutive alpha-secretase of the amyloid precursor protein in primary neurons. *EMBO J* **2010**, *29* (17), 3020-32.
97. Bandyopadhyay, S.; Goldstein, L. E.; Lahiri, D. K.; Rogers, J. T., Role of the APP non-amyloidogenic signaling pathway and targeting alpha-secretase as an alternative drug target for treatment of Alzheimer's disease. *Curr Med Chem* **2007**, *14* (27), 2848-64.
98. Hong-Qi, Y.; Zhi-Kun, S.; Sheng-Di, C., Current advances in the treatment of Alzheimer's disease: focused on considerations targeting A $\beta$  and tau. *Transl Neurodegener* **2012**, *1* (1), 21.
99. Marcade, M.; Bourdin, J.; Loiseau, N.; Peillon, H.; Rayer, A.; Drouin, D.; Schweighoffer, F.; Désiré, L., Etazolate, a neuroprotective drug linking GABA(A) receptor pharmacology to amyloid precursor protein processing. *J Neurochem* **2008**, *106* (1), 392-404.
100. Vellas, B.; Sol, O.; Snyder, P. J.; Ousset, P. J.; Haddad, R.; Maurin, M.; Lemarié, J. C.; Désiré, L.; Pando, M. P.; group, E. s., EHT0202 in Alzheimer's disease: a 3-month, randomized, placebo-controlled, double-blind study. *Curr Alzheimer Res* **2011**, *8* (2), 203-12.
101. Obregon, D. F.; Rezai-Zadeh, K.; Bai, Y.; Sun, N.; Hou, H.; Ehrhart, J.; Zeng, J.; Mori, T.; Arendash, G. W.; Shytle, D.; Town, T.; Tan, J., ADAM10 activation is required for green tea (-)-epigallocatechin-3-gallate-induced alpha-secretase cleavage of amyloid precursor protein. *J Biol Chem* **2006**, *281* (24), 16419-27.
102. Rezai-Zadeh, K.; Shytle, D.; Sun, N.; Mori, T.; Hou, H.; Jeanniton, D.; Ehrhart, J.; Townsend, K.; Zeng, J.; Morgan, D.; Hardy, J.; Town, T.; Tan, J., Green tea epigallocatechin-3-gallate (EGCG) modulates amyloid precursor protein cleavage and reduces cerebral amyloidosis in Alzheimer transgenic mice. *J Neurosci* **2005**, *25* (38), 8807-14.
103. Saïdo, T.; Leissring, M. A., Proteolytic degradation of amyloid  $\beta$ -protein. *Cold Spring Harb Perspect Med* **2012**, *2* (6), a006379.
104. Saito, T.; Iwata, N.; Tsubuki, S.; Takaki, Y.; Takano, J.; Huang, S. M.; Suemoto, T.; Higuchi, M.; Saïdo, T. C., Somatostatin regulates brain amyloid beta peptide Abeta42 through modulation of proteolytic degradation. *Nat Med* **2005**, *11* (4), 434-9.
105. Jacobsen, J. S.; Comery, T. A.; Martone, R. L.; Elokdah, H.; Crandall, D. L.; Oganessian, A.; Aschmies, S.; Kirksey, Y.; Gonzales, C.; Xu, J.; Zhou, H.; Atchison, K.; Wagner, E.; Zaleska, M. M.; Das, I.; Arias, R. L.; Bard, J.; Riddell, D.; Gardell, S. J.; Abou-Gharbia, M.; Robichaud, A.; Magolda, R.; Vlasuk, G. P.; Bjornsson, T.; Reinhart, P. H.; Pangalos, M. N., Enhanced clearance of Abeta in brain by sustaining the plasmin proteolysis cascade. *Proc Natl Acad Sci U S A* **2008**, *105* (25), 8754-9.
106. Solomon, B.; Koppel, R.; Hanan, E.; Katzav, T., Monoclonal antibodies inhibit in vitro fibrillar aggregation of the Alzheimer beta-amyloid peptide. *Proc Natl Acad Sci U S A* **1996**, *93* (1), 452-5.
107. Legleiter, J.; Czilli, D. L.; Gitter, B.; DeMattos, R. B.; Holtzman, D. M.; Kowalewski, T., Effect of different anti-Abeta antibodies on Abeta fibrillogenesis as assessed by atomic force microscopy. *J Mol Biol* **2004**, *335* (4), 997-1006.
108. Solomon, B.; Koppel, R.; Frankel, D.; Hanan-Aharon, E., Disaggregation of Alzheimer beta-amyloid by site-directed mAb. *Proc Natl Acad Sci U S A* **1997**, *94* (8), 4109-12.
109. Mullard, A., Alzheimer amyloid hypothesis lives on. *Nat Rev Drug Discov* **2016**, *16* (1), 3-5.
110. Reiman, E. M., Alzheimer's disease: Attack on amyloid- $\beta$  protein. *Nature* **2016**, *537* (7618), 36-7.

111. Sevigny, J.; Chiao, P.; Bussière, T.; Weinreb, P. H.; Williams, L.; Maier, M.; Dunstan, R.; Salloway, S.; Chen, T.; Ling, Y.; O'Gorman, J.; Qian, F.; Arastu, M.; Li, M.; Chollate, S.; Brennan, M. S.; Quintero-Monzon, O.; Scannevin, R. H.; Arnold, H. M.; Engber, T.; Rhodes, K.; Ferrero, J.; Hang, Y.; Mikulskis, A.; Grimm, J.; Hock, C.; Nitsch, R. M.; Sandrock, A., The antibody aducanumab reduces A $\beta$  plaques in Alzheimer's disease. *Nature* **2016**, *537* (7618), 50-6.
112. Therapeutics. Alzforum (n.d.). Retrieved February 25, 2017, from <https://www.alzforum.org/therapeutics>.
113. Herrup, K., The case for rejecting the amyloid cascade hypothesis. *Nat Neurosci* **2015**, *18* (6), 794-9.
114. Nelson, P. T.; Alafuzoff, I.; Bigio, E. H.; Bouras, C.; Braak, H.; Cairns, N. J.; Castellani, R. J.; Crain, B. J.; Davies, P.; Del Tredici, K.; Duyckaerts, C.; Frosch, M. P.; Haroutunian, V.; Hof, P. R.; Hulette, C. M.; Hyman, B. T.; Iwatsubo, T.; Jellinger, K. A.; Jicha, G. A.; Kövari, E.; Kukull, W. A.; Leverenz, J. B.; Love, S.; Mackenzie, I. R.; Mann, D. M.; Masliah, E.; McKee, A. C.; Montine, T. J.; Morris, J. C.; Schneider, J. A.; Sonnen, J. A.; Thal, D. R.; Trojanowski, J. Q.; Troncoso, J. C.; Wisniewski, T.; Woltjer, R. L.; Beach, T. G., Correlation of Alzheimer disease neuropathologic changes with cognitive status: a review of the literature. *J Neuropathol Exp Neurol* **2012**, *71* (5), 362-81.
115. Serrano-Pozo, A.; Qian, J.; Monsell, S. E.; Frosch, M. P.; Betensky, R. A.; Hyman, B. T., Examination of the clinicopathologic continuum of Alzheimer disease in the autopsy cohort of the National Alzheimer Coordinating Center. *J Neuropathol Exp Neurol* **2013**, *72* (12), 1182-92.
116. Smith, D. G.; Cappai, R.; Barnham, K. J., The redox chemistry of the Alzheimer's disease amyloid beta peptide. *Biochim Biophys Acta* **2007**, *1768* (8), 1976-90.
117. Mecocci, P.; MacGarvey, U.; Beal, M. F., Oxidative damage to mitochondrial DNA is increased in Alzheimer's disease. *Ann Neurol* **1994**, *36* (5), 747-51.
118. Jo, D. G.; Arumugam, T. V.; Woo, H. N.; Park, J. S.; Tang, S. C.; Mughal, M.; Hyun, D. H.; Park, J. H.; Choi, Y. H.; Gwon, A. R.; Camandola, S.; Cheng, A.; Cai, H.; Song, W.; Markesbery, W. R.; Mattson, M. P., Evidence that gamma-secretase mediates oxidative stress-induced beta-secretase expression in Alzheimer's disease. *Neurobiol Aging* **2010**, *31* (6), 917-25.
119. Glabe, C. C., Amyloid accumulation and pathogenesis of Alzheimer's disease: significance of monomeric, oligomeric and fibrillar A $\beta$ . *Subcell Biochem* **2005**, *38*, 167-77.
120. Mattson, M. P., Pathways towards and away from Alzheimer's disease. *Nature* **2004**, *430* (7000), 631-9.
121. Querfurth, H. W.; LaFerla, F. M., Alzheimer's disease. *N Engl J Med* **2010**, *362* (4), 329-44.
122. Siegel, S. J.; Bieschke, J.; Powers, E. T.; Kelly, J. W., The oxidative stress metabolite 4-hydroxynonenal promotes Alzheimer protofibril formation. *Biochemistry* **2007**, *46* (6), 1503-10.
123. Liu, L.; Komatsu, H.; Murray, I. V.; Axelsen, P. H., Promotion of amyloid beta protein misfolding and fibrillogenesis by a lipid oxidation product. *J Mol Biol* **2008**, *377* (4), 1236-50.
124. Keller, J. N.; Pang, Z.; Geddes, J. W.; Begley, J. G.; Germeyer, A.; Waeg, G.; Mattson, M. P., Impairment of glucose and glutamate transport and induction of mitochondrial oxidative stress and dysfunction in synaptosomes by amyloid beta-peptide: role of the lipid peroxidation product 4-hydroxynonenal. *J Neurochem* **1997**, *69* (1), 273-84.
125. Shringarpure, R.; Grune, T.; Sitte, N.; Davies, K. J., 4-Hydroxynonenal-modified amyloid-beta peptide inhibits the proteasome: possible importance in Alzheimer's disease. *Cell Mol Life Sci* **2000**, *57* (12), 1802-9.

126. Tamagno, E.; Parola, M.; Bardini, P.; Piccini, A.; Borghi, R.; Guglielmotto, M.; Santoro, G.; Davit, A.; Danni, O.; Smith, M. A.; Perry, G.; Tabaton, M., Beta-site APP cleaving enzyme up-regulation induced by 4-hydroxynonenal is mediated by stress-activated protein kinases pathways. *J Neurochem* **2005**, *92* (3), 628-36.
127. Stadtman, E. R.; Moskovitz, J.; Levine, R. L., Oxidation of methionine residues of proteins: biological consequences. *Antioxid Redox Signal* **2003**, *5* (5), 577-82.
128. Butterfield, D. A.; Sultana, R., Methionine-35 of a $\beta$ (1-42): importance for oxidative stress in Alzheimer disease. *J Amino Acids* **2011**, *2011*, 198430.
129. Gabbita, S. P.; Aksenov, M. Y.; Lovell, M. A.; Markesbery, W. R., Decrease in peptide methionine sulfoxide reductase in Alzheimer's disease brain. *J Neurochem* **1999**, *73* (4), 1660-6.
130. Misiti, F.; Clementi, M. E.; Giardina, B., Oxidation of methionine 35 reduces toxicity of the amyloid beta-peptide(1-42) in neuroblastoma cells (IMR-32) via enzyme methionine sulfoxide reductase A expression and function. *Neurochem Int* **2010**, *56* (4), 597-602.
131. Brown, A. M.; Lemkul, J. A.; Schaum, N.; Bevan, D. R., Simulations of monomeric amyloid  $\beta$ -peptide (1-40) with varying solution conditions and oxidation state of Met35: implications for aggregation. *Arch Biochem Biophys* **2014**, *545*, 44-52.
132. Hou, L.; Shao, H.; Zhang, Y.; Li, H.; Menon, N. K.; Neuhaus, E. B.; Brewer, J. M.; Byeon, I. J.; Ray, D. G.; Vitek, M. P.; Iwashita, T.; Makula, R. A.; Przybyla, A. B.; Zagorski, M. G., Solution NMR studies of the A beta(1-40) and A beta(1-42) peptides establish that the Met35 oxidation state affects the mechanism of amyloid formation. *J Am Chem Soc* **2004**, *126* (7), 1992-2005.
133. Nguyen, T.; Nioi, P.; Pickett, C. B., The Nrf2-antioxidant response element signaling pathway and its activation by oxidative stress. *J Biol Chem* **2009**, *284* (20), 13291-5.
134. Kobayashi, M.; Yamamoto, M., Nrf2-Keap1 regulation of cellular defense mechanisms against electrophiles and reactive oxygen species. *Adv Enzyme Regul* **2006**, *46*, 113-40.
135. de Vries, H. E.; Witte, M.; Hondius, D.; Rozemuller, A. J.; Drukarch, B.; Hoozemans, J.; van Horsen, J., Nrf2-induced antioxidant protection: a promising target to counteract ROS-mediated damage in neurodegenerative disease? *Free Radic Biol Med* **2008**, *45* (10), 1375-83.
136. Dinkova-Kostova, A. T.; Talalay, P., NAD(P)H:quinone acceptor oxidoreductase 1 (NQO1), a multifunctional antioxidant enzyme and exceptionally versatile cytoprotector. *Arch Biochem Biophys* **2010**, *501* (1), 116-23.
137. Ye, S.; Chen, M.; Jiang, Y.; Zhou, T.; Wang, Y.; Hou, Z.; Ren, L., Polyhydroxylated fullerene attenuates oxidative stress-induced apoptosis via a fortifying Nrf2-regulated cellular antioxidant defence system. *Int J Nanomedicine* **2014**, *9*, 2073-87.
138. Ramsey, C. P.; Glass, C. A.; Montgomery, M. B.; Lindl, K. A.; Ritson, G. P.; Chia, L. A.; Hamilton, R. L.; Chu, C. T.; Jordan-Sciutto, K. L., Expression of Nrf2 in neurodegenerative diseases. *J Neuropathol Exp Neurol* **2007**, *66* (1), 75-85.
139. Eftekharzadeh, B.; Maghsoudi, N.; Khodaghali, F., Stabilization of transcription factor Nrf2 by tBHQ prevents oxidative stress-induced amyloid beta formation in NT2N neurons. *Biochimie* **2010**, *92* (3), 245-53.
140. Lee, C.; Park, G. H.; Lee, S. R.; Jang, J. H., Attenuation of  $\beta$ -amyloid-induced oxidative cell death by sulforaphane via activation of NF-E2-related factor 2. *Oxid Med Cell Longev* **2013**, *2013*, 313510.
141. An, Y. W.; Jhang, K. A.; Woo, S. Y.; Kang, J. L.; Chong, Y. H., Sulforaphane exerts its anti-inflammatory effect against amyloid- $\beta$  peptide via STAT-1 dephosphorylation and activation of Nrf2/HO-1 cascade in human THP-1 macrophages. *Neurobiol Aging* **2016**, *38*, 1-10.

142. Wang, Y.; Miao, Y.; Mir, A. Z.; Cheng, L.; Wang, L.; Zhao, L.; Cui, Q.; Zhao, W.; Wang, H., Inhibition of beta-amyloid-induced neurotoxicity by pinocembrin through Nrf2/HO-1 pathway in SH-SY5Y cells. *J Neurol Sci* **2016**, *368*, 223-30.
143. Joshi, G.; Gan, K. A.; Johnson, D. A.; Johnson, J. A., Increased Alzheimer's disease-like pathology in the APP/PS1 $\Delta$ E9 mouse model lacking Nrf2 through modulation of autophagy. *Neurobiol Aging* **2015**, *36* (2), 664-79.
144. Liu, Y.; Deng, Y.; Liu, H.; Yin, C.; Li, X.; Gong, Q., Hydrogen sulfide ameliorates learning memory impairment in APP/PS1 transgenic mice: A novel mechanism mediated by the activation of Nrf2. *Pharmacol Biochem Behav* **2016**, *150-151*, 207-216.
145. Beckerman, R.; Prives, C., Transcriptional regulation by p53. *Cold Spring Harb Perspect Biol* **2010**, *2* (8), a000935.
146. Checler, F.; Alves da Costa, C., p53 in neurodegenerative diseases and brain cancers. *Pharmacol Ther* **2014**, *142* (1), 99-113.
147. Chatoo, W.; Abdouh, M.; Bernier, G., p53 pro-oxidant activity in the central nervous system: implication in aging and neurodegenerative diseases. *Antioxid Redox Signal* **2011**, *15* (6), 1729-37.
148. Chui, D. H.; Dobo, E.; Makifuchi, T.; Akiyama, H.; Kawakatsu, S.; Petit, A.; Checler, F.; Araki, W.; Takahashi, K.; Tabira, T., Apoptotic neurons in Alzheimer's disease frequently show intracellular Abeta42 labeling. *J Alzheimers Dis* **2001**, *3* (2), 231-239.
149. Ohyagi, Y.; Asahara, H.; Chui, D. H.; Tsuruta, Y.; Sakae, N.; Miyoshi, K.; Yamada, T.; Kikuchi, H.; Taniwaki, T.; Murai, H.; Ikezoe, K.; Furuya, H.; Kawarabayashi, T.; Shoji, M.; Checler, F.; Iwaki, T.; Makifuchi, T.; Takeda, K.; Kira, J.; Tabira, T., Intracellular Abeta42 activates p53 promoter: a pathway to neurodegeneration in Alzheimer's disease. *FASEB J* **2005**, *19* (2), 255-7.
150. Buizza, L.; Cenini, G.; Lanni, C.; Ferrari-Toninelli, G.; Prandelli, C.; Govoni, S.; Buoso, E.; Racchi, M.; Barcikowska, M.; Styczynska, M.; Szybinska, A.; Butterfield, D. A.; Memo, M.; Uberti, D., Conformationally altered p53 as an early marker of oxidative stress in Alzheimer's disease. *PLoS One* **2012**, *7* (1), e29789.
151. Uberti, D.; Lanni, C.; Carsana, T.; Francisconi, S.; Missale, C.; Racchi, M.; Govoni, S.; Memo, M., Identification of a mutant-like conformation of p53 in fibroblasts from sporadic Alzheimer's disease patients. *Neurobiol Aging* **2006**, *27* (9), 1193-201.
152. Lanni, C.; Racchi, M.; Mazzini, G.; Ranzenigo, A.; Polotti, R.; Sinforiani, E.; Olivari, L.; Barcikowska, M.; Styczynska, M.; Kuznicki, J.; Szybinska, A.; Govoni, S.; Memo, M.; Uberti, D., Conformationally altered p53: a novel Alzheimer's disease marker? *Mol Psychiatry* **2008**, *13* (6), 641-7.
153. Zhou, X.; Jia, J., P53-mediated G(1)/S checkpoint dysfunction in lymphocytes from Alzheimer's disease patients. *Neurosci Lett* **2010**, *468* (3), 320-5.
154. Lanni, C.; Nardinocchi, L.; Puca, R.; Stanga, S.; Uberti, D.; Memo, M.; Govoni, S.; D'Orazi, G.; Racchi, M., Homeodomain interacting protein kinase 2: a target for Alzheimer's beta amyloid leading to misfolded p53 and inappropriate cell survival. *PLoS One* **2010**, *5* (4), e10171.
155. Lanni, C.; Necchi, D.; Pinto, A.; Buoso, E.; Buizza, L.; Memo, M.; Uberti, D.; Govoni, S.; Racchi, M., Zyxin is a novel target for  $\beta$ -amyloid peptide: characterization of its role in Alzheimer's pathogenesis. *J Neurochem* **2013**, *125* (5), 790-9.
156. Rudy, C. C.; Hunsberger, H. C.; Weitzner, D. S.; Reed, M. N., The role of the tripartite glutamatergic synapse in the pathophysiology of Alzheimer's disease. *Aging Dis* **2015**, *6* (2), 131-48.

157. Hardingham, G. E.; Fukunaga, Y.; Bading, H., Extrasynaptic NMDARs oppose synaptic NMDARs by triggering CREB shut-off and cell death pathways. *Nat Neurosci* **2002**, *5* (5), 405-14.
158. Liu, Y.; Wong, T. P.; Aarts, M.; Rooyackers, A.; Liu, L.; Lai, T. W.; Wu, D. C.; Lu, J.; Tymianski, M.; Craig, A. M.; Wang, Y. T., NMDA receptor subunits have differential roles in mediating excitotoxic neuronal death both in vitro and in vivo. *J Neurosci* **2007**, *27* (11), 2846-57.
159. Talantova, M.; Sanz-Blasco, S.; Zhang, X.; Xia, P.; Akhtar, M. W.; Okamoto, S.; Dziewczapolski, G.; Nakamura, T.; Cao, G.; Pratt, A. E.; Kang, Y. J.; Tu, S.; Molokanova, E.; McKercher, S. R.; Hires, S. A.; Sason, H.; Stouffer, D. G.; Buczynski, M. W.; Solomon, J. P.; Michael, S.; Powers, E. T.; Kelly, J. W.; Roberts, A.; Tong, G.; Fang-Newmeyer, T.; Parker, J.; Holland, E. A.; Zhang, D.; Nakanishi, N.; Chen, H. S.; Wolosker, H.; Wang, Y.; Parsons, L. H.; Ambasadhan, R.; Masliah, E.; Heinemann, S. F.; Piña-Crespo, J. C.; Lipton, S. A., A $\beta$  induces astrocytic glutamate release, extrasynaptic NMDA receptor activation, and synaptic loss. *Proc Natl Acad Sci U S A* **2013**, *110* (27), E2518-27.
160. Jürgensen, S.; Ferreira, S. T., Nicotinic receptors, amyloid-beta, and synaptic failure in Alzheimer's disease. *J Mol Neurosci* **2010**, *40* (1-2), 221-9.
161. Lauderback, C. M.; Hackett, J. M.; Huang, F. F.; Keller, J. N.; Szweda, L. I.; Markesbery, W. R.; Butterfield, D. A., The glial glutamate transporter, GLT-1, is oxidatively modified by 4-hydroxy-2-nonenal in the Alzheimer's disease brain: the role of Abeta1-42. *J Neurochem* **2001**, *78* (2), 413-6.
162. Klein, W. L.; Lacor, P. N.; De Felice, F. G.; Ferreira, S. T., Molecules that Disrupt Memory Circuits in Alzheimer's Disease: The Attack on Synapses by A $\beta$  Oligomers (ADDLs). In *Memories: Molecules and Circuits*, Bontempi, B.; Silva, A. J.; Christen, Y., Eds. Springer Berlin Heidelberg: Berlin, Heidelberg, 2007; pp 155-179.
163. Danysz, W.; Parsons, C. G., Alzheimer's disease,  $\beta$ -amyloid, glutamate, NMDA receptors and memantine--searching for the connections. *Br J Pharmacol* **2012**, *167* (2), 324-52.
164. Alley, G. M.; Bailey, J. A.; Chen, D.; Ray, B.; Puli, L. K.; Tanila, H.; Banerjee, P. K.; Lahiri, D. K., Memantine lowers amyloid-beta peptide levels in neuronal cultures and in APP/PS1 transgenic mice. *J Neurosci Res* **2010**, *88* (1), 143-54.
165. Rosini, M.; Simoni, E.; Caporaso, R.; Minarini, A., Multitarget strategies in Alzheimer's disease: benefits and challenges on the road to therapeutics. *Future Med Chem* **2016**, *8* (6), 697-711.
166. Bolognesi, M. L.; Matera, R.; Minarini, A.; Rosini, M.; Melchiorre, C., Alzheimer's disease: new approaches to drug discovery. *Curr Opin Chem Biol* **2009**, *13* (3), 303-8.
167. Morphy, R.; Rankovic, Z., Designed multiple ligands. An emerging drug discovery paradigm. *J Med Chem* **2005**, *48* (21), 6523-43.
168. Gauthier, S.; Molinuevo, J. L., Benefits of combined cholinesterase inhibitor and memantine treatment in moderate-severe Alzheimer's disease. *Alzheimers Dement* **2013**, *9* (3), 326-31.
169. Grossberg, G. T.; Edwards, K. R.; Zhao, Q., Rationale for combination therapy with galantamine and memantine in Alzheimer's disease. *J Clin Pharmacol* **2006**, *46* (7 Suppl 1), 17S-26S.
170. Namzaric Alzheimer's disease treatment website. [www.Namzaric.com](http://www.Namzaric.com).
171. Rosini, M., Polypharmacology: the rise of multitarget drugs over combination therapies. *Future Med Chem* **2014**, *6* (5), 485-7.
172. Morphy, R.; Rankovic, Z., Designing multiple ligands - medicinal chemistry strategies and challenges. *Curr Pharm Des* **2009**, *15* (6), 587-600.
173. Peters, J. U., Polypharmacology - foe or friend? *J Med Chem* **2013**, *56* (22), 8955-71.

174. Castro, A.; Martinez, A., Targeting beta-amyloid pathogenesis through acetylcholinesterase inhibitors. *Curr Pharm Des* **2006**, *12* (33), 4377-87.
175. Rosini, M.; Simoni, E.; Milelli, A.; Minarini, A.; Melchiorre, C., Oxidative stress in Alzheimer's disease: are we connecting the dots? *J Med Chem* **2014**, *57* (7), 2821-31.
176. Rosini, M.; Andrisano, V.; Bartolini, M.; Bolognesi, M. L.; Hrelia, P.; Minarini, A.; Tarozzi, A.; Melchiorre, C., Rational approach to discover multipotent anti-Alzheimer drugs. *J Med Chem* **2005**, *48* (2), 360-3.
177. Rosini, M.; Simoni, E.; Bartolini, M.; Tarozzi, A.; Matera, R.; Milelli, A.; Hrelia, P.; Andrisano, V.; Bolognesi, M. L.; Melchiorre, C., Exploiting the lipoic acid structure in the search for novel multitarget ligands against Alzheimer's disease. *Eur J Med Chem* **2011**, *46* (11), 5435-42.
178. Tirosh, O.; Sen, C. K.; Roy, S.; Kobayashi, M. S.; Packer, L., Neuroprotective effects of alpha-lipoic acid and its positively charged amide analogue. *Free Radic Biol Med* **1999**, *26* (11-12), 1418-26.
179. Minarini, A.; Milelli, A.; Tumiatti, V.; Rosini, M.; Simoni, E.; Bolognesi, M. L.; Andrisano, V.; Bartolini, M.; Motori, E.; Angeloni, C.; Hrelia, S., Cystamine-tacrine dimer: a new multi-target-directed ligand as potential therapeutic agent for Alzheimer's disease treatment. *Neuropharmacology* **2012**, *62* (2), 997-1003.
180. Pi, R.; Mao, X.; Chao, X.; Cheng, Z.; Liu, M.; Duan, X.; Ye, M.; Chen, X.; Mei, Z.; Liu, P.; Li, W.; Han, Y., Tacrine-6-ferulic acid, a novel multifunctional dimer, inhibits amyloid- $\beta$ -mediated Alzheimer's disease-associated pathogenesis in vitro and in vivo. *PLoS One* **2012**, *7* (2), e31921.
181. Huang, W. Y.; Chao, X. J.; Ouyang, Y.; Liu, A. M.; He, X. X.; Chen, M. H.; Wang, L. H.; Liu, J.; Yu, S. W.; Rapposelli, S.; Pi, R. B., Tacrine-6-ferulic acid, a novel multifunctional dimer against Alzheimer's disease, prevents oxidative stress-induced neuronal death through activating Nrf2/ARE/HO-1 pathway in HT22 cells. *CNS Neurosci Ther* **2012**, *18* (11), 950-1.
182. Chen, Z.; Digiacomio, M.; Tu, Y.; Gu, Q.; Wang, S.; Yang, X.; Chu, J.; Chen, Q.; Han, Y.; Chen, J.; Nesi, G.; Sestito, S.; Macchia, M.; Rapposelli, S.; Pi, R., Discovery of novel rivastigmine-hydroxycinnamic acid hybrids as multi-targeted agents for Alzheimer's disease. *Eur J Med Chem* **2017**, *125*, 784-792.
183. Rosini, M.; Simoni, E.; Minarini, A.; Melchiorre, C., Multi-target design strategies in the context of Alzheimer's disease: acetylcholinesterase inhibition and NMDA receptor antagonism as the driving forces. *Neurochem Res* **2014**, *39* (10), 1914-23.
184. Busquet, P.; Capurro, V.; Cavalli, A.; Piomelli, D.; Reggiani, A.; Bertorelli, R., Synergistic effects of galantamine and memantine in attenuating scopolamine-induced amnesia in mice. *J Pharmacol Sci* **2012**, *120* (4), 305-9.
185. Simoni, E.; Daniele, S.; Bottegoni, G.; Pizzirani, D.; Trincavelli, M. L.; Goldoni, L.; Tarozzo, G.; Reggiani, A.; Martini, C.; Piomelli, D.; Melchiorre, C.; Rosini, M.; Cavalli, A., Combining galantamine and memantine in multitargeted, new chemical entities potentially useful in Alzheimer's disease. *J Med Chem* **2012**, *55* (22), 9708-21.
186. Doody, R. S.; Gavrilova, S. I.; Sano, M.; Thomas, R. G.; Aisen, P. S.; Bachurin, S. O.; Seely, L.; Hung, D.; investigators, d., Effect of dimebon on cognition, activities of daily living, behaviour, and global function in patients with mild-to-moderate Alzheimer's disease: a randomised, double-blind, placebo-controlled study. *Lancet* **2008**, *372* (9634), 207-15.
187. Miller, G., Pharmacology. The puzzling rise and fall of a dark-horse Alzheimer's drug. *Science* **2010**, *327* (5971), 1309.

188. Rosini, M.; Simoni, E.; Bartolini, M.; Soriano, E.; Marco-Contelles, J.; Andrisano, V.; Monti, B.; Windisch, M.; Hutter-Paier, B.; McClymont, D. W.; Mellor, I. R.; Bolognesi, M. L., The bivalent ligand approach as a tool for improving the in vitro anti-Alzheimer multitarget profile of dimebon. *ChemMedChem* **2013**, *8* (8), 1276-81.
189. Makhaeva, G. F.; Lushchekina, S. V.; Boltneva, N. P.; Sokolov, V. B.; Grigoriev, V. V.; Serebryakova, O. G.; Vikhareva, E. A.; Aksinenko, A. Y.; Barreto, G. E.; Aliev, G.; Bachurin, S. O., Conjugates of  $\gamma$ -Carbolines and Phenothiazine as new selective inhibitors of butyrylcholinesterase and blockers of NMDA receptors for Alzheimer Disease. *Sci Rep* **2015**, *5*, 13164.
190. Prati, F.; De Simone, A.; Bisignano, P.; Armirotti, A.; Summa, M.; Pizzirani, D.; Scarpelli, R.; Perez, D. I.; Andrisano, V.; Perez-Castillo, A.; Monti, B.; Massenzio, F.; Polito, L.; Racchi, M.; Favia, A. D.; Bottegoni, G.; Martinez, A.; Bolognesi, M. L.; Cavalli, A., Multitarget drug discovery for Alzheimer's disease: triazinones as BACE-1 and GSK-3 $\beta$  inhibitors. *Angew Chem Int Ed Engl* **2015**, *54* (5), 1578-82.
191. Llorens-Martín, M.; Jurado, J.; Hernández, F.; Avila, J., GSK-3 $\beta$ , a pivotal kinase in Alzheimer disease. *Front Mol Neurosci* **2014**, *7*, 46.
192. Davinelli, S.; Sapere, N.; Zella, D.; Bracale, R.; Intrieri, M.; Scapagnini, G., Pleiotropic protective effects of phytochemicals in Alzheimer's disease. *Oxid Med Cell Longev* **2012**, *2012*, 386527.
193. Singh, M.; Arseneault, M.; Sanderson, T.; Murthy, V.; Ramassamy, C., Challenges for research on polyphenols from foods in Alzheimer's disease: bioavailability, metabolism, and cellular and molecular mechanisms. *J Agric Food Chem* **2008**, *56* (13), 4855-73.
194. Handique, J. G.; Baruah, J. B., Polyphenolic compounds: an overview. *Reactive and Functional Polymers* **2002**, *52* (3), 163-188.
195. Porat, Y.; Mazor, Y.; Efrat, S.; Gazit, E., Inhibition of islet amyloid polypeptide fibril formation: a potential role for heteroaromatic interactions. *Biochemistry* **2004**, *43* (45), 14454-62.
196. Porat, Y.; Abramowitz, A.; Gazit, E., Inhibition of amyloid fibril formation by polyphenols: structural similarity and aromatic interactions as a common inhibition mechanism. *Chem Biol Drug Des* **2006**, *67* (1), 27-37.
197. Hamaguchi, T.; Ono, K.; Yamada, M., REVIEW: Curcumin and Alzheimer's disease. *CNS Neurosci Ther* **2010**, *16* (5), 285-97.
198. Shimmyo, Y.; Kihara, T.; Akaike, A.; Niidome, T.; Sugimoto, H., Epigallocatechin-3-gallate and curcumin suppress amyloid beta-induced beta-site APP cleaving enzyme-1 upregulation. *Neuroreport* **2008**, *19* (13), 1329-33.
199. Yang, F.; Lim, G. P.; Begum, A. N.; Ubeda, O. J.; Simmons, M. R.; Ambegaokar, S. S.; Chen, P. P.; Kaye, R.; Glabe, C. G.; Frautschy, S. A.; Cole, G. M., Curcumin inhibits formation of amyloid beta oligomers and fibrils, binds plaques, and reduces amyloid in vivo. *J Biol Chem* **2005**, *280* (7), 5892-901.
200. Ma, Q. L.; Yang, F.; Rosario, E. R.; Ubeda, O. J.; Beech, W.; Gant, D. J.; Chen, P. P.; Hudspeth, B.; Chen, C.; Zhao, Y.; Vinters, H. V.; Frautschy, S. A.; Cole, G. M., Beta-amyloid oligomers induce phosphorylation of tau and inactivation of insulin receptor substrate via c-Jun N-terminal kinase signaling: suppression by omega-3 fatty acids and curcumin. *J Neurosci* **2009**, *29* (28), 9078-89.
201. Fu, Z.; Aucoin, D.; Ahmed, M.; Ziliox, M.; Van Nostrand, W. E.; Smith, S. O., Capping of a $\beta$ 42 oligomers by small molecule inhibitors. *Biochemistry* **2014**, *53* (50), 7893-903.

202. Yanagisawa, D.; Shirai, N.; Amatsubo, T.; Taguchi, H.; Hirao, K.; Urushitani, M.; Morikawa, S.; Inubushi, T.; Kato, M.; Kato, F.; Morino, K.; Kimura, H.; Nakano, I.; Yoshida, C.; Okada, T.; Sano, M.; Wada, Y.; Wada, K. N.; Yamamoto, A.; Tooyama, I., Relationship between the tautomeric structures of curcumin derivatives and their Abeta-binding activities in the context of therapies for Alzheimer's disease. *Biomaterials* **2010**, *31* (14), 4179-85.
203. Reinke, A. A.; Gestwicki, J. E., Structure-activity relationships of amyloid beta-aggregation inhibitors based on curcumin: influence of linker length and flexibility. *Chem Biol Drug Des* **2007**, *70* (3), 206-15.
204. Weinreb, O.; Amit, T.; Youdim, M. B., The application of proteomics for studying the neurorescue activity of the polyphenol (-)-epigallocatechin-3-gallate. *Arch Biochem Biophys* **2008**, *476* (2), 152-60.
205. Mandel, S.; Youdim, M. B., Catechin polyphenols: neurodegeneration and neuroprotection in neurodegenerative diseases. *Free Radic Biol Med* **2004**, *37* (3), 304-17.
206. Ehrnhoefer, D. E.; Bieschke, J.; Boeddrich, A.; Herbst, M.; Masino, L.; Lurz, R.; Engemann, S.; Pastore, A.; Wanker, E. E., EGCG redirects amyloidogenic polypeptides into unstructured, off-pathway oligomers. *Nat Struct Mol Biol* **2008**, *15* (6), 558-66.
207. Dragicevic, N.; Smith, A.; Lin, X.; Yuan, F.; Copes, N.; Delic, V.; Tan, J.; Cao, C.; Shytle, R. D.; Bradshaw, P. C., Green tea epigallocatechin-3-gallate (EGCG) and other flavonoids reduce Alzheimer's amyloid-induced mitochondrial dysfunction. *J Alzheimers Dis* **2011**, *26* (3), 507-21.
208. Baur, J. A.; Sinclair, D. A., Therapeutic potential of resveratrol: the in vivo evidence. *Nat Rev Drug Discov* **2006**, *5* (6), 493-506.
209. Anekonda, T. S.; Reddy, P. H., Neuronal protection by sirtuins in Alzheimer's disease. *J Neurochem* **2006**, *96* (2), 305-13.
210. Chen, J.; Zhou, Y.; Mueller-Steiner, S.; Chen, L. F.; Kwon, H.; Yi, S.; Mucke, L.; Gan, L., SIRT1 protects against microglia-dependent amyloid-beta toxicity through inhibiting NF-kappaB signaling. *J Biol Chem* **2005**, *280* (48), 40364-74.
211. Saibabu, V.; Fatima, Z.; Khan, L. A.; Hameed, S., Therapeutic Potential of Dietary Phenolic Acids. *Adv Pharmacol Sci* **2015**, *2015*, 823539.
212. Moosavi, F.; Hosseini, R.; Saso, L.; Firuzi, O., Modulation of neurotrophic signaling pathways by polyphenols. *Drug Des Devel Ther* **2016**, *10*, 23-42.
213. Kim, J. H.; Wang, Q.; Choi, J. M.; Lee, S.; Cho, E. J., Protective role of caffeic acid in an A $\beta$ 25-35-induced Alzheimer's disease model. *Nutr Res Pract* **2015**, *9* (5), 480-8.
214. Razzaghi-Asl, N.; Garrido, J.; Khazraei, H.; Borges, F.; Firuzi, O., Antioxidant properties of hydroxycinnamic acids: a review of structure- activity relationships. *Curr Med Chem* **2013**, *20* (36), 4436-50.
215. Scapagnini, G.; Vasto, S.; Sonya, V.; Abraham, N. G.; Nader, A. G.; Caruso, C.; Calogero, C.; Zella, D.; Fabio, G., Modulation of Nrf2/ARE pathway by food polyphenols: a nutritional neuroprotective strategy for cognitive and neurodegenerative disorders. *Mol Neurobiol* **2011**, *44* (2), 192-201.
216. Satoh, T.; Lipton, S. A., Redox regulation of neuronal survival mediated by electrophilic compounds. *Trends Neurosci* **2007**, *30* (1), 37-45.
217. Zhang, D.; Lee, B.; Nutter, A.; Song, P.; Dolatabadi, N.; Parker, J.; Sanz-Blasco, S.; Newmeyer, T.; Ambasudhan, R.; McKercher, S. R.; Masliah, E.; Lipton, S. A., Protection from cyanide-induced brain injury by the Nrf2 transcriptional activator carnosic acid. *J Neurochem* **2015**, *133* (6), 898-908.

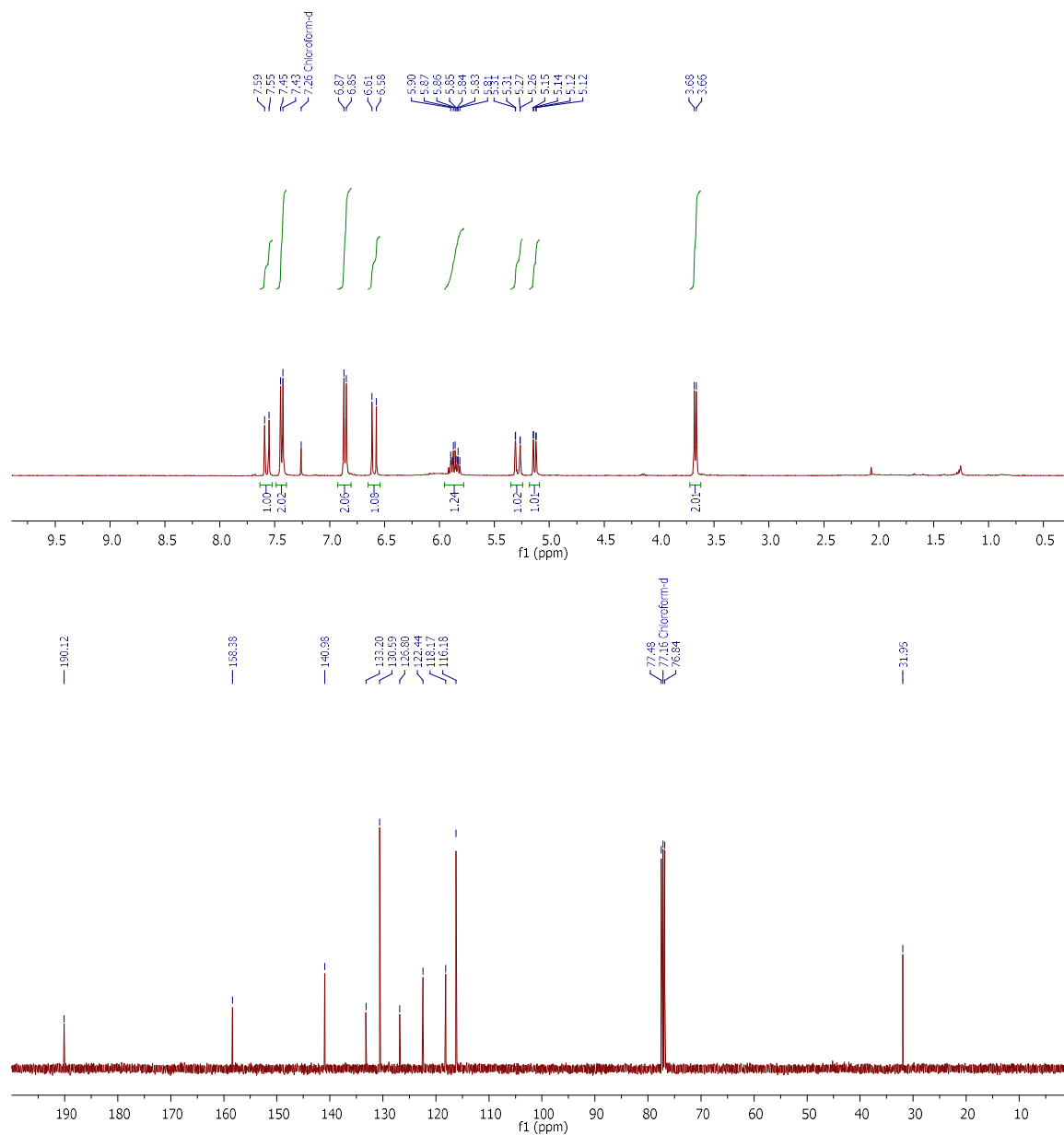
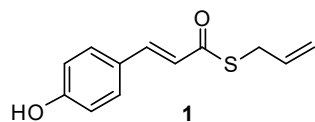
218. Satoh, T.; McKercher, S. R.; Lipton, S. A., Nrf2/ARE-mediated antioxidant actions of pro-electrophilic drugs. *Free Radic Biol Med* **2013**, *65*, 645-57.
219. Lipton, S. A.; Rezaie, T.; Nutter, A.; Lopez, K. M.; Parker, J.; Kosaka, K.; Satoh, T.; McKercher, S. R.; Masliah, E.; Nakanishi, N., Therapeutic advantage of pro-electrophilic drugs to activate the Nrf2/ARE pathway in Alzheimer's disease models. *Cell Death Dis* **2016**, *7* (12), e2499.
220. Kim, S.; Lee, H. G.; Park, S. A.; Kundu, J. K.; Keum, Y. S.; Cha, Y. N.; Na, H. K.; Surh, Y. J., Keap1 cysteine 288 as a potential target for diallyl trisulfide-induced Nrf2 activation. *PLoS One* **2014**, *9* (1), e85984.
221. Gupta, V. B.; Indi, S. S.; Rao, K. S., Garlic extract exhibits anti-amyloidogenic activity on amyloid-beta fibrillogenesis: relevance to Alzheimer's disease. *Phytother Res* **2009**, *23* (1), 111-5.
222. Chauhan, N. B., Effect of aged garlic extract on APP processing and tau phosphorylation in Alzheimer's transgenic model Tg2576. *J Ethnopharmacol* **2006**, *108* (3), 385-94.
223. Mandal, S.; Mukherjee, S.; Chowdhury, K. D.; Sarkar, A.; Basu, K.; Paul, S.; Karmakar, D.; Chatterjee, M.; Biswas, T.; Sadhukhan, G. C.; Sen, G., S-allyl cysteine in combination with clotrimazole downregulates Fas induced apoptotic events in erythrocytes of mice exposed to lead. *Biochim Biophys Acta* **2012**, *1820* (1), 9-23.
224. Tsai, S. J.; Chiu, C. P.; Yang, H. T.; Yin, M. C., s-Allyl cysteine, s-ethyl cysteine, and s-propyl cysteine alleviate  $\beta$ -amyloid, glycation, and oxidative injury in brain of mice treated by D-galactose. *J Agric Food Chem* **2011**, *59* (11), 6319-26.
225. Manral, A.; Meena, P.; Saini, V.; Siraj, F.; Shalini, S.; Tiwari, M., DADS Analogues Ameliorated the Cognitive Impairments of Alzheimer-Like Rat Model Induced by Scopolamine. *Neurotox Res* **2016**, *30* (3), 407-26.
226. Manral, A.; Saini, V.; Meena, P.; Tiwari, M., Multifunctional novel Diallyl disulfide (DADS) derivatives with  $\beta$ -amyloid-reducing, cholinergic, antioxidant and metal chelating properties for the treatment of Alzheimer's disease. *Bioorg Med Chem* **2015**, *23* (19), 6389-403.
227. Butterfield, D. A.; Swomley, A. M.; Sultana, R., Amyloid  $\beta$ -peptide (1-42)-induced oxidative stress in Alzheimer disease: importance in disease pathogenesis and progression. *Antioxid Redox Signal* **2013**, *19* (8), 823-35.
228. Lanni, C.; Racchi, M.; Memo, M.; Govoni, S.; Uberti, D., p53 at the crossroads between cancer and neurodegeneration. *Free Radic Biol Med* **2012**, *52* (9), 1727-33.
229. Lu, M. C.; Ji, J. A.; Jiang, Z. Y.; You, Q. D., The Keap1-Nrf2-ARE Pathway As a Potential Preventive and Therapeutic Target: An Update. *Med Res Rev* **2016**, *36* (5), 924-63.
230. Rizzo, S.; Waldmann, H., Development of a natural-product-derived chemical toolbox for modulation of protein function. *Chem Rev* **2014**, *114* (9), 4621-39.
231. Meanwell, N. A., Synopsis of some recent tactical application of bioisosteres in drug design. *J Med Chem* **2011**, *54* (8), 2529-91.
232. Tulla-Puche, J.; Marcucci, E.; Prats-Alfonso, E.; Bayó-Puxan, N.; Albericio, F., NMe amide as a synthetic surrogate for the thioester moiety in thiocoraline. *J Med Chem* **2009**, *52* (3), 834-9.
233. Xia, C. N.; Li, H. B.; Liu, F.; Hu, W. X., Synthesis of trans-caffeate analogues and their bioactivities against HIV-1 integrase and cancer cell lines. *Bioorg Med Chem Lett* **2008**, *18* (24), 6553-7.
234. Gisch, N.; Balzarini, J.; Meier, C., Enzymatically activated cycloSal-d4T-monophosphates: The third generation of cycloSal-pronucleotides. *J Med Chem* **2007**, *50* (7), 1658-67.
235. Ferino, G.; Cadoni, E.; Matos, M. J.; Quezada, E.; Uriarte, E.; Santana, L.; Vilar, S.; Tatonetti, N. P.; Yáñez, M.; Viña, D.; Picciau, C.; Serra, S.; Delogu, G., MAO inhibitory activity of

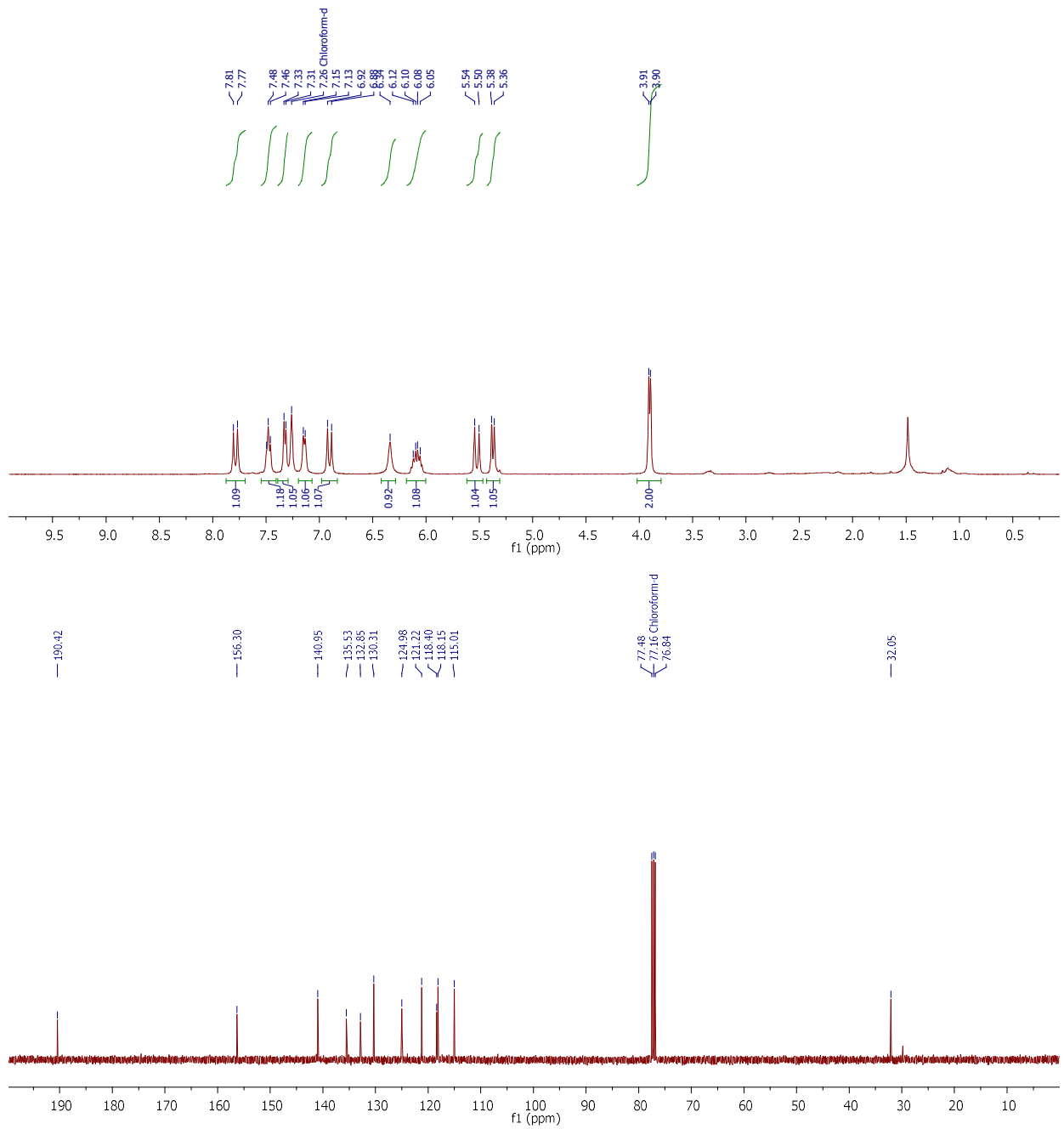
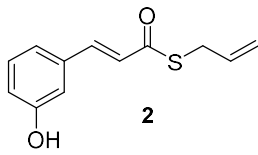
- 2-arylbenzofurans versus 3-arylcoumarins: synthesis, in vitro study, and docking calculations. *ChemMedChem* **2013**, *8* (6), 956-66.
236. Liu, Y.; Liu, Z.; Shi, J.; Chen, H.; Mi, B.; Li, P.; Gong, P., Synthesis and cytotoxicity of novel 10-substituted dihydroartemisinin derivatives containing N-arylphenyl-ethenesulfonamide groups. *Molecules* **2013**, *18* (3), 2864-77.
237. Simoni, E.; Serafini, M. M.; Bartolini, M.; Caporaso, R.; Pinto, A.; Necchi, D.; Fiori, J.; Andrisano, V.; Minarini, A.; Lanni, C.; Rosini, M., Nature-Inspired Multifunctional Ligands: Focusing on Amyloid-Based Molecular Mechanisms of Alzheimer's Disease. *ChemMedChem* **2016**, *11* (12), 1309-17.
238. Bartolini, M.; Naldi, M.; Fiori, J.; Valle, F.; Biscarini, F.; Nicolau, D. V.; Andrisano, V., Kinetic characterization of amyloid-beta 1-42 aggregation with a multimethodological approach. *Anal Biochem* **2011**, *414* (2), 215-25.
239. Lambert, M. P.; Barlow, A. K.; Chromy, B. A.; Edwards, C.; Freed, R.; Liosatos, M.; Morgan, T. E.; Rozovsky, I.; Trommer, B.; Viola, K. L.; Wals, P.; Zhang, C.; Finch, C. E.; Krafft, G. A.; Klein, W. L., Diffusible, nonfibrillar ligands derived from Abeta1-42 are potent central nervous system neurotoxins. *Proc Natl Acad Sci US A* **1998**, *95* (11), 6448-53.
240. Walsh, D. M.; Klyubin, I.; Fadeeva, J. V.; Cullen, W. K.; Anwyl, R.; Wolfe, M. S.; Rowan, M. J.; Selkoe, D. J., Naturally secreted oligomers of amyloid beta protein potently inhibit hippocampal long-term potentiation in vivo. *Nature* **2002**, *416* (6880), 535-9.
241. Forester, S. C.; Lambert, J. D., The role of antioxidant versus pro-oxidant effects of green tea polyphenols in cancer prevention. *Mol Nutr Food Res* **2011**, *55* (6), 844-54.
242. Fiori, J.; Naldi, M.; Bartolini, M.; Andrisano, V., Disclosure of a fundamental clue for the elucidation of the myricetin mechanism of action as amyloid aggregation inhibitor by mass spectrometry. *Electrophoresis* **2012**, *33* (22), 3380-6.
243. Hou, L.; Kang, I.; Marchant, R. E.; Zagorski, M. G., Methionine 35 oxidation reduces fibril assembly of the amyloid abeta-(1-42) peptide of Alzheimer's disease. *J Biol Chem* **2002**, *277* (43), 40173-6.
244. Méplan, C.; Richard, M. J.; Hainaut, P., Redox signalling and transition metals in the control of the p53 pathway. *Biochem Pharmacol* **2000**, *59* (1), 25-33.
245. Uberti, D.; Carsana, T.; Bernardi, E.; Rodella, L.; Grigolato, P.; Lanni, C.; Racchi, M.; Govoni, S.; Memo, M., Selective impairment of p53-mediated cell death in fibroblasts from sporadic Alzheimer's disease patients. *J Cell Sci* **2002**, *115* (Pt 15), 3131-8.
246. Hayakawa, K.; Hasegawa, M.; Kawashima, M.; Nakamura, Y.; Matsuura, M.; Toda, H.; Mitsuhashi, N.; Niibe, H., Comparison of effects of doxorubicin and radiation on p53-dependent apoptosis in vivo. *Oncol Rep* **2000**, *7* (2), 267-70.
247. Lorenzo, E.; Ruiz-Ruiz, C.; Quesada, A. J.; Hernández, G.; Rodríguez, A.; López-Rivas, A.; Redondo, J. M., Doxorubicin induces apoptosis and CD95 gene expression in human primary endothelial cells through a p53-dependent mechanism. *J Biol Chem* **2002**, *277* (13), 10883-92.
248. Wang, S.; Konorev, E. A.; Kotamraju, S.; Joseph, J.; Kalivendi, S.; Kalyanaraman, B., Doxorubicin induces apoptosis in normal and tumor cells via distinctly different mechanisms. Intermediacy of H(2)O(2)- and p53-dependent pathways. *J Biol Chem* **2004**, *279* (24), 25535-43.
249. Hardingham, G. E.; Bading, H., Synaptic versus extrasynaptic NMDA receptor signalling: implications for neurodegenerative disorders. *Nat Rev Neurosci* **2010**, *11* (10), 682-96.

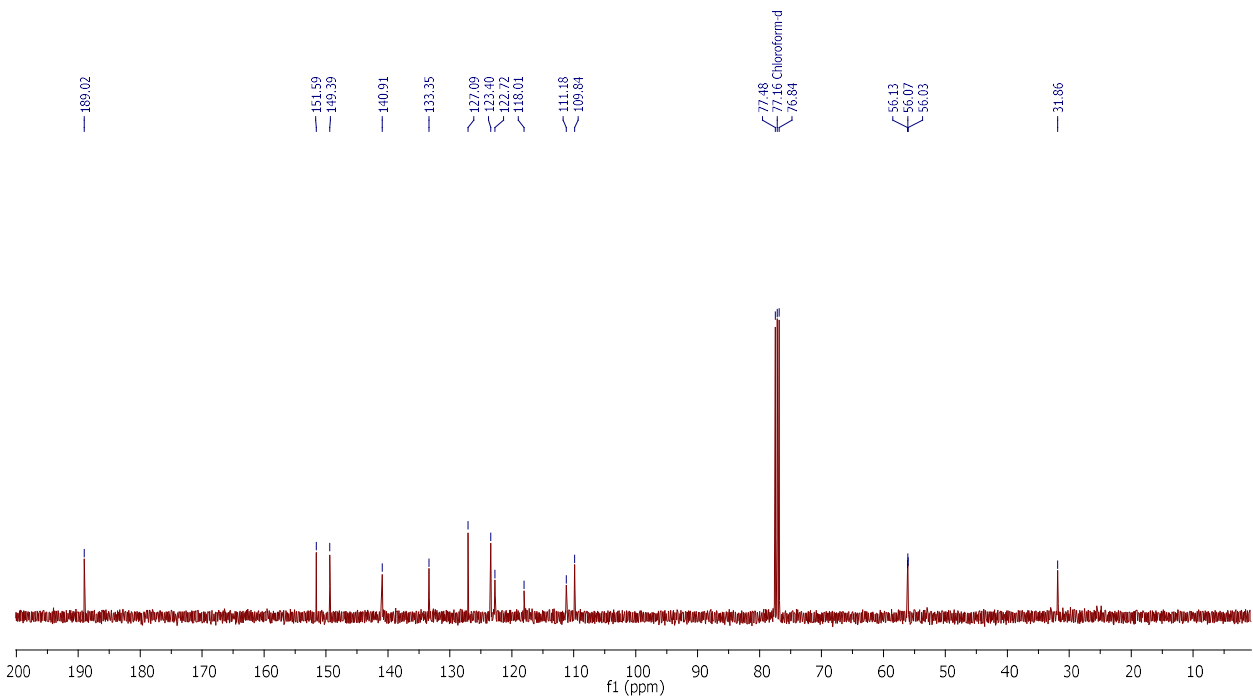
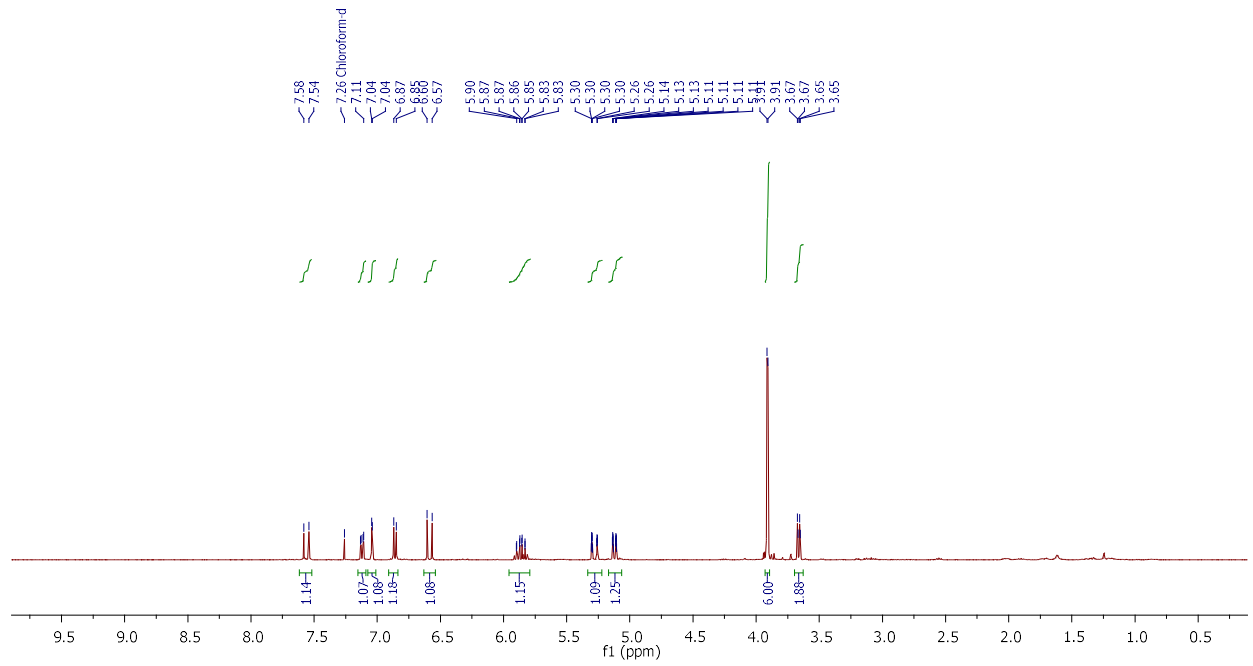
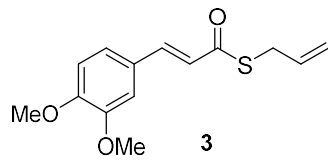
250. Wanka, L.; Cabrele, C.; Vanejews, M.; and Schreiner, P. R.,  $\gamma$ -Aminoadamantanecarboxylic Acids Through Direct C–H Bond Amidations. *European Journal of Organic Chemistry* **2007**, 2007 (9), 16.
251. Bartolini, M.; Bertucci, C.; Bolognesi, M. L.; Cavalli, A.; Melchiorre, C.; Andrisano, V., Insight into the kinetic of amyloid beta (1-42) peptide self-aggregation: elucidation of inhibitors' mechanism of action. *Chembiochem* **2007**, 8 (17), 2152-61.
252. Naiki, H.; Higuchi, K.; Hosokawa, M.; Takeda, T., Fluorometric determination of amyloid fibrils in vitro using the fluorescent dye, thioflavin T1. *Anal Biochem* **1989**, 177 (2), 244-9.
253. LeVine, H., Thioflavine T interaction with synthetic Alzheimer's disease beta-amyloid peptides: detection of amyloid aggregation in solution. *Protein Sci* **1993**, 2 (3), 404-10.

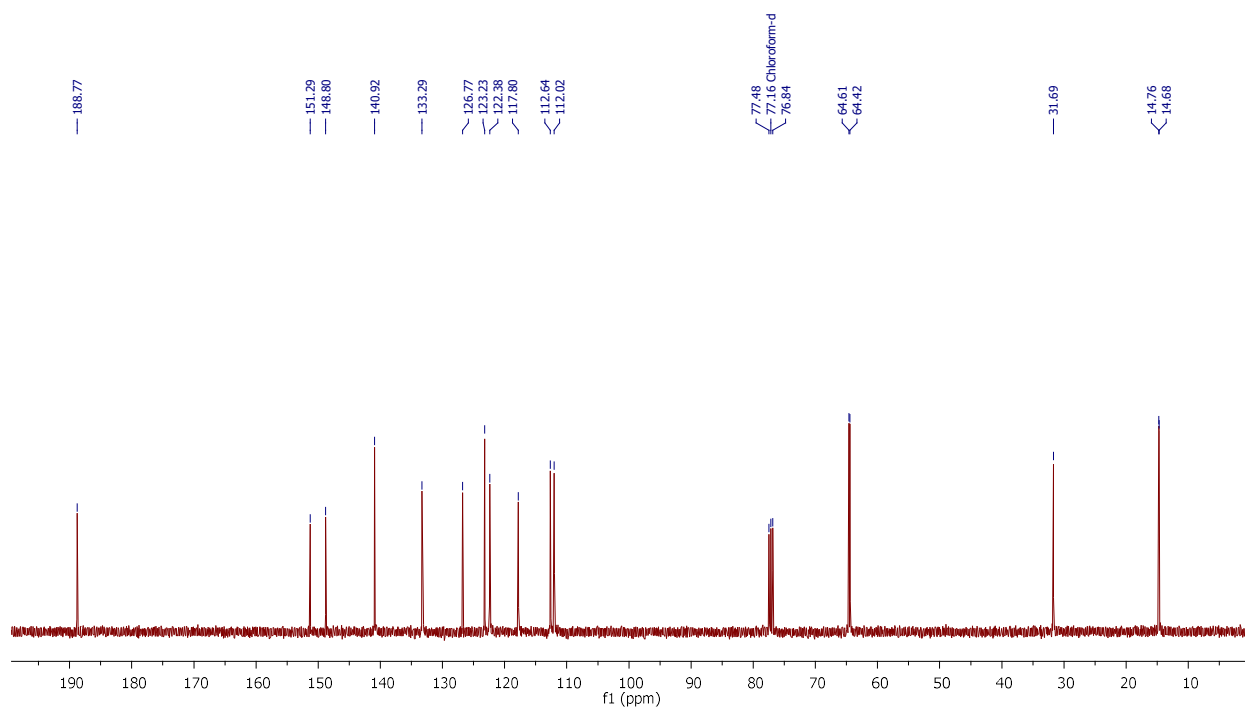
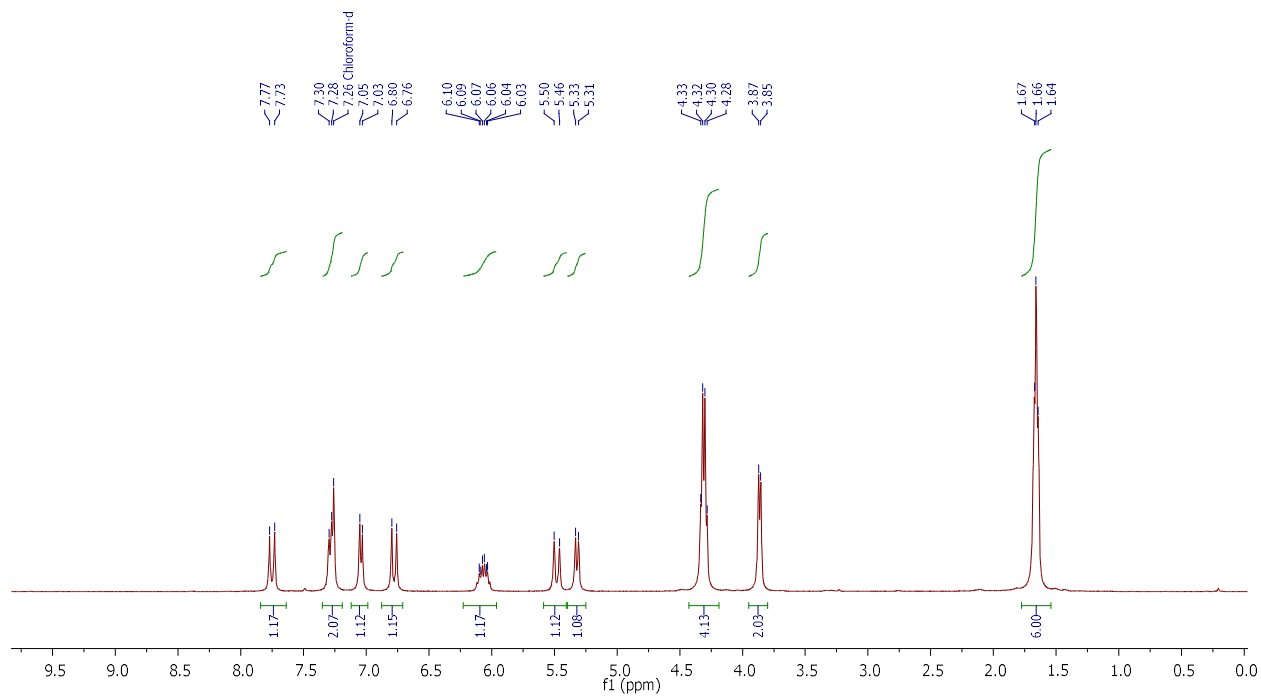
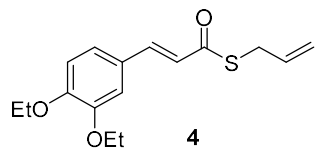
## Appendix

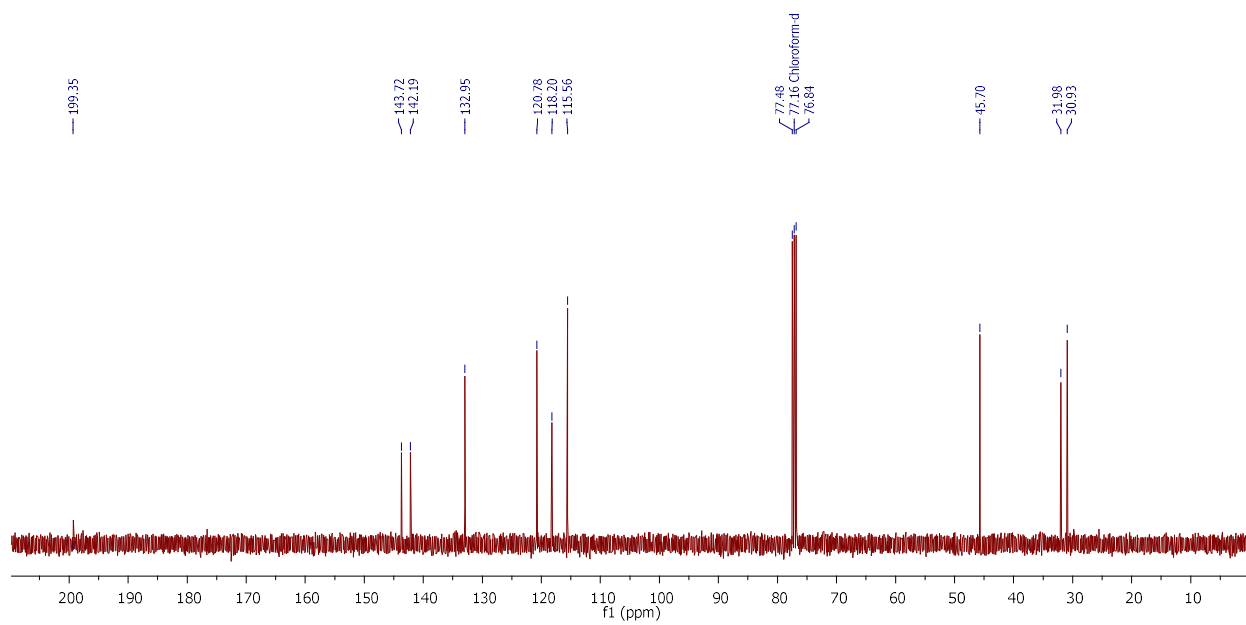
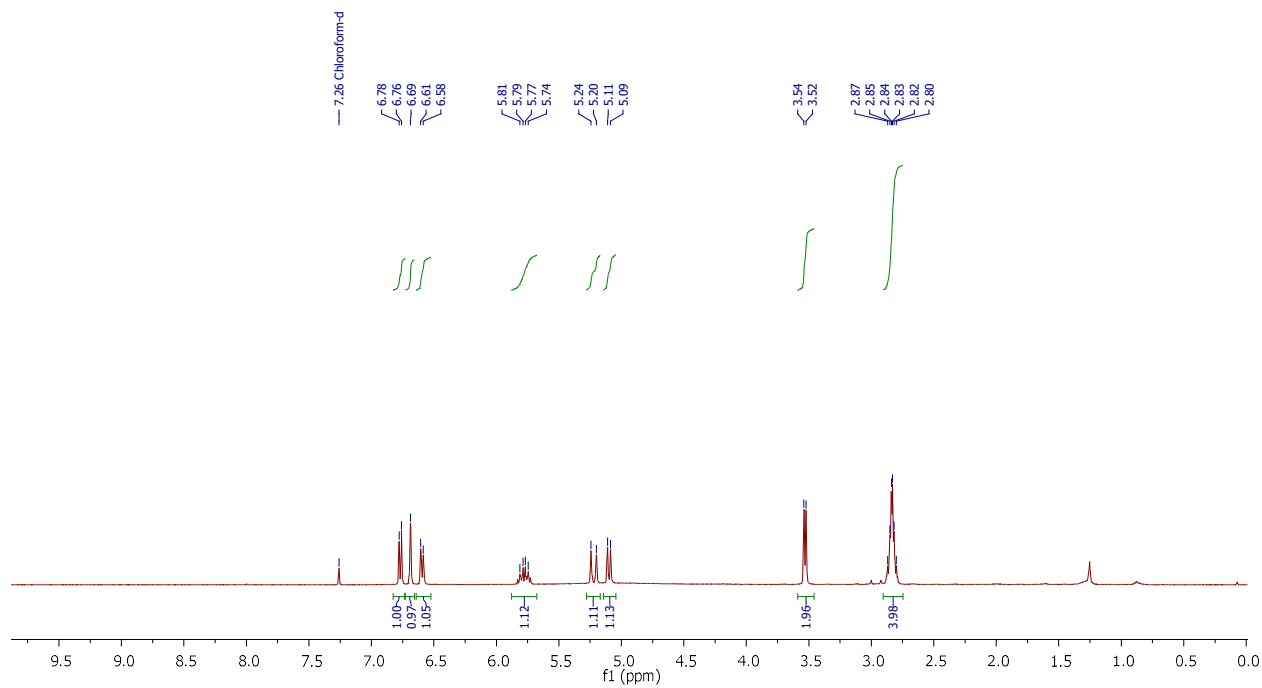
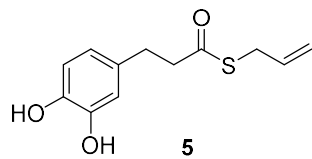
Copies of  $^1\text{H}$  and  $^{13}\text{C}$  NMR spectra of final compounds 1-23.

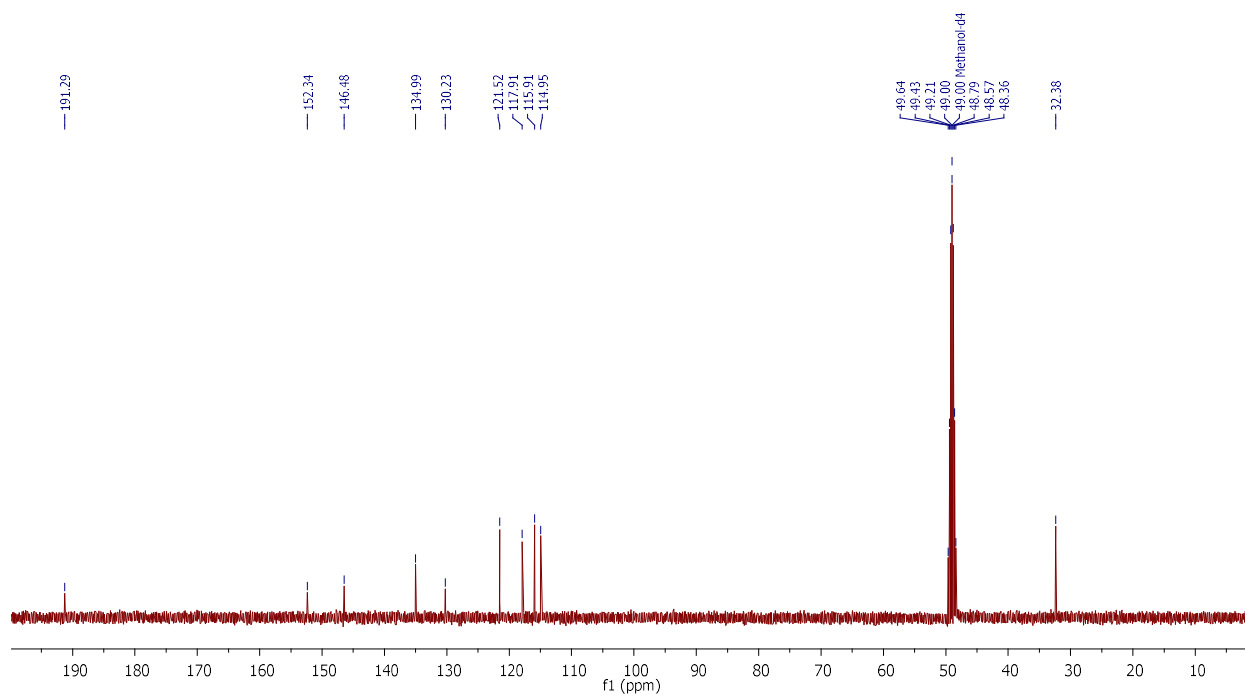
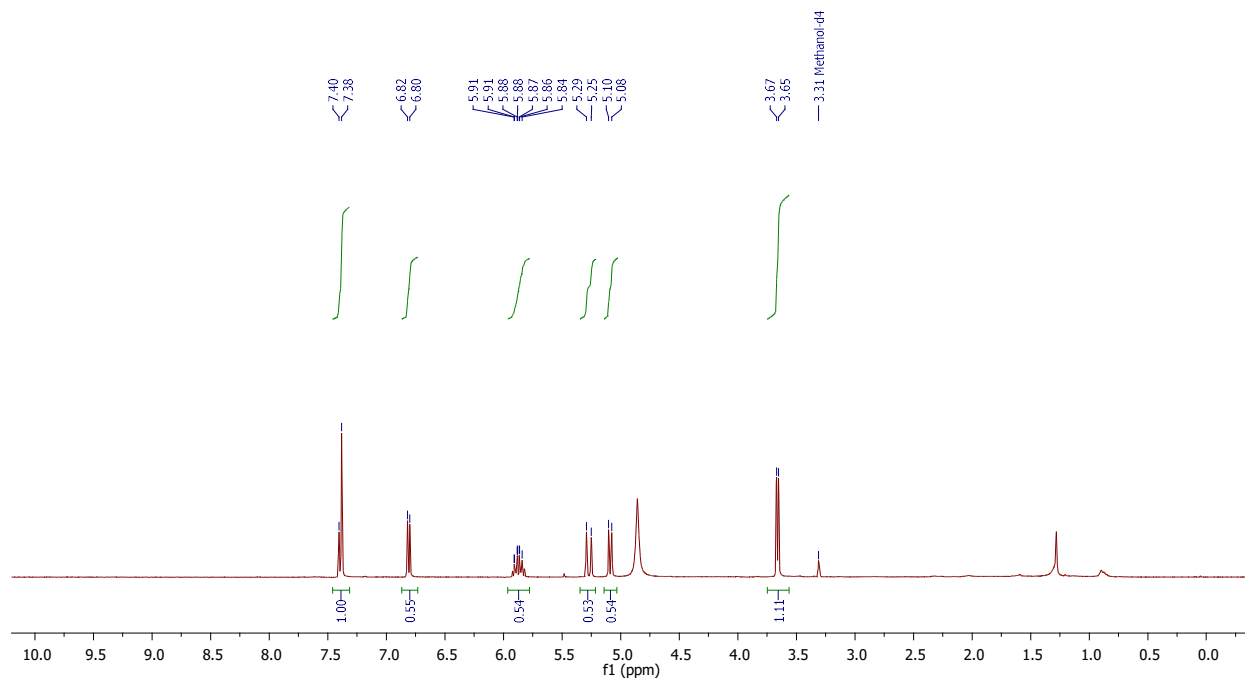
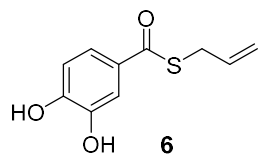


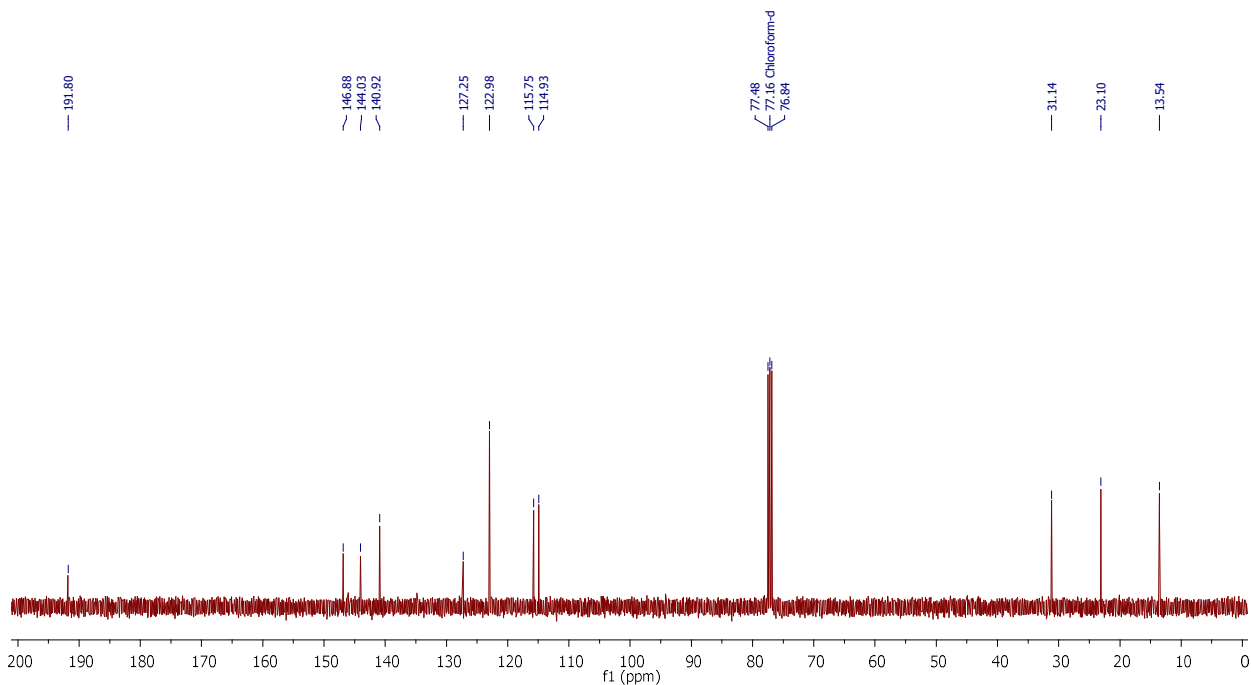
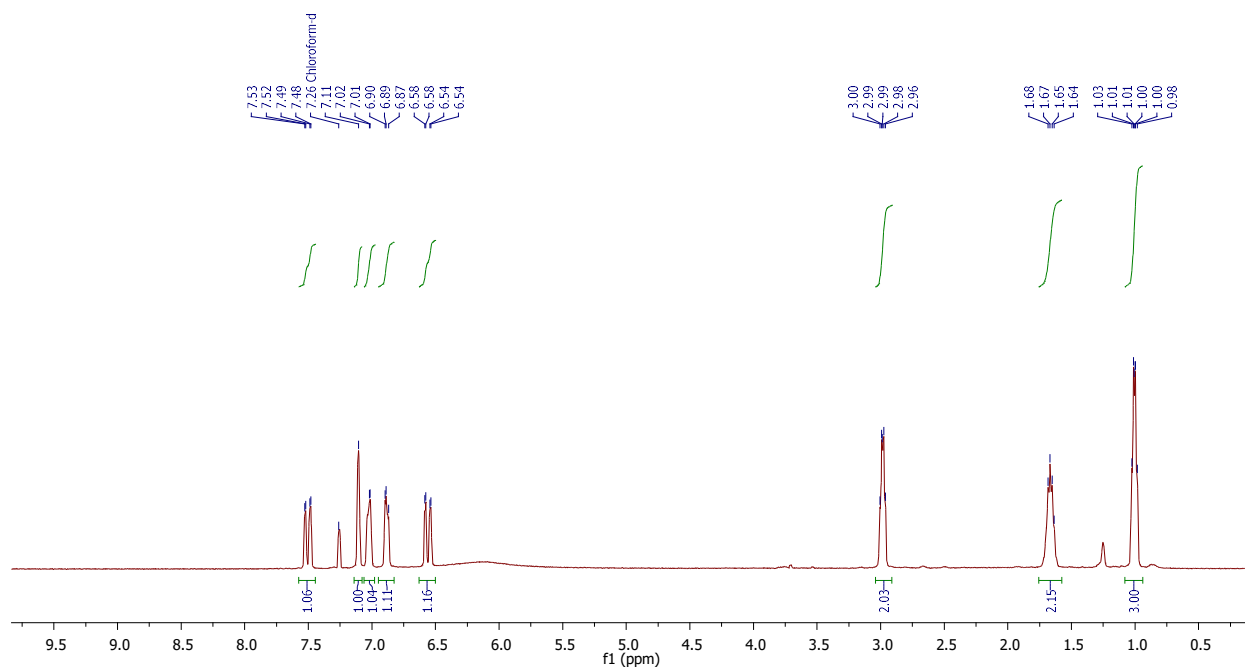
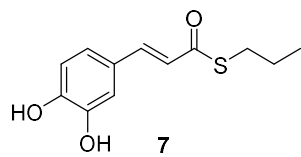


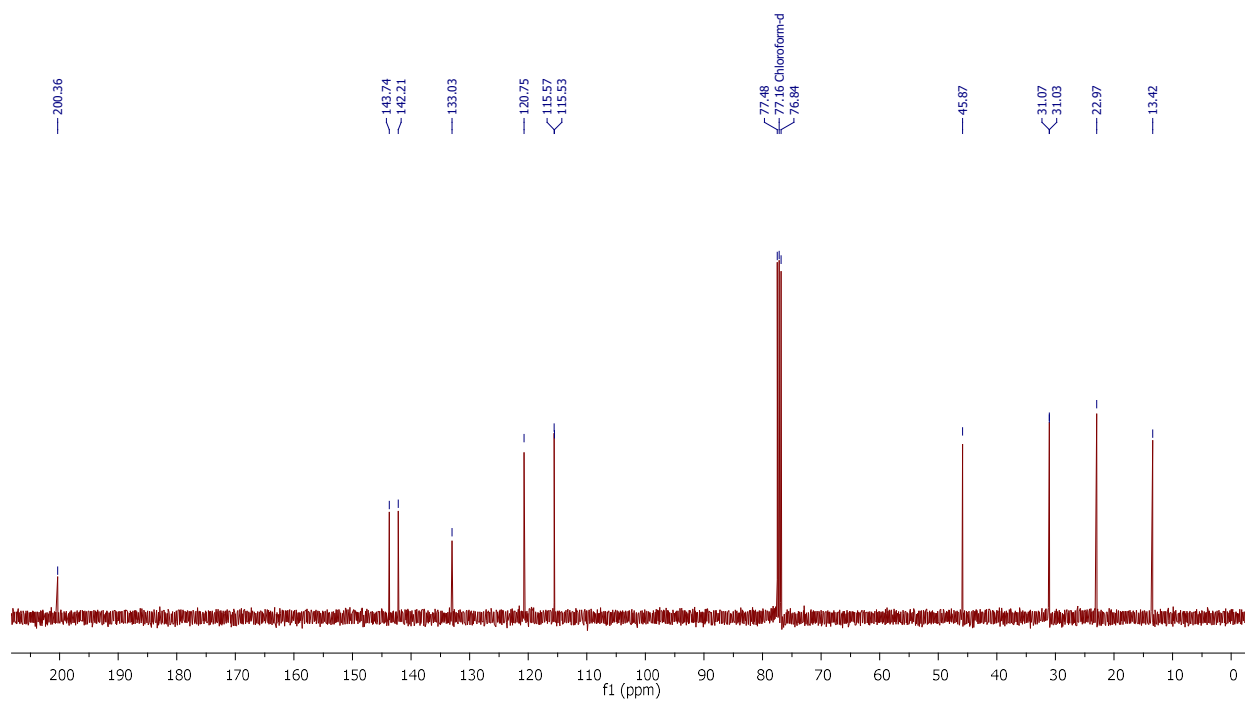
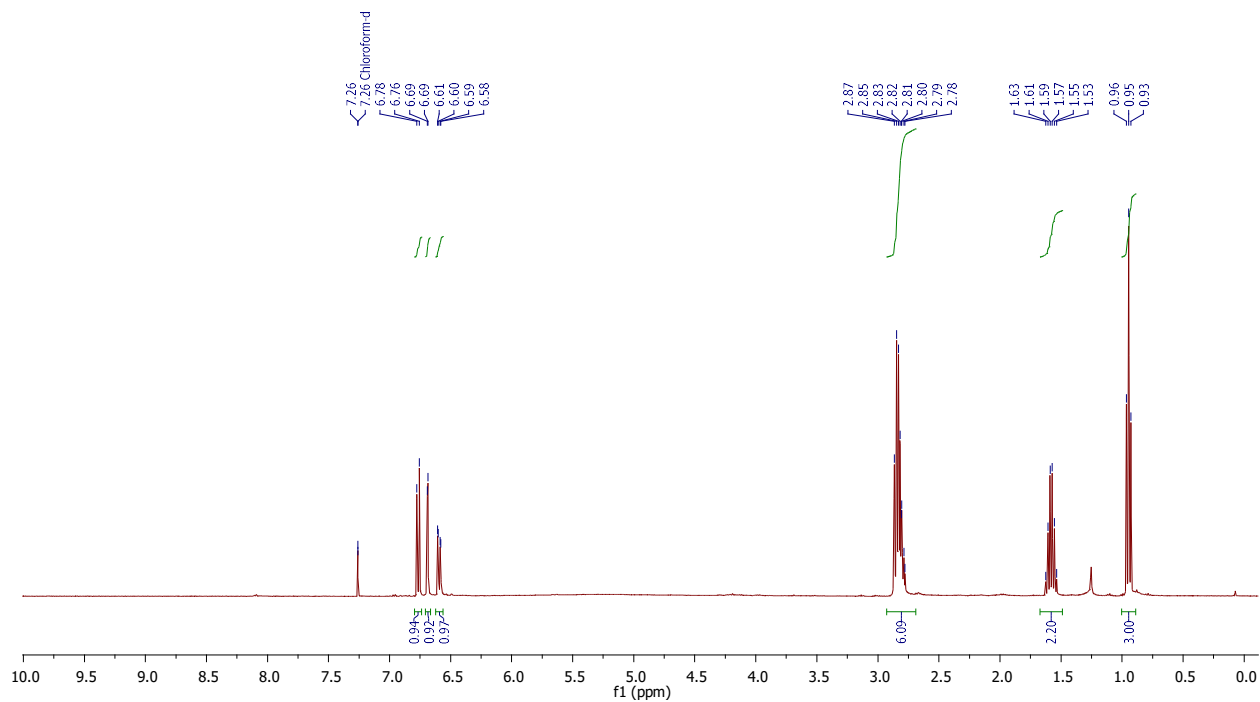
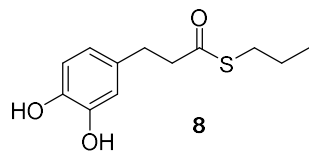


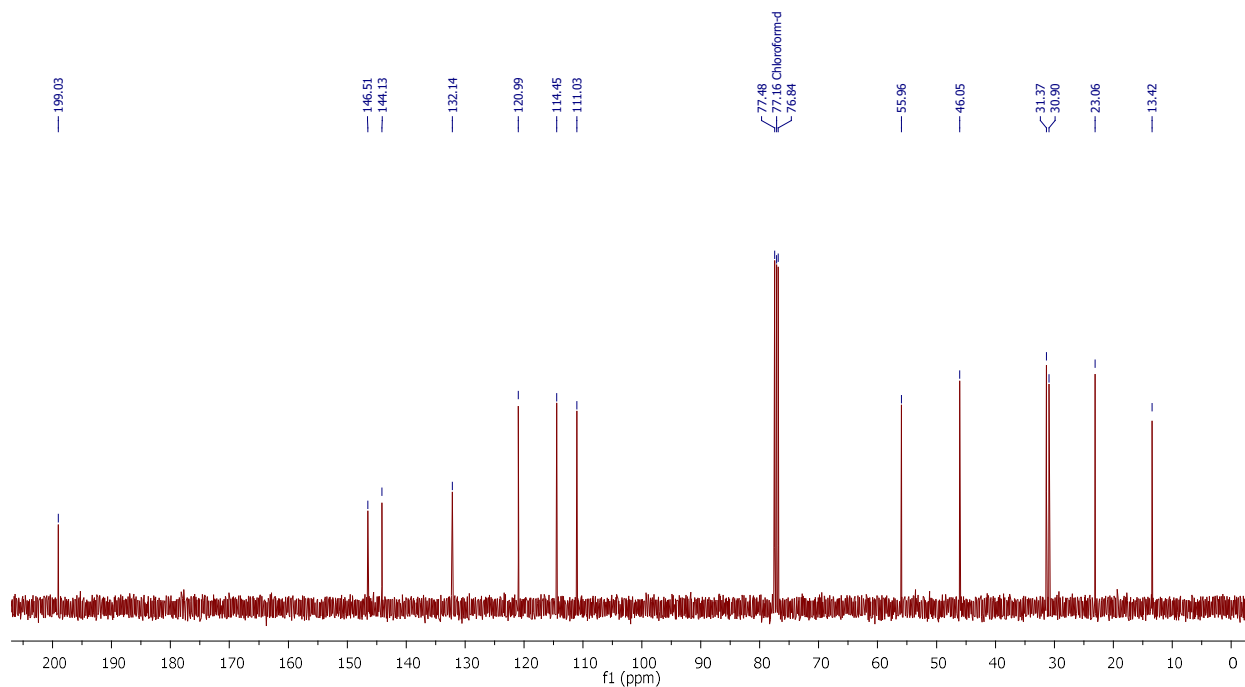
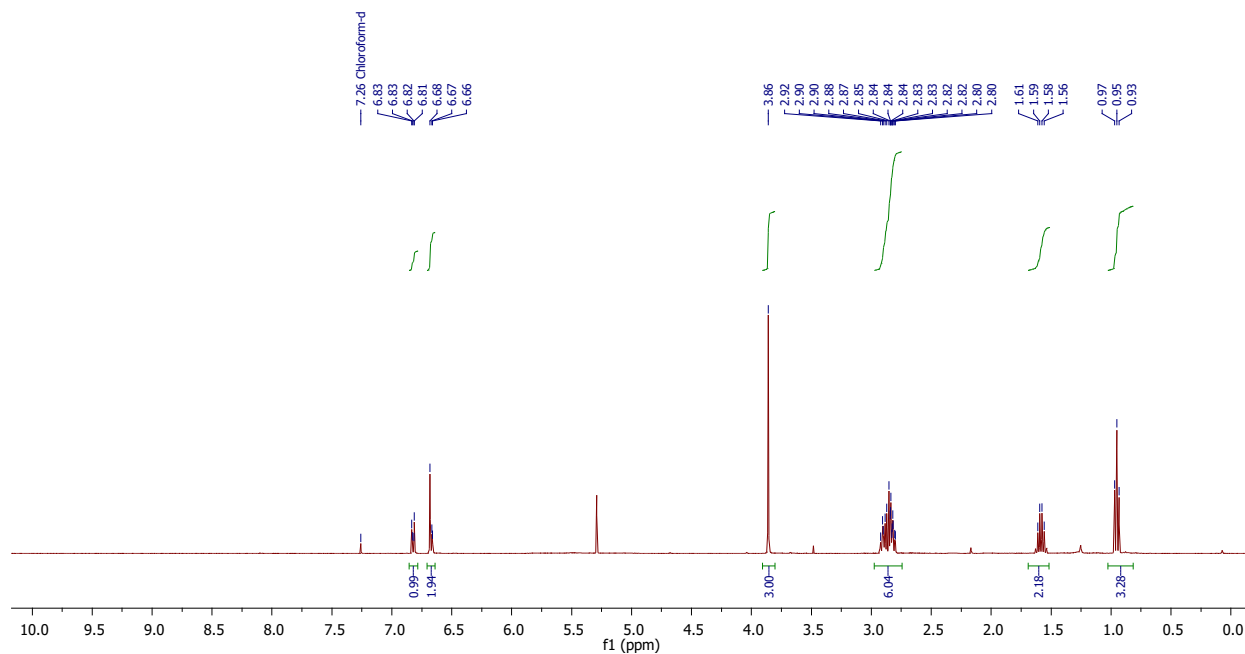
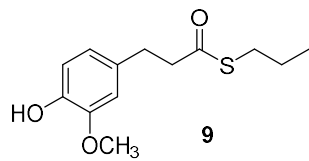


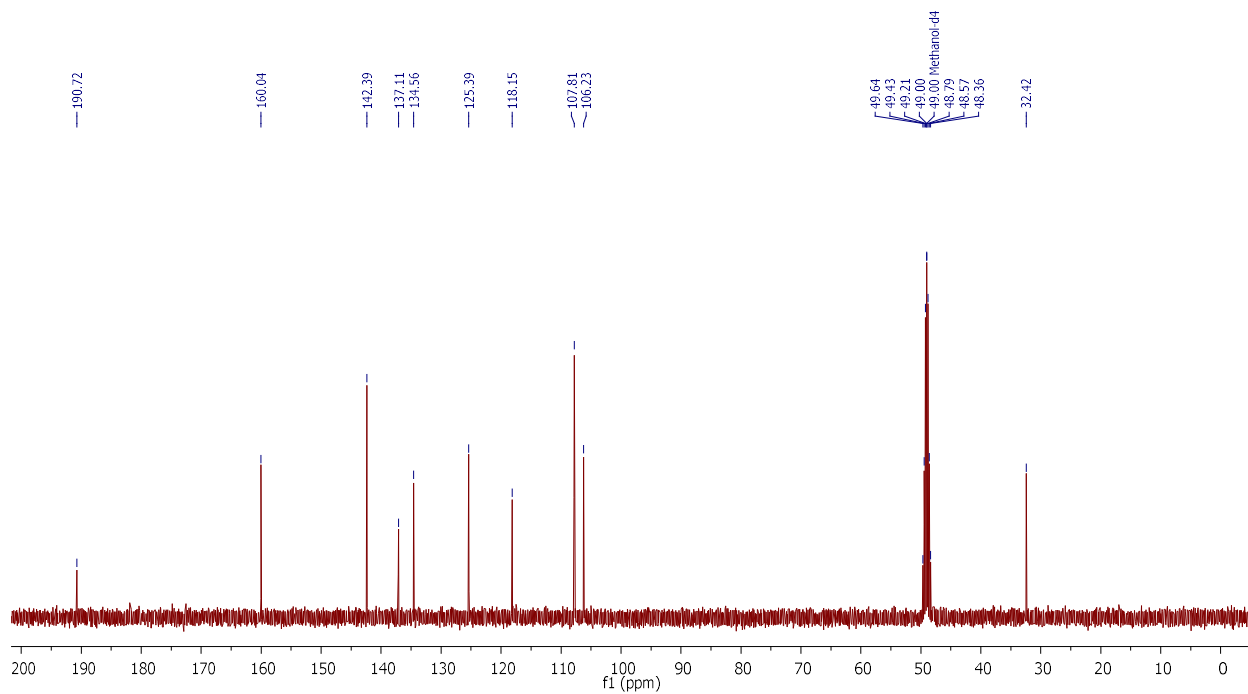
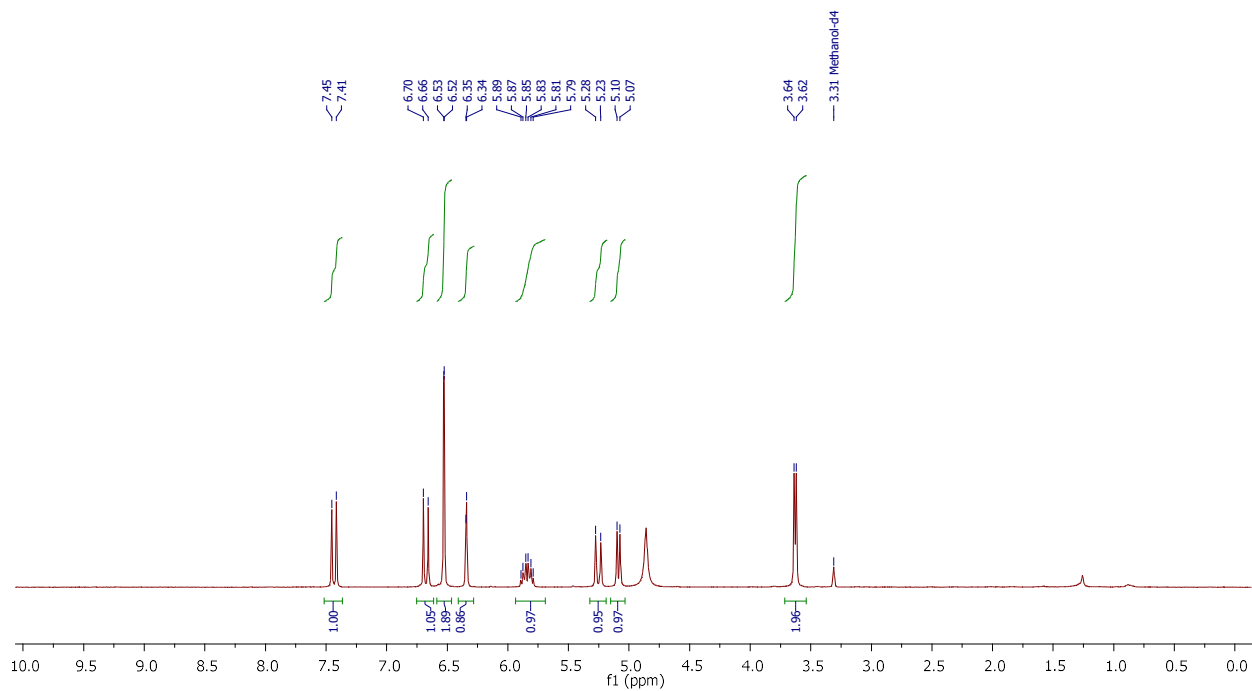
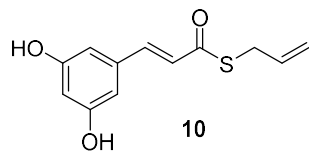


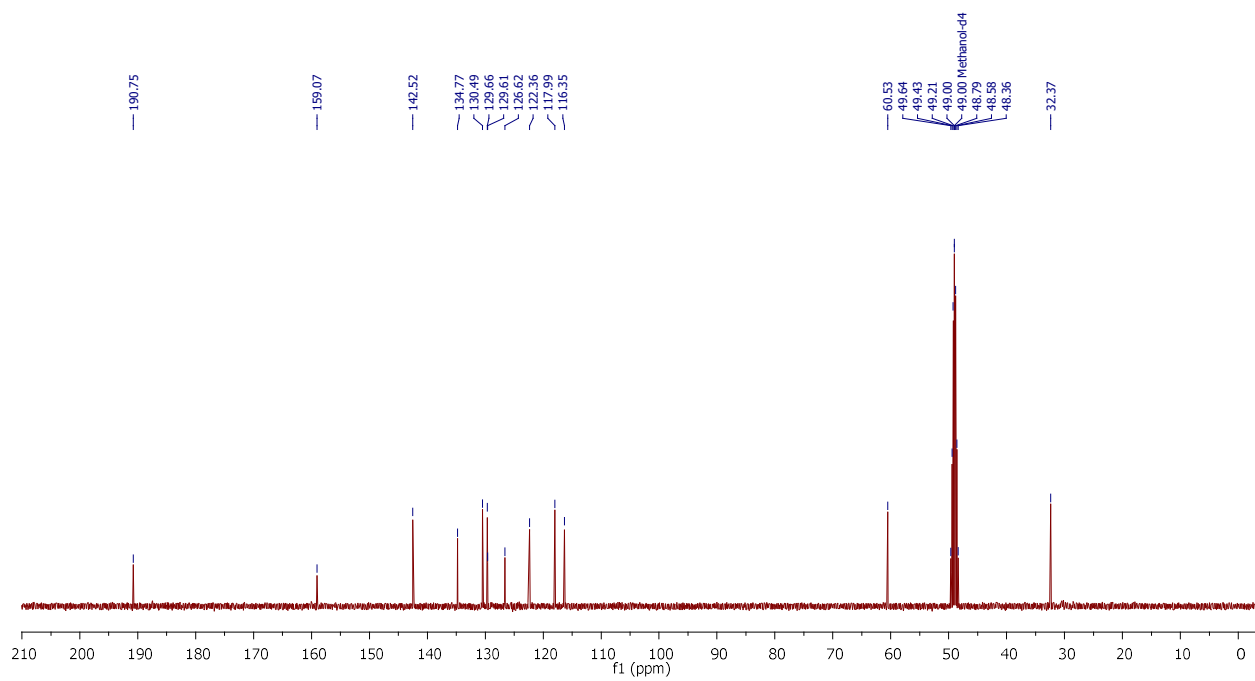
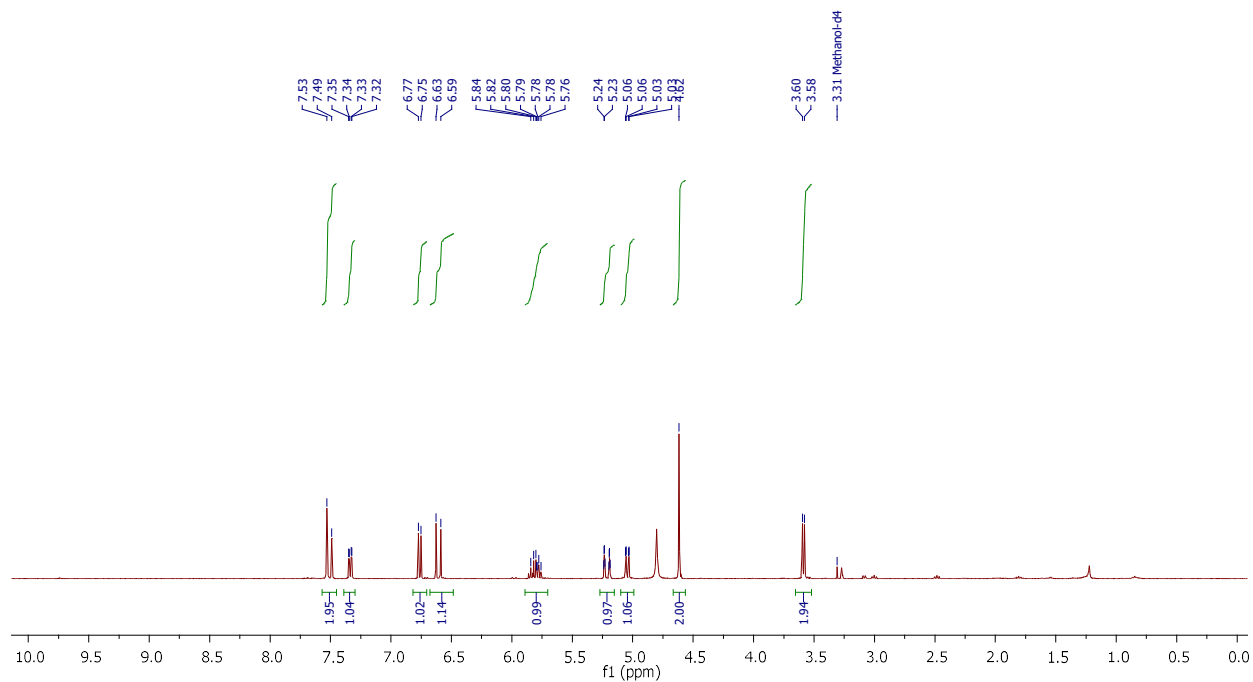
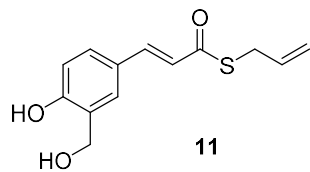


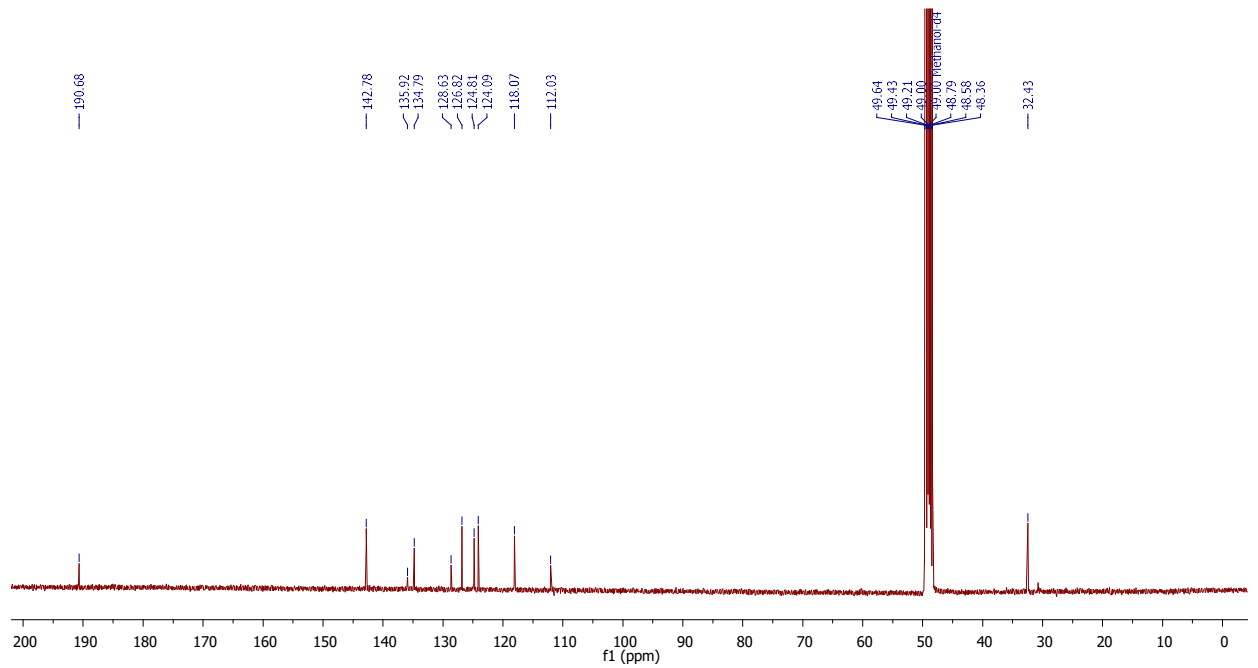
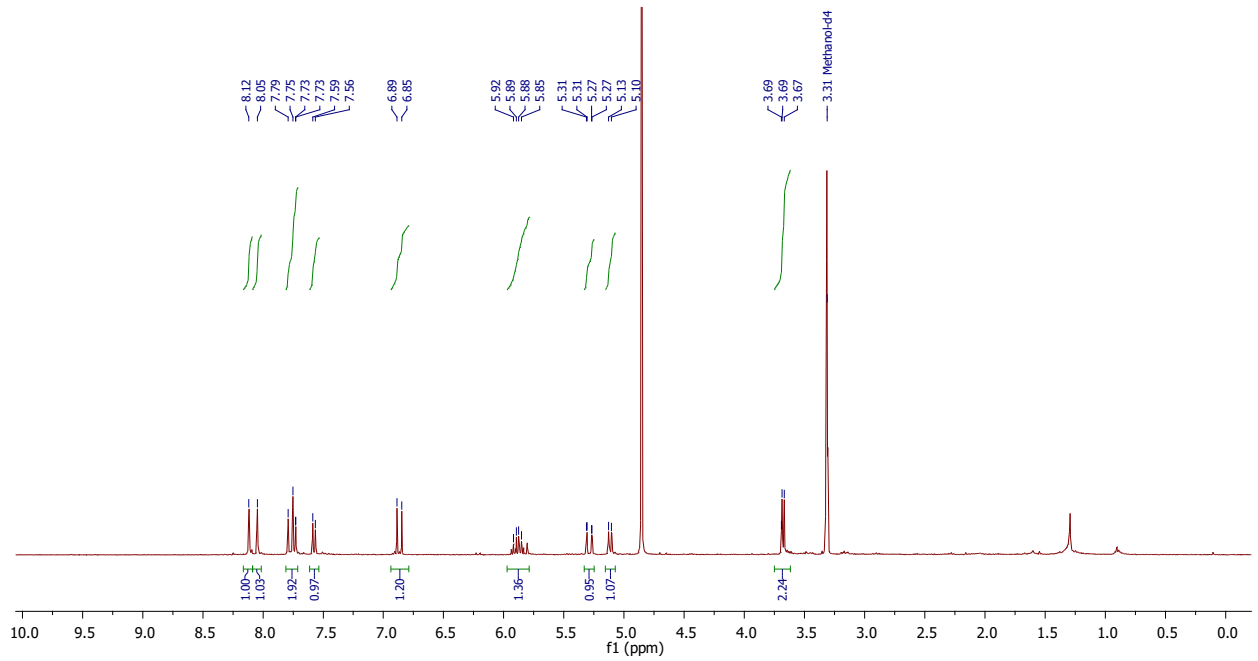
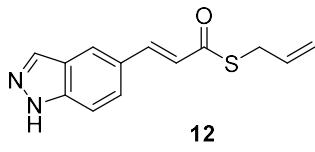


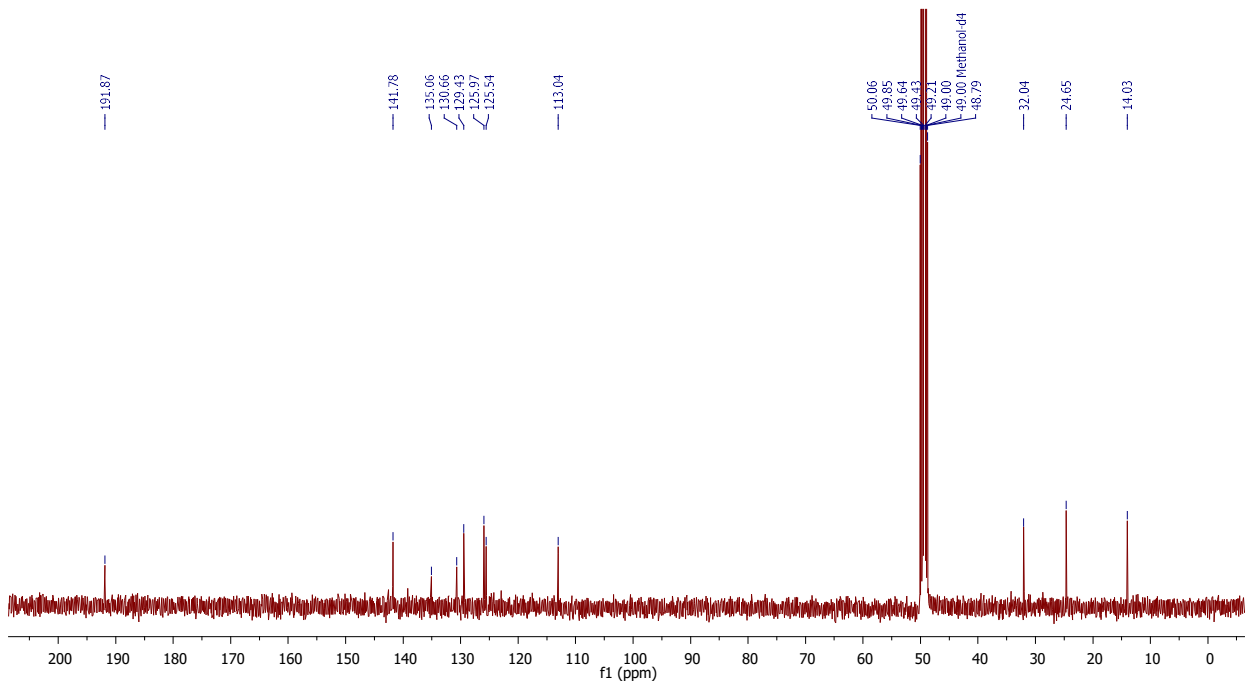
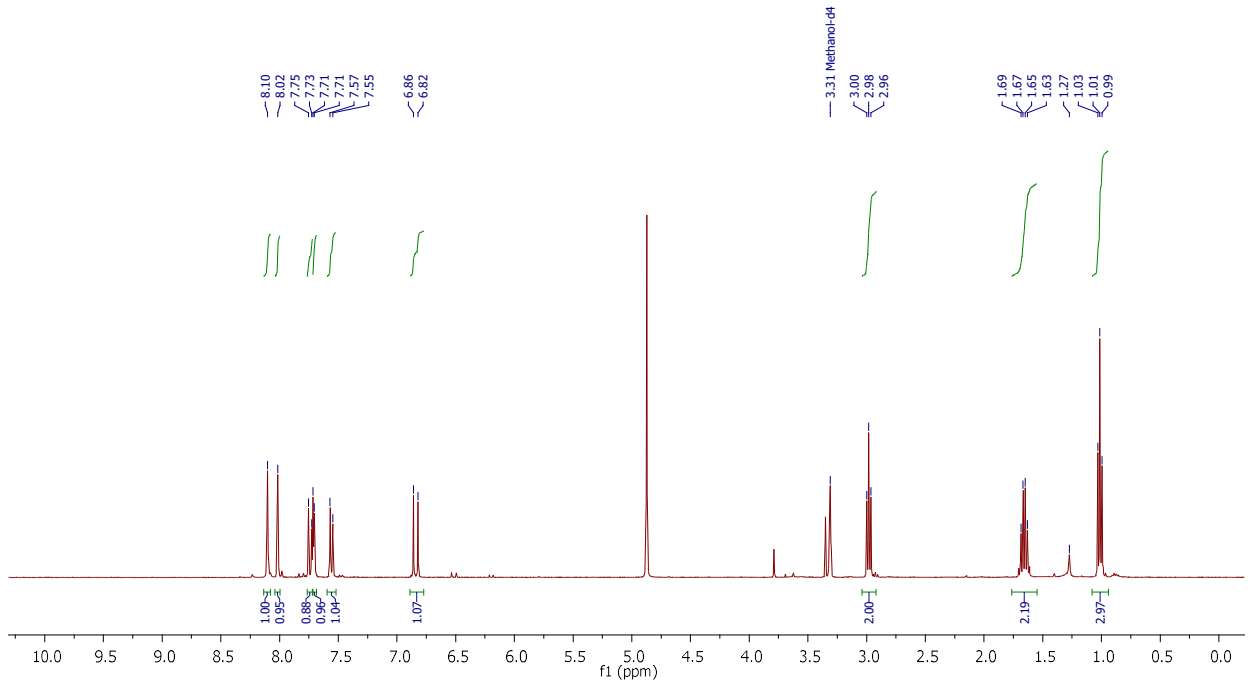
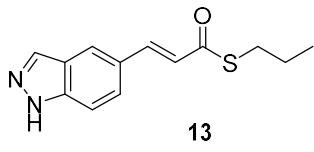


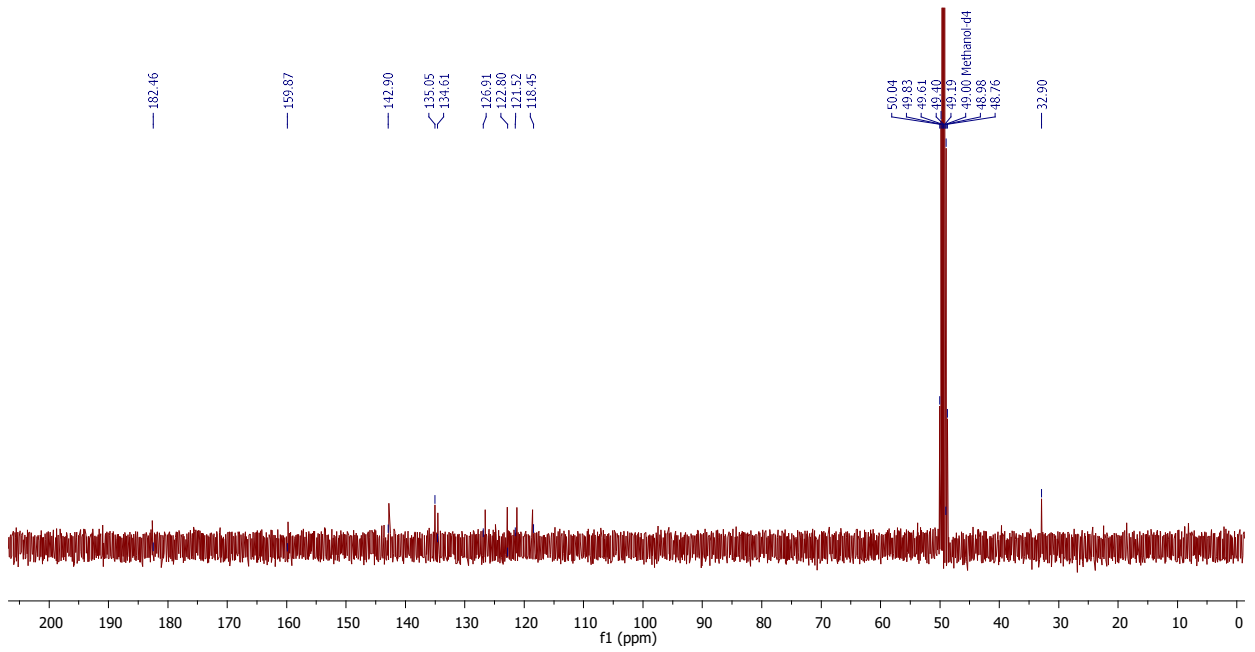
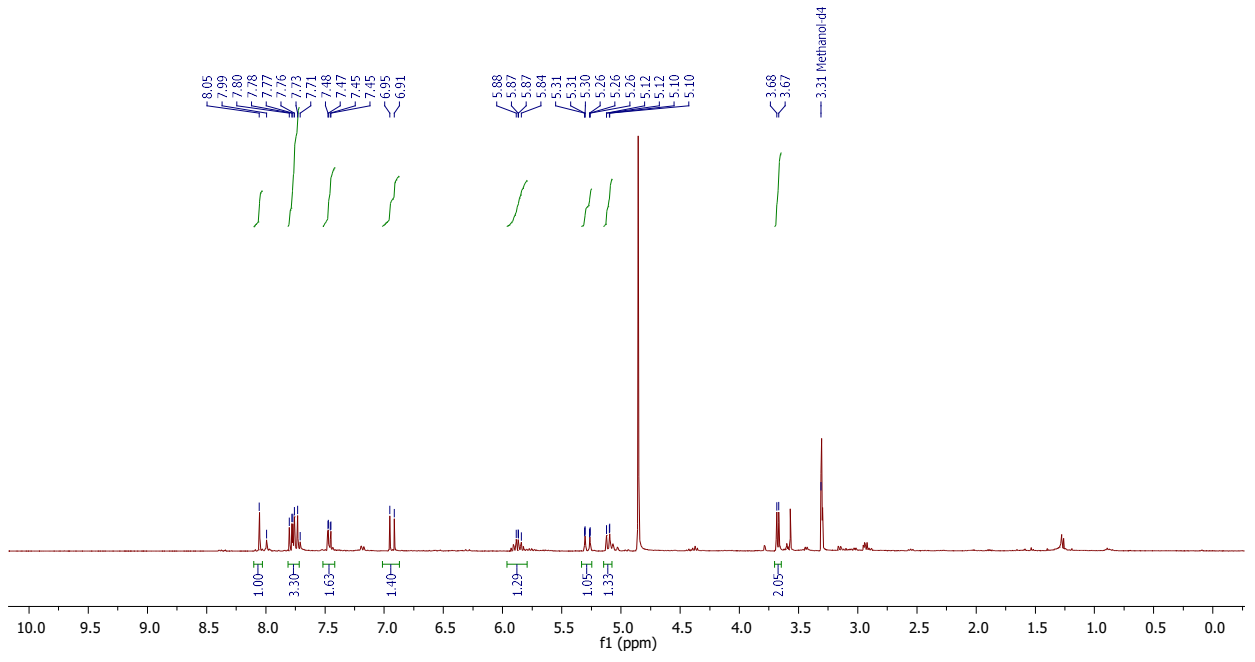
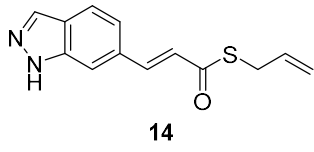


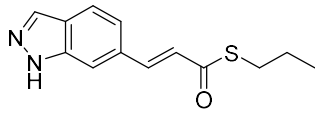












15

